NATIONAL ADVISORY COMMITTEE FOR AERONAUTICS

NACA 1957 FLIGHT PROPULSION CONFERENCE

Lewis Flight Propulsion Laboratory
Cleveland, Ohio

December 21-22, 1957

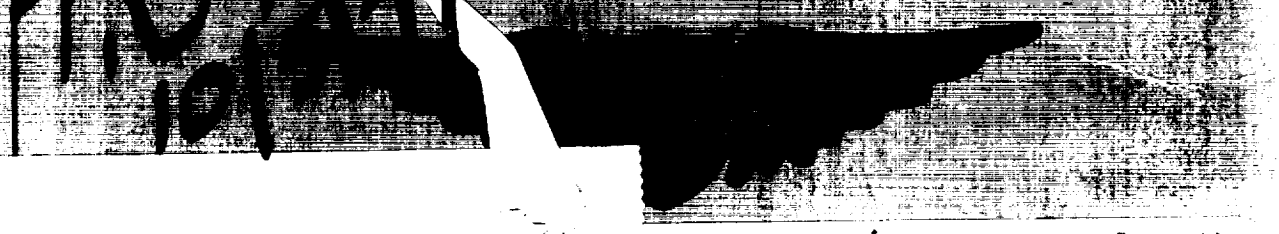

NACA 1957 FLIGHT PROPULSION CONFERENCE

Lewis Flight Propulsion Laboratory
Cleveland, Ohio

November 21, 22, 1957

INTRODUCTION

This volume contains copies of the technical papers presented at the "NACA 1957 Flight Propulsion Conference," held at the Lewis Flight Propulsion Laboratory on November 21 and 22, 1957. A list of those attending the conference is included.

The original presentation and this record are considered supplementary to, rather than substitutes for, the Committee's system of complete and formal reports.

NATIONAL ADVISORY COMMITTEE
FOR AERONAUTICS

TABLE OF CONTENTS

VOLUME I

LIST OF CONFEREES

The following conferees were registered at the NACA 1957 Flight Propulsion Conference, Lewis Flight Propulsion Laboratory, Cleveland, Ohio, November 21 and 22, 1957:

Aldrich, D. E.	Rocketdyne, North American
Alexander, S. R.	Bureau of Aerodynamics
Allen, J. L.	NACA - Lewis
Altman, D.	Aeronutronics Systems
Antoniak, C.	Solar Aircraft
Appold, Col. N. C.	ARDC
Atkinson, A. S.	Bureau of Aeronautics
Audano, P. A.	Convair
Auld, C. D.	Naval Ordnance Laboratory
Bailey, F. J.	NACA - Langley
Baldwin, L. V.	NACA - Lewis
Barnard, D. P.	Subcommittee on Aircraft Fuels
Barnes, J. L.	Subcommittee on Power Plant Control
Bashark, N.	WADC
Beck, N. J.	Douglas Aircraft
Beckelman, B. F.	Subcommittee on Internal Flow
Bell, E. B.	WADC
Benneche, R. A.	Bureau of Aeronautics
Bennet, W. J.	Marquardt Aircraft
Berkey, D. C.	General Electric
Berteling, Lt. Col. J.	U. S. Marine Corps.
Birmingham, Bascom W.	National Bureau of Standards, Boulder
Bjork, C. F.	Subcommittee on Power Plant Controls
Blackshear, Perry L., Jr.	University of Minnesota
Bliss, Cdr. L. K.	Subcommittee on Compressors and Turbines
Blum, Lt. Col. E.	Headquarters - USAF
Bodemuller, R.	Subcommittee on Engine Performance and Operations
Boksenbom, A. S.	NACA - Lewis
Bollay, W.	OASD
Border, R. L.	USN - Lake Denmark
Bortell, Lt. Col. C. K.	ARDC
Boyer, R. P.	AEDC
Breitwieser, C. J.	Giannini Co.
Breitwieser, R.	NACA - Lewis
Briggs, E. J., Jr.	Civil Aeronautics Administration
Brill, Capt. J. R.	ARDC
Brown, A. E.	General Motors Corp.
Brown, E. D.	Pratt and Whitney

[redacted]

Brown, R.	Bureau of Aeronautics
Browne, T. P.	Douglas Aircraft
Bruckman, B. W.	General Electric
Brun, R. J.	NACA - Lewis
Bryan, G. J.	Naval Ordnance Laboratory
Bunze, Col. H. F.	WADC
Calderbank, Col. J. J.	Committee on Power Plants
Calvert, C. S.	General Electric
Campbell, K.	Curtiss Wright
Canright, R. B.	Subcommittee on Rocket Engines
Carhart, H. W.	Naval Research Laboratory
Chapman, C. E.	Convair
Charshatian, J. O.	Wright Aeronautical
Childs, J. H.	NACA - Lewis
Christensen, R. G.	OASD
Cole, D. M.	Martin Co.
Connelly, Lt. J. J.	Atomic Energy Commission
Connors, J. F.	NACA - Lewis
Conrad, E. W.	NACA - Lewis
Cooley, J. L.	Subcommittee on Aircraft Fuels
Cornell, W. G.	Subcommittee on Compressors and Turbines
Cortright, E. M.	NACA - Lewis
Courson, R. G.	North American Aviation
Craigie, Gen. L. C.	Giannini Co.
Daley, J.	NAMC - Philadelphia
Davis, W. F.	NACA - Ames
Delio, G.	NATTS - Trenton
Demler, Brig. Gen. M. C.	ARDC
Deodati, Cdr. J. B.	Bureau of Aeronautics
Dibble, C. G.	Committee on Power Plants
Dietz, R. O.	AEDC
Disher, J. H.	NACA - Lewis
Dixon, T. F.	OASD
Dougherty, F. G.	Subcommittee on Aircraft Fuels
Douglass, H. W.	NACA - Lewis
Drake, J. A.	Subcommittee on Internal Flow
Drake, J. F.	Marquardt Aircraft
Drell, H.	Subcommittee on Internal Flow
Dryer, M.	NACA - Lewis
DuBois, Maj. J. M.	ARDC
Duckworth, J. B.	Standard Oil of Indiana
Dugan, J. F.	NACA - Lewis
Dukek, W. G., Jr.	Subcommittee on Aircraft Fuels
Dunholter, H. F.	Subcommittee on Rocket Engines

[redacted]

Eads, D	Callery Chemical
Eber, G. R.	Holloman Air Force Base
Edkins, D. P.	General Electric
Ehrich, F. F.	General Electric
Ellis, B.	Lockheed Aircraft
Ellis, F. E., Jr.	Bureau of Aeronautics
English, R. E.	NACA - Lewis
Erkeneff, N.	ARDC
Everett, Maj. P. E.	ARDC
Fischer, L. J.	General Electric
Fisher, J. H.	Ramo Wooldridge
Fisher, R. E.	Marquardt Aircraft
FitzMaurice, W. A.	Bendix Aviation
Fleming, F. M.	Douglas Aircraft
Fletcher, E. A.	NACA - Lewis
Forsten, I.	USN - Lake Denmark
Francis, H. E.	Subcommittee on Power Plant Materials
Friedrich, H. R.	Subcommittee on Power Plant Materials
Gabriel, D. S.	NACA - Lewis
Gamman, Ben	NACA - Washington
Gebhardt, W. A.	Bendix Prod.
Gerdan, D.	Committee on Power Plants
Gerstein, M.	NACA - Lewis
Giannini, G. M.	Giannini Co.
Godfrey, P. W.	McDonnell Aircraft
Goranson, R. F.	NACA - Washington
Gordon, S.	NACA - Lewis
Gorman, Cdr. F. B.	Bureau of Aeronautics
Graham, R. W.	NACA - Lewis
Grant, A. F., Jr.	Jet Propulsion Laboratory
Gregory, A. T.	Fairchild Engine and Airplane
Grizzell, J. O., Jr.	WADC
Gross, R. A.	Fairchild Engine and Airplane
Haber, B. D.	North American Aviation
Haley, Capt. T. B.	Bureau of Aeronautics
Hall, R. S.	Subcommittee on Engine Performance
Hallowell, F. C.	NADC - Johnsville
Hand, W. H.	Subcommittee on Power Plant Controls
Hanger, Capt. W. M.	Bureau of Aeronautics
Hanzalek, W. V.	Subcommittee on Combustion
Harkleroad, Capt. N.	Bureau of Aeronautics
Harned, Capt. R. W.	USAF
Hartman, E. P.	NACA - Los Angeles
Harvie, S.	Grumman Aircraft
Hasel, L. E.	NACA - Langley

[redacted]

Hausmann, G. F.	United Aircraft
Havenstein, Lcdr. P.	Bureau of Aeronautics
Haxby, L. P.	Shell Oil
Hazen, R. M.	Allison
Hedberg, J. H.	Firestone Tire and Rubber
Henneberry, H. M.	NACA - Lewis
Hill, P. R.	NACA - Langley
Himmel, S. C.	NACA - Lewis
Holden, F. R.	NADC - Johnsville
Holmes, V. V.	OASD
Holtsinger, C. E.	Pratt and Whitney
House, W. C.	Aerojet
Hribar, Capt. E. W.	NADC - Johnsville
Hunczak, H. R.	NACA - Lewis
Hunter, J. A.	Martin Co.
Hunter, M. W.	Douglas Aircraft
Hurt, J. B.	Convair
Hyatt, A.	Committee on Aerodynamics
Ivey, H. R.	TAC - Langley Air Force Base
Jackson, J. E.	OASD
Jacobs, R. M.	National Bureau of Standards, Boulder
Jenkins, H. P., Jr.	NOTS-Inyokern
Jirsa, L. A.	Convair
Johnson, E.	WADC
Johnson, J. A.	U.S. Army - Fort Eustis
Johnson, K. P.	Martin Co.
Johnson, P. G.	NACA - Lewis
Johnson, W. A.	Thompson Products
Joline, E. S.	Sperry Gyroscope
Kapelion, V. S.	Subcommittee on Internal Flow
Kappus, P. G.	Subcommittee on Power Plant Materials
Karlovitz, B.	Subcommittee on Combustion
Kartveli, A.	Committee on Aerodynamics
Kaufman, Lt. Col. F.	USAF
Keating, T. J.	WADC
Kelso, Lt. Col. W. R.	USAF
Kerrebrock, J. L.	Oak Ridge
Klenke, E.	WADC
Knapp, W.	WADC
Kochendorfer, F. D.	NACA - Lewis
Kolk, F. W.	OASD
Kotcher, E.	WADC
Kramer, F.	Redstone Arsenal
Krase, W. H.	Rand Corp.
Kuhrt, W. A.	United Aircraft

[redacted]

Lamar, W. E.	ARDC
Lavacot, F. J.	NOTS - Inyokern
Lawrence, H. R.	OASD
Lee, Lcdr. A. S.	O.N.R.
Lee, L. W.	Redstone Arsenal
Levitt, B. B.	Northrop Aircraft
Lewis, B.	Subcommittee on Combustion
Liddell, C. J., Jr.	Lockheed Aircraft
Littlewood, W.	OASD
Loh, W. H. T.	Chance Vought
Lorenzo, M.	USAF
Low, G. M.	NACA - Lewis
Lubarsky, B.	NACA - Lewis
Lubick, R. L.	NACA - Lewis
Mallett, Lt. W. E.	NATC - Patuxent
Mandel, M. W.	Sperry Gyroscope
Manganiello, E. J.	NACA - Lewis
Maravel, J.	Republic Aviation
Martin, C. J.	Thompson Products
Martz, R. B.	WADC
Maslen, S. H.	NACA - Lewis
McDowall, C. J.	Allison
McKee, J. W.	Douglas Aircraft
McNickle, Col. M.	ARDC
McRae, A. H.	WADC
Meghreblian, R. V.	Oak Ridge
Melrose, R.	Reaction Motors
Mercer, Capt. W.	Subcommittee on Power Plants
Meuser, R. B.	University of California
Michaels, C. M.	WADC
Mickelson, L.	Subcommittee on Rocket Engines
Millsaps, K.	Holloman Air Force Base
Mitcham, G. L.	Naval Ord.
Moeckel, W. E.	NACA - Lewis
Moyers, Col. F. N.	USAF
Mulholland, D. R.	NACA - Los Angeles
Multhopp, H.	Martin Co.
Mumford, N. V. S.	Chance Vought
Munger, W. P.	Subcommittee on Rocket Engines
Munier, A. E.	Grumman Aircraft
Muse, T. C.	OASD
Nadler, Lt. Col. P. O.	USAF
Nagey, T. F.	Martin Co.
Nassetta, F. C.	O.N.R.
Nay, Col. P. F.	ARDC
Nesbitt, M. W.	Pesco Products
Nichols, M. R.	NACA - Langley

[redacted]

Norman, T. E.	Subcommittee on Rocket Engines
Novik, D.	NACA - Washington
O'Donnell, W. J.	Committee on Aerodynamics
Offutt, W. F.	OASD
O'Malley, J. A.	Bell Aircraft
Ordin, P. M.	NACA - Lewis
Ormsby, R. B., Jr.	Lockheed Aircraft
Pake, F. A.	Goodyear Aircraft
Palmer, C.	NACA - Washington
Parke, D. B.	Subcommittee on Internal Flow
Parrett, Cdr. G. S.	Subcommittee on Aircraft Construction
Pattillo, Lt. Col. L. G.	ARDC - Cleveland
Patton, J. R.	Committee on Power Plants
Paxhia, V. B.	Bell Aircraft
Pearce, R. B.	North American Aviation
Pearson, R. Adm. J.	North American Aviation
Pellini, W. S.	Naval Research Lab.
Perchonok, E.	Marquardt Aircraft
Petersen, Lcdr. F. C.	NATC - Patuxent
Phillips, F. W.	NACA - Washington
Pinkel, B.	OASD
Pinnes, R. W.	Bureau of Aeronautics
Posner, D. L.	Lockheed Aircraft
Povolny, J. H.	NACA - Lewis
Priem, R. J.	NACA - Lewis
Prince, W. R.	Los Alamos Lab.
Rall, F. T., Jr.	Subcommittee on Internal Flow
Ray, G. D.	Subcommittee on Aircraft Construction
Redding, A. H.	Subcommittee on Engine Performance
Reese, B. A.	Purdue University
Reichel, R. H.	Bell Aircraft
Reid, J. A.	Subcommittee on Aircraft Fuels
Reinhardt, T. F.	Bell Aircraft
Reinhardt, W. J.	Reaction Motors
Rethman, Lt. Col. V. C.	ATIC
Reynolds, T. W.	NACA - Lewis
Rice, J. S.	Garrett Corp.
Rich, B.	Lockheed Aircraft
Ring, E.	Martin Co.
Robert, K. F.	NACA - Langley
Robbins, Lt. Col. H. W.	ARDC
Robinson, R. G.	NACA - Ames
Rochen, H. D.	Subcommittee on Compressors and Turbines
Rogers, J. D, Jr.	Los Alamos Lab.
Rohl, H. T.	WADC
Rom, F. E.	NACA - Lewis
Rostkowski, Capt. F. J.	ARDC - Cleveland

[redacted]

Sadler, C., Jr.	McDonnell Aircraft
Sanders, J. E.	Subcommittee on Compressors and Turbines
Savage, C. A.	Convair
Scarborough, R. W.	Martin Co.
Schamberg, R.	Rand Corp.
Scheller, K.	Subcommittee on Combustion
Schiavone, D. C.	Committee on Power Plants
Schloesser, V. V.	Subcommittee on Compressors and Turbines
Schmidt, Maj. H. R.	A.E.C.
Schmidt, J.	WADC
Schnare, C. W.	WADC
Schramm, W. B.	NACA - Lewis
Schuldenfrei, M.	Bureau of Aeronautics
Schulman, F.	O.N.R.
Scull, W. E.	NACA - Lewis
Seaberg, Lt. Col. J. D.	ARDC
Sears, R. E.	Hughes Aircraft
Seifert, H. S.	Subcommittee on Rocket Engines
Sens, W. H.	Pratt and Whitney
Shapiro, A. H.	OASD
Sharp, Dr. E. R.	NACA - Lewis
Shippen, W. B.	Subcommittee on Combustion
Silverstein, Abe	NACA - Lewis
Simon, D. M.	Avco Mfgr.
Simpson, E. C.	Subcommittee on Compressors and Turbines
Slawsky, M. W.	USAF
Slivka, W.	NATTS - Trenton
Smith, C. B.	United Aircraft
Smith, S. B.	Bendix Prod.
Sorem, S. S.	Subcommittee on Combustion
Sorensen, H. P.	Minneapolis Honeywell
Sorgen, C. C.	OASD
Stein, H.	Republic Aviation
Stenning, A. H.	Subcommittee on Compressors and Turbines
Stewart, W. L.	NACA - Lewis
Stoolman, L.	Hughes Aircraft
Stranges, P. A.	Olin Mathieson Chem. Co.
Struble, Cdr. A.	Bureau of Aeronautics
Sturgis, B. M.	Subcommittee on Aircraft Fuels
Sulkin, M. A.	Subcommittee on Compressors and Turbines
Tanczos, F. I.	Subcommittee on Rocket Engines
Tangren, R. F.	Aerojet
Taylor, E. B.	Subcommittee on Engine Performance and Operations
Thoren, T. R.	Thompson Products
Tilgner, C., Jr.	Committee on Aerodynamics
Tischler, A. O.	NACA - Lewis
Tormey, J. F.	Subcommittee on Rocket Engines
Towle, Cdr. B. L.	Subcommittee on Aircraft Fuels
Tuman, C.	[redacted] Mugu

47y3-I

Underwood, W. J.	NACA - Wright Field
VanVoorhis, S. N.	OASD
Vasu, G.	NACA - Lewis
Voedisch, A.	ATIC
Vogt, P. R.	North American Aviation
VonOhain, H.	OASD
Walker, C. J.	Wright Aeronautical
Walker, J. H.	Johns Hopkins
Walker, Lt. Col. W.	USAF
Walter, D. L.	Subcommittee on Engine Performance
Wang, C. J.	Ramo Wooldridge
Weber, R. J.	NACA - Lewis
Weidhuner, D. D.	Subcommittee on Engine Performance
Weiss, R. A.	U.S. Army
Weissman, C. C.	O.N.R.
Weitzen, W.	USAF
Wetherington, R. L.	Redstone Arsenal
Wetzler, J. M.	Subcommittee on Compressors and Turbines
Whitmire, Maj. W. T.	TAC - Langley Air Force Base
Widmer, R. H.	Convair
Wilcox, W. W.	NACA - Lewis
Williams, T. W.	Subcommittee on Internal Flow
Wilsted, H. D.	Allison
Wislicenus, G. F.	Subcommittee on Compressors and Turbines
Wohl, K.	Subcommittee on Combustion
Woodworth, L. R.	Subcommittee on Engine Performance
Word, C. L.	WADC
Worth, W.	WADC
Worthington, Capt. R.	OASD
Wyatt, D. D.	NACA - Lewis
Young, C. G., Jr.	McDonnell Aircraft
Young, W. H.	Bureau of Aeronautics
Ziemer, R. R.	NACA - Lewis
Zimmerman, A. V.	NACA - Lewis
Zimmerman, J. E.	WADC
Zubko, L. M.	Subcommittee on Combustion
Zucrow, M. J.	Subcommittee on Rocket Engines

1. INTRODUCTORY CONCEPTS

By Edgar M. Cortright, J. Howard Childs, DeMarquis D. Wyatt,
and David S. Gabriel

THE CHOICE

It is clear that the military planners today face some difficult and far-reaching decisions concerning the choice of deterrent weapons to be developed for the future. These weapons systems include the manned bomber and the unmanned missile for sustained flight within the atmosphere; the glide bomber; and, beyond the atmosphere, the intercontinental ballistic missile and the satellite bomber. All these systems have their chemical and nuclear counterparts. Although each has its own virtues, only the ICBM has been assured of vigorous support at the moment of this writing.

This situation is at least in part due to the fact that these various weapons systems have a common vice. They are all expensive and time-consuming to develop. This does not mean that only the least expensive system should be developed, however, or that only one should be developed. Since each unit is capable of such vast destruction, fewer units are needed. Therefore, the choice may be made on the basis of criteria other than cost. It is probable, however, that all these systems cannot be developed simultaneously.

One of the most tensely awaited outcomes of this deliberation will be the role of the air-breathing engine. Most of the aircraft industry has been developed around this type of engine and the airframe it powers. Before a rational decision can be made, however, a vast amount of information must be gathered about the various weapons systems. This is the purpose of these first five papers - to contribute to this fund of information by presenting an appraisal of the ultimate performance capabilities of aircraft and missiles powered by air-breathing engines.

CRITERIA OF MERIT

There are many criteria of merit to be considered in evaluating any type of weapons system. Some of the more important are range, speed, weight, payload, accuracy, reliability, vulnerability, development time, useful life, cost, flexibility, and logistics. Of these, only range, speed, weight, and payload have been evaluated. The other criteria, with

the exception of development time, are beyond the scope of this study. In this regard it seems probable that ten years would be required to develop an aircraft or missile utilizing the powerplants discussed herein.

REGIONS OF SUSTAINED FLIGHT

The probable regions of future sustained flight within the atmosphere are presented in figure 1. Today none of our subsonic manned aircraft has an unrefueled radius approaching the 5500-mile target distance established by the military some years ago (the 6500- and 8500-mile marks in the figure are hypothetical future goals considered in paper 5 on Mission Studies). Admittedly, the manned aircraft can extend the useful radius by aerial refueling, "fly-over" missions, and, from a deterrent point of view, could even be considered for their one-way capability. The unmanned Snark, however, attains the 5500-mile range, since its missions are all one way.

The supersonic bomber, the B-58, utilizes a split-speed mission to achieve a fairly limited unrefueled radius. The currently proposed second generation of supersonic bombers, the WS-110, are designed to cruise at Mach 3 over ranges approaching those of our current subsonic bombers. Still longer ranges are certainly desirable, and again the one-way missile can achieve them, as typified by the now defunct advanced version of the Navaho. This missile represented the only ramjet-powered bombardment vehicle.

The WS-110 and the advanced Navaho probably represent about the limits to which present technology can be pushed. The question is whether additional research and development can yield appreciably better performance for both the piloted bomber and the unmanned missile. Examination of figure 1 indicates that the most obvious need of the manned bomber is greater range capability. If missile performance is to advance appreciably beyond that projected for the Navaho, flight at very high stagnation temperature will be necessary.

COOLING

The temperature problems of high-speed flight are visualized in figure 2 where various skin temperatures are plotted as functions of flight Mach number. Also indicated are some assumed materials limits for combustor and other surfaces.

Radiation cooling at the high altitudes accompanying high speeds is sufficient to maintain the external surfaces at marginally acceptable levels. Unfortunately, the interior passages cannot radiate. Above Mach 4.5 the subsonic diffuser temperature exceeds the materials limits and,

hence, these surfaces must be cooled. Since this temperature would also apply to the compressor of turbojet-type engines, and since cooled compressors are not foreseeable, Mach 4.5 probably represents the absolute upper limit for this type engine. Actually, an upper limit closer to Mach 4 is probably more reasonable, and even at this speed the lubricants must be cooled.

For the range of flight speeds where the diffuser temperatures are well below combustor temperatures, film cooling can be used to minimize fuel-cooling requirements even though the temperature of the cooling film of inlet air actually exceeds materials limits.

FUELS AS COOLANTS

Because the concept of cooling with the fuel as it flows from the tank to the combustor has been introduced, the adequacy of such a source of cooling should be discussed. JP fuels and ethyldecaborane break down if they are permitted to heat up much. Cryogenic fuels like diborane, liquefied methane, and liquefied hydrogen cannot be maintained as liquids if their temperatures are allowed to rise. However, since they are burned as gases, this is not particularly worrisome provided that any phase change occurs before the cooling passages and that the resulting gas has a reasonably high specific heat and can be heated to elevated temperatures.

In figure 3 the resulting cooling capacities of the aforementioned fuels are compared. It was assumed that no fuel cooling is required below Mach 4 and that all cooling is done by the fuel above that speed. Only liquefied methane and hydrogen showed appreciable cooling capacity above Mach 5. Hydrogen is markedly the best fuel for cooling purposes, largely because it can be heated close to the limiting temperature of the cooled surfaces.

It should be pointed out that the Mach number at which the heat load exceeds the fuel sink capacity can be extended by flowing excess fuel into the combustor. This fuel-rich operation reduces the impulse, of course, but at a rate that decreases with increasing speeds.

RANGE

It has thus been indicated that there exists no fundamental limit that precludes flight in the atmosphere to Mach numbers approaching and exceeding 10. This does not mean that flight at that speed is desirable. One obvious question is what ranges are attainable at these hypersonic speeds. Some of the considerations necessary to answering this question are shown in figure 4. The range equation,

[redacted]

$$\text{Range} = IV \frac{L/D}{1-(V/V_s)^2} \ln \frac{1}{1-W_f/W_g}$$

consists of the terms, impulse, velocity, lift-drag ratio, centrifugal-force effect, and a log function of fuel- to initial-gross-weight ratio. All of these terms except velocity and centrifugal force decrease with increasing flight speed in the indicated manner. The net result is that range will maximize at some point in this speed range.

Much of the material in the following papers will discuss how to attain the highest possible values of the terms over which there is some control: impulse, lift-drag ratio, and fuel- to initial-gross-weight ratio. In this regard it should be noted that the discontinuity in the variation of fuel- gross-weight ratio illustrates one method of maximizing this value at the start of cruise. That is, to provide a disposable booster as must be done in the case of the ramjet engine.

SELF-BOOST

Since the ramjet engine requires at least some boost, differentiation is necessary between this engine type and those utilizing turbine-driven compressors with take-off capabilities. The distinction may be clarified with the aid of figure 5. At speeds much below Mach 1 the ramjet produces no useful thrust, whereas relatively low pressure ratio compressors are quite effective. In general, at low speeds, the higher the pressure ratio, the better the performance. As speed is increased, however, the higher the pressure ratio, the sooner the performance falls below that of the ramjet. The compressor and turbine are merely in the way at high speeds where most of the compression occurs in the air-induction system.

Because the self-boost capabilities of the turbine type engine are essential in some applications, paper 3 is devoted to discussing the various turbine cycles that may be utilized to drive the compressor.

MATCHING

Among the many problems introduced by operation over a wide speed range, as required by self boost, is that of matching the air inlet and the jet exit nozzle to the air-handling capacity of the engine. This problem is illustrated in figure 6 where relative areas of an ideal inlet and exit are plotted as a function of flight Mach number for a hypothetical turbojet engine. The ideal areas are merely the areas of the capture stream tube and the discharged jet at ambient static pressure.

[redacted]

The problem is simplified by considering the engine as approximating a fixed throttling device. The higher the flight speed, the more air can be forced through the engine. Conversely, if the inlet and nozzle are sized (as in the sketch of fig. 6) to capture and discharge the airflows at Mach 4, they are much too large at Mach 1.5. Unless the inlet is varied to bypass the excess air in a sophisticated manner at off-design speeds, large drags can result. The nozzle must also be adjusted to the discharge stream-tube area or suffer thrust penalties. At the same time, the adjustment must not incur large boattail drags.

Although these curves are for a turbojet engine, they look much the same for a ramjet engine having a fixed combustor and nozzle throat. At the higher operating speeds of the ramjet, the matching problem becomes much more severe as indicated by the increasing rate of change of stream-tube area with Mach number. Nozzle-throat-area variation somewhat mitigates this problem by providing a degree of engine flexibility. Nevertheless, it is very difficult to make a good cruise engine provide much self-boost capability for the hypersonic ramjet.

FUEL HEATING VALUE

The basic engine types and some of their inherent off-design problems having been introduced, it is of interest to return to design-point operation and the problem of maximizing the terms of the range equation over which some control is possible. When the impulse term is considered, the heating value of the fuel is certainly of paramount importance. In figure 7 the heating values of the more prominent fuels are shown. The superiority of hydrogen is clearly indicated by a heating value 70 percent greater than that of its nearest competitor, diborane. This fact, combined with its greatly superior cooling capacity, makes hydrogen extremely interesting as a fuel for long-range hypersonic flight. One of its disadvantages, low density, will be considered later.

DISSOCIATION LOSSES

It is not at all certain that all the heating value of the fuels listed in figure 7 can be realized. The combination of high temperatures and moderate pressures in the combustion chamber at high Mach numbers results in dissociation of the fuel and air into many components. This dissociation absorbs energy and unless the components recombine into the products of combustion within the nozzle, the full heating value of the fuel is not realized.

The implications of this possibility are illustrated in figure 8 where thrust per unit airflow is plotted as a function of flight Mach number. The upper curve represents the thrust obtained with equilibrium

expansion (full recombination) and thus represents full realization of the heating value. The lower curve, denoted frozen expansion, corresponds to the maximum loss due to dissociation. The difference between the two curves thus represents the loss in sensible enthalpy.

RECOMBINATION

The possible losses clearly become very large at hypersonic speeds and whether or not equilibrium expansion occurs is a question of major import. Figure 9 illustrates this question with an example using hydrogen as a fuel. The various constituents at the entrance to the nozzle are listed along with that percent of the sensible enthalpy loss that is tied up in the particular constituent. Within the nozzle the temperature drops because of the expansion of the flow. As the temperature drops, the indicated reactions begin to take place recombining the many constituents into the two products of combustion. If all these reactions go to completion, there are no dissociation losses.

Unfortunately, the rates of all these reactions are not known. In particular, those involving hydrogen molecules and hydroxyl radicals are in doubt, and these chemical species contain 58 percent of the potential enthalpy loss due to dissociation. While research proceeds to establish these recombination rates, the hope is that the reactions will go nearly to completion in the large nozzles which will be of concern. Most of the calculations to be presented will thus assume equilibrium flow, although the effect of frozen composition will occasionally be illustrated.

COMPONENT PERFORMANCE

Obtaining large values of impulse involves more than large heating values. High efficiencies must be attained in the inlet and the exit nozzle as illustrated in figure 10 along with some other interesting observations. It is immediately apparent from this figure that very high impulse levels relative to a rocket may be realized. This, of course, is necessary for sustained flight in the atmosphere but also indicates the potential of the ramjet as a booster.

Spotted on the curves for Mach 4 and 7 ramjets are the inlet kinetic energy efficiencies corresponding to the particular values of impulse and inlet pressure recovery (kinetic-energy efficiency η_{KE} is the efficiency of the inlet in converting the free-stream kinetic energy into pressure within the engine). The highest indicated value of $\eta_{KE} = 0.97$ represents the best of current inlets and corresponds to realization of most of the available impulse. It is interesting to note that this value may be achieved with a much lower pressure recovery at Mach 7 than at Mach 4

and that good values of impulse may be obtained with much lower values of pressure recovery. In general, it should be remembered that $\eta_{KE} = 0.95$ represents good inlet efficiency.

The fact that increasing pressure recovery from 0.35 to 0.70 does not result in correspondingly large increases in impulse should not be taken to mean that the attainment of high pressure recovery is not important in itself. Under some circumstances it can be vitally important since, for a given developed engine, doubling the recovery doubles the airflow through the engine and more than doubles the thrust. For lightweight engines designed to fit a particular mission, however, η_{KE} is more indicative of the impulse and the range.

Also shown in figure 10 is the decrement from ideal impulse due to using an actual nozzle having a velocity coefficient of 0.97 in addition to being slightly underexpanded (this decrement is smaller at Mach 4). Refined nozzle design may regain up to half of this loss. The following paper on Inlets, Exits, and Cooling Problems discusses in more detail the problems of attaining efficient performance of these components.

LIFT-DRAG RATIO

Efficient performance of the inlet and exit components must include low drag as a factor, since this influences another term of the range equation, L/D. Of course, L/D is more importantly influenced by other factors that are discussed in paper 4.

Shown in figure 11 is the variation of L/D with flight Mach number for currently efficient wing-body combinations. The problem is to obtain as good or better values of L/D with actual long-range configurations, with powerplants installed, and with sufficient fuselage volume to store the required quantities of fuel. That this may be difficult is better understood when one realizes that the powerplants become an increasingly large part of the total configuration with increasing speeds. Also, use of hydrogen as a fuel necessitates low-density fuselages, which are detrimental to the attainment of high values of both L/D and high values of fuel- to gross-weight ratio, the remaining term of the range equation to be considered.

REMARKS

This paper constitutes a sketch of the basic ideas to be explored in more detail by papers 2, 3, 4, and 5. The requirement of a new engine for the ultimate in manned bombers with take-off capabilities will be considered. The requirement of a new technology for the hypersonic ramjet missile will also be considered. Here, is invisioned a "cooled" missile

[redacted]

with all surfaces glowing red hot; a missile that contains hydrogen fuel in both a cold liquid and a hot gaseous form. As imposing as the attendant problems may seem, they certainly lie ahead if the ultimate capabilities of the type of weapon are to be realized.

[redacted]

ULTIMATE AIR BREATHING ENGINES REQUIREMENTS

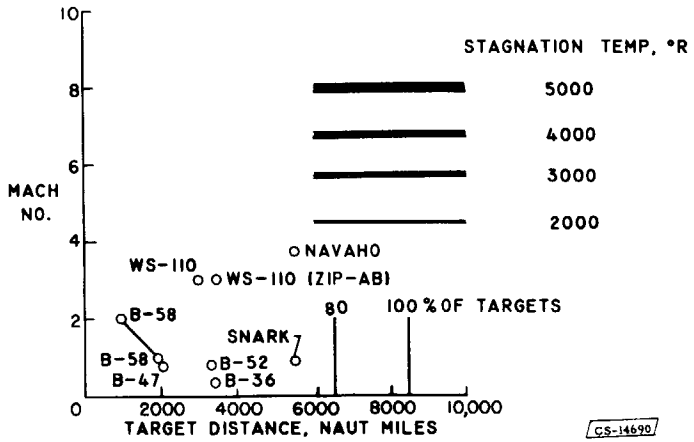

Figure 1

COOLING IS REQUIRED

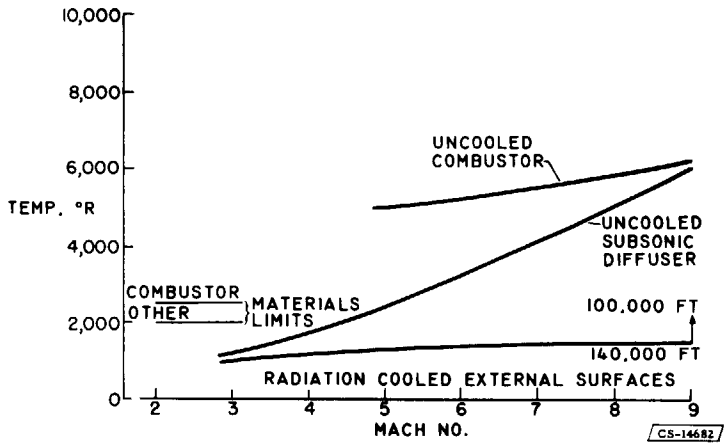

Figure 2

FUELS AS COOLANTS

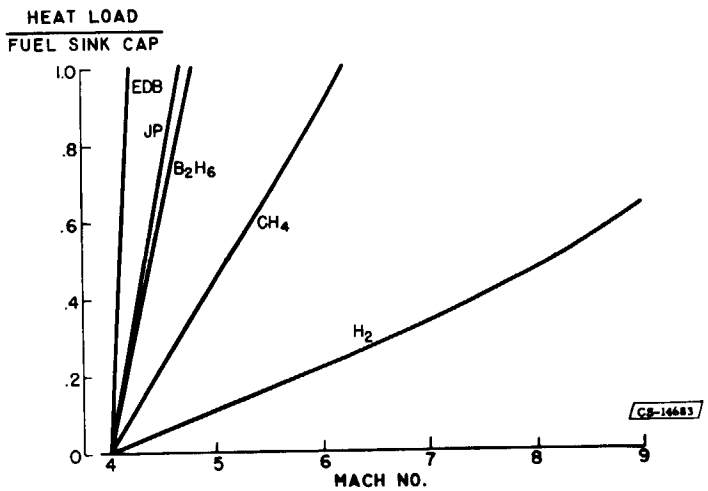

Figure 3

RANGE CONSIDERATIONS

$$\text{RANGE} = IV\frac{L/D}{1-(V/V_s)^2}\ln\frac{1}{1-W_f/W_G}$$

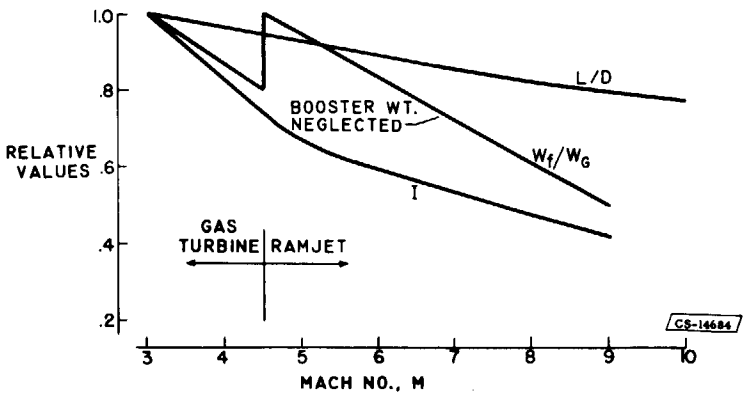

Figure 4

SELF-BOOST PENALIZES HIGH-SPEED PERFORMANCE

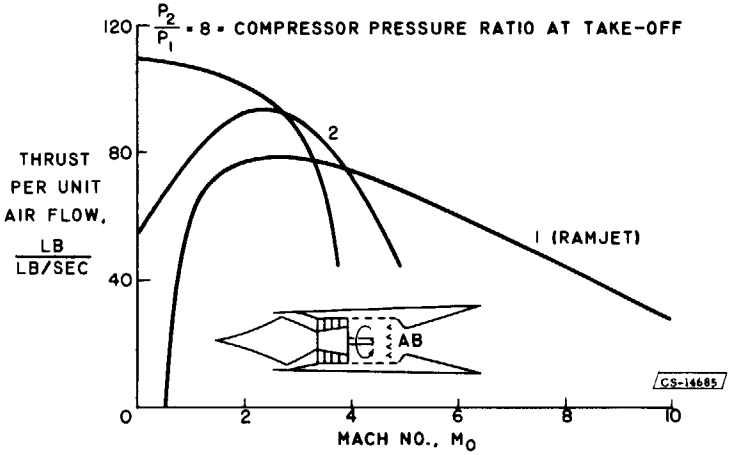

Figure 5

TURBINE ENGINES HAVE MATCHING PROBLEMS

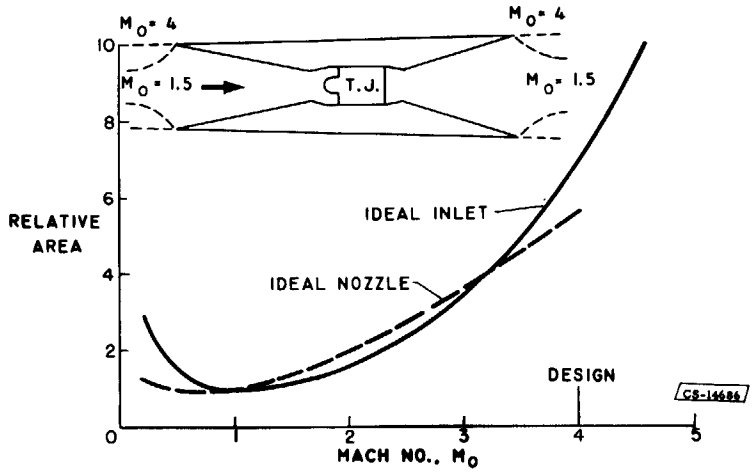

Figure 6

FUEL HEATING VALUES

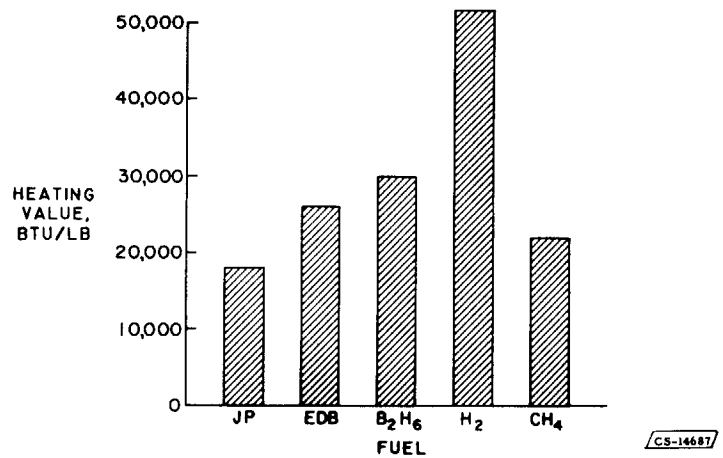

Figure 7

DISSOCIATION LOSES THRUST

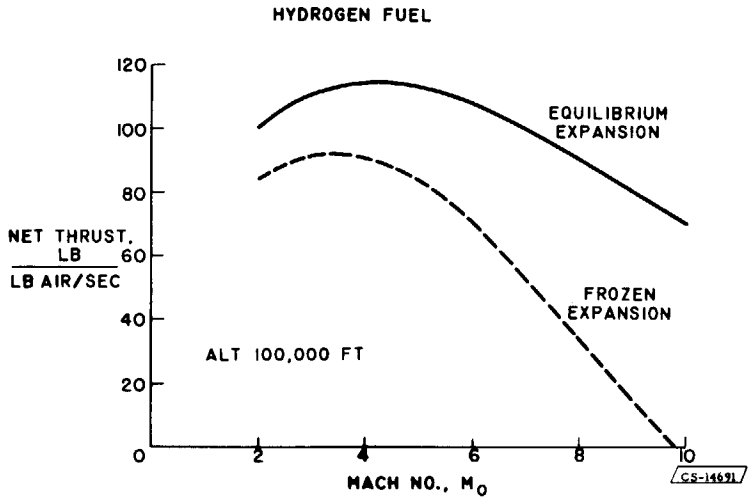

Figure 8

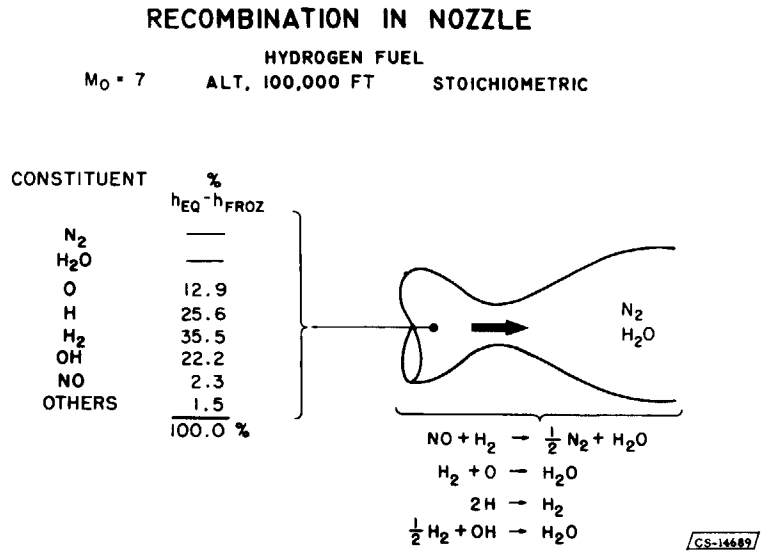

Figure 9

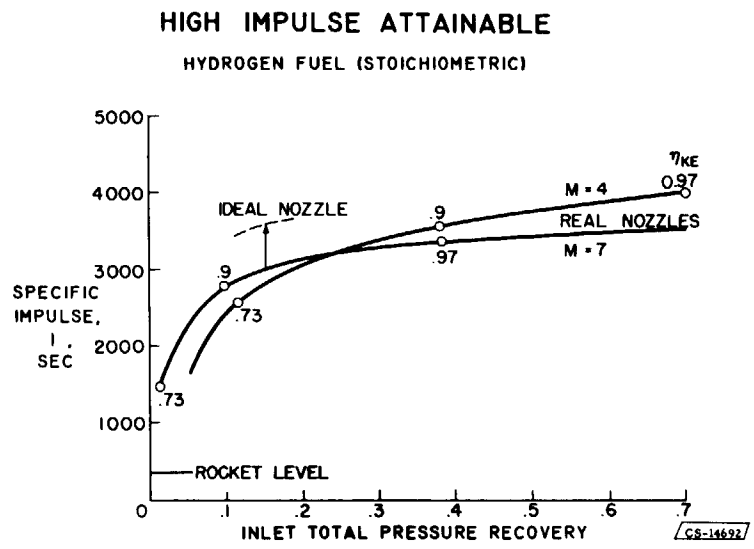

Figure 10

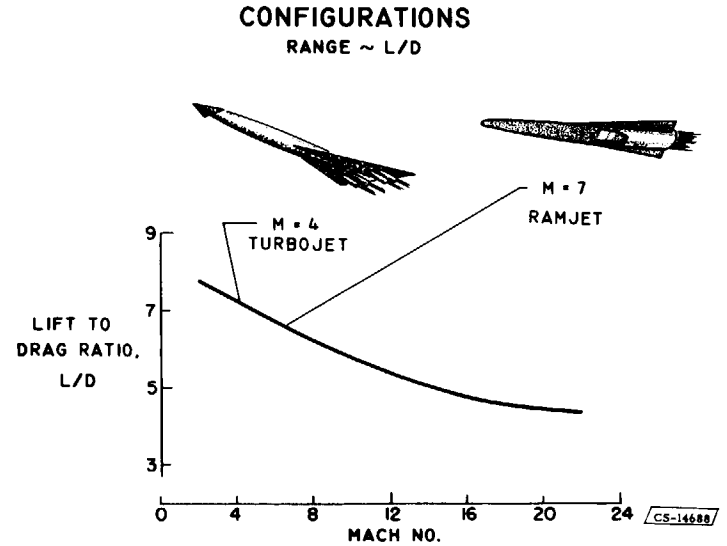

Figure 11

2. INLETS, EXITS, AND COOLING PROBLEMS

I. - INLETS

By James F. Connors and John L. Allen

Introduction

As design flight speeds are pushed progressively higher, the supersonic inlet becomes an increasingly important component of air-breathing propulsion systems. Currently, the turbojet engine is being considered for application at Mach numbers up to approximately 4 and the ramjet engine for application in the hypersonic region, or Mach numbers of 5 and above. Herein the inlet situation is surveyed and the merits of the various inlet-design philosophies are assessed on the basis of recent experimental data obtained at Mach numbers up to 5. These trends are then extrapolated into the hypersonic range for an analysis of the performance potentialities of the various ramjet-inlet configurations.

General Inlet Discussion

The three basic types of compression system that will be considered are illustrated in figure 1. These schemes shall be referred to according to their mode of compressing the flow, i.e., external or internal compression relative to the cowl lip. External supersonic compression is accomplished outside the cowl by turning the flow in one direction, radially outward by means of a protruding ramp or spike. The internal-compression scheme, on the other hand, accomplishes all the compression inside the cowl and is capable of high performance, provided that the characteristic starting problem can be handled. In order to start a highly contracted supersonic inlet, complexity must be added in the form of variable geometry, because the contraction ratio between the entrance and the throat must be decreased drastically before supersonic flow can be established within the inlet. The lower sketch in figure 1 shows a system utilizing both external and internal compression. This scheme has a similar starting problem as the all-internal-compression configuration, although to a somewhat lesser degree.

In order to demonstrate graphically this starting problem, which is characteristic of any inlet employing large internal contraction and, secondly, to illustrate the shock-boundary-layer interactions that occur within the inlet duct, selected frames of a motion-picture sequence of a two-dimensional, external-plus-internal compression inlet at Mach 3.05

are shown in figure 2. This configuration was similar to that schematically represented in the lower sketch of figure 1, but had a variable bypass door ahead of the throat to permit starting. Rectangular glass sideplates were installed on the model to allow schlieren observations of the flow inside the inlet. Figure 2 illustrates one complete cycle of the starting procedure, which must be repeated each time the terminal shock is expelled. Note the extensive separation occurring in the vicinity of the terminal shock system (fig. 2(d)) during supercritical operation. The point of incipient separation moves forward towards the throat as the back pressure is increased until critical operation (fig. 2(e)) is attained. These observations accentuate the need for boundary-layer control in the high-Mach-number inlets.

The geometry and performance variations obtained for these various compression systems will now be considered in detail. With respect to the inlet, the two parameters that best describe over-all performance are total-pressure recovery and external drag. This drag, of course, can consist of cowl-pressure drag, additive or spillage drag due to flow deflection ahead of the cowl lip, and bleed drag due to flow being removed internally for boundary-layer control and then being returned to the free stream. Obviously, at any given Mach number, a good inlet would be one having both high recovery and low drag.

In figure 3, the interrelation between recovery and drag is examined for various flight Mach numbers. As determined in reference 1, the ordinate indicates the increase in drag coefficient (based on the captured free-stream tube area) that can be tolerated for a unit increase in pressure recovery in order to maintain a constant range. This is referred to as a range "break-even" condition. At low Mach numbers, a large increase in drag coefficient is permissible for a given increase in recovery. At high Mach numbers, only a small increase in drag coefficient is tolerable for the same increment in recovery. For example, this difference between Mach 2.0 and 5.0 is a factor of 5 to 1. Thus, there is an increasing sensitivity to drag coefficient with increasing flight speeds.

External-compression inlets. - Historically, large amounts of experimental performance data have been obtained on the various types of external-compression inlet. Attention here (fig. 4) is on the most refined form of external compression, that is, an inlet utilizing a continuously contoured isentropic-compression surface. This inlet attains the highest level of recovery for all-external compression, but it also has a theoretical limit (ref. 2) based upon flow conditions at the compression-fan focus point. This limit on maximum compressive turning is determined by the requirements of a pressure balance and equal flow direction across the vortex sheet emanating from and immediately downstream of the focal point.

Generally, peak recovery is attained when the cowl lip is alined with the local flow behind the compression fan. This results in an inclined lip and, hence, drag. Thus, with increased turning, both recovery and drag would increase. In practice, compromises are usually made wherein an internal shock off the cowl is taken in order to reduce the cowl-lip angle.

Boundary-layer control was provided through a ram scoop located in the throat. This is schematically represented by the sketch inserted in figure 4. Significant performance gains are to be had with this type of bleed (see ref. 3 for two-cone-inlet results).

The inlet shown in the lower part of figure 4 was designed specifically for high Mach number application ($M > 4.0$). In this case, the cowl-lip drag has been eliminated by sacrificing some potential recovery by limiting the amount of external compression. This limit was determined by the requirements for shock attachment on a cylindrical cowl. At these high design speeds, the subsonic entrance Mach number was low enough to permit the use of an abrupt area discontinuity, or subsonic dump, without large loss in recovery. In fact, at Mach 4.0, the calculated turning loss for a cylindrical cowl with a constant-area throat section (as discussed in ref. 4) is about the same order of magnitude as this dumping loss which is based on a recovery of only the static pressure behind the normal shock.

Boundary-layer control through a rearward-facing flush slot is provided in the throat to handle any pressure feedback originating downstream thereof. The short-length, light-weight possibilities of this arrangement are obvious.

The theoretical recovery limits for these external-compression inlets are shown for a wide range of Mach numbers in figure 5. Reference lines of constant kinetic-energy efficiency are also included. In the turbojet range of application, the theoretical limit for maximum turning is quite high and has decreased from 0.99 at Mach 2.0 to 0.68 at Mach 4.0. In the ramjet range, where kinetic-energy efficiency can be used as a guide, recovery levels corresponding to efficiencies of approximately 95 percent can be attained up to Mach 7.0. For the zero-cowl-drag, limited-compression case, kinetic-energy efficiencies of about 92 percent can be achieved. For this case, dumping losses have been taken into account. The corresponding recoveries are based on a recovery of only the static pressure behind the normal shock, or a full loss of the subsonic dynamic pressure.

Internal-compression inlets. - Cowl-lip drags can be eliminated by using an internal-compression system which, furthermore, does not appear to have any theoretical limits on recovery. Two axisymmetric versions of this system are shown in figure 6. The upper sketch illustrates a

configuration without any centerbody, which simply is a convergent-divergent diffuser with small included angles (approximately 8°). This inlet is quite long, 2 to 4 inlet diameters in the supersonic portion alone. This length is dictated by the necessity of maintaining small pressure gradients on the boundary layer in order to avoid separation difficulties. For starting, a large throat bypass is provided. After starting has been accomplished, boundary-layer bleed around the throat periphery and some constant-area section are generally needed for shock stabilization.

The lower sketch shows an internal-compression inlet that utilizes a small angle centerbody which can be translated to vary the contraction ratio between the entrance and the throat. For starting, long translation distances are required, approximately 2 inlet diameters. Otherwise this inlet is similar to the upper configuration in that both are long because of boundary-layer considerations and both are in need of throat bleed.

External-plus-internal-compression inlets. - The all-internal-compression inlets, thus, do not appear attractive on the basis of over-all length and spike translation requirements. In comparison, several configurations using combined external-plus-internal-compression systems look somewhat better in this respect. These configurations are illustrated in figure 7. The top sketch shows an axisymmetric version having a low-angle centerbody. A cylindrical cowl is used with the lip located back on the initial conical shock. Internal compression is accomplished by a number of reflecting shocks in the gradually convergent passage ahead of the throat. With this inlet, the spike translation requirement for starting is only about half of that for the corresponding all-internal-compression scheme, shown previously in figure 6. The over-all length of this inlet is still quite large.

In the center sketch of figure 7, another axisymmetric version of the combined external-plus-internal-compression system is shown. This inlet has a larger angle centerbody (e.g., a 20° half-angle cone at Mach 3.0 was used in ref. 5) than the top arrangement and accomplishes the internal compression of the flow through a system of shocks, generated by the internal cowl surface and focused on the sharp shoulder of the centerbody. Boundary-layer bleed is provided in the form of a flush slot ahead of the throat. In this case, the starting translation requirements for the centerbody are only a fraction of that required by the top inlet. The over-all length of this configuration is also much less than that of the top inlet.

In the bottom sketch of figure 7, a two-dimensional version of an external-plus-internal compression inlet is illustrated. This configuration was used in the motion-picture sequence of figure 2. Briefly, isentropic

contoured ramps are used to generate both external and internal focused compression with a low drag cowl. A small variable bypass door is provided ahead of the throat to cope with the starting problem. This bypass is a relatively small component of the over-all inlet system and, compared with translation or rotation of major compression surfaces, should be mechanically much simpler and faster. In the flush or design position of the bypass door, a small gap is left for boundary-layer bleed.

Experimental results. - Detailed performance data obtained with these various inlet geometries in recent experimental investigations are given in table I. Peak performance levels are indicated for each type. These experimental results will serve as the basis for trends and conclusions to be drawn in the subsequent discussion.

Experimental pressure-recovery levels obtained with the various inlet systems are indicated in figure 8. Bands of recovery against Mach number are presented and identified only by the basic type of compression system. The all-internal-compression systems attained the highest recovery levels corresponding to kinetic-energy efficiencies greater than 0.97 with zero cowl-lip drags. However, with the attainment of these exceptionally high recoveries, there was an attendant large bleed requirement; e.g., 30 and 25 percent of the air entering the cowl had to be removed at Mach 3 and 5, respectively. When attempts were made to reduce this bleed at Mach 5, the recovery correspondingly decreased. At this particular Mach number, a 6 percent bleed requirement existed at the lower boundary and the recovery was down to 0.41. The rest of the inlets all had moderate bleed requirements (less than 10 percent of the inlet mass flow). Of the three systems, the external-compression inlets showed the lowest levels of peak performance. The maximum-turning case, however, still attained kinetic-energy-efficiency levels of 97 percent at Mach 2 and 95 percent at Mach 4. The cylindrical-cowl version indicated kinetic-energy efficiencies of 90 to 92 percent at Mach numbers from 4 to 5.

Turbojet Inlet Considerations

So far, the discussion has dealt only with the general inlet problem of attaining high pressure recovery with low external drag. In the application of these various geometries to the high-Mach-number turbojet, additional inlet operating problems such as the following arise: (1) subcritical operation, (2) angle-of-attack effect, (3) diffuser exit flow distortion, and (4) engine matching. With the high-recovery inlets there is no stable subcritical operating range at design speeds. The high-performance external-compression inlets encounter "buzz" or shock instability, whereas the other types with large internal contraction suffer large performance penalties due to expelled-shock operation. All axisymmetric inlets with high recovery capability are sensitive to

angle of attack with rather severe losses occurring at angles of 5° or more. However, the inlets may be sheltered from angle-of-attack effects by favorable environmental locations on the airplane configuration, such as under the wing or under a flat-bottom fuselage. This is discussed in paper 4 on Configuration Considerations. Design criteria for maintaining low distortion levels (refs. 6 and 7) have been established for Mach numbers up to 3 or 4. At the higher speeds, inlet data per se are generally lacking. Some consideration will now be given to the primary problem of matching an inlet to the high-Mach-number turbojet.

Engine matching. - The off-design matching requirements for the handling of excess inlet airflow are shown in figure 9 for a hypothetical Mach 4 turbojet engine operating with an assumed recovery schedule. Typically, large quantities of air must be diverted from the engine at the low Mach numbers; e.g., at Mach 2.0, as much as 70 percent of the possible inlet airflow must be spilled in some manner. This is entirely a function of the particular engine airflow schedule and is independent of any additional boundary-layer bleed requirements. The efficiency of handling such excess air can be vitally important to the over-all powerplant performance at off-design speeds.

The associated drag penalties in percentage of net engine thrust for the various methods of handling this excess air are shown in figure 10. The additive or spillage drags attendant with diverting flow around the cowl by means of a bow shock or an oblique shock generated by a 30°-half-angle cone result in clearly prohibitive drag penalties. These values bracket those resulting from inlets having large-angle centerbodies (as is typical of the axisymmetric external-compression inlets). If the corresponding spillage were achieved through an oblique shock generated by a 15°-half-angle cone, the drags would be quite low. This would be the type of spillage achieved by the axisymmetric low-angle-centerbody external-plus-internal-compression inlet. Two-dimensional external-compression inlets, of course, may achieve low drags by reducing ramp angle at the lower speeds.

The drags associated with taking the excess inlet air aboard and then returning it to the free stream by means of a bypass ahead of the compressor face are also shown in figure 10 for the conditions of sonic and full-expansion discharge. A thrust coefficient of 0.9, which corresponds to about a 15° discharge angle, was assumed in the calculation. Both bypass drags are somewhat higher than the oblique shock values for a 15°-half-angle cone.

Other possibilities for handling excess airflows (which will not be considered here) include bypassing the excess air around the engine and using it in the base area, in the overexpanded portion of the exhaust nozzle, or even in conjunction with heat addition in the bypass duct for thrust augmentation (as in the turbofan engine).

Inlet comparisons. - The design-point characteristics of the various inlet systems for the Mach 4.0 turbojet application are summarized in table II. The three basic inlet types (i.e., external, internal, and combined external-plus-internal compression systems) are compared on the basis of factors that would influence the selection of a particular geometry. Weak points in the argument for any inlet type are indicated by shaded areas within the table. The total-pressure recovery at Mach 4.0, as shown previously in figure 8, was highest for the all-internal-compression system with a maximum of 0.75, corresponding to a kinetic-energy efficiency of approximately 97 percent. The lowest recovery was realized with the external-compression scheme, which shows a maximum of 0.60, or a kinetic-energy efficiency of 95 percent. Cowl-lip drag, of course, was only a problem for the maximum-turning version of the external-compression inlet. This can be a big penalty; for example, at Mach 3, cowl-lip drag alone amounted to 10 to 12 percent of engine thrust. Variable-geometry requirements for starting are large for the all-internal-compression scheme and somewhat less for the combined compression system. Boundary-layer bleed requirements were moderate for all except the all-internal-compression inlet. In this case, in order to achieve its exceptionally high recoveries, there was an attendant large bleed requirement (25 to 30 percent of the maximum possible inlet airflow), which is far in excess of any airflow needed for secondary engine systems. If it were assumed that this quantity of bleed air were returned to the free stream by means of a bypass ahead of the compressor, even with a complete-expansion bypass nozzle, the resulting drag at Mach 4.0 would be about 10 percent of net engine thrust. The over-all length of the all-internal-compression system is also higher than that of the other systems.

Based on these qualitative results, the inlet that appears best suited for the Mach 4.0 turbojet application is the combined external-plus-internal-compression inlet. The all-external system is eliminated because of its large cowl-lip drags, while the all-internal system is penalized because of its large variable-geometry and boundary-layer bleed requirements, and its high over-all length. The combined compression system offers the best compromise for the Mach 4.0 turbojet.

Hypersonic Ramjet Inlet Considerations

The attainment of good off-design performance for a hypersonic ramjet engine is even more difficult than that for a turbojet engine primarily because of the larger inlet- and exit-area variations required with the high design flight Mach numbers. This was shown in paper 1. The associated variable geometry requirements are formidable problems because of the extreme temperatures.

If the engine is designed for good range at cruise, the excess thrust at below-design speeds is generally small. If the cruise engine is

compromised in order to increase the excess thrust during self-acceleration, the penalties at the cruise condition are large. An alternate approach, for some applications might be to use an expendable engine for the boost phase. This problem is beyond the scope of this study and, hence, only inlets for on-design ramjet engines will be discussed.

Effect of flight Mach number on ramjet thrust and drag coefficients. - The variation of design-point thrust and nacelle drag coefficients (based on capture area) for Mach 5 to 7 is shown in figure 11. For this and subsequent figures, the cycle calculations are for real gas properties for stoichiometric combustion of hydrogen. The exhaust pressure was 2.5 times the ambient pressure and the velocity coefficient was 0.97, which is defined as the ratio of the axial exit velocity to the ideal velocity for the stated exit pressure. Thrust coefficients are shown for inlet kinetic-energy efficiencies of 97 percent, which might be obtained with a high-pressure-recovery all-internal-contraction inlet, 90 percent, which is obtainable with external compression inlets, and 72 percent, which approximates normal-shock-inlet performance. The assigned boundary-layer-bleed requirements of 20 percent for the high-efficiency inlet and 10 percent for the 90 percent kinetic-energy efficiency were optimistically extrapolated from lower Mach number experimental data. The normal-shock inlet requires no bleed and, hence, the total drag for the engine is composed of friction and wave or external pressure drag as shown by the shaded region of figure 11. Wave drag was calculated by the method of reference 8 and friction drag for radiation equilibrium temperature by means of reference 9. (Blunt-lip drag has not been considered but should be relatively small and not affect the relative comparison.) The friction and wave drag for the high-efficiency engine is of similar magnitude. However, the drag associated with discharging boundary-layer bleed air can be from 2 to 4 times the sum of the friction and wave drag, depending on whether a sonic or completely expanded exhaust is used. The thrust coefficient decreases with increasing Mach number while the drag coefficient remains nearly constant. Thus, drag becomes relatively more important at higher Mach numbers. The difference between the thrust and drag coefficients, or thrust minus drag, which must be equal to the drag coefficient of the remainder of the missile, decreases not only with increasing Mach number but also with decreasing kinetic-energy efficiency, particularly for efficiencies less than 90 percent. Thus, the required engine size would depend on the inlet-kinetic-energy efficiency.

Effect of inlet type. - Some of the interacting effects, such as level of pressure recovery, various drags, size, and weight, can be illustrated by designing engines with different types of inlet to provide equal thrust minus drag. A pictorial comparison is shown in figure 12 for Mach 7.0 and an altitude of 100,000 feet. The same "ground rules" such as nozzle and diffuser angles were used for all the engines. The combustor length was constant and the engines are illustrated with combustors alined.

Bleed-air passages are shown schematically, although the calculations were for full expansion with a nozzle coefficient of 0.9 at a constant bleed-air total temperature equal to free-stream stagnation temperature.

Engines having all-internal-compression inlets are shown for a probably unrealistic recovery of 0.50 and for a recovery of 0.15. Both inlets had 10°-included-angle compression surfaces and were of approximately equal length. Although the high-recovery inlet has the greater compression, the normal shock occurs at a Mach number of about 2.4 compared with a Mach number of 3.6 for the 0.15-recovery inlet. Because of these contra-acting effects and the absence of experimental data, it was assumed that the boundary-layer bleed would be 20 percent of the capture flow for both inlets.

Two engines having external-compression isentropic spike inlets with a boundary-layer bleed requirement of 10 percent are shown. An inclined cowl lip having an area of 10 percent of the capture area was required for the 0.25 pressure recovery. The 0.10-pressure-recovery inlet had limited compression, zero cowl-lip drag, and a dump diffuser. A normal-shock engine is shown for comparison.

The relative sizes of the engines primarily reflect the effect of pressure recovery or kinetic-energy efficiency on internal-thrust coefficient. Since the requirement was for equal net thrust, or thrust minus drag, the various drag components also influence the size and will be discussed later.

Also shown on figure 12 are preliminary values of engine-to-missile gross-weight ratio. These values are for the primary structure and include regenerative cooling of the internal surfaces. In regions where the fuel pressure would not cause local buckling, a corrugated-type material was used. In regions where fuel pressure was high compared with air pressure, such as the inlet and nozzle, a circumferential, wrapped tube construction (similar to some rocket-engine nozzles) was used. A 0.05-inch thickness of zirconia was assumed for the combustor and a 0.035-inch thickness for the remainder of the internal areas. The coating surface temperatures were the same as those used in part III of this paper. A tensile-stress level of about 18,000 pounds per square inch was used for Inconel X. In the interest of minimizing thermal-stress gradients, the outer skin was assumed to be supported only at the cowl lip and the nozzle exit. The mount for the engine was attached to the external skin, which was stressed for an engine weight of 3 g's. No allowance was made for controls, fuel pumps, manifolding, or variable geometry where needed.

The weight ratio was influenced by both inlet type and pressure recovery. For example, the change in weight ratio for the engines having all-internal-compression inlets is primarily due to the nearly 3 to 1

ratio of internal pressures (30 atm against 9 atm) since the sizes of the engines are about equal. In contrast, the normal-shock engine, which had a low internal pressure (0.6 atm), was very large and had the second highest weight ratio.

The engine with the 0.25-recovery isentropic spike had the highest weight ratio primarily because of the high load on the base of the spike and the structure needed to hold the spike. It should be emphasized, however, that the weight factors neglected in this analysis would very likely result in heavier weights for the all-internal-compression engines because of the inherently needed variable geometry. In addition, more powerful fuel pumps would be required to raise the injection pressure above the internal pressure and, hence, the weight of this item would be a function of both discharge pressure and flow rate.

A breakdown of the various drag components as a ratio of drag to net thrust for these engines is shown in the lower portion of figure 13. Here, the engines are arranged according to pressure recovery. For the normal-shock engine, friction was about 70 percent of the total drag because of the large surface area; the remainder of the drag was wave or external pressure drag. The largest portion of the drag for the other engines was that due to bleed or cowl-lip drag for the high-recovery isentropic spike engine (configuration C). The sum of cowl-lip and bleed drag is the same magnitude as the bleed drag for the all-internal-compression inlet, which was assigned the higher bleed requirement. However, both the amount of lip inclination and the length of alinement are also rather arbitrary assignments. Wave drag was not an important component except for the normal-shock engine previously mentioned.

The relative heights of the drag columns represent the engine size increase needed in order to provide equal thrust minus drag.

In the upper portion of figure 13 the range relative to that for the normal-shock engine is plotted as a function of pressure recovery for the various engines. In the basic range equation, the thrust minus drag has been used in the impulse term and the effect of engine weight has been accounted for in the logarithm term by maintaining a fixed ratio of fuel plus engine weight to missile gross weight of 0.5.

As pressure recovery is increased from the normal-shock value of 0.011, the relative range increases rapidly to a value of about 2.2 at a recovery of 0.10 or a kinetic-energy efficiency of 90 percent. The relative range does not change much for pressure recoveries up to 0.25 and then increases slowly to a value of about 2.5 at a recovery of 0.50.

In summary, inlet kinetic-energy efficiencies greater than about 90 to 95 percent result in only small increases in range for hypersonic ramjet missiles. Serious cooling and weight problems are associated with the

variable geometry necessary to establish or start supersonic flow for the all-internal-compression inlet needed to obtain higher kinetic-energy efficiencies (greater than 95 percent). Even when these factors are ignored, the increase in range over that for the simple, self-starting all-external-compression inlet is only about 15 percent.

REFERENCES

1. Weber, Richard J., and Luidens, Roger W.: A Simplified Method for Evaluating Jet-Propulsion-System Components in Terms of Airplane Performance. NACA RM E56J26, 1956.

2. Connors, James F., and Meyer, Rudolph C.: Design Criteria for Axisymmetric and Two-Dimensional Supersonic Inlets and Exits. NACA TN 3589, 1956.

3. Connors, James F., Lovell, J. Calvin, and Wise, George A.: Effects of Internal-Area Distribution, Spike Translation, and Throat Boundary-Layer Control on Performance of Double-Cone Axisymmetric Inlet at Mach Numbers from 3.0 to 2.0. NACA RM E57F03, 1957.

4. Meyer, Rudolph C.: Flow-Turning Losses Associated with Zero-Drag External Compression Supersonic Inlets. NACA TN 4096, 1957.

5. Obery, Leonard J., and Stitt, Leonard E.: Performance of External-Internal Compression Inlet with Abrupt Internal Turning at Mach Numbers 3.0 and 2.0. NACA RM E57H07a, 1957.

6. Piercy, Thomas G.: Factors Affecting Flow Distortions Produced by Supersonic Inlets. NACA RM E55L19, 1956.

7. Sterbentz, William H.: Factors Controlling Air-Inlet Flow Distortions. NACA RM E56A30, 1956.

8. Willis, J. H., and Randall, D. G.: The Theoretical Wave Drag of Open-Nose Axisymmetrical Forebodies with Varying Fineness Ratio, Area Ratio, and Nose Angle. Tech. Note Aero. 2360, British RAE, Feb. 1955.

9. Eckert, E. R. G.: Engineering Relations for Friction and Heat Transfer to Surfaces in High Velocity Flow. Jour. Aero. Sci., vol. 22, no. 8, Aug. 1955, pp. 585-587.

INLET RESEARCH EXPERIMENTAL RESULTS

	M_0	P_3/P_0	C_D cowl (ref A_{MAX})	$\dot{m}_{BLEED}/\dot{m}_0$	$\dot{m}_{SPILLAGE}/\dot{m}_0$
1	3.01	0.81	0.10	0.05	0.06
	3.01	0.74	0.10	0.03	0.06
2	3.85	0.41	0	0.08	
	3.85	0.47	0		
	4.95	0.33	0	0.25	
	4.95	0.23	0		
3	2.97	0.88–0.91	0	0.29	0
	4.95	0.59	0	0.25	0
		0.415	0	0.06	
4	2.5	0.91	0	0.13	0
5					
6	3.01	0.78	0.01	0.02	0
7	3.05	0.79	0	0.05	0
	4.95	0.40	0		

CS-14882

Table I

INLET COMPRESSION SYSTEMS

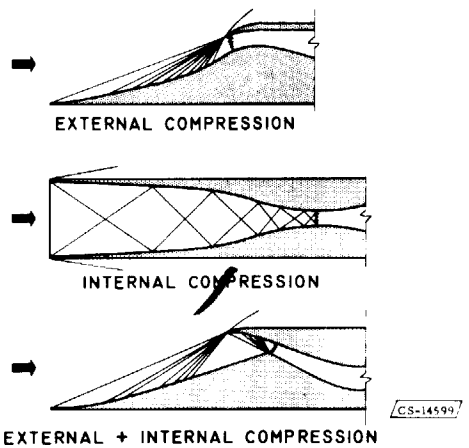

Figure 1

MACH 4.0 TURBOJET INLET CHARACTERISTICS

INLET TYPE →	EXTERNAL COMPRESSION (MAX TURNING)	INTERNAL COMPRESSION	EXTERNAL + INTERNAL COMPRESSION
RECOVERY LEVEL, M = 4	0.55–0.60	0.65–0.75	0.62–0.69
COWL-LIP DRAG	HIGH, 10 to 12% of F_N at M~3	0	0
VAR-GEOM REQUIREMENT FOR STARTING	0	LARGE	INTERMEDIATE
BLEED REQUIREMENT	0.03 to 0.05 m_0	0.25 to 0.30 m_0 at M_0 = 3 to 5	0.05 to 0.10 m_0
OVERALL LENGTH	MODERATE	LONG	MODERATE

CS-14627

Table II

STARTING AND OPERATING PROCEDURE FOR TWO-DIMENSIONAL EXTERNAL + INTERNAL-COMPRESSION INLET

M_0 = 3.05

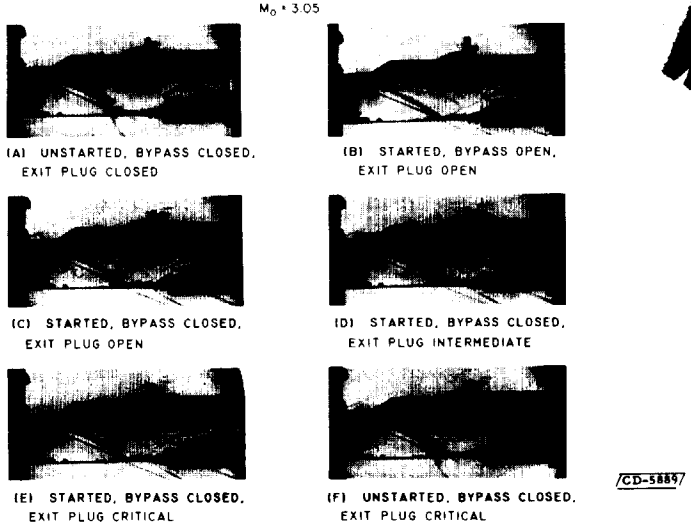

Figure 2

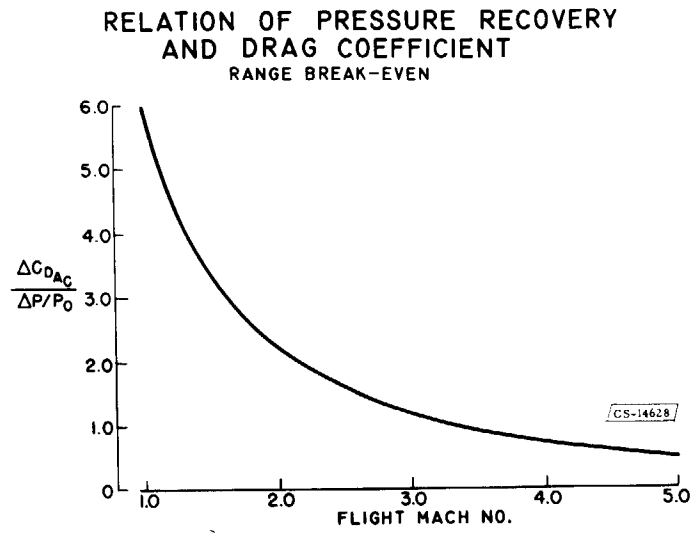

Figure 3

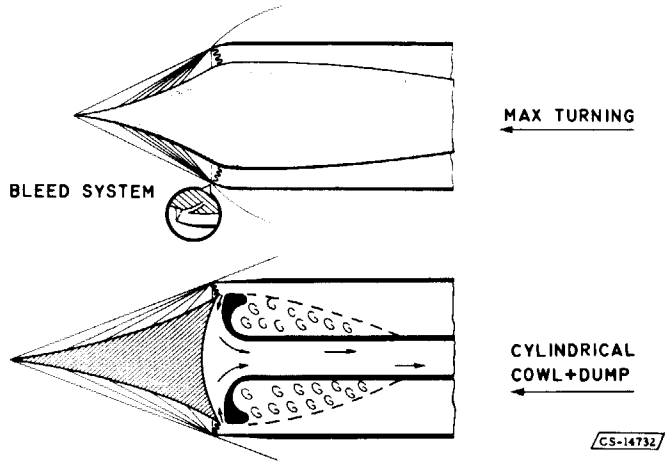

Figure 4

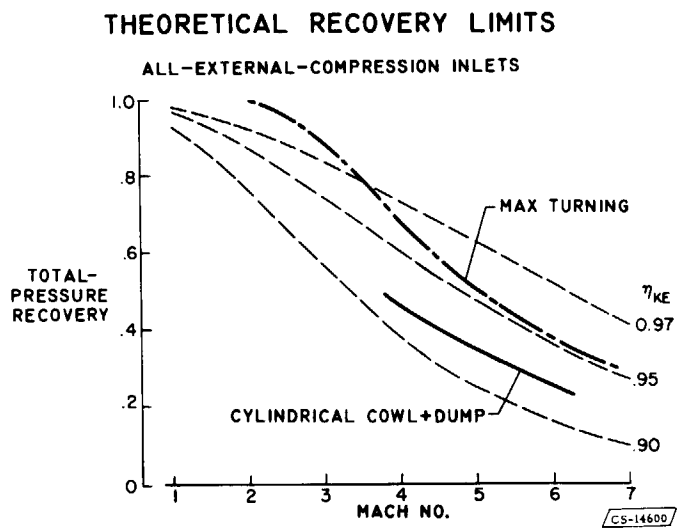

Figure 5

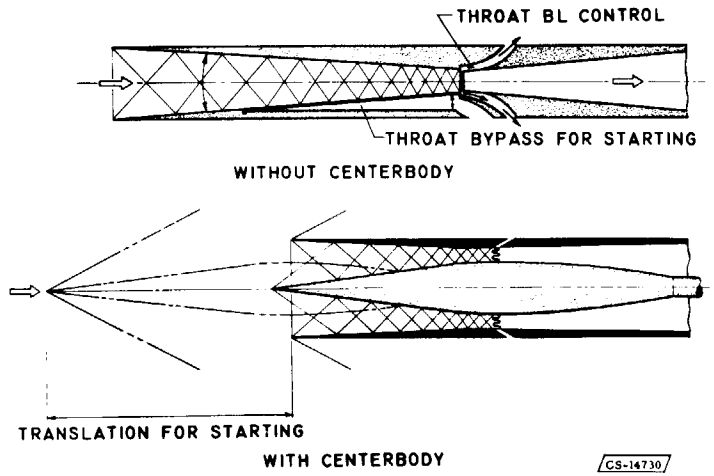

Figure 6

EXTERNAL+INTERNAL-COMPRESSION INLETS

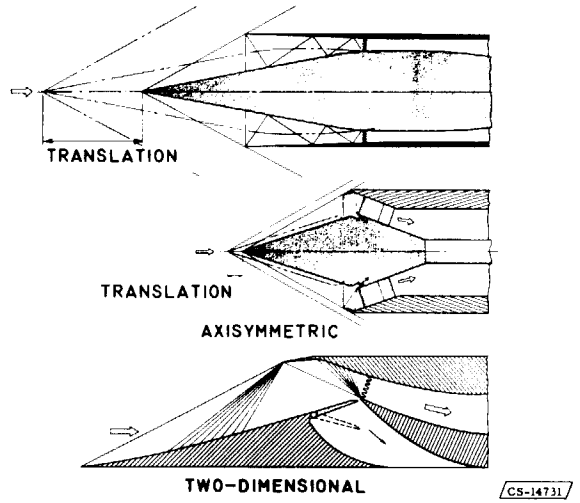

Figure 7

EXPERIMENTAL PRESSURE - RECOVERY LEVELS

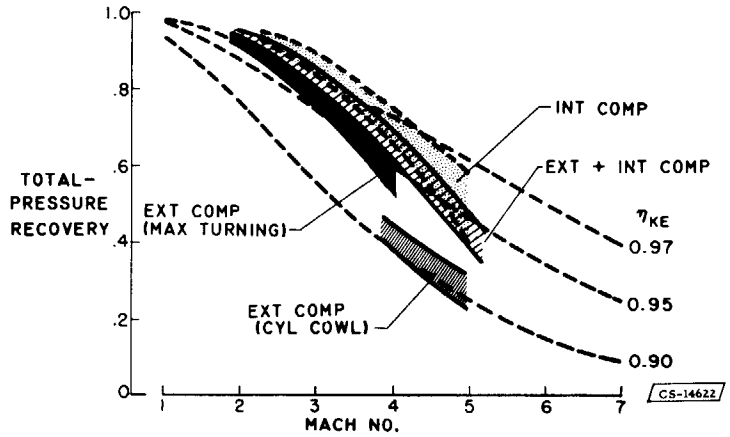

Figure 8

TURBOJET MATCHING REQUIREMENTS

M_{DESIGN} = 4.0

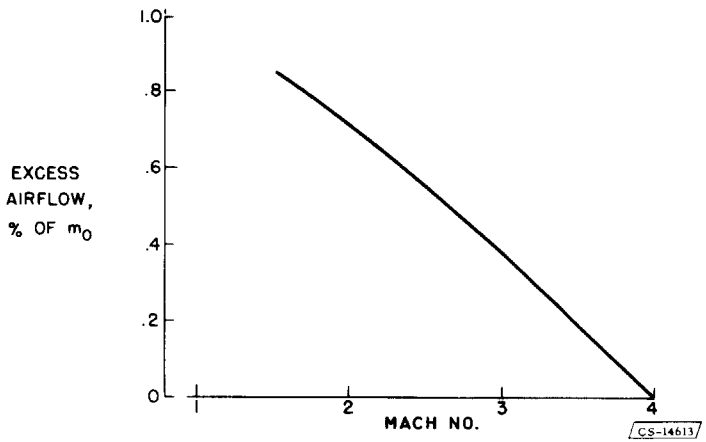

Figure 9

TURBOJET MATCHING DRAG PENALTIES

M_{DESIGN} = 4.0

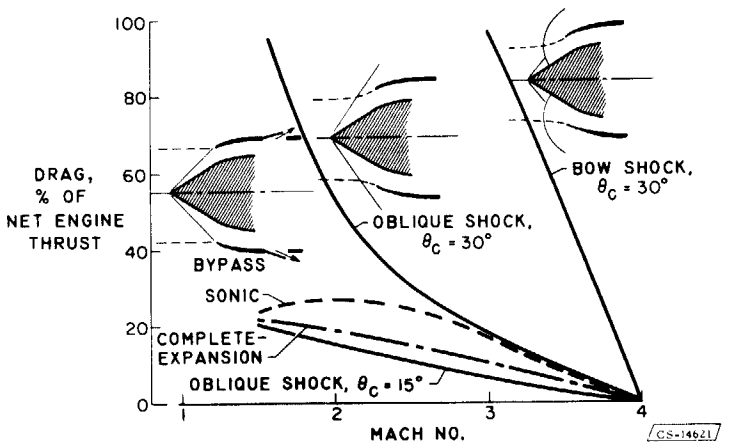

Figure 10

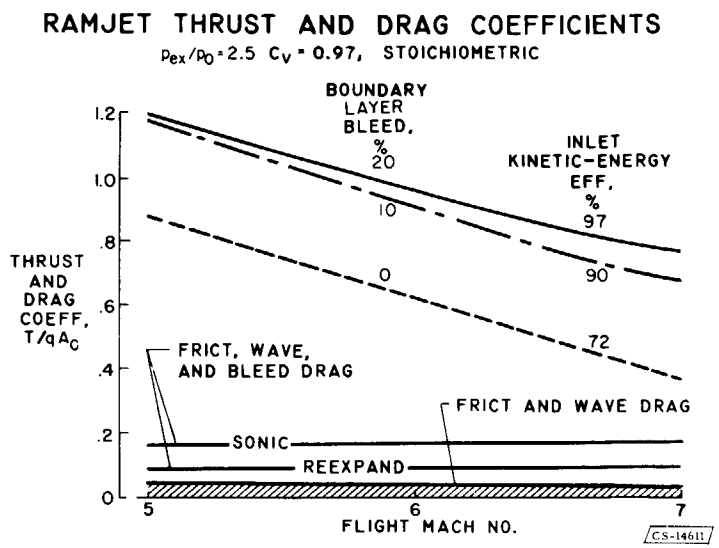

Figure 11

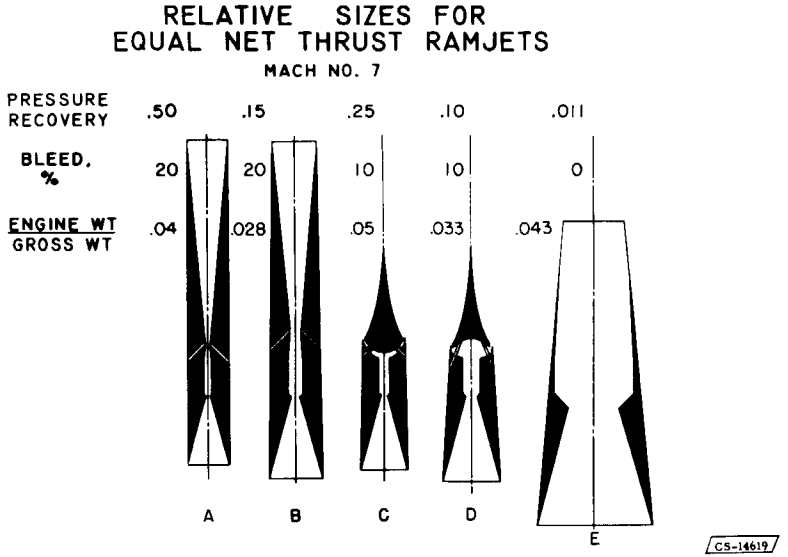

Figure 12

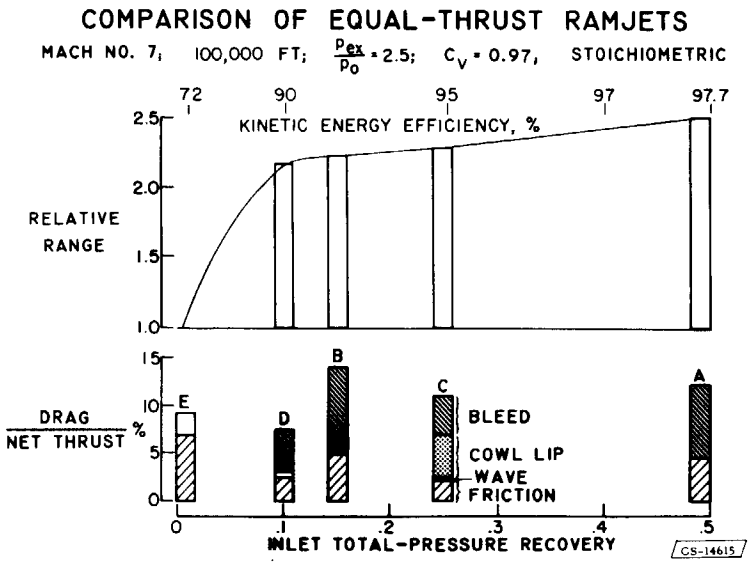

Figure 13

II. EXITS

By Fred D. Kochendorfer and Gerald W. Englert

Introduction

The exit nozzle for air-breathing engines should perform two functions. First, it should control airflow in a manner consistant with optimum engine performance. Second, it should provide optimum thrust. These requirements will be satisfied if the nozzle has the correct throat and exit areas.

If the aircraft is to operate at one flight speed only, the nozzle problem is relatively simple compared with those problems that have been discussed for the inlet. Because the static pressure decreases continually through the nozzle, the boundary layer has no tendency to separate and the flow can be essentially shock free. Nozzle thrusts within 98 percent of the ideal can be obtained without too much trouble.

If the aircraft is to operate over a range of flight speeds, however, nozzle geometry must be varied to obtain optimum performance at all speeds. For air-breathing engines, nozzle pressure ratio increases rapidly with flight speed at the higher speeds, so that, in general, large exit area variations will be required.

At the higher speeds, the problem is further aggravated because even small nozzle losses are reflected as large losses in net engine thrust. The relation between engine thrust (which includes the effect of the inlet momentum of the engine airflow) and nozzle thrust depends on inlet and engine performance and on flight plan; a typical case is shown in figure 1. The loss ratio increases rapidly with flight speed and at Mach 7, for example, a 1-percent loss in nozzle thrust results in a 4.2-percent loss in engine thrust.

This discussion studies the compromise between the mechanical complexity and weight of the variable nozzle and the performance penalties of the fixed nozzle. A Mach 4 turbojet and a Mach 7 ramjet will be considered.

[redacted]

Mach 4 Turbojet

Area variations. - Throat and exit area variations required for a typical Mach 4 turbojet engine are shown in figure 2. The curves depend on engine details and on flight plan and are used only to illustrate the magnitudes of the required area variations.

A 60-percent throat area modulation will be needed, and exit area must be changed by a factor of about 3.0 if maximum thrust is to be obtained.

Nozzle geometry. - Probably the simplest method for obtaining the required area variations is to construct both the throat and the divergent portion of overlapping leaves or flaps as shown in figure 3(a). An ejector-type nozzle is illustrated because it cools easier and has better off-design characteristics than the convergent-divergent nonejector nozzle. A third nozzle type, the plug nozzle, does, of course, give excellent off-design performance in quiescent air (ref. 1). However, reference 2 shows that in a transonic stream the jet overexpands and large thrust penalties result. Other data, as yet unpublished, obtained in the Lewis 8- by 6-foot supersonic wind tunnel show that the plug nozzle is inferior to the fixed ejector at supersonic speeds as well.

In the ejector (fig. 3(a)) secondary or cooling air is admitted between the primary flow and the shroud. Throat area is controlled by flaps. Exit area is controlled by shroud flaps that must be quite long if the exit angles are to be small. If base area is to be avoided, flaps must also be provided for the outer skin and these outer flaps must also be quite long if boattail angles are to be small.

Another possibility for the outer skin is illustrated in figure 3(b). From the inlet discussion (Part 1, INLETS), it will be recalled that excess air is available at speeds below design. If all or part of this air can be ducted aft, it can be used to fill the base area as indicated for the Mach 2 position. The outer skin can be left fixed.

The question to be considered, then, is whether or not the thrust advantage of the variable nozzle will warrant the mechanical complexity and weight of the required flaps, actuators, and controls.

Fixed nozzle thrust. - Nozzle thrust coefficient is shown as a function of flight Mach number for several fixed nozzles in figure 4. Also shown for reference is the variable nozzle.

The dashed curves represent the calculated performance of fixed nonejector nozzles designed for Mach 3 and Mach 4. Clearly, the nozzle designed for the maximum speed is not useable at lower speeds. The important point, however, is that by designing the nozzle for a lower than maximum Mach number large off-design thrust gains can be made. For

[redacted]

the case shown in figure 4, designing for Mach 3 gives better performance at all speeds less than Mach 3.65. The penalty at the maximum speed point is 1.5 percent in nozzle thrust.

It can be seen, however, that designing a nozzle for a lower speed is not a complete solution to the problem; at transonic speeds, thrust losses still reach 30 percent. The ejector nozzle designed for Mach 3 (solid curves) is clearly superior to the nonejector at all Mach numbers below approximately 2.5. The lower portion of the ejector curves represents performance with 2-percent secondary flow; the upper represents the optimum. The data points are from recent tests in the Lewis 8- by 6-foot wind tunnel.

Shroud pressures. - The best way to explain the improved performance of the ejector is to consider in some detail conditions in the divergent portion of these nozzles at one of the lower-speed points. Conditions at Mach 1.5 are shown in figure 5.

For the nonejector, shroud pressures were calculated from trailing and nozzle shock-pressure-rise data (refs. 3 and 4). Shroud pressures fall far below the ambient pressure p_0. This results from two factors:

(1) The stream and the separated jet aspirate the separated region to a pressure of 0.5 p_0.

(2) The nozzle expands the flow to a pressure below that of the separated region. The pressure just upstream of the nozzle shock is 0.3 p_0.

The large thrust losses of figure 4 reflect these low pressures. Actually, the nonejector thrust at Mach 1.5 is essentially that which would result from a calculation assuming the flow to be completely overexpanded.

For the ejector with 2-percent secondary flow, the pressure measured at the shroud exit was 0.6 p_0 (indicated in fig. 5). Furthermore, this was the lowest pressure within the shroud. The amount of overexpansion is less than for the nonejector, because the low-energy secondary flow cannot sustain a large shock-pressure rise.

If the secondary flow is increased and additional low-energy air is bled in through perforations, as indicated in the lower part of figure 5, shroud pressures will get even higher. However, since there is an inlet momentum charge for the additional air, an optimum will exist.

With optimum secondary flow, the thrust penalty for using a fixed nozzle reaches 11 percent at Mach 1 (fig. 4). For a true comparison, however, an additional factor should be considered. In order to produce

good thrust at the lower speeds, the variable nozzle must be closed. As a result, even with long outer flaps the variable nozzle will have larger boattail angles than the fixed nozzle (fig. 3(a)) and, hence, higher drags.

The fixed and variable nozzles are compared on a thrust-minus-drag basis in figure 6. The boattail angles corresponding to the outer flap length of figure 3(a) are indicated. Because of the higher drag of the variable nozzle, the advantage of the variable nozzle on a thrust-minus-drag basis is reduced to 5.5 percent at Mach 1.

Whether or not the thrust penalties of the fixed nozzle offset the complexities and weight of the variable nozzle, will depend on factors difficult to generalize. Certainly, excess thrust for acceleration at the lower speeds and relative lengths of flight time at the various speeds will be important parameters.

Mach 7 Ramjet

Nozzle problems in the higher speed range are similar to those discussed for the Mach 4 turbojet. However, since the change in nozzle pressure ratio per unit change in flight Mach number increases with speed, the fixed nozzle will be limited to a much smaller range of flight speeds.

Nozzle thrust coefficient is shown as a function of flight Mach number for both a variable and a fixed nozzle in figure 7. Consider first the chemical equilibrium curves. The fixed nozzle is sized for conditions at Mach 4; data are from the Lewis 10- by 10-foot supersonic wind tunnel. At Mach 7, the penalty in nozzle thrust for using the fixed nozzle is 3.5 percent. This penalty is 15 percent in net engine thrust. Furthermore, the loss at Mach 2 is clearly prohibitive. Even if the losses at the lower speeds could be reduced by means of an ejector, a fixed nozzle is limited to a small range of flight speeds unless large thrust penalties are acceptable.

Another factor that can affect performance at high speeds is that cycle temperatures exceed 4000° R. At these temperatures large amounts of energy go into dissociation and excitation of the vibrational modes of the working fluid. If the expansion in the nozzle is so fast that this energy is not returned as kinetic energy, additional losses will result. The frozen expansion curve represents the result of a calculation for which the energies were assumed to be "frozen" at their high-temperature (combustor outlet) values. At Mach 7 the additional loss in nozzle thrust is 12 percent.

It was pointed out in paper 1, Introductory Concepts, that many of the important energies should reach equilibrium. However, even small nozzle losses can cause large losses in engine thrust and it is clear that additional tests are required.

Conclusions

Mach 4 turbojet. - A fixed nozzle of the ejector type provides reasonably good performance over the speed range. Whether or not penalties in nozzle thrust minus afterbody drag varying from 2 percent at Mach 4 to 5.5 percent at Mach 1 will offset the complexity and weight of a variable nozzle will depend on aircraft and flight plane details that are difficult to generalize.

Mach 7 ramjet. - At high speeds (Mach 5 and above), the thrust of a fixed nozzle falls off rapidly as speed is increased above and especially as speed is decreased below the design speed. It must therefore be concluded that, if operation over a range of speeds is necessary, the variable nozzle with its extreme mechanical and cooling difficulties must be used unless large thrust losses are acceptable.

Recombination rates within the nozzle need further investigation.

References

1. Krull, H. George, Beale, William T., and Schmiedlin, Ralph F.: Effect of Several Design Variables on Internal Performance of Convergent-Plug Exhaust Nozzles. NACA RM E56G20, 1956.

2. Salmi, R. J., and Cortright, E. M., Jr.: Effects of External Stream Flow and Afterbody Variations on the Performance of a Plug Nozzle at High Subsonic Speeds. NACA RM E56F11a, 1956.

3. Baughman, L. Eugene, and Kochendorfer, Fred D.: Jet Effects on Base Pressures of Conical Afterbodies at Mach 1.91 and 3.12. NACA RM E57E06, 1957.

4. Love, Eugene S.: Pressure Rise Associated with Shock-Induced Boundary-Layer Separation. NACA TN 3601, 1955.

ENGINE THRUST

NOZZLE THRUST COEFF ≈ E; ENGINE THRUST COEFF ≈ E - I

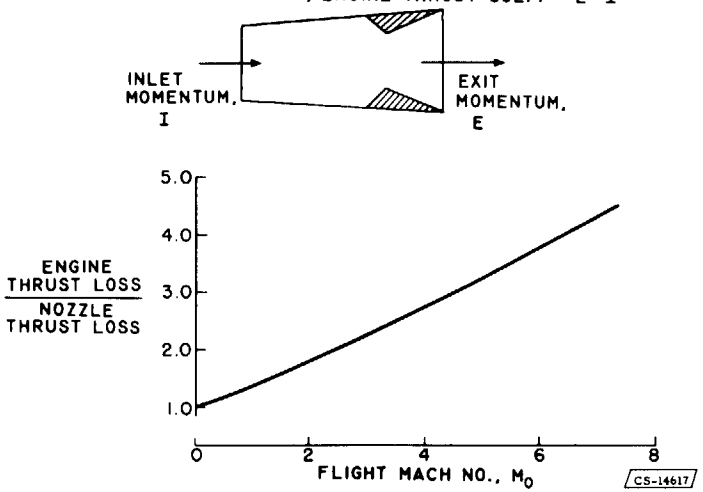

Figure 1

NOZZLE AREA REQUIREMENTS OF A TURBOJET

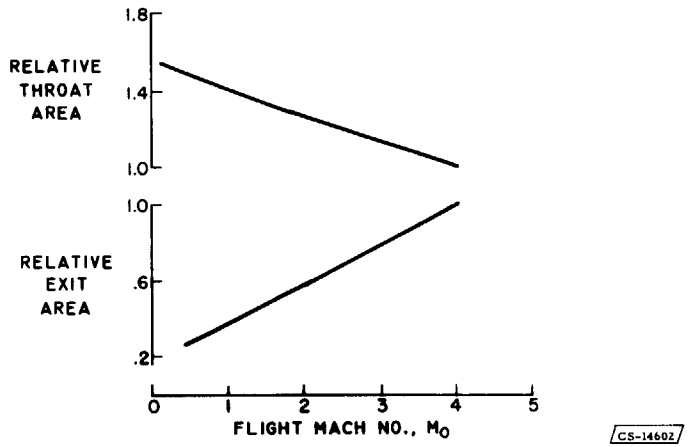

Figure 2

TYPICAL NOZZLE

MACH NO. 4 TURBOJET

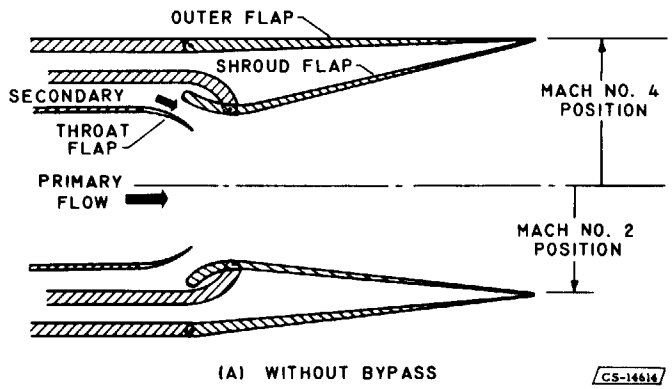

TYPICAL NOZZLE

MACH NO. 4 TURBOJET

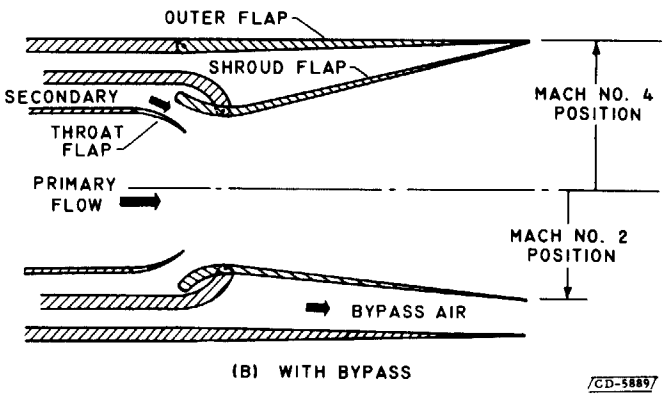

Figure 3

FIXED NOZZLE DESIGN

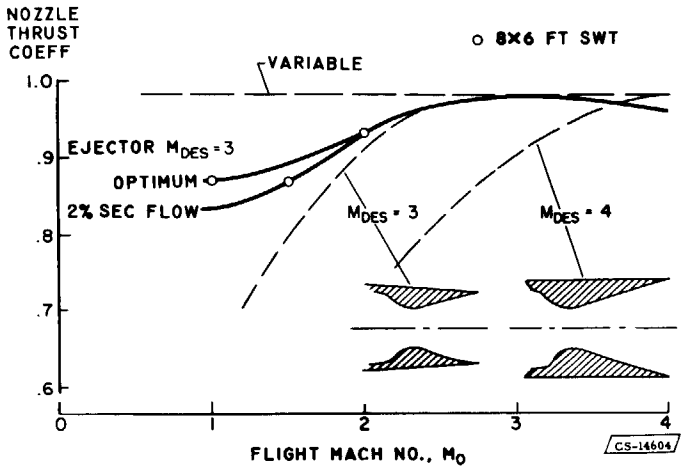

Figure 4

FIXED NOZZLE PENALTIES

MACH NO. 4 TURBOJET

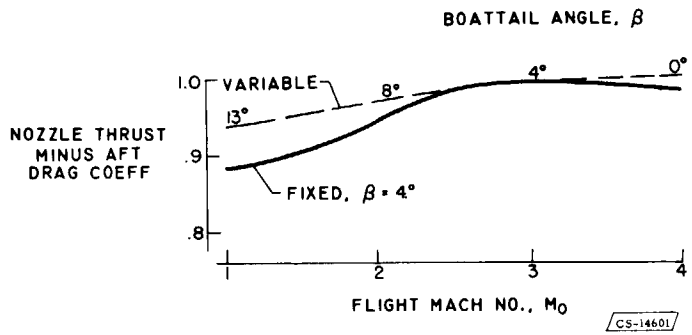

Figure 6

FIXED NOZZLES AT MACH 1.5

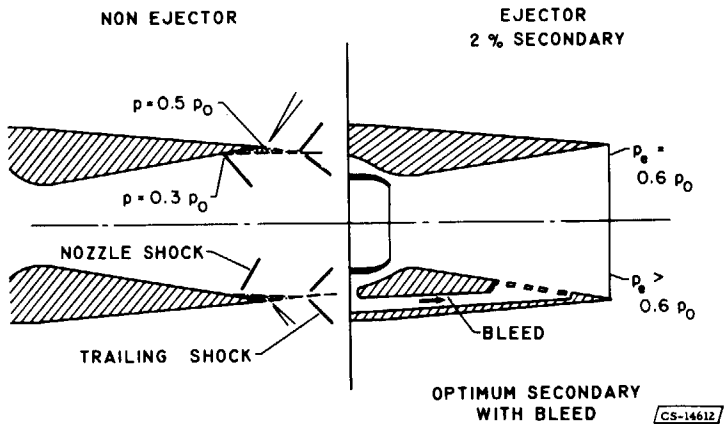

Figure 5

RAMJET NOZZLE

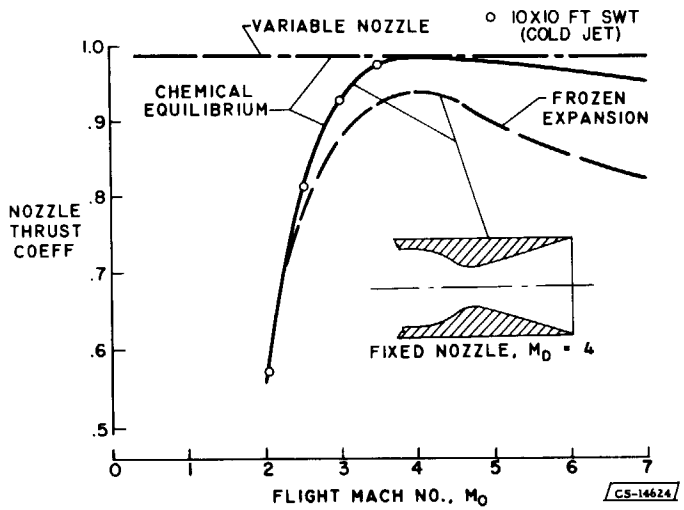

Figure 7

III. PRELIMINARY ANALYSIS OF HYPERSONIC RAMJET COOLING PROBLEMS

By Henry R. Hunczak and George M. Low

Introduction

One of the basic differences between flight at supersonic and hypersonic speeds lies in the temperatures encountered in these two flight regimes. At supersonic speeds, stagnation temperatures are sufficiently low so that internal components of ramjet engines upstream of the combustor do not have to be cooled. The hot parts of an engine (combustor and nozzle) can generally be film-cooled with ram air.

At hypersonic speeds, on the other hand, temperatures may reach a high enough level to make the cooling of all internal components mandatory. Furthermore, since the ram air will also be hot, it cannot be used as a coolant.

At sufficiently high speeds, therefore, all internal components of ramjet engines will have to be cooled either with an expendable coolant or regeneratively with the fuel; an alternative cooling scheme which transports the internally generated heat to the external surfaces, whence it can be radiated to the atmosphere, may also be feasible.

This paper presents the results of preliminary calculations of the heat loads sustained by ramjet engines in hypersonic flight. The heat-sink capacity of several fuels is examined, and the heat load is compared to the available cooling capacity.

Symbols

a velocity of sound, ft/sec

h enthalpy, Btu/lb

M Mach number

Pr Prandtl number

Q heat load, Btu/sec

[redacted]

q heat-transfer rate, Btu/(sq ft)(sec)

T temperature, ^{o}R

v velocity, ft/sec

x distance parallel to surface from origin of boundary layer, ft

α absorptivity of gas

ε emissivity of wall

ε' effective emissivity of wall, $(\varepsilon + 1)/2$

ε_g emissivity of gas

ν kinematic viscosity, sq ft/sec

ρ density, lb/cu ft

σ Stefan-Boltzmann constant, 0.48×10^{-12} Btu/(sq ft)(sec)($^{o}R^4$)

Subscripts:

aw adiabatic wall conditions

e local conditions at outer edge of boundary layer

o stagnation conditions at outer edge of boundary layer

w wall or surface conditions

rad radiation

ref conditions evaluated at reference enthalpy as given in ref. 5

0 free stream

Calculation Procedure

The numerical calculations can, for convenience, be divided into two groups. The first comprises the inviscid-flow calculations which determine the internal aerodynamics and geometry of the configurations; the second group includes the viscous-flow and radiation analyses which are used to evaluate the heat loads.

[redacted]

Inviscid flow. - The free-stream conditions were based on the ICAO standard atmosphere as obtained from reference 1. For the supersonic inlet and subsonic diffuser the stagnation and local static pressures, temperature, and enthalpy for air were obtained by using real gas properties. Charts of these properties are published in reference 2.

For internal-compression inlets, isentropic one-dimensional flow was assumed with all flow losses occurring through a normal shock at the throat. For other inlet types, the oblique-shock losses were accounted for. At a Mach number of 7 and below, where the stagnation temperatures were below 5000° R, throat-shock Mach numbers were determined by using the methods of reference 3. These methods account for caloric imperfections but neglect gaseous imperfections such as dissociation. At a Mach number of 9, the stagnation temperatures were above 5000° R, and graphical solutions of the gas charts were used.

The diffuser-discharge Mach number was 0.2, at which point a stoichiometric fuel flow was added. The heat release was assumed to be instantaneous and was determined from the thermodynamic charts of reference 4. The momentum pressure loss due to combustion was neglected. However, for a free-stream Mach number of 7, calculations indicate that this loss is not large for a diffuser-discharge Mach number of 0.2.

The combustor length was held fixed at 2 feet, and the exhaust nozzles were assumed to be fully expanded.

Viscous flow. - Convective heat transfer: The convective heat loads were calculated using reference enthalpies (ref. 5) in the method outlined in reference 6 for turbulent boundary layers. A zero pressure gradient, variable property solution was employed in order to obtain preliminary results for comparison purposes. This simplified the analysis so that a wide range of variables could be investigated and trends could be established. The basic equation for the local heating rate is

$$q = 0.043\ \rho_e v_e (h_{aw} - h_w)\left(\frac{h_o}{h_e}\right)^{0.452}\left(\frac{h_e}{h_{ref}}\right)^{0.571}\left(\frac{M_e a_o}{\nu_o}\,x\right)^{-0.22}(Pr)_{ref}^{-2/3}$$

Sample calculations indicated that this equation yields results which are in excellent agreement with the semiempirical method of reference 5.

Flow properties, as previously indicated, were obtained from Mollier charts (refs. 2 and 4). Transport properties were obtained from the following sources:

(1) Prandtl number for air: Reference 7 for temperatures up to 4500° R; extrapolated values from 4500° to 6500° R.

[redacted]

(2) Viscosity of air: Reference 8 for temperatures up to 3400° R; above 3400° R viscosities were calculated by methods of reference 8 using self-diffusion coefficients.

(3) Prandtl number and viscosity for the combustion products of hydrogen and air: Calculated by methods proposed in reference 9.

For integration purposes the boundary layer was considered to originate at the cowl lip, the beginning of the subsonic diffuser, and the start of the combustor. The latter two assumptions were made because it was anticipated that some bleed would be required at the inlet throat, and the fuel nozzles and combustion process would disturb the boundary layer sufficiently to wipe a large part of it away.

The majority of the calculations were made for wall temperatures of 2000° R in the inlet and subsonic diffuser and 2500° R in the combustor and exhaust nozzle. Heat-transfer calculations for different temperatures were made by changing only the wall enthalpy in the heat-transfer equation; the effects of this change on reference enthalpy and Prandtl number were neglected. (This assumption is equivalent to assuming that the heat-transfer coefficient is independent of surface temperature.)

Radiation heat transfer: Radiation from the hot stream to the cold wall contributes to the heat transfer when water vapor or carbon dioxide is present. Since hydrogen fuel was used in the heat-transfer analysis, only water vapor contributed to the radiation heat load in the combustor and exhaust nozzle.

Calculation procedures suggested in references 10 to 12 were employed. The equation for radiation heat flux is

$$q_{rad} = \sigma \epsilon_w' (\epsilon_g T_e^4 - \alpha T_w^4)$$

An emissivity of 0.35 was assumed for the wall.

Although the local convective heat loads could be scaled with engine size, the radiation heat load cannot be scaled. Instead, radiation heat-transfer rates were recalculated for each of the altered conditions investigated.

Total heat load: Total heat loads were obtained by a planimeter integration of a plot of the local heat-transfer rate as a function of the wetted surface area.

[redacted]

Results and Discussion

Representative engine. - In order to study the effect of the variation of many parameters on the heat load, a representative engine was selected (fig. 1). An internal-compression inlet was chosen in order to facilitate the computations. The combustor length was fixed at 2 feet, while the combustion-chamber Mach number equaled 0.2. An inlet diameter of 10 feet was assumed for many of the calculations. All other pertinent dimensions are given in figure 1.

Temperatures and heat flux. - External temperatures: If the engine is free to radiate in all directions, the external surfaces will assume an equilibrium temperature which results when the aerodynamic heat input is balanced by the heat radiated away from the engine.

Typical radiation equilibrium temperatures for an emissivity of 0.8 are presented as the dashed curves of figure 2. With the exception of a small region near the leading edge, these temperatures are sufficiently low to make the cooling of external surfaces unnecessary. At a constant Mach number, radiation equilibrium temperatures decrease with increasing altitude. From external temperature considerations, therefore, it is beneficial to fly at the highest possible altitude.

Internal temperatures: The internal temperature distributions of an uncooled engine are also shown in figure 2. As the Mach number increases, these temperatures become intolerably high in all parts of the engine. Because these high temperatures exceed the limits of all known materials, all internal components require some form of cooling. The question then arises as to the rate at which heat must be carried away in order to maintain allowable temperatures.

Internal heat-transfer rates of cooled engine: The heat-transfer rate, or heat flux, of the representative engine is presented in figure 3. The curve is for flight at Mach 9 and an altitude of 140,000 feet; hydrogen fuel was used for this calculation. Wall temperatures in the inlet and subsonic diffuser were assumed to be 2000° R; in the combustor and exhaust nozzle, where oxidation problems do not exist, a wall temperature of 2500° R was assumed.

High heat fluxes occur in the throat regions and in the combustion chamber (fig. 3). But even at this very high Mach number, the peak heat-transfer rate is only about 400 Btu/(sq ft)(sec). This heat flux is about 25 percent of the heat-transfer rates currently being handled successfully in rocket motors. It should, therefore, be possible to cool ramjet engines in hypersonic flight without serious difficulties.

Regenerative cooling system. - The magnitude of the heat flux suggests that a regenerative cooling system be used which makes use of the fuel as

a coolant. The cooling capacities and impulses of several fuels are shown in the following table:

Fuel	Minimum temperature, ^{o}R	Maximum temperature, ^{o}R	Relative specific impulse	Relative cooling capacity	
				Inlet and subsonic diffuser	Combustor and nozzle
Hydrogen	37	2500	100	100	100
Diborane	194	600	45	5.4	10.2
Ethyl decaborane	520	760	38	2.0	2.7
Methane	201	1520	35	15.2	28.6
Stable JP type	520	1060	31	5.4	11.5

Results in this table are for stoichiometric fuel-air ratio and flight at Mach 7 with the engines scaled to provide equal internal thrust. The minimum temperatures for the cryogenic fuels are their boiling point. The maximum temperatures for all fuels except hydrogen were determined from limits imposed by the degradation of the fuel; hydrogen has no such limit, and the material temperature limit of 2500^{o} R was, therefore, chosen as a maximum.

The relative cooling capacity is a function not only of the heat-sink capacity of the fuel but also of the relative heat load of the several fuels. The heat-sink capacity is related to both the specific heat of the fuel and the temperature rise during the cooling process. The heat load depends on the heat-transfer coefficient, the surface area, and the enthalpy of the gas (air or combustion products) at the wall and adiabatic wall temperatures. The difference in relative cooling capacities of the cold parts (inlet and diffuser) and the hot parts (combustor and nozzle) of the engine is due to the different enthalpies of air and of the products of combustion. Heat-transfer coefficients were not adjusted for the different fuel types.

When compared with hydrogen, the cooling capacities of the two boron fuels and the jet fuel are very low. This fact stems from a combination of a low specific heat and a low allowable temperature rise. Methane, which has an impulse somewhat better than that of jet fuel, has also a somewhat better cooling capacity. The two cooling capacities of methane (28.6 for the combustor plus nozzle and 15.2 for the inlet and diffuser) can be combined into a single value if the proportion of the total heat load in each engine component is known. If it is assumed that three-quarters of the total heat load is in the combustor and nozzle, and one-quarter is in the inlet and diffuser, the over-all cooling capacity of methane is 25 percent that of hydrogen. This may be sufficient for some

applications. But when both cooling capacity and impulse are considered, none of the fuels measures up to hydrogen. All the subsequent heat-transfer calculations were, therefore, based on hydrogen fuel.

Of course, not all the heat-sink capacity of the fuel is available to cool the engine. In a regenerative cooling scheme the engine walls become a rather complex heat exchanger. An analysis has shown that such a heat exchanger using hydrogen fuel can be 80 to 85 percent efficient at Mach 7. In addition, some of the cooling capacity may be required to cool the airplane structure, the instruments, and the payload. These other uses, together with the 15- to 20-percent heat-exchanger losses, have led to the assumption that 50 percent of the fuel cooling capacity is available to cool the engine.

Total heat load. - The heat flux throughout the engine was integrated to yield the total heat load. The effects of Mach number, altitude, and pressure recovery were investigated for the engine with an internal compression inlet. An inlet diameter of 10 feet and wall temperatures of 2000° R in the inlet and diffuser and 2500° R in the combustor and nozzle were chosen. Next, the effect of wall temperature was investigated for the same 10-foot engine; the effect of engine size was also calculated. Finally, the effect of other inlet types on total heat load was analyzed.

Effect of Mach number: In figure 4 the heat load, relative to the cooling capacity, is plotted as a function of Mach number. An altitude schedule corresponding to a constant dynamic pressure of 400 pounds per square foot and a pressure recovery schedule corresponding to a kinetic energy efficiency of about 92 percent were chosen. If 50 percent of the heat-sink capacity of the hydrogen fuel is available to cool the engine, a limiting Mach number of slightly over 8 can be reached.

Effect of altitude: It is well known that the heat load decreases with increasing altitude. But, for a fixed inlet size, the airflow (and hence, the fuel flow) decreases with increasing altitude; this causes a reduction in heat-sink capacity. The net result is that the heat load increases relative to the cooling capacity as the altitude is increased. However, as shown in figure 5, this increase is not very pronounced at Mach 7.

Effect of total-pressure recovery: The effect of total-pressure recovery for a family of similar internal compression inlets is rather interesting in that two opposing factors are of importance. As the pressure recovery is increased, the local heat flux increases. But at the same time the wetted areas of the subsonic diffuser, the combustor, and the exhaust nozzle are reduced. The resulting total heat load is shown in figure 6. For the conditions of these calculations, the heat load peaks at a pressure recovery between 0.15 and 0.18. But the over-all effect of pressure recovery (for geometrically similar engines) is very small.

Effect of metal surface temperature: Up to this point all results were presented for the rather high surface temperatures of 2000° R in the inlet and subsonic diffuser and 2500° R in the combustor and exhaust nozzle. Although these temperatures are high, they are not completely unrealistic; alloys are now being developed that have satisfactory strength at temperatures approaching 2500° R.

However, if the high temperatures cannot be maintained, it is still possible to cool the engine by using a larger portion of the cooling capacity of the fuel. The effect of surface temperature on the ratio of heat load relative to cooling capacity is shown in figure 7. This ratio increases with decreasing surface temperature for two reasons: First, the local heat flux is increased as the difference between the wall and the adiabatic wall temperatures increases; second, the heat-sink capacity of the fuel decreases as the maximum fuel temperature decreases.

If only 50 percent of the heat-sink capacity of the fuel is available to cool the engine, the minimum allowable surface temperature is about 2000° R (fig. 7). This minimum can be decreased slightly by applying a high-temperature insulating coating, as shown by the dashed line in figure 7. A 0.05-inch coating of zirconia can be used to reduce the average metal surface temperature by about 100° without raising the heat load. (The previously mentioned numbers, of course, apply only at the specified conditions: namely, M_0, 7; altitude, 120,000 ft; inlet diameter, 10 ft; fuel, hydrogen.)

The penalty for applying a high-temperature coating is the resulting increased engine weight. The 0.05-inch coating, when applied to the reference engine, adds 30 to 40 percent to its weight. In a practical application, therefore, coatings should be applied only in regions of high heat flux, because they are most effective in these regions.

Effect of engine size: So far all results were for an engine with the rather large inlet diameter of 10 feet. An engine of this size may be required for missions of semiglobal range. But for shorter ranges, such as the intercontinental mission, smaller engines are wanted. The effect of engine size at a Mach number of 7 and an altitude of 120,000 feet and with hydrogen fuel is shown in figure 8. The heat load increases rather rapidly relative to the cooling capacity as the engine size is decreased. For 50-percent heat-sink utilization the minimum allowable inlet diameter is 4 feet.

Comparison of several inlet types: As mentioned earlier, the parametric study of heat loads was made for an engine with an all-internal-compression inlet. In order to start and control this inlet, rather large area variations are required. The problem of cooling large movable components is exceedingly difficult. Also, with this type of inlet, large quantities of hot boundary-layer bleed flow must be handled. The inlet therefore does not appear to be very practical for application at high hypersonic speeds.

In figure 9(a) the total heat loads of several other inlet types are shown. These inlets are drawn schematically in figure 9(b). All engines were sized for equal thrust at a Mach number of 7 and an altitude of 120,000 feet. The inlet types are described in the following table:

Engine	Inlet type	Total-pressure recovery
A	Internal compression	0.12
B	Three-dimensional isentropic spike, external compression	0.12
C	Three-dimensional isentropic spike, rapidly expanding diffuser	0.12
D	Three-dimensional isentropic spike, external plus internal compression	0.25
E	Two-dimensional isentropic wedge, external compression	0.12
F	Two-dimensional isentropic wedge, external plus internal compression	0.12
G	Two-dimensional single wedge	0.04

Engine A is the reference engine with the internal compression inlet. Its total heat load is unity. About one-half of the heat load is in the exhaust nozzle, one-fourth in the combustion chamber, and the remainder in the inlet and subsonic diffuser. The total load is relatively low because the regions of high heat flux occur where the surface areas are small. (Surface areas in square feet are indicated by the numbers in fig. 9(b)).

Engine B is three dimensional with an isentropic external-compression inlet. The supersonic inlet has a very low heat load because it can radiate to the atmosphere. The subsonic diffuser, on the other hand, has a very high heat load that results from a large surface area in a region of high heat flux.

The heat flux in the subsonic diffuser can be minimized by providing a rapid area expansion or perhaps by allowing the flow to separate. Engine C is identical to engine B, with the exception that the area in the subsonic diffuser is expanded rapidly. The heat load for this component was computed with the assumption that the flow remains attached. With this modification, the total heat load of the inlet with external compression is slightly less than that of the internal-compression inlet.

Engine D represents another modification of engine B. The pressure recovery was increased from 0.12 to 0.25 by incorporating some internal compression in addition to the external compression. This modification

increased the heat load in the supersonic inlet and decreased the nozzle heat load. The changes in the subsonic diffuser and combustor heat loads were minor. The total heat load of engine D is somewhat higher than that of engine B.

Engines E and F both have two-dimensional inlets with isentropic compression surfaces. Engine E has all external compression, while engine F has combined internal and external compression. Pressure recoveries of 0.12 were assigned to both inlets. The internal compression again raises the heat load of the supersonic inlet. The total heat load of engine E is about 30 percent higher than that of engine A, while the heat load of engine F exceeds that of the reference engine by 50 percent.

Engine G has a two-dimensional single-wedge inlet with a total-pressure recovery of 0.04. Its total heat load is relatively low and can probably be reduced further by modifying the subsonic diffuser.

Closed cooling cycle. - It has been shown that at Mach 5 only about 15 percent of the cooling capacity of hydrogen is needed to cool the engine. Therefore, methane might also be satisfactory for cooling up to Mach 5 or perhaps even Mach 6. But at Mach 7 and above, more than 30 percent of the cooling capacity of hydrogen is required for the engine alone. None of the other fuels that were considered have even this much cooling capacity with stoichiometric combustion. From cooling considerations it must therefore be concluded that hydrogen is the only practical fuel for flight at high hypersonic speeds if a regenerative cooling system is to be used.

A different type of cooling system not using the fuel as a coolant was also investigated. It was shown in figure 2 that the external surfaces of the engine are at temperatures below the material limits. It may therefore be possible to transport the internal heat to the external surfaces and to radiate it to the atmosphere. This system is shown schematically in the upper part of figure 10. The heat picked up along the internal surfaces is carried to the external surfaces through a heat exchanger, probably of the liquid-metal type. A pump for the heat-exchanger agent is also required.

The performance of this system is shown in the lower part of figure 10. The dashed line represents the heat to be removed for the conditions indicated at the top of the figure. If the external surfaces can be maintained at a temperature of 2400° R, the system is good at Mach numbers even above 9. But the 2400° R temperature allows for only a 100° temperature drop in the heat exchanger; this may be very unrealistic. If the external temperature is kept at 1900° R, the closed cooling cycle cannot be used at Mach numbers much above 5. These results should, however, be qualified. First of all, they apply only for a very specific set of conditions. Second, the external engine surface area was used as a radiator

surface. This area would be decreased if the engine is not free to radiate in all directions; it could also be increased by using other parts of the aircraft surfaces as radiators.

The system has some inherent disadvantages. It would probably be quite heavy. All parts of the engine structure would be very much hotter than in a fuel-cooled system. The development of a liquid-metal pump is also required.

If hydrogen fuel is acceptable, a regenerative cooling scheme is probably the simplest and most practical. If for some reason the use of hydrogen is ruled out, a cooling cycle such as shown in figure 10 will have to be developed.

CONCLUDING REMARKS

The results of a preliminary study of the cooling requirements of ramjet engines have been presented. Although the general trends and approximate magnitudes of these results are believed to be correct, the exact values and cooling limits are probably a function of the assumptions inherent in the analysis.

Perhaps one of the major assumptions lies in the use of a stoichiometric fuel-air ratio. The cooling capacity is almost directly proportional to fuel-air ratio. Therefore, all the cooling limits can be increased by burning at equivalence ratios greater than 1; of course, the specific impulse is thereby decreased.

The low bleed flow requirements and the absence of moving parts suggest the use of an external-compression inlet for flight at high hypersonic speeds. The cooling requirements of this inlet need not exceed those of an internal-compression inlet.

At Mach numbers of 7 and above, regenerative cooling is probably the simplest and most practical scheme. Fuels such as jet fuel, diborane, and ethyl decaborane are ruled out because of their almost negligible cooling capacity. Methane may give satisfactory performance up to some low hypersonic speeds.

The calculated results indicate that hydrogen fuel is outstanding for the purpose of regenerative cooling at Mach 7 and above, in that it has both a high heat capacity and a high heat of combustion.

[redacted]

REFERENCES

1. Air Force Cambridge Research Center: Atmospheric Models. Doc. No. 56SD233, Missile and Ord. Systems Dept., General Electric, Phila. (Pa.).

2. Moeckel, W. E., and Weston, Kenneth C.: Composition and Thermodynamic Properties of Air in Chemical Equilibrium. (To be published.)

3. Ames Research Staff: Equations, Tables, and Charts for Compressible Flow. NACA Rep. 1135, 1953. (Supersedes NACA TN 1428.)

4. Hall, Eldon W., and Weber, Richard J.: Tables and Charts for Thermodynamic Calculations Involving Air and Fuels Containing Boron, Carbon, Hydrogen, and Oxygen. NACA RM E56B27, 1956.

5. Eckert, E. R. G.: Engineering Relations for Friction and Heat Transfer to Surfaces in High Velocity Flow. Jour. Aero. Sci., vol. 22, no. 8, Aug. 1955, pp. 585-587.

6. Reshotko, Eli, and Tucker, Maurice: Approximate Calculation of the Compressible Turbulent Boundary Layer with Heat Transfer and Arbitrary Pressure Gradient. NACA TN 4154, 1957.

7. Glassman, Irvin, and Bonilla, Charles F.: The Thermal Conductivity and Prandtl Number of Air at High Temperatures. Preprints of papers for Heat Transfer Symposium, Am. Inst. Chem. Eng., Dec. 1951.

8. Hilsenrath, Joseph, et al.: Tables of Thermal Properties of Gases. Cir. 564, NBS, Nov. 1, 1955.

9. Hirschfelder, Joseph O., Curtiss, Charles F., and Bird, R. Byron: Molecular Theory of Gases and Liquids. John Wiley & Sons, Inc., 1954.

10. McAdams, William H.: Heat Transmission. Second ed., McGraw-Hill Book Co., Inc., 1942.

11. Hottel, A. C.: Radiant Heat from Water Vapor. Trans. Am. Inst. Chem. Eng., vol. 38, 1942, p. 531.

12. Penner, S. S., and Thomson, A.: Determination of Equilbrium Infrared Gas Emissivities from Spectroscopic Data. Presented at Second Biennial Gas Dynamics Symposium, Tech. Inst., Northwestern Univ., Aug. 26-28, 1957.

[redacted]

REPRESENTATIVE ENGINE
USED IN HEAT-TRANSFER ANALYSIS

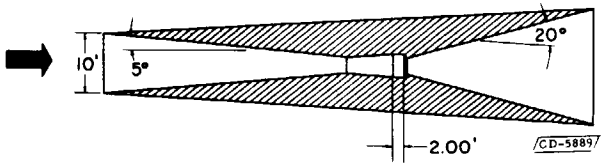

Figure 1

EQUILIBRIUM TEMPERATURES OF
UNCOOLED ENGINE

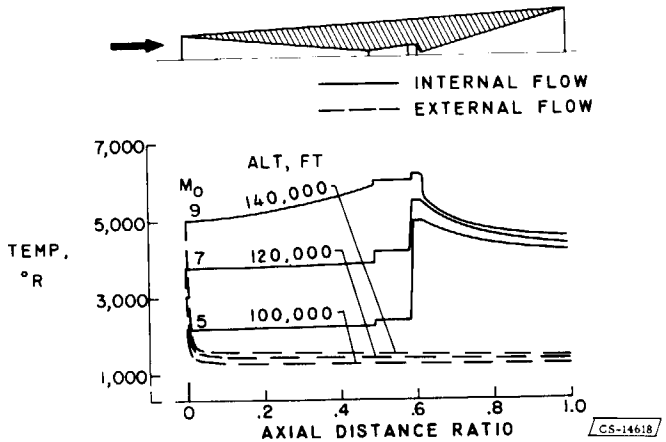

Figure 2

LOCAL INTERNAL HEAT TRANSFER RATES OF
COOLED ENGINE
M_0, 9, ALTITUDE, 140,000 FT

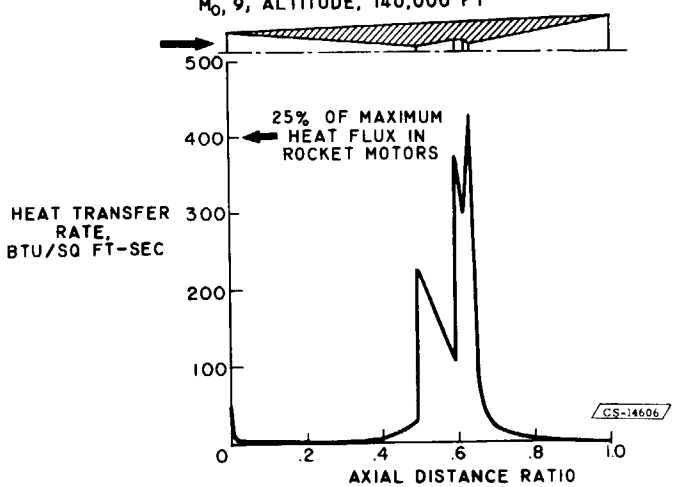

Figure 3

INCREASING MACH NUMBER RAISES HEAT LOAD

FUEL, HYDROGEN, D_{INLET}, 10 FT, DYNAMIC PRESSURE, 400 PSF

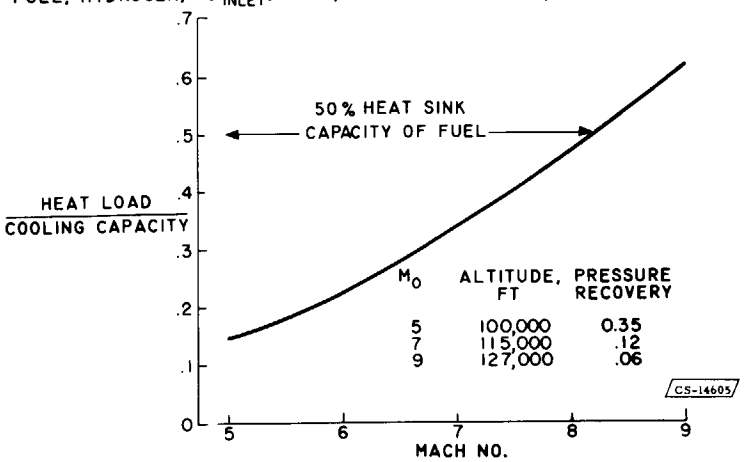

Figure 4

HIGHER ALTITUDE REDUCES COOLING RESERVE

M_o, 7, D_{INLET}, 10 FT, FUEL, HYDROGEN

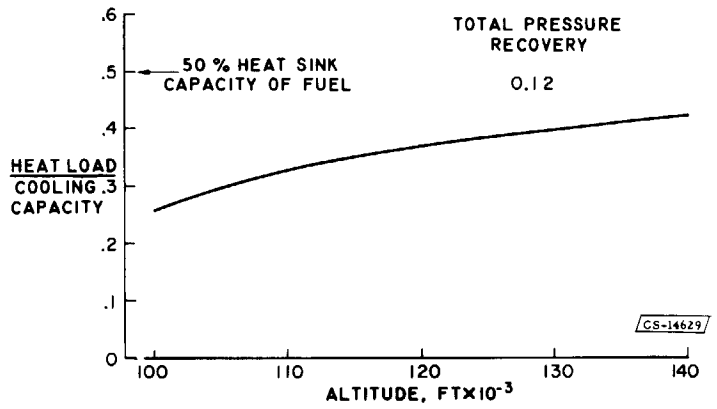

Figure 5

EFFECT OF TOTAL-PRESSURE RECOVERY ON HEAT LOAD

(M_o, 7, D_{INLET}, 10 FT, FUEL, HYDROGEN, ALT, 120,000 FT)

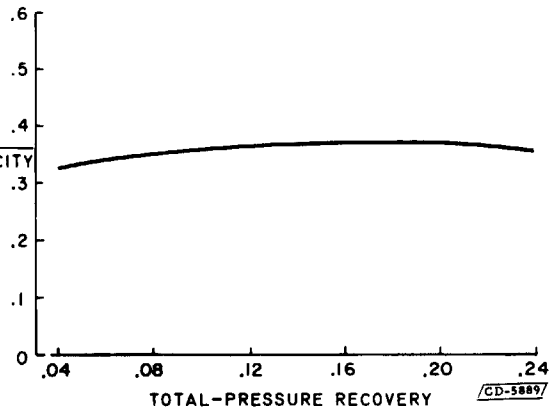

Figure 6

LOWER SURFACE TEMPERATURE YIELDS HIGHER HEAT LOAD

D_{INLET}, 10 FT, M_o, 7, ALTITUDE, 120,000 FT, FUEL, HYDROGEN

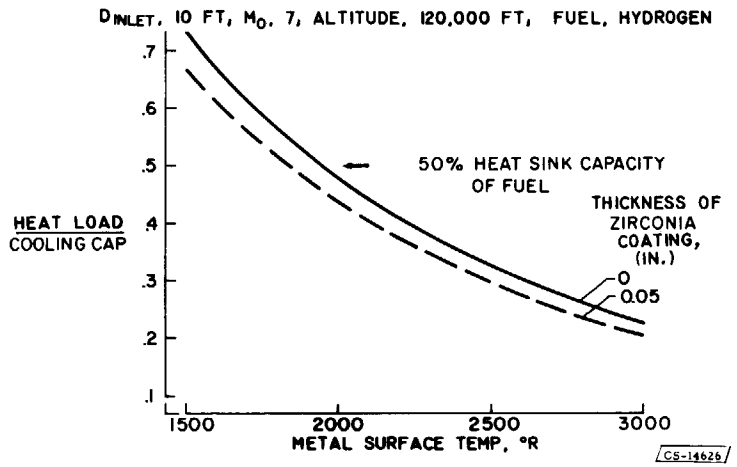

Figure 7

LARGE ENGINES ARE EASIER TO COOL THAN SMALL ONES

M_o, 7; ALTITUDE, 120,000 FT, HYDROGEN FUEL

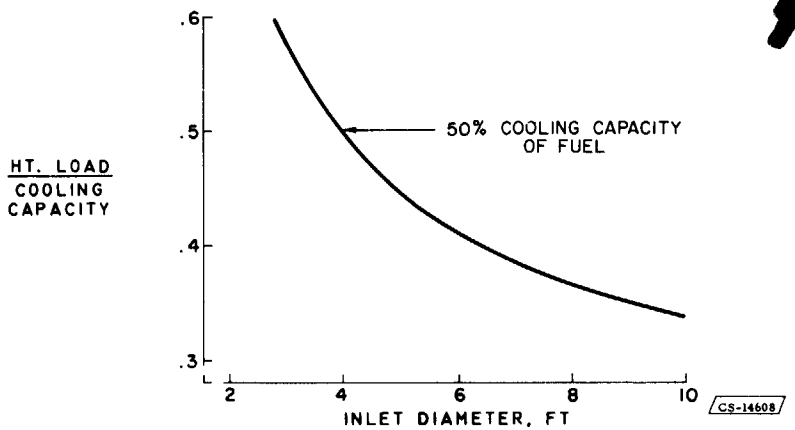

Figure 8

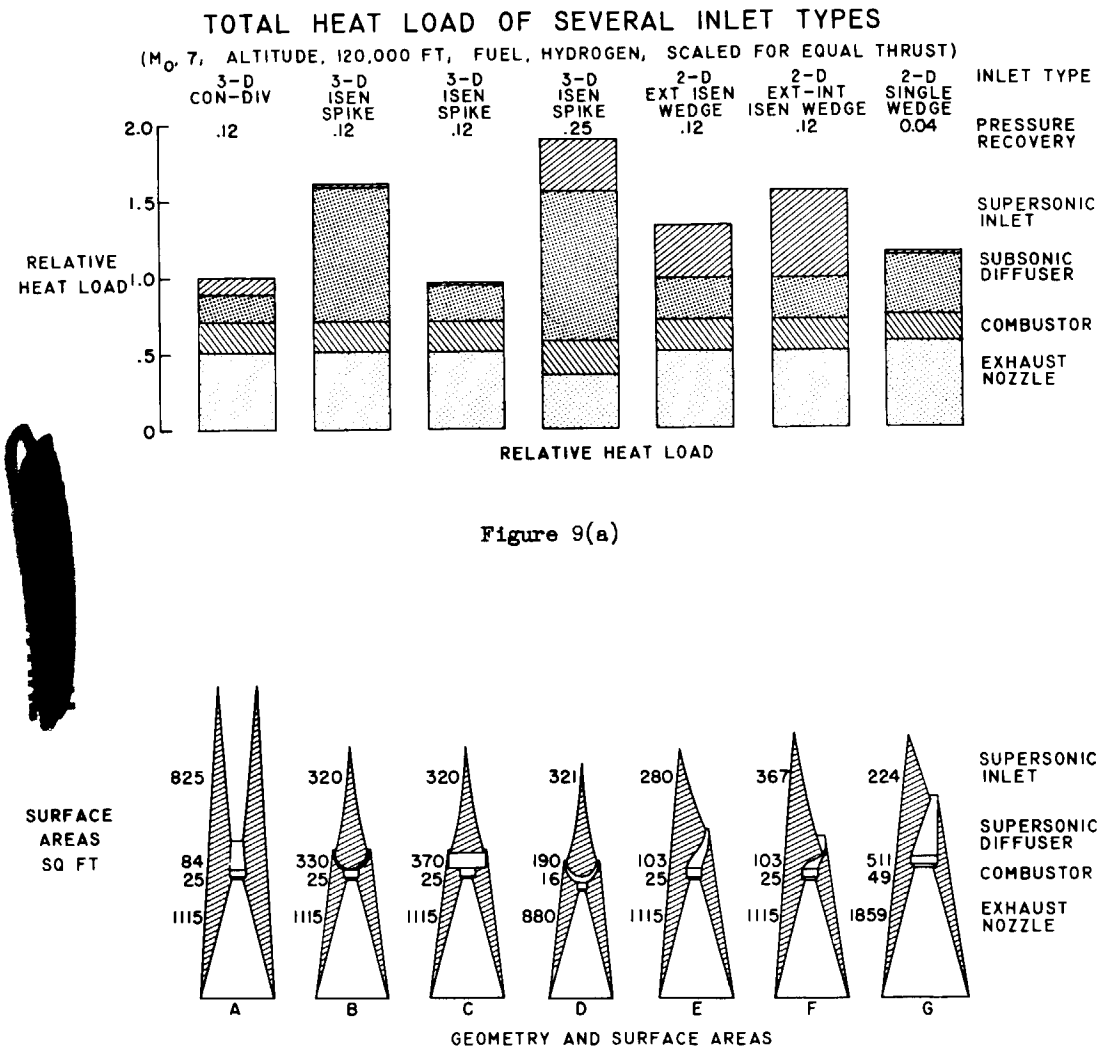

Figure 9(a)

Figure 9(b)

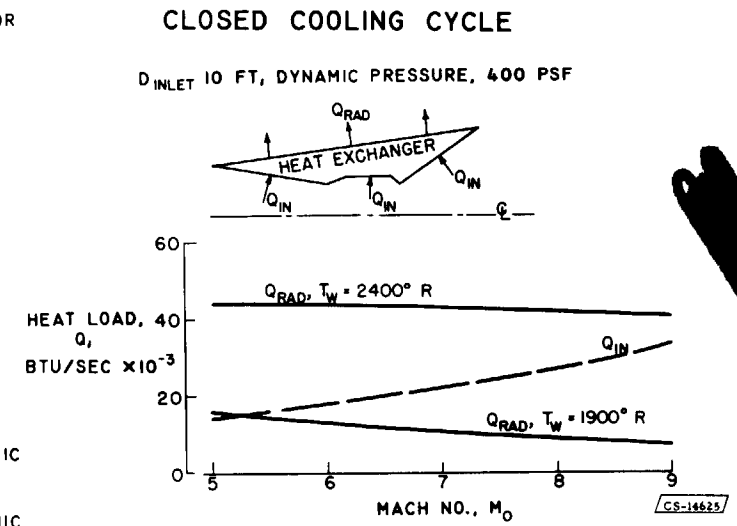

Figure 10

3. ENGINES

By H. M. Henneberry, A. V. Zimmerman, J. F. Dugan, W. B. Schramm, R. Breitwieser, and J. H. Povolny

INTRODUCTION

Present air-breathing engines and those being developed are capable of unassisted flight to Mach numbers of 2.0 or 3.0. This paper investigates the potentialities of air-breathing engines at Mach numbers above 3.0. Suitable engine types have been described in paper 1. A comparison of these engine types over a range of flight Mach numbers is presented in figure 1. Thrust per unit airflow is used as a measure of engine feasibility for four general classes of air-breathing engines: high-pressure-ratio gas turbines, low-pressure-ratio gas turbines, conventional ramjets, and high Mach number fuel-rich ramjets.

The high-pressure-ratio gas-turbine engine is included for reference. It is typical of present-day turbojet engines capable of flight to Mach 2.0. A sea-level compressor pressure ratio of 12 and full afterburning have been assumed for this engine, and its Mach number potential is limited to 2 or 2.5. The low-pressure-ratio gas turbine can be characterized by an afterburning turbojet engine with a sea-level compressor pressure ratio of 2 or 3. It is inferior to contemporary engines at subsonic Mach numbers, but it can produce useful thrust to Mach numbers of 4 or 4.5. Analysis has indicated that the poor subsonic performance of this engine can be tolerated in missions requiring all-supersonic cruise at Mach numbers above 3.

As Mach number increases, the conventional ramjet becomes an attractive powerplant. However, below Mach 2.0 its thrust falls rapidly; it requires low-speed thrust assistance. Conventional ramjet thrust also falls off at the higher Mach numbers, and the fuel-rich ramjet becomes the superior powerplant. The fuel-rich ramjet would also need thrust assistance at low speeds, but preliminary calculations indicate it may produce useful thrust to Mach numbers as high as 18. The performance of this engine is indicated as an area rather than a line because the analysis of this cycle is still preliminary and definitive results have not been obtained.

This paper will treat in order the low-pressure-ratio gas turbines, the conventional ramjet, and the fuel-rich ramjet. The major emphasis will be on their long-range supersonic mission capabilities.

LOW-PRESSURE-RATIO GAS-TURBINE ENGINES

For the low-pressure-ratio gas-turbine engines, all-supersonic Mach 4.0 missions are emphasized. Split missions (i.e., subsonic cruise and supersonic dash) are not treated, since calculations indicated no advantages for this mission when the supersonic portion is at Mach 4.0. Furthermore, the engine-airplane combinations of this analysis are assumed to be capable of unassisted flight over the entire mission; that is, they are capable of climb, acceleration, and cruise without external thrust assistance. Obviously, some compromises in the direction of rocket assist, such as small jet-assisted takeoff units for takeoff or transonic accelerations, could be made without a great sacrifice in airplane flexibility. In order to demonstrate the potentialities of the gas-turbine engines for unassisted flight, such compromises are not assumed.

A variety of gas-turbine engines has been proposed for high-speed flight. In this paper, four representative types are examined: the turbojet, the fuel-rich turbofan, the air-turborocket, and the hydrogen expansion engines. Actually, a strong similarity exists among these engine types. This similarity is indicated in figure 2, which illustrates the components common to all the engine types. Detailed descriptions of these engines are presented later. In figure 2 the upper vertical vector represents the heat input into the afterburner necessary to obtain the cycle temperature, and the lower vertical vector represents the heat that must be removed to cool critical engine areas. The torque vector represents the shaft work that must be provided to drive the fan or compressor. The engines differ primarily in the means used to provide this shaft work, which ranges from essentially an air-driven turbine in the turbojet to a fuel-driven turbine in the hydrogen expansion engine. All the engines require an inlet diffuser, an afterburner, an exhaust nozzle, a nacelle, and a compressor or fan. The weight estimates of this analysis indicate that these components account for over two-thirds of the total engine weight. Therefore, only small differences in over-all weight were revealed in analyzing the various gas-generator types.

The turbojet engine will be examined in some detail because it is the most familiar engine type and because its over-all potentialities are very attractive in the Mach 4 speed region. The other three cycles will then be examined briefly and all four engine types will be compared before the higher speed regions are discussed.

Turbojet Engine

Component design. - Compressor: Operating a turbojet engine up to a flight Mach number of 4.0 results in a number of severe compressor problems, and special provisions need to be taken in the compressor design to alleviate these problems as far as possible. For example, if a conventional compressor, one suitable for a Mach 2.5 turbojet, is used at Mach 4.0, three major problems will arise: (1) At Mach 4.0, the compressor will be operating in rotating stall; (2) the compressor efficiency will be low; and (3) the level of compressor weight flow will be low.

One solution to these problems is indicated by the compressor map of figure 3, which shows compressor pressure ratio as a function of corrected weight flow. Included on the map is an engine operating line with operating points at various flight conditions indicated by the circles. This compressor has three stages, and the map was obtained by analytically stacking data from an experimental single-stage compressor. A photograph of this single-stage compressor is included in figure 3.

To obtain the performance shown on the map, three changes from conventional practice were made in both the compressor and the operating line. The most significant change was using a low value of compressor pressure ratio (2.3) at takeoff. The second change was moving the aerodynamic design point of the compressor from takeoff to near the Mach 2.0 operating point, as indicated by the location of the 100-percent-equivalent-speed line. The third change was departing from conventional constant-mechanical-speed operation. The mechanical speed of the compressor was increased 18 percent between the takeoff and Mach 3.3 and then held constant to Mach 4.0.

The net effect of these changes is a compressor less sensitive to rotating stall, with a wide range of high efficiency. The Mach 4.0 operating point is at 78 percent of design equivalent speed. It is in a region free from rotating stall and the efficiency is over 80 percent. The corrected weight flow at Mach 4.0 is also high; it is 85 percent of the takeoff weight flow, resulting in a good cruise specific weight of the engine. More important, this small weight-flow variation between takeoff and Mach 4.0 matches closely the critical weight-flow variation of simple conical inlets. This avoids high subcritical additive drags at off-design flight conditions.

It should be noted that the improvements in Mach 4.0 engine performance effected by these compressor changes are obtained at a sacrifice in low-speed performance. This is particularly true in using a low value of takeoff pressure ratio. However, high compressor pressure ratios are not beneficial at Mach 4.0, and compromises in low-speed engine performance were accepted in an effort to improve the Mach 4.0 performance.

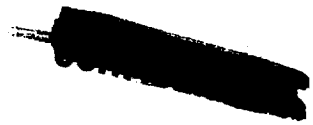

In view of the high stagnation temperatures at Mach 4.0, careful consideration must also be given to the structural problems of the compressor. Stagnation temperature on the order of 1600° R requires the use of a super alloy for the compressor blades and disks. At Mach 4.0, the actual tip speed of the compressor is 1085 feet per second, which results in a centrifugal blade-root stress of 30,000 psi.

Turbine: The turbine for a Mach 4.0 turbojet engine also presents some unique problems. Using a low value of compressor pressure ratio results in a low turbine work output and a high turbine flow requirement, which lead to long flat turbine blades. An example of the type of blade that will be required is shown in figure 4. It is apparent that this type of blade will lead to structural problems, especially of a vibrational nature. Since turbine losses do not decrease with decreasing work when high axial velocities are required, lower turbine efficiencies can also be anticipated with a low turbine work output. With a single-stage turbine, losses associated with the rotor and stator surfaces are principally a function of axial velocity; and, as work output decreases, the efficiency will drop.

One solution to the structural problem appears to be the use of unconventional aerodynamic designs to achieve a large chord taper. Tapering the chord and giving the blade a more triangular shape will make it less subject to vibrational problems by eliminating some of the flat portions. Furthermore, tapering the chord will lower the centrifugal stress in the blade by providing a more favorable area distribution.

Some experimental turbine work has been directed toward unconventional aerodynamic design in an effort to get a sound structural blade for this class of turbine. Figure 5 shows the results of some of these tests. A photograph of the rotor from the single-stage turbine on which the data were obtained is also included. In designing blades for this rotor, aerodynamic compromises were made in order to obtain a tip-to-root chord taper of 0.79 and an area taper of 0.33. The design-speed performance is shown as turbine efficiency against turbine work. At the design point, the efficiency is 82.5 percent. Even if aerodynamic compromises had not been made to favor structural requirements, a design-point efficiency of only 83 percent would be expected. The fact that only half a point in efficiency was sacrificed suggests that further compromises in aerodynamic design should be investigated.

The small variation in efficiency over a range of turbine work is also encouraging in that it suggests a degree of insensitivity that would be desirable in actually operating a practical engine.

Afterburner: Figure 6 shows the afterburner temperature ratios and pressures encountered with a hydrogen-fueled airplane over a typical flight path consisting of takeoff, climb, and cruise at Mach 4.0. A

curve for JP and EDB fuels is also included. The symbols represent the conditions at the end of cruise, the square representing the conditions in a typical JP or EDB engine and the circle representing the conditions in a typical hydrogen engine. Because hydrogen-fueled airplanes inherently have a lower density, they tend to cruise at higher altitudes and thus will encounter lower afterburner pressures. However, even at the end of cruise the pressure is 0.8 atmosphere, which presents no problem for efficient combustion of hydrogen. The pressure at the end of cruise for the dense fuels is 1.2 atmosphere, which again presents no problem.

The highest temperature ratio achieved over the flight path is slightly over 2.4 and occurs at a Mach number of 0.9. Because the temperature ratio is high during climb, the afterburner-inlet velocity must be low. Also, with a low-pressure-ratio turbojet, the afterburner-inlet density is low. These conditions of low velocity and low density lead to large afterburner frontal area, which for the case under consideration is about twice the compressor frontal area. This does not result in any drag penalties, however, since the required inlet and outlet areas for a Mach 4.0 turbojet are even larger than this. In addition, the weight penalties will be minimized when hydrogen or boron fuels are used, since short afterburner lengths can be obtained. This is not true for the JP engine, where the afterburner is necessarily a long and heavy component.

In a typical Mach 4 mission, more than 90 percent of the total airplane fuel is consumed in the engine afterburner. Therefore, in applying boron hydride fuels to this mission it appears practical to consider the use of the high-energy fuel in the afterburner only. Retention of JP in the primary burner will avoid the troublesome solid-product problem in the turbine and will have little effect on radius capability because primary-burner fuel is such a small percent of total fuel.

Fuel system: For JP and EDB fuels, no new fuel-pump problems are evident. Because heat input to these fuels will have to be kept to a minimum, bypass-type pumps will not be satisfactory. This is already true in the Mach 2.5 to 3.0 region. When hydrogen is considered, new pump techniques will be necessary. In the turbojet these can be low-pressure pumps, 8 atmospheres being the maximum required at any flight condition. It appears likely that the fuel would not have to be pumped at all during cruise, since a 2-atmosphere tank pressure would be sufficient to feed the burners. This is particularly advantageous, since a large part of the fuel would be vaporized during cruise because of heat leaks into the tanks and lines at the high-temperature Mach 4 cruise condition. Calculations have indicated that, with $1\frac{1}{2}$ inches of tank insulation, approximately 70 percent of the engine cruise fuel requirement would be vaporized by these heat leaks. During climb, heat leakage to the fuel would be much lower but combustor pressures would be higher.

[redacted]

Therefore, a liquid-hydrogen pump would be required for this portion of the flight.

In view of the high stagnation temperatures at Mach 4.0, it is necessary to provide a cooling system for critical engine components such as bearings and accessories. For hydrogen fuel, one attractive possibility is the use of a fuel-to-air heat exchanger that would cool compressor bleed air. This bleed air could then be diverted to the critical engine areas. Such a heat exchanger could be small and light, since only 2 or 3 percent of the engine airflow would be required for cooling.

Cycle variables. - To obtain engine performance, the various mechanical elements were combined into practical engine configurations. Engine weights were then estimated, and both design and off-design engine performance was analyzed. Engine performance was then evaluated in typical long-range airplanes. In doing this, the radius capabilities of airplanes of fixed gross weight were used as a criterion to establish desirable values of the engine cycle variables such as compressor pressure ratio and turbine-inlet temperature. The influence of both design and off-design engine performance on the airplane is indicated in figure 7. Impulse and total thrust are shown over a typical mission profile for two hydrogen-fueled airplanes. One is powered by turbojet engines with three-stage compressors and sea-level pressure ratios of 2.3, and the other by engines with four-stage compressors and sea-level pressure ratios of 3.0. The thrust shown is the total thrust for all the engines installed in the airplane. A typical airplane drag curve is also included so that thrust margins available for acceleration can be noted.

The climb path used consisted of acceleration at sea level to Mach 0.9, climb at Mach 0.9 to 20,000 feet, then climb and acceleration through Mach 2 and 36,000 feet to Mach 4 and 70,000 feet, and then climb at Mach 4 to the cruise altitude. Cruise afterburner temperature for the engines was 3000° R, and during climb the afterburner temperature was 4000° R. At the end of acceleration, thrust margins are very high. However, after acceleration, the altitude is increased and the afterburner temperature is decreased to reach the cruise condition, where the thrust margin is zero. During acceleration and climb, the thrust margins are large. Even at Mach 1.5, where transonic drag losses are high, the thrust is almost twice the drag. In this figure, engine drag losses have been charged against engine performance. This accounts for the dip in the impulse and thrust curves around Mach 1.5 where inlet additive drag losses are high.

The airplanes of figure 7 had target altitudes of over 100,000 feet. This resulted in large engine sizes and led to the large thrust margins shown in figure 7. The high target altitude data were chosen in order to separate the curves and facilitate their presentation. However, even at a more optimum target altitude of 95,000 feet, the thrust was 50 percent higher than the drag at Mach 1.5.

[redacted]

The comparison between the two engines is typical of those encountered in most of the engine comparisons. In general, the important considerations are thrust margin during climb and impulse at cruise. No one engine is able to dominate both of these regions at once. During the early part of climb, the engines with the four-stage compressors have better thrust margins. At the higher Mach numbers the three-stage engines have the larger thrust margins, and they also have a slightly higher impulse at cruise. In this example, the differences are small because the pressure ratios of the two engines are quite similar.

Compressor pressure ratio: The only way the trends of figure 7 can be evaluated is to observe their effect on the total airplane radius, as shown in figure 8. Airplane radius is shown as a function of sea-level compressor pressure ratio. The airplane was hydrogen-fueled and cruised at a Mach number of 4.0 with a target altitude of 95,000 feet. The pressure ratios shown on the abscissa represent those obtained by using two-, three-, or four-stage compressor designs. Radius has been normalized to the value obtained for the three-stage engine. Thus a relative radius of 1.0 is indicated at a pressure ratio of 2.3. The engines all had maximum turbine-inlet temperatures of 1900° R and cruised at optimum afterburner temperature, which was near 3000° R in all cases. From figure 8 it appears that three- or four-stage compressor designs are best for the Mach 4.0 mission. This same result was obtained for JP and EDB fuels, even though airplane and altitude requirements were much different with the higher-density fuels. For subsequent turbojet analyses, a three-stage compressor is used.

Turbine-inlet temperature: The effect of turbine-inlet temperature on relative radius is presented in figure 9. The airplane was similar to the one investigated in figure 8, and the engine had a three-stage compressor. Radius is normalized at 1.0 for a turbine-inlet temperature of 1900° R.

The important aspect of this curve is its flat slope at high values of turbine-inlet temperature. At cruise, the low-pressure-ratio turbojet is very similar to a ramjet; therefore, the only purpose of a high turbine-inlet temperature is to drive the compressor. With the low-pressure-ratio compressor selected, modest turbine-inlet temperatures are adequate. This engine had a turbine centrifugal stress of about 30,000 psi; consequently, even with good materials, 1900° R is near the maximum temperature that could be used without turbine cooling. Severe turbine-cooling problems would be encountered at the highest temperatures shown in figure 9, especially in view of the high-temperature environment in which the entire engine is immersed. Since radius increases are only about 13 percent at the highest temperature, the uncooled turbine appears to be a good selection. Better transonic inlet characteristics would reduce the importance of high turbine-inlet temperatures even more.

[redacted]

Selected design. - As a result of studying the component problems and the cycle variables of the low-pressure-ratio turbojet engine, a particular design was arrived at that appears suitable for the all-supersonic Mach 4 mission under consideration. A layout of this engine is presented in figure 10. The inlet, outlet, and afterburner are the largest engine components, and the gas-generator section is rather small by comparison. The engine has a three-stage compressor and a single-stage high-flow uncooled turbine. The burners illustrated are suitable for EDB or hydrogen. Use of JP fuel would require burners over twice as long, with a consequent increase in engine weight.

The inlet is a two-cone axisymmetric design. Simple geometry variation could be included, such as a translating forward spike to reduce transonic additive drags. The outlet is a variable-convergent, fixed-divergent ejector nozzle. Nozzle secondary air is obtained from compressor bleed; and nozzle tertiary air, which is ducted to the perforated divergent section, is obtained from the boundary-layer scoop at the inlet shoulder.

The layout also includes a representation of a cooling-air heat exchanger. Compressor discharge air is bled off along the outer circumference of the inlet diffuser of the primary combustor. This simplifies the diffuser problem and saves some diffuser length. Part of this compressor bleed is ducted to a heat exchanger located at the outer circumference of the turbine rotor. If hydrogen fuel is used, the cold side of the heat exchanger can be supplied with a portion of the engine fuel flow. Part of the cooled bleed air is diverted to the engine bearings, and the rest is introduced into the afterburner liner to cool the afterburner shell and the variable convergent nozzle.

The weight of this engine would be about 65 percent greater than the weight of a comparable ramjet engine. Control requirements are similar to those encountered in present-day turbojets and can be met by existing techniques. The turbojet of figure 10 is not a good subsonic engine. Best efficiency at Mach 0.9 is only about 70 percent as high as the efficiency obtained by contemporary high-pressure-ratio turbojets. But the engine appears to have adequate transonic thrust margins and is well suited to the all-supersonic Mach 4 mission under consideration. It has conventional components and could be developed in a minimum time compared with the development time for the other cycles to be considered. It is an attractive solution to the problem of flight at Mach 4.

Besides the turbojet engine, a variety of other gas-turbine cycles has been proposed for Mach 4.0 flight. An investigation of these engines together with their many variations revealed that a number of them are suitable for a Mach 4.0 mission. The investigations also revealed a strong similarity between these engine types. As a result of this similarity, only three of the cycles are considered in detail here. In de-

[redacted]

scribing the engines it will be apparent that the principal difference between them lies in the method of work extraction used to obtain the power needed to drive the fan. These differences in work extraction lead to different mechanical devices and determine the adaptability of the engines to various fuels.

Fuel-Rich Turbofan

A number of turbofan engines suitable for a Mach 4 mission were investigated. One interesting variation that will be discussed is the fuel-rich turbofan. In contrast to the turbojet, the fuel-rich turbofan obtains shaft work from essentially a fuel-driven turbine. As a result, this cycle is of interest only when hydrogen is used as a fuel.

A representative layout of the fuel-rich turbofan is shown in figure 11. The engine contains all the elements of a conventional turbofan: that is, a fan that compresses the engine airflow, a bypass duct that delivers the fan air to the afterburner, and a separate compressor-turbine unit that drives the fan. The cycle works as follows: at the fan exit, about 10 percent of the engine airflow is bled off into a second compressor, compressed, and delivered to a combustor. Here the engine fuel flow is heated by fuel-rich combustion with the compressor air. The resulting hydrogen-rich gases are expanded through turbines that drive both the compressor and the fan. These fuel-rich gases are then diverted to the afterburner where they provide the fuel for combustion. As is apparent from figure 11, the compressor and turbines for this engine are small in diameter compared with the fan. In order to achieve acceptable wheel speeds on these components, a twin-spool version was assumed. The inner spool consists of the compressor and a single-stage turbine, while the outer spool consists of the fan and a two-stage turbine.

The cycle variables for this engine were studied, and for a Mach 4.0 application the following values were selected: a two-stage fan with a takeoff pressure ratio of 1.7, a four-stage compressor with a takeoff pressure ratio of 3.0, and a maximum turbine-inlet temperature of 2500° R.

Many of the component problems in the fuel-rich turbofan are similar to those of the turbojet. For example, the fan and compressor have the same problems as the turbojet compressor, and a similar approach could be applied to their solution. The required fuel-pump pressures and weight flows are comparable to those of the turbojet. The primary combustor is not conventional, of course, because it is fuel-rich, but experimental work has already been done at the NACA Lewis laboratory demonstrating that this is feasible.

The afterburner problem, however, is more difficult. Current experience with hydrogen indicates that achieving short afterburner lengths

and high combustion efficiencies requires using a multiplicity of fuel-injection points and high fuel-injection velocities, which result in a high-pressure-drop fuel-distribution system. The fuel-rich cycle, on the other hand, requires a low-pressure-drop fuel-distribution system in order to avoid high back pressures on the turbine that would reduce the turbine work output. No solution to the problem of achieving an effective low-pressure-drop afterburner fuel-distribution system has as yet been demonstrated.

Another difference between the fuel-rich turbofan and the turbojet lies in the turbines. Since only 10 percent of the engine airflow passes through the turbines of the fuel-rich turbofan, the turbine diameters are small compared with the turbojet turbine. However, with this low flow the turbine work requirement will be high - over 200 Btu per pound of turbine flow. To keep the number of turbine stages to a minimum requires taking advantage of the high sonic velocities of the hydrogen-rich turbine gases by using high jet velocities in the turbine design. For the fuel-rich turbofan, these considerations will lead to turbine designs utilizing low values of blade- to jet-speed ratio; and experience indicates a lower efficiency for turbines of this type.

The weight of the fuel-rich turbofan is comparable to that of the turbojet. However, since this is a fuel-rich cycle, the control problems for this engine will be more difficult than for a turbojet. In summary, the use of a fuel-rich turbofan at Mach 4.0 appears feasible. However, the engine will be substantially more complex than a turbojet, and it will create a number of new and difficult development problems.

Hydrogen Expansion Engine

A third powerplant considered for the Mach 4.0 mission was a hydrogen expansion engine. One variation of this type of engine is shown in figure 12. The engine airflow is compressed by the two-stage fan. Most of the air then flows through a bypass duct to the afterburner. A small amount of the fan exit air enters the primary combustor and burns fuel-rich with hydrogen. The resulting fuel-rich combustion products pass through the hot side of the heat exchanger and then mix with additional hydrogen and the main body of bypassed air. In the afterburner, final combustion occurs and the hot gas expands through the exhaust nozzle to produce thrust.

The hydrogen starts out as a liquid in the fuel tank. First it is pumped to a very high pressure and then it is used as a heat sink for various cooling requirements. By the time it reaches the cold side of the heat exchanger, the hydrogen is a gas. After being heated, the high-pressure high-temperature gas is ducted to a small three-stage turbine which drives the fan through a suitable gear. The hydrogen from the turbine exit is then injected into the primary combustor.

A study of the hydrogen expansion engine has indicated that it is a suitable powerplant for the Mach 4.0 mission and that numerous problems would be encountered in developing such an engine. Although there are no moving parts in the heat exchanger, a number of development problems might be anticipated because of large temperature gradients throughout and because of very high pressure on the hydrogen side. The fuel-pump problems might be an order of magnitude more difficult than those for the turbojet because of the very high pressures required by the hydrogen turbine. Finally, the control of the hydrogen expansion engine is expected to be more complex than the control of the turbojet.

The hydrogen expansion engine shown in figure 12 was estimated to be about 10 percent heavier than the turbojet engine. The hydrogen expansion engine could be used in performing the Mach 4.0 mission, but the development problems appear to be many and difficult.

Air-Turborocket Engine

A fourth possible Mach 4.0 powerplant is the air-turborocket engine. Fuels considered for the turborocket drives in the past have included the monopropellants such as methyl acetylene, and many of the standard rocket propellant combinations. The arrangement considered here is the liquid-air turborocket (fig. 13).

In this engine, the cooling capacity of liquid-hydrogen fuel is exploited by using it to liquefy a sufficient quantity of air to serve as the oxidizer in the rocket combustion chambers. Liquid hydrogen is brought into the nacelle at high pressure and passed through the cold side of the air-liquefaction heat exchanger. The hydrogen then passes directly to the rocket combustion chambers.

The engine airflow is compressed by the two-stage fan. Most of the air then flows to the inlet of the afterburner. A small portion of the fan exit air is bled off into the heat exchanger where it is condensed and collected and subsequently pumped at high pressure into the rocket combustion chambers. Here, the air and hydrogen burn fuel-rich. The resulting combustion products expand through the turbine which drives the fan through a suitable gear. The fuel-rich turbine exhaust then passes into the afterburner for final combustion with the main body of bypassed air and additional hydrogen as required.

Many elements of this engine have development and application problems similar to those of the fuel-rich turbofan and hydrogen expansion engines. An additional complication is icing in the air-liquefaction heat exchanger at low altitudes where a significant amount of water is present. Thus far, no practical solution to the icing problem has been suggested.

[redacted]

The liquid-air turborocket engine appears feasible as a Mach 4.0 engine, provided its difficult development problems can be mastered.

Gas-Turbine Summary

The four cycles studied are quite similar once they are optimized, or nearly optimized, for the long-range Mach 4.0 mission. A study of the engines powering suitable airplanes revealed that the best target altitude for hydrogen fuel is about 95,000 feet. With an airplane designed for this altitude, the thrust-to-drag ratios are similar for all four engine types, the minimum being about 1.5 to 1 at Mach 1.5. For an airplane of 300,000-pound gross weight, six gas-turbine engines would be required, each with a fan or compressor diameter of about 39 inches.

A comparison of the range capability of the four engine types is shown in figure 14 as relative radius against target altitude for hydrogen-fueled airplanes. Radius is normalized at the 95,000-foot turbojet point. Maximum differences are about 30 percent at the extremely high altitude where radius capability is limited. At the more interesting altitudes, 90,000 to 95,000 feet, total spread is only 10 percent.

The inlets assumed for the calculations of figure 14 were simple axisymmetric designs with a minimum of geometry variation used to obtain some reduction in transonic additive drag. Total-pressure recovery at Mach 4.0 cruise was 0.57, which was obtained by assuming a 2-cone inlet favorably located in the pressure field of the airplane wing. The divergent portion of the exhaust nozzle was assumed fixed so that overexpansion losses were encountered at transonic conditions. If inlets and exits with better off-design performance were provided, the spread among the four engine types would be even less than that shown in figure 14. This is true because off-design climb performance was an area in which some engine differences were apparent, and these differences become less important as inlet and exit performance improves.

From a consideration of radius capability and development problems, the low-pressure-ratio turbojet engine shows the greatest promise for the long-range Mach 4.0 mission. Some range advantage can be demonstrated for other engines, especially at high altitude, but the advantage is not large and can be expected to decrease as inlet and exhaust-nozzle technologies improve. The turbojet is by far the simplest engine and would require the least development effort. It is also most adaptable to a wide variety of fuels.

The effect of cruise Mach number on turbojet radius is shown in figure 15 for airplanes powered by a family of turbojet engines. At Mach 3, engines with five-stage compressors and two-stage turbines were assumed; at Mach 4.0, engines with three-stage compressors and one-stage

[redacted]

turbines were used; and at Mach 4.5, similar engines were analyzed except that turbine and compressor cooling were assumed. Target altitude varied from 75,000 feet at Mach 3 to 100,000 feet at Mach 4.5. Radius, which is normalized at Mach 4.0, continuously decreases as cruise Mach number increases. For Mach 4.5 cruise, the engine is greatly complicated by compressor and turbine cooling. Moreover, climb fuel becomes a major portion of total fuel. These considerations suggest that some sort of staging will be necessary to obtain long range at Mach numbers higher than about 4.0.

RAMJET ENGINE

When staging is considered to obtain long range at cruise Mach numbers above 4.0, the conventional ramjet appears to be an attractive powerplant. The mission for the ramjet is different from the mission for the gas-turbine engines in that only missiles are considered. This mission is considered because staging is required and because the second stage is relatively small and expendable. For this system, range is the index of performance rather than radius. Because the missile design does not have to be compromised for the presence of a crew, savings can be effected; on the other hand, flexibility is sacrificed when the man is removed from the airplane. In this study, no attempt is made to compare these two weapon systems. Rather, ramjet capabilities are examined as simply another way of flying long distances at high speed. Cruise Mach numbers of 5 to 9 are considered, because it appears that the ramjet has most to offer in this speed region.

The basic ramjet engine was assumed to be installed in a system with a combined missile-plus-rocket-booster weight of 150,000 pounds including a payload of 10,000 pounds. A fuselage engine installation is assumed because it results in longer range than the nacelle type. Although several other fuels such as diborane and liquid methane were examined, the results are presented only for hydrogen because of its superior cooling and performance characteristics in the Mach number range considered.

The effect of nozzle expansion on range is shown in figure 16 as relative range against the ratio of nozzle-exit static pressure to ambient static pressure. Performance is for a cruise Mach number of 7 and a target altitude of 110,000 feet. Chemical equilibrium was assumed through the exhaust nozzle. As would be expected with the fuselage installation, maximum range occurs when the exhaust nozzle is fully expanded. The ratio of exit to throat area for maximum range is about 55.

In figure 17, the effect of burner equivalence ratio on ramjet relative range is presented for Mach numbers of 5, 7, and 9. Chemical equilibrium was assumed to exist in the exhaust nozzle, and each Mach

number curve is for optimum operating altitude. In general, optimum or nearly optimum range is attainable over a wide range of equivalence ratios. For example, at Mach 5 it is possible to operate at equivalence ratios from 0.4 to 1.0 with only a 5-percent variation in range.

Figure 17 also shows that, as flight Mach number increases, the decrease in range with equivalence ratios greater than 1.0 becomes less. Thus, if additional cooling capacity is required at the higher Mach numbers, it may be obtained with only a small sacrifice in range by operating fuel-rich. For example, by operating at Mach 9 with an equivalence ratio of 1.25, an additional 25-percent cooling capacity is available and range is only 10 percent less than optimum.

The fact that range decreases with Mach number is a result of holding the missile-plus-booster weight constant. If missile weight were held constant, the range would be about the same at each Mach number.

One of the greatest uncertainties involved in ramjet-powered flight is concerned with the expansion process in the exhaust nozzle; the question is whether there is sufficient time for chemical equilibrium to exist or whether all or part of the process is frozen. A rough calculation made for the Mach 7 engine indicated that there was sufficient time for vibrational equilibrium to exist, but the calculation was inconclusive with respect to reassociation. It has been estimated that the actual process in the exhaust nozzle is closer to that for chemical equilibrium than for frozen composition; but at the present time no reliable or accurate data exist.

The effect of expansion processes on ramjet-engine efficiency is shown in figure 18, in which efficiency is plotted against flight Mach number for the two processes of complete chemical equilibrium and frozen composition. The latter process assumes no reassociation but does allow for specific heat (vibrational) adjustment with temperature. Two curves are shown for the frozen-composition process. The upper one is for the optimum altitude at each Mach number, and the lower one is for altitudes 20,000 feet higher than optimum. Although the differences in the two processes are small at Mach 5, both the differences in the two processes and the effect of altitude on the frozen-composition process increase considerably with increasing Mach number. This means that, if ramjets are to be used at Mach numbers over 5, it is essential that data be obtained which will indicate the nature of the actual process. Work in this area is being conducted at the Lewis laboratory at the present time.

An indication of the general performance trends of the ramjet propulsion system with Mach number is presented in figure 19. Specific impulse and over-all efficiency are plotted against flight Mach number. Although specific impulse decreases with Mach number, its value at Mach 9.0 is still over 2000 and is thus superior to that of a rocket. The

decrease in specific impulse with Mach number is largely a result of the increased amounts of dissociation and the resulting inability to get an appreciable temperature rise across the combustion chamber.

The over-all efficiency, on the other hand, increases slightly as flight Mach number increases from 5 to 9. The over-all efficiency does not peak below Mach 9 because of the fuselage installation, which allows full or nearly full expansion in the exhaust nozzle. Naturally, if chemical equilibrium is not achieved in the exhaust nozzle, the performance at the higher Mach numbers will be below that indicated. However, if the expansion process is near that for chemical equilibrium, thrust and fuel consumption will not limit the performance attainable; the limits undoubtedly will be set by the cooling considerations.

A Mach 7 ramjet engine designed for a fuselage installation is shown in figure 20. An engine such as this weighing about 1500 pounds could power a missile of about 30,000 pounds. Exhaust-nozzle-exit diameter would be about $7\frac{1}{2}$ feet, and the divergent section would be about 7 feet long. This nozzle should be capable of achieving a velocity coefficient of about 0.96. The combustion chamber, 2 feet in length and $1\frac{1}{2}$ feet in diameter, would provide a burner-inlet Mach number of about 0.3. The double-wedge external compression inlet, which is not quite as long as the exhaust nozzle, would have an over-all kinetic-energy efficiency of slightly over 90 percent. With the $5\frac{1}{2}$-atmosphere pressure and the 4000° R temperature at the inlet to the combustion chamber, a combustion efficiency of 95 percent should be easily obtained with hydrogen fuel. All parts of the engine would be jacketed and fuel-cooled. It appears possible to build such an engine within the limits of present-day technology.

FUEL-RICH RAMJET ENGINE

The thrust of the conventional ramjet drops rapidly as Mach numbers of 10 are approached. This thrust loss can be eliminated by large increases in fuel flow, which leads directly to the fuel-rich ramjet cycle. The objective here will be simply to demonstrate high thrust capability for this engine, together with the possibility of reasonable specific impulse over a large Mach number range.

The conventional and fuel-rich ramjets are contrasted in figures 21 and 22. Enthalpy per pound of air is plotted against engine axial station for a conventional Mach 3 ramjet (fig. 21) and for a fuel-rich Mach 17 ramjet (fig. 22). The kinetic energy of the Mach 3 air is converted to about 170 Btu per pound in the diffuser. Fuel is added in the combustor, and the heat released increases the enthalpy to about 1120 Btu

per pound. Expansion of these gases then converts the enthalpy back to kinetic energy. The net thrust attainable from this high-velocity gas is shown in the bar graph as the difference between the exit and inlet momentum. For conventional-ramjet operation, the increased mass at the exit contributes only slightly to the thrust.

The fuel-rich ramjet (fig. 22) operates on the same cycle. The stagnation enthalpy for Mach 17 operation is 33 times the Mach 3 value. The heat of combustion is essentially the same because no more than the stoichiometric amount of fuel can be burned. For this example, 0.58 pound of fuel was used per pound of air. The excess fuel, about 0.55 pound per pound of air, reduces the combustor temperature to about 3800° R. The combustion gases expand to ambient pressure with an increase in kinetic energy. The net thrust shown by the bar graphs results more from the increased mass flow than from the increased velocity. In actual practice, the jet velocity could be lower than the inlet velocity because of incomplete expansion and internal losses. Thus, in actual practice the net thrust is even more dependent on the increased mass flow.

To help evaluate the fuel-rich ramjet, a mission of boosting an airplane from a Mach number of 2 to about 18 was considered. The engine was operated lean at the lower Mach numbers but rich at Mach numbers higher than 7. Hydrogen was selected as the fuel, although other fuels may be used. The fuel-air ratios were chosen primarily on the basis of highest impulse, but sufficient fuel was used to provide cooling of the internal and external parts of the airplane-engine combination. Also, sufficient fuel was used to keep the combustor temperatures below the point where severe dissociation and recombination problems are encountered. Maximum allowable acceleration forces (tentatively selected as 4 to 7 g's) were obtained, thus demonstrating the high thrust capabilities of the fuel-rich ramjet engine.

The configuration selected for this preliminary analysis is shown in figure 23 along with engine performance. The flight vehicle is essentially a two-dimensional wedge with fixed-area normal-shock inlets located at the rear of the structures. At high Mach numbers, the inlets captured most of the high-pressure air generated by the wedge. The exhaust exit area was fixed, while the exhaust throat area was allowed to vary. An initial wing loading of 100 pounds per square foot was assumed in calculating induced drag.

The performance curves of figure 23 are impulse as a function of Mach number. The top curve is the net internal impulse based on the exit momentum minus the inlet momentum. The lower impulse curve is based on engine thrust minus frictional, wave, and induced drag of the aircraft and engine. Because this device must climb rapidly to avoid excessive internal pressure, a gravity force associated with angle of climb is also included in the lower curve. Very high impulse

characterizes the low Mach number range. Impulse decreases as Mach number increases up to around Mach 12, where the curves level off. At Mach 18, the net impulse is about 300 seconds, and impulse including associated drag is about 200 seconds.

Before the fuel-rich ramjet can be compared with other propulsion devices such as a rocket, the application must be considered. If the mission is boosting a glider where the engine can be installed in the large glider fuselage, net impulse values should be considered for comparison. If the application is a single stage of a satellite boosting system, the lower impulse values, which account for propulsion-system drag, are more significant.

The fuel-rich ramjet is an air-breathing powerplant whose performance is potentially attractive for flight Mach numbers up to 18. It appears to be technically feasible, but more work is needed to indicate its practicality.

SUMMARY

Air-breathing engines have been considered over a wide Mach number range from 4 to 18. For flight at Mach 4, several cycles can be considered. The best one appears to be the low-pressure-ratio turbojet, which is competitive on a performance basis and could be developed in a minimum amount of time using existing techniques. It is also most adaptable to a variety of fuels.

From Mach 5 to 9, the "conventional" ramjet appears to be a feasible powerplant. Its performance is excellent, and the cooling problems appear capable of solution, at least when hydrogen fuel is considered.

The fuel-rich ramjet may extend the usefulness of air-breathing engines to Mach numbers as high as 18. It offers the possibility of high thrust capability and, at the same time, high impulse over most of its Mach number range.

EFFECT OF MACH NUMBER ON ENGINE THRUST

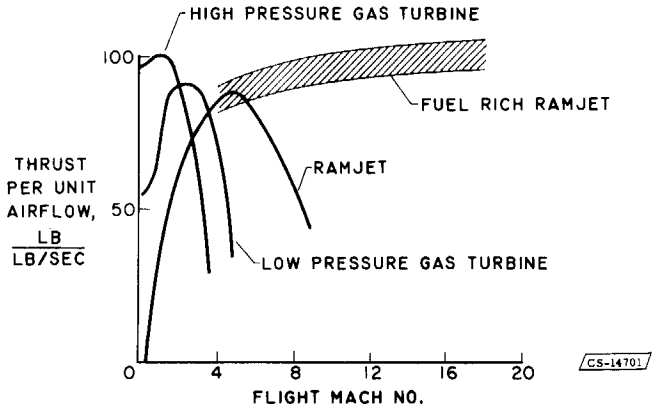

Figure 1

GENERALIZED ENGINE SCHEMATIC

TURBOJET
FUEL RICH TURBOFAN
HYDROGEN EXPANSION
LIQUID AIR TURBOROCKET

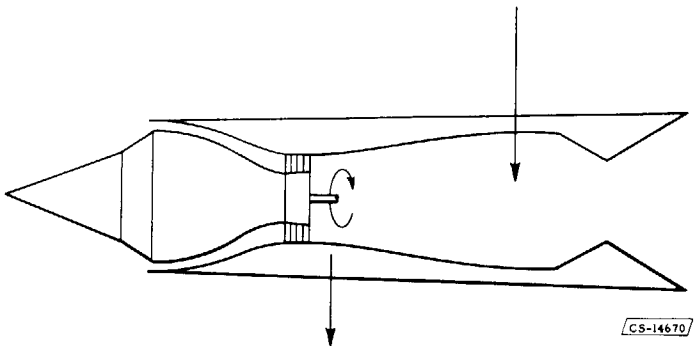

Figure 2

3-STAGE COMPRESSOR MAP

MACH NO., 4 TURBOJET ENGINE

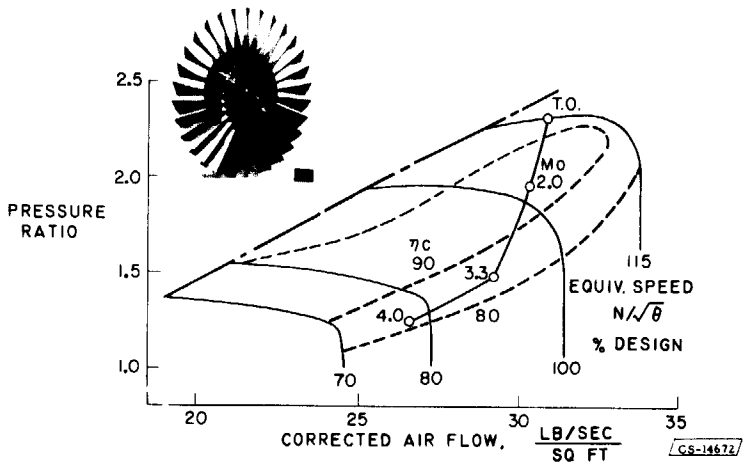

Figure 3

LOW-CAMBER TURBINE BLADE

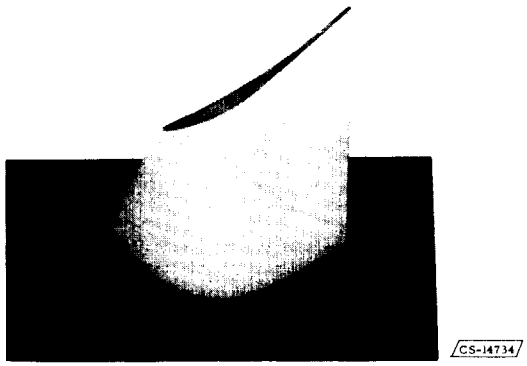

Figure 4

DESIGN SPEED PERFORMANCE
OF EXPERIMENTAL TURBINE

C_T/C_R = 0.79 A_T/A_R = 0.33

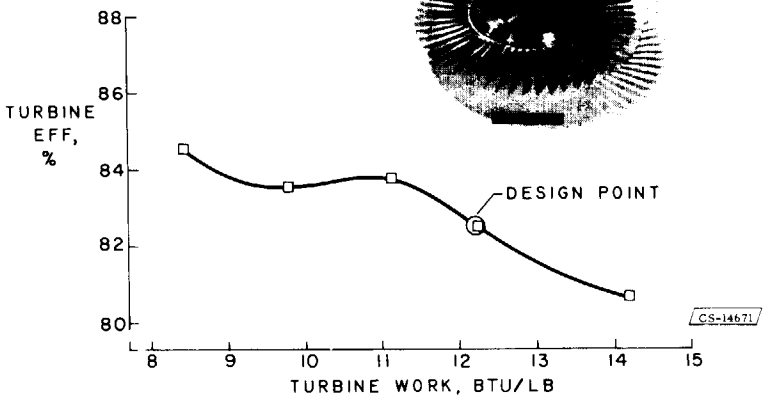

Figure 5

TURBOJET AFTERBURNER CONDITIONS

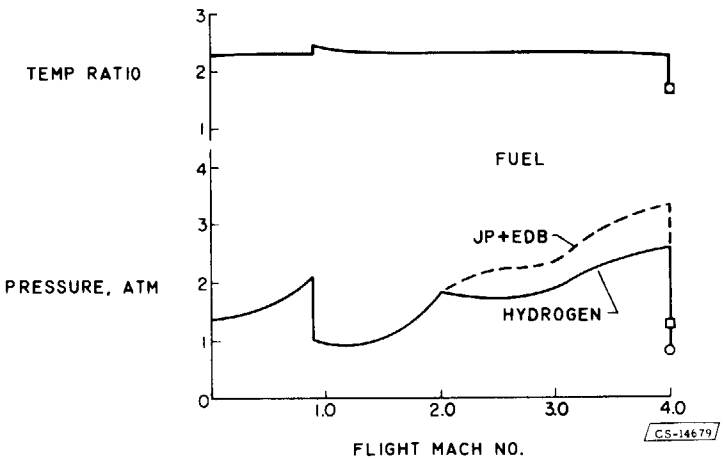

Figure 6

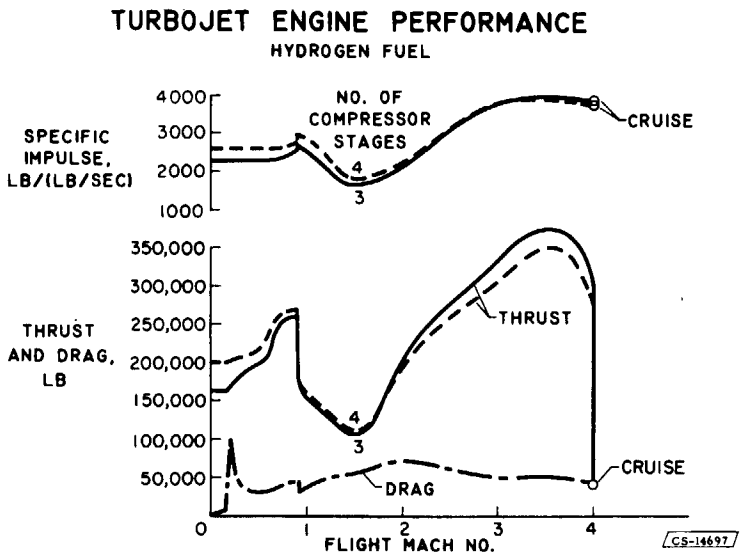

Figure 7

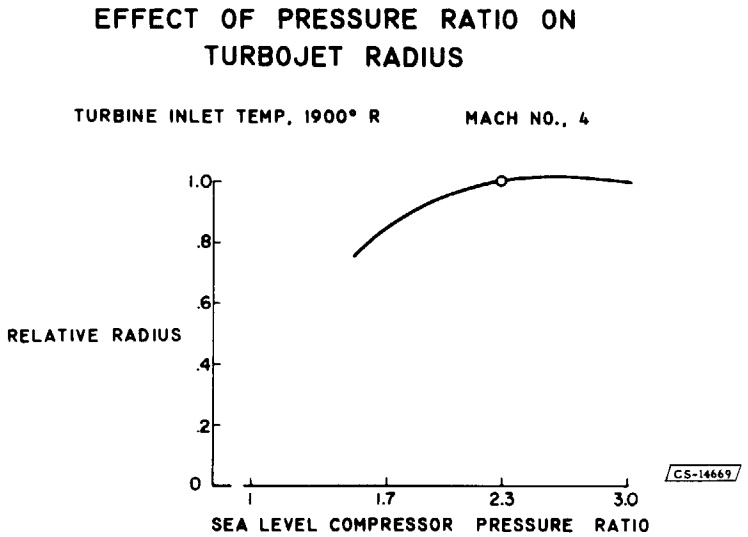

Figure 8

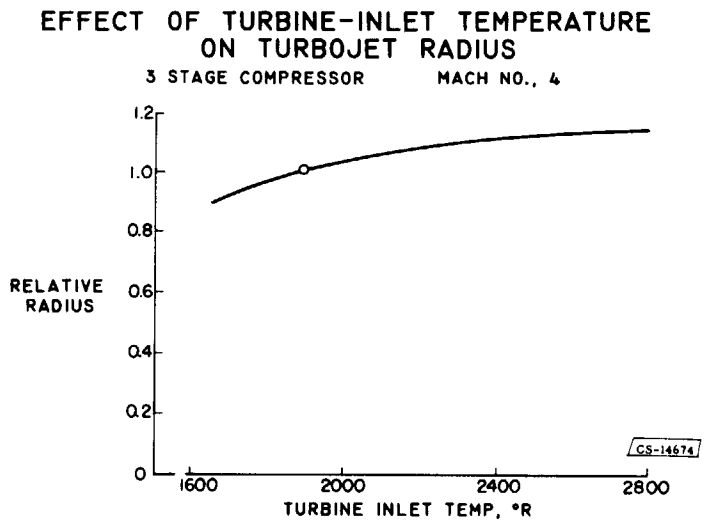

Figure 9

TURBOJET ENGINE

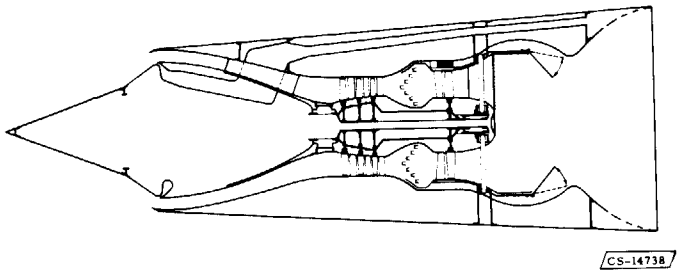

Figure 10

FUEL-RICH TURBOFAN ENGINE

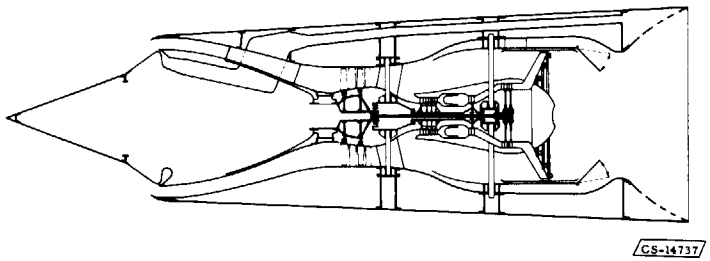

Figure 11

HYDROGEN EXPANSION ENGINE

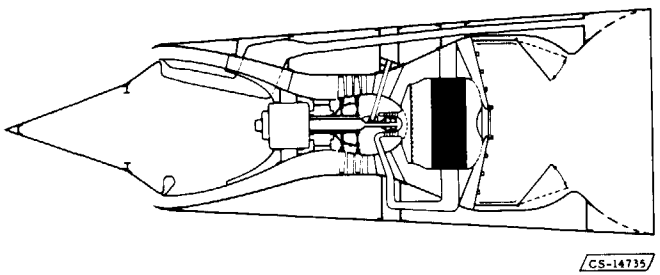

Figure 12

LIQUID-AIR TURBOROCKET ENGINE

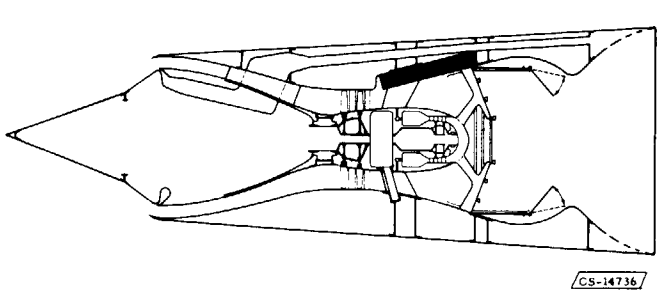

Figure 13

COMPARISON OF ENGINES
WITH SIMPLE INLET AND EXIT
HYDROGEN FUEL MACH NO., 4

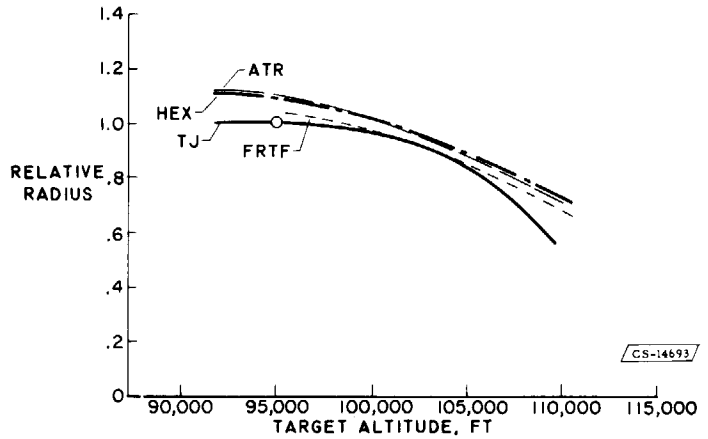

Figure 14

EFFECT OF CRUISE MACH NUMBER
ON TURBOJET RADIUS

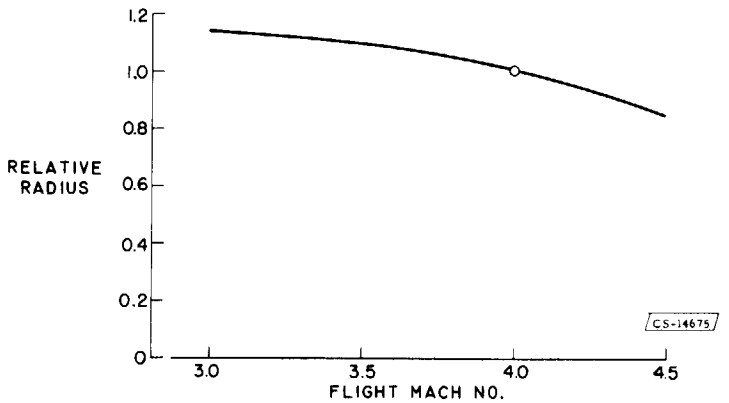

Figure 15

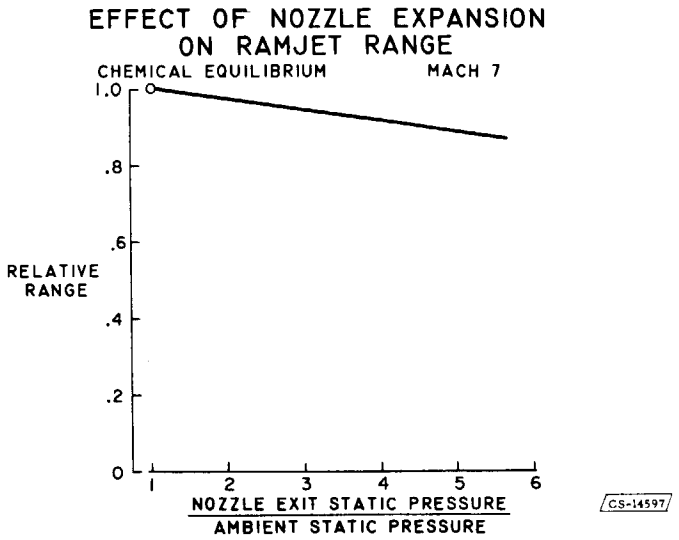

Figure 16

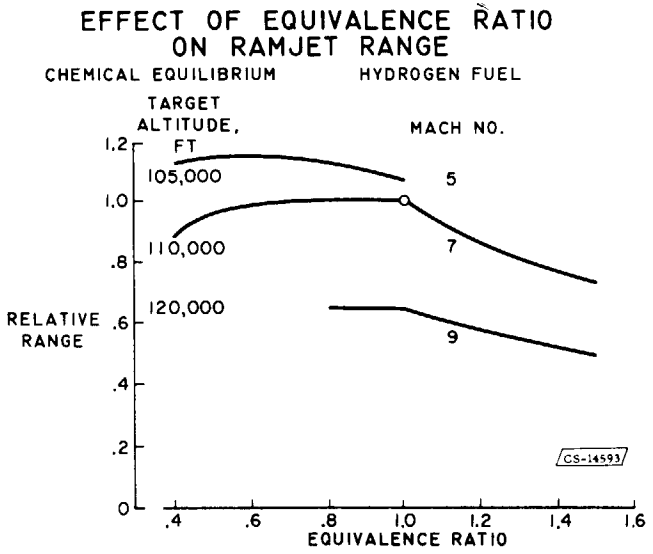

Figure 17

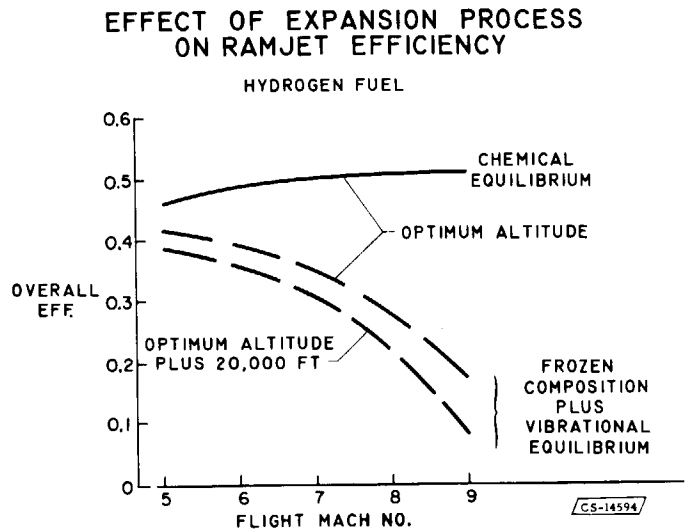

Figure 18

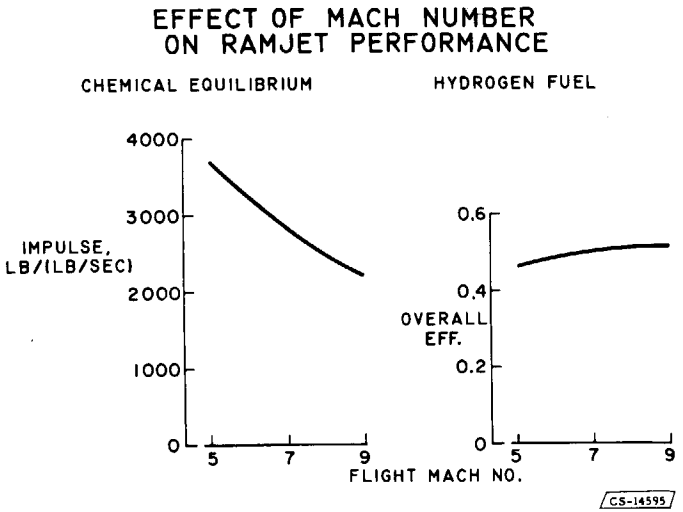

Figure 19

RAMJET ENGINE

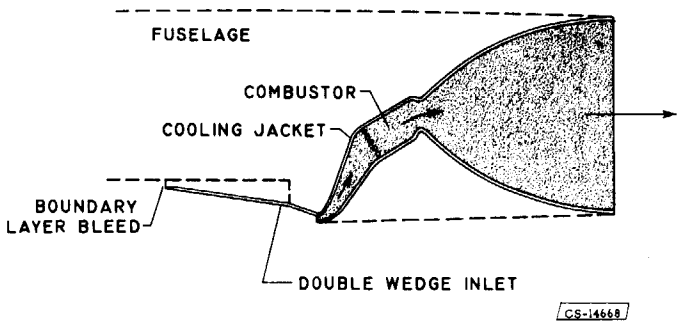

Figure 20

CONVENTIONAL RAMJET

HYDROGEN FUEL-AIR RATIO ~ 0.02 MACH NO., 3

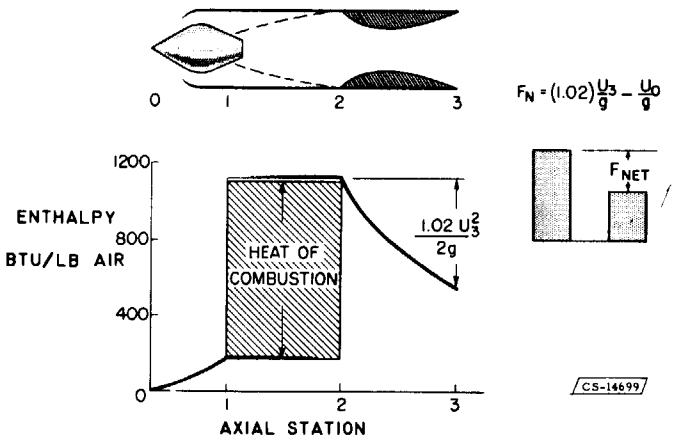

Figure 21

HYPERSONIC FUEL-RICH RAMJET

HYDROGEN FUEL-AIR RATIO, 0.58 MACH NO. 17

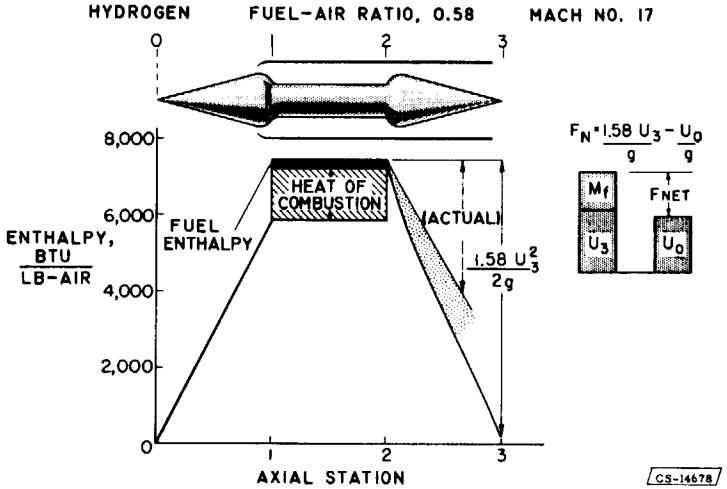

Figure 22

PERFORMANCE OF FUEL-RICH RAMJET

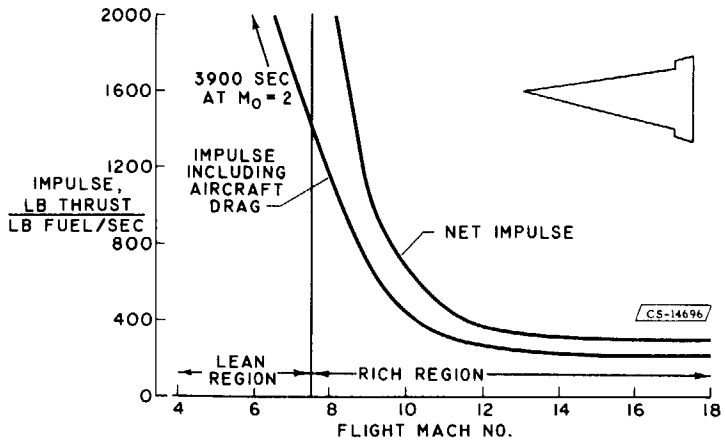

Figure 23

4. CONFIGURATIONS CONSIDERATIONS

By Roger W. Luidens, John H. Disher, Murray Dryer,
and Thaine W. Reynolds

This paper provides a bridge between the preceding discussions of engines and the following discussion of the range capabilities of airplanes. Hence, consideration is given to the aerodynamics of configurations in terms of their lift-drag ratios and the effect of the propulsion system on the configuration. Finally, some factors affecting airframe structural weight are discussed.

The range equation is as follows:

$$\mathscr{R} = IV \frac{L/D}{1 - \left(\frac{V}{V_S}\right)^2} \ln \frac{1}{\frac{W_e}{W_G} + \frac{W_s}{W_G} + \frac{W_p}{W_G}} \qquad (1)$$

where

I specific impulse

V velocity

V_S satellite velocity

W_e engine weight

W_s structural weight

W_p payload weight

W_G gross weight

At a specified altitude,

$$\frac{W_e}{W_G} \approx \frac{1}{L/D}$$

The lift-drag ratio L/D is important because it affects the range directly and it also affects the range through the engine weight W_e. It affects engine weight in such a way that increasing lift-drag ratios

[redacted]

decrease engine weight. The airplane structural weight W_s enters the range equation in the same manner as the engine weight. Decreasing engine and structure weights increase range.

Consideration will first be given to configuration L/D. The drag of an airplane may be broken down in several ways. One way is (1) friction drag, (2) pressure drag at zero lift, and (3) drag due to lift. Another classification might be (1) fuselage drag, (2) wing drag, and (3) engine drag. Unfortunately, it is not possible to consider these items as isolated topics. Therefore, although each of the items mentioned is discussed, it is always discussed in relation to the over-all problem of achieving long range.

The lift-drag ratios considered today are much higher than those considered several years ago. This fact is related in a large part to a very fundamental effect - airplane size.

Two schematic airplanes, one with a gross weight of 20,000 pounds and the other with a gross weight of 500,000 pounds, are shown in figure 1. The equation at the top of the figure is for the zero-lift drag coefficient of the airplane based on wing area $C_{D,0}$. It is equal to the zero-lift drag coefficient of the wing $C_{D,0,W}$ plus the zero-lift drag coefficient of the body based on the body area $C_{D,0,b}$ times the ratio of body area to wing area A_b/S_W. The latter ratio is necessary to make the equation consistent. The so-called "square-cube law" states that, if the linear dimensions of a body are increased, the areas will increase as the square of the linear dimension and the volume will increase as the cube. For example, if the size of the small airplane is doubled, the wing area will be four times as big as the original area, and the volume will be eight times larger than the original volume. If it is assumed that the two airplanes shown in the figure have the same wing loading, scaling up the small configuration will result in more volume in the body than needed. In addition, there is relatively more usable volume in the wing of a large airplane. This means that the ratio of body area to wing area can be reduced; and therefore the last term in the drag equation is reduced.

The airplane size also reduces the coefficients in the drag equation. Figure 2 is the familiar plot of the variation of mean skin-friction coefficient with free-stream Reynolds number. This particular curve is for a turbulent boundary layer at Mach 4. The coefficient that might be expected for a 20,000-pound airplane is about 0.0013, and for a 500,000-pound airplane is about 0.0010. The larger airplane has a lower friction coefficient.

These two effects, reduction of skin-friction coefficient and reduced body drag coefficient as a result of increased size, have been combined

[redacted]

in a calculation of maximum lift-drag ratio as a function of gross weight (on a log scale) in figure 3. The 20,000-pound airplane has a maximum L/D of about 6.0, whereas the larger airplane has a value of about 8.5. By increasing the gross weight still further, a point is reached where all the necessary volume is readily available in the wing, and an even higher L/D results.

The flight Mach numbers of interest have also increased over the last several years. Figure 4 is a plot of friction coefficient against Reynolds number for flight Mach numbers of 2, 4, and 7. Increasing M_O also tends to decrease the friction coefficient. However, there is another factor that influences $(L/D)_{max}$. One form of the equation for maximum L/D is as follows:

$$\left(\frac{L}{D}\right)_{max} = \frac{1}{2}\sqrt{\frac{dC_L/d\alpha}{C_{D,O}}} \qquad (2)$$

Besides the drag $C_{D,O}$, the lift-curve slope $dC_L/d\alpha$ also enters into the determination of $(L/D)_{max}$. In general, the lift-curve slope decreases more rapidly with increasing Mach number than the drag decreases. The net result is that $(L/D)_{max}$ generally decreases somewhat with increasing M_O. This effect will be evident in several of the later figures.

The drag of an airplane is also affected by the nature of the boundary layer, whether it is turbulent or laminar. Figure 5, which shows friction coefficients for laminar and turbulent boundary layers, indicates that, if the boundary layer is laminar, the skin-friction coefficient is considerably lower than if the boundary layer is turbulent. This decrease in the friction coefficient may be reflected in a considerable increase in the lift-drag ratio. Since this is the case, one should look into the probability of obtaining laminar flow at the flight conditions being considered.

Figure 6 shows a band of Reynolds numbers for a 60-foot-long surface calculated for the particular altitude and Mach number variations shown in the upper right corner of the figure. The points plotted are experimental values and are some of the highest Reynolds numbers at which laminar flow has been observed in free flight. The arrows on the points indicate that the flow, in fact, was laminar at the last measuring station on the body, and that transition to turbulent flow would have occurred at higher values of Reynolds numbers than those indicated. The fact that the range of Reynolds numbers of interest may be below values at which laminar flow has been observed would indicate that a good chance of obtaining laminar flow exists in these cases.

However, Reynolds number is not the only criterion for determining the transition from laminar to turbulent flow. The effects of some of

[redacted]

the additional factors that influence boundary-layer transition are shown in figures 7 and 8. The Reynolds number of figures 6, 7, and 8 is based on length from the stagnation point of the body and on free-stream conditions. Figure 7 shows calculated transition characteristics for blunt-nosed bodies at Mach 5 (based on data of refs. 1 to 4 and theory of ref. 5), and figure 8 presents flight and wind-tunnel transition data for sharp-tipped bodies at Mach numbers of 3 to 5 (refs. 1 and 4). Both figures show the favorable effect of low wall to stream temperature ratios on increased transition Reynolds number. The unfavorable effect of surface roughness is shown by the decrease in transition Reynolds number at a given temperature ratio. Approximate values of average surface roughness for the "smooth" and "rough" data were 2 to 16 microinches and 200 microinches, respectively. The favorable effect of tip bluntness on increased transition Reynolds number is apparent. This effect is due to the lowering of Reynolds number and the increase of static temperature at the edge of the boundary layer, as discussed in reference 5. The size of the blunt tip required to achieve the favorable effect varies with model length and with stream conditions. When the nose of the body is blunted in order to enhance the chances for laminar flow, the added pressure drag due to bluntness must of course be weighed against the decreased friction drag. In addition, if the tip bluntness becomes too large, transition may occur on the tip itself; thus, the amount of tip bluntness must be carefully considered.

To illustrate the place of typical flight conditions in these curves, a flight condition for Mach 5 at 100,000 feet altitude with a 60-foot-long body at radiation equilibrium wall temperature is shown on the coordinates of figures 7 and 8. If the body is blunt tipped the flight condition lies in the laminar region for smooth bodies, but when roughness is considered it appears likely that turbulent flow would exist over much of the body. With a sharp-tipped body, the flight condition would be in the turbulent region even with smooth surfaces. In order for the flight condition to lie in the laminar region for the sharp-tipped body, the wall would have to be cooled well below the equilibrium temperature.

Additional adverse effects on laminar boundary layers are caused by control-surface-body or wing-body junctures and protuberances such as pilot canopies. The transition data shown are for bodies alone. The limited amount of data available indicate that early transition to turbulent flow is likely to occur aft of body-wing junctures.

The amount of wing friction drag can be large compared with the total drag for configurations with large wings. Therefore the amount of laminar flow that might be expected on a wing must be considered. Some experimental data in figure 9 show the effect of wing sweep on transition. The sketch defines the distance X_T where transition occurs perpendicular to the wing leading edge. The distance, shown as a fraction of the distance for a zero-sweptback wing, is plotted as a function of the angle of

[redacted]

sweep. The Mach 4 experimental data (ref. 6) agree quite well with the cosine-cubed of the sweepback angle. If highly swept wings (65° to 75°) are to be used, it appears very unlikely that significant runs of laminar flow can be expected.

The boundary-layer discussion may be summarized as follows. On some highly polished, slightly blunted research models, laminar flow has been observed to very high Reynolds numbers. But on a practical airplane that flys at angle of attack, has a pilot canopy and canard surfaces on the fuselage forebody, and has skin joints, or on a wing that is highly swept, long laminar runs seem improbable.

It is appropriate to discuss another point here. A hot, highly stressed structure such as the wing will probably develop a surface waviness. This waviness will generate a pressure drag that is not usually included in the form drag and is often charged to the surface drag. With this waviness condition, the drag chargeable to the surface can be larger than that calculated by assuming all-turbulent skin friction. (The Missions Studies paper (5) assumes all-turbulent boundary layer in calculations.)

Consider next the pressure drag, in particular as it relates to fuselage design. There are two philosophies about fuselage design. One is that the fuselage should house a given volume at the minimum cost in drag. If this is the point of view, the analysis shown on figure 10 may be made. The drag per fuselage volume is plotted against fuselage fineness ratio l/d. Increasing the fineness reduces the pressure drag but increases the friction drag because the wetted area increases. (A sphere, $l/d = 1.0$, has a minimum wetted area for given volume.) The sum of the friction and pressure drag reaches a minimum at l/d of about 25 in this example. From an engineering point of view, this minimum drag is essentially reached at l/d of 18 or 20. The airplane models with circular fuselages have finenesses of 18 and 20.

A second approach to fuselage design is to find the fuselage shape that will give the best airplane L/D. An example of the results from such an approach is shown in figure 11. In this example the fuselage volume and flight altitude are held constant. The lift-drag ratio is plotted against the width to height ratio of the fuselage and against the length over the equivalent diameter of fuselage. The upper curve is the L/D of the wing alone, which is 8.3. The point at $w/h = 1$ is for a circular nonlifting fuselage, and at this point L/D of the wing-body combination is 6.0. Carrying lift on the fuselage and widening it to make it a better lifting shape increases the L/D of the wing-body combination to a value approaching 7.0. For $w/h = 4.0$, the effect of equivalent fineness is shown on the right side of figure 11. The best l/d, about 16, is somewhat less than the l/d of about 25 for the previous analysis.

[redacted]

There are other ways of generating lift from the fuselage. The Ames configuration uses a half cone under an arrow wing. Antonio Ferri discusses still another design approach that might be applied to a fuselage in the Journal of the Aeronautical Sciences for November 1957.

The choice of design approach is related in part to the fuel-tankage problem, as will be discussed shortly. The idea here is that, for a configuration design to have the highest aerodynamic efficiency, all the components of the airplane must do their share of the work. The fuselage generates a pressure and friction drag; it should also generate its share of the lift.

The next drag term to be examined is the drag due to lift, illustrated in figure 12. There are ways to minimize this drag term. In supersonic flow with a conventional supersonic airfoil at angle of attack (illustrated as a flat plate in the upper left corner of fig. 12), it is evident that the resultant force vector for the airfoil lies perpendicular to the surface and that a drag direction force D_i equal to the resultant force R times the sine of the angle of attack α exists. In subsonic flow, illustrated at the lower left of the figure, camber and a rounded leading edge on an airfoil make it possible to take advantage of leading-edge suction and thus bring the resultant force vector, in the idealized two-dimensional case, normal to the free stream and eliminate the drag term. A concept that would apply this subsonic principle to supersonic flow is illustrated at the lower right. Here a subsonic airfoil is swept back so far that the Mach number normal to the leading edge of the airfoil is subsonic. In this situation, leading-edge suction can be utilized to bring the resultant force vector nearly perpendicular to the free stream.

Figure 13 shows calculated lift-drag ratios for this type of wing, which has been called the oblique wing. The calculated values are based on experimental section data for the 64A-506 subsonic airfoil section. For comparison, calculated lift-drag ratios for a conventional supersonic airfoil of $2\frac{1}{2}$-percent thickness are shown by the dashed line. At a Mach number of 2, the oblique wing shows over twice the maximum lift-drag ratio of the conventional wing. Of course, the calculations shown apply to the two-dimensional case. When finite aspect ratios are considered, the values will decrease. Recent experiments with an oblique wing in the Lewis 1- by 1-foot Mach 3 wind tunnel have yielded encouraging results.

It should be remarked that the oblique-wing concept is about 12 years old; and, although it appears to be very interesting, it evidently has not been thoroughly exploited. Section data for airfoils up to 10 or 12 percent thick indicate that they may also yield good L/D. For very large airplanes, using wings of such thickness, it is possible to conceive a flying-wing airplane where all the required volume is in wing. Such a flying-wing configuration would be expected to have a very high L/D. This is certainly an interesting possibility.

This concludes the discussion of wing and fuselage drag. One topic remains that can have a marked effect on the airplane configuration and its lift-drag ratio; that is, the effect of the propulsion system - fuel type and engine location.

Two fuels have been prominent in the discussions of the preceding papers - JP fuel and hydrogen. One of the significant differences in these fuels is their density. JP fuel has a density of 47 pounds per cubic foot; hydrogen, 4.4 pounds per cubic foot. The effect of this density difference on the airplane configuration is illustrated by the two models in figure 14. The JP airplane has a gross weight of 500,000 pounds. The hydrogen airplane actually has a lower gross weight, 300,000 pounds, but is almost twice as long. In addition, the hydrogen airplane has a larger ratio of fuselage to wing area. This has an adverse effect on the L/D, as previously discussed.

The other propulsion-system factor of interest is the engine installation. Of course, the objective is to find a way to install the engine to the mutual benefit of both the engine and the airframe.

Consider first the question of engine inlet location. There are a number of reasons why it is desirable to locate the engine inlet under a wing or fuselage to take advantage of the compression field there. Some of these reasons are illustrated in figure 15, which shows two examples of locating the engine inlet under a wing. First, the size of the inlet is reduced from what it would be if located in the free stream. At Mach 4, the inlet area is reduced about 30 percent. At Mach 7, the area reduction is about 50 percent. This reduced inlet area for the turbojet engine ($M = 4.0$) would ease the matching problem at lower speeds. Another reason is that the Mach number ahead of the inlet is reduced below the free-stream value, and this would tend to increase the pressure recovery of the inlet. Also, shielding the inlet in this way would make the performance of the inlet insensitive to variations in angle of attack.

This inlet area reduction has an effect on the over-all engine proportions, as illustrated in figure 16. Here the engine frontal area is shown in a two-dimensional fashion for a Mach 4 turbojet installation. Assuming that an exit static-pressure ratio of 1.7 is acceptable as a compromise between the jet thrust and cowl pressure drag for a nacelle installation, the top sketch illustrates the frontal area when the inlet is located in the free stream. When the inlet is located under the wing or body, the frontal area will be increased, as shown by the middle sketch. If complete expansion is desired, the frontal area increases still further, as shown by the bottom sketch. This increased frontal area can be an advantage or a disadvantage, as illustrated by the configurations in figures 17 and 18. Figure 17 shows the engines mounted in nacelles beneath the wing. The pressure drag on the engines will be higher than it would be if the nacelles were in the free stream, because the pressures and the

[redacted]

frontal areas are larger. The configuration of figure 18 has the inlet beneath the body. Complete expansion is utilized in the nozzle. The pressure drag on the engine frontal area has been avoided because the engine frontal area is hidden behind the main body frontal area. In addition, the fuselage afterbody pressure drag, which is unavoidable on the previous configuration, is decreased or eliminated.

Another way the engine can be used to improve the performance of the configuration is to take lift from the exhaust jet. This can be done by canting the jet downward. An example of this is given in figure 19 for a Mach 4.0 turbojet. Relative range is plotted as a function of the angle of jet cant below the flight direction θ. Airplane performance is often calculated as if the jet is alined in the flight direction ($\theta = 0$). By canting the jet to the optimum angle, which is about twice the wing angle of attack, a 4-percent gain in range is available. The size of this range gain depends for one thing on the airplane L/D. For lower values of L/D, the range gain would be larger. With respect to maintaining faired external lines on the over-all airplane and avoiding unbalance moments, it often is inconvenient to cant the exhaust jet more or less than the wing angle of attack. A range gain resulting from canting the exhaust at the angle of the wing, in this case 3 percent, exists in most airplane designs.

Another consideration associated with engine inlet location is directional stability. Figure 20(a) illustrates an airplane with a circular fuselage cross section and with the engine inlet located at the front. This is a poor location with respect to stability, since, if the airplane is yawed slightly, the force required to turn the incoming air tends to increase the yaw angle. The unstable condition is indicated in figure 20(a) by the "inlet" curve. The body is also directionally unstable; this condition of instability for the inlet-body combination is also indicated in figure 20(a).

The area of a tail required to make this airplane neutrally stable at Mach 7 can be calculated. This configuration would be more stable at lower Mach numbers, indicating that the condition that designs the tail is the high Mach number. The addition of such a tail surface might reduce the L/D of the configuration from 7.5 to around 7.1.

Figure 20(b) shows a configuration with the engine inlet located to the rear of the airplane center of gravity and with a flattened fuselage. This fuselage has the same volume as the circular one of figure 20(a). The advantage of this flattening to obtain lift from the fuselage was mentioned earlier. This shape also reduces the cross section of the body normal to the yaw direction, and so directional instability of the body is reduced. Since the engine inlet is behind the center of gravity, the turning force tends to restore the airplane to the flight direction. This combination, then, can be made directionally stable without the addition of any tail surface. A tail surface might be required, however, for proper control and dynamic characteristics.

[redacted]

In figure 21 some experimental maximum lift-drag ratios are plotted as a function of free-stream Mach number for several airplane concepts. One scheme is the Ames configuration sketched in figure 22. This model, tested in the Ames 10- by 14-inch tunnel, incorporates half of a hypersonic body of revolution mounted beneath an arrow wing. The pressure field of the body therefore produces lifting pressures on the underside of the wing. The data shown as solid symbols in figure 21 were obtained at Reynolds numbers of 5.2×10^6 to 1×10^6 based on the model length of 7 inches. The Reynolds number decreased with increasing Mach number. The maximum L/D varies from a little over 7 at Mach 3 and 4 to about 5 at Mach 6.2.

Another configuration investigated recently in the Lewis 10- by 10-foot tunnel is the flat-bottom design shown in figure 23. This fuselage has a semielliptical cross section and a canopy that was necessary to accommodate the sting and strain-gage balance assembly. The wing is swept back at about 74° and is hexagonal in cross section. Thickness of 1/4 inch gives a thickness-chord ratio at the mean aerodynamic chord of less than 1 percent. The wing is made of aluminum and is extremely flexible, but no flutter was encountered. The data were obtained at Reynolds numbers of 6.6×10^6, 20×10^6, and 29×10^6, based on the body length of 13.2 feet, and at Mach numbers of 3.0 and 3.5. At Mach 3.0 the maximum L/D of 6.9 at 6.6×10^6 Reynolds number was increased to 9.3 at Re_l of 20×10^6. This is due in large part to the effect of Reynolds number on the friction coefficient, which was discussed earlier.

Data for a third configuration are also shown. These data were obtained for what might be called a conventional wing-body configuration (fig. 24). The data shown are for the configuration without the engines. At the high Reynolds number of 29×10^6 the data fall from about 6 at Mach 2 to about 5.5 at Mach 3.5. It should be emphasized that all these data are for configurations without engine installations or tail surfaces.

Consider again the range equation (eq. (1)). Several factors affect the airplane structural weight W_S/W_G. The discussion of inlets and outlets in paper 2 pointed out the large effect of the temperature environment on the engine design. The temperature environment around the airplane structure can also have an important effect on the airframe structural design and weight. Another item that can make a substantial contribution to structural weight is the fuel tank. This is particularly true for hydrogen. And, of course, this tank problem is aggravated by its temperature environment.

Shown in figure 25 are radiation equilibrium surface temperatures at selected locations on a typical airframe. These temperatures are shown as a function of Mach number for the Mach number and altitude schedule shown on the figure. The calculations are for turbulent flow with 0.8 emissivity. The lower curves show wing upper- and lower-surface

[redacted]

temperatures at 5° angle of attack. At Mach 9, the wall temperature is less than 1700° R. If necessary, the entire wing structure could be built to withstand this temperature. At the wing leading edge, the temperature exceeds 2400° R at Mach numbers above 7, and leading-edge cooling would be required. The wing temperatures shown would also apply approximately to the upper and lower surfaces of the fuselage and to the fuselage stagnation region.

The amount of cooling required for the airframe is shown in figure 26. The airframe configurations are those chosen for the range calculations in the Mission Studies paper (5). Although it should be possible to build a wing to withstand equilibrium temperature, it may be more efficient structurally to have a cool internal structure. For that reason, the cooling requirements have been based on 600° F internal wing temperature. The leading-edge requirement has arbitrarily been taken as 1600° F, and the fuselage interior other than fuel tankage areas as 170° F. The use of 1 inch of insulation is assumed, where required. The cooling requirement is expressed in percent of available cooling capacity for hydrogen fuel. At Mach numbers of 4 to 5 only a slight amount of cooling is required. At Mach 7, about 6 percent of that available is needed, and at Mach 9 this has risen to 10 percent. It was shown in paper 2 that about 50 percent of the available fuel cooling capacity is required for the engine alone. Thus, the total required cooling capacity for airframe and engines would be approximately 60 percent of the total available cooling capacity of the fuel at Mach 9.0. The requirement is conservative in the sense that a cooled wing structure is provided for.

With regard to fuel storage in the airplane, this discussion merely presents some considerations indicating the order of magnitude of the tank weights and fuel vaporization rates with hydrogen. Consider, first, just the weight of the tank shell required to house a given quantity of fuel. As shown on figure 27, the weight of tank per unit weight of fuel will be proportional to the surface-volume ratio of the tank and to the thickness and density of the construction materials, and inversely proportional to the fuel density. If one considers making this tank from a minimum-gage-thickness material (in this case 0.015-inch stainless steel), the weight of the tank shell alone for hydrogen is shown by the middle curve of figure 27 as a function of tank diameter. Since the surface-volume ratio is inversely proportional to the diameter, the increase of weight at small diameters represents one penalty connected with configurations that require a small tank diameter. Tanks of the particular thickness shown would have the maximum operating pressures shown on the curve; that is, the yield limit would be reached at these pressures and any desired higher operating pressure would require proportionately heavier tanks.

Similarly, the weight of any insulation required would be governed in the same manner, ρ and t being the density and thickness of the

[redacted]

insulation. A curve of insulation weight for a 2-inch layer is also shown. The use of this insulation will be discussed shortly. The combined weight of a tank shell plus 2 inches of insulation, again for hydrogen, is shown by the top curve of figure 27. In the range of tank diameters that are involved in some of the configurations presented in the following paper (6 to 7 ft), minimum tank weights would be in the neighborhood of 15 percent of the fuel weight with present materials. The higher density of JP fuels, 10 times that of hydrogen, would give much smaller tank weights by these criteria.

The weight of insulation shown in figure 27 has been used in two different ways, as shown in figure 28. In one way, which is labeled "nonregenerative," the insulation is a simple barrier between the fuel tank and the fuselage. Heat flowing into the fuel tank all goes into latent heat and vaporizes fuel. The other way of using the same amount of insulation is called a "regenerative" system. This scheme essentially splits the insulation into two layers and permits vaporized gas to circulate between the layers. Using this principle, it is possible to take advantage of considerably more of the heat-sink capacity of the fuel than in the nonregenerative system, which absorbs only latent heat. In effect, in the regenerative system, heat that flows through the inner layer of insulation goes to the vaporizing fuel, while gas circulating between the layers intercepts and carries off a large portion of the heat flowing through the outer layer.

A comparison of the performance with these two methods is shown in figure 29 as a function of flight Mach number. The heat-transfer performance of the insulation at the higher Mach numbers is related to two different effects. One is the higher fuselage temperatures which lead to greater heat-transfer rates. The other is the higher fuel-flow rate. This higher fuel flow may be considered a counteracting effect, since the general concern is with the rate of fuel vaporization compared to the fuel-flow rate to the engines. In this illustration the higher fuel-flow rates at the higher Mach numbers more than counteracted the effect of the higher temperatures.

With the nonregenerative insulating scheme (top curve of fig. 29), vaporization rates of the order of 60 to 70 percent of the fuel-flow rate were calculated for a particular configuration over a range of conditions. With vaporization rates of this order of magnitude, pumping large quantities of vapor fuel would be necessary. This increased pumping would require either higher-pressure tanks (using tank pressure as the pumping means), which means heavier tanks, or vapor pumps, which also may be large and heavy.

Using the regenerative scheme, calculated vaporization rates were only 6 to 7 percent of the fuel-flow rate, or about one-tenth of that for the nonregenerative system (fig. 29). It would seem, then, that some such scheme as the regenerative one will be required to avoid the necessity for handling large quantities of vapor fuel.

[redacted]

To summarize the ideas discussed in this paper, several models incorporating as many of the favorable features as possible were built and are shown in figure 30. Figure 30(a) is a Mach 4.0 airplane of 500,000-pound gross weight using JP fuel. Because tank weight is not a problem with JP fuel, a flattened fuselage is used to develop fuselage lift. The forebody is shaped in plan form for low center-of-pressure shift from subsonic to supersonic speeds and is cambered in side view for self trim without a canard surface. The shape of the bottom of the fuselage results in a favorable pressure gradient. Since there is no canard surface, it is hoped that a long run of laminar boundary layer will exist. The inlet is located under the fuselage to take advantage of the compression existing there and to shield the inlet from angle-of-attack effects. It is located behind the center of gravity to contribute to the directional stability. The engine frontal area is hidden behind the fuselage, eliminating engine pressure drag and fuselage afterbody drag. The exhaust is at the wing angle of attack to develop some jet lift. The airplane probably does not require airframe structural cooling.

The airplane shown in figure 30(b) is designed for Mach 4.0 using hydrogen and has a gross weight of 300,000 pounds. Despite the lower gross weight, the hydrogen-fueled airplane is about twice as long. Because fuel tankage is a problem of prime importance for the hydrogen airplane, only a partially widened fuselage was used. A canard surface was chosen for trim and control. Most of the other features of the airplane are consistent with those previously described.

The final airplane shown in figure 30(c) is an adaptation of the oblique wing to an arrow-wing configuration. This type of configuration shows great analytical possibilities below $M = 3$ or 4. More experimental evidence is needed, however.

The ideas about airplane configurations and their lift-drag ratios discussed in this paper have been incorporated in the range and mission calculations that are presented in paper 5.

REFERENCES

1. Rabb, Leonard, and Disher, John H.: Boundary-Layer Transition at High Reynolds Numbers as Obtained in Flight of a 20° Cone-Cylinder with Wall to Local Stream Temperature Ratios Near 1.0. NACA RM E55I15, 1955.

2. Disher, John H., and Rabb, Leonard: Observation of Laminar Flow on a Blunted 15° Cone-Cylinder in Free Flight at High Reynolds Numbers and Free-Stream Mach Numbers to 8.17. NACA RM E56G23, 1956.

[redacted]

3. Rabb, Leonard, and Krasnican, Milan J.: Observation of Laminar Flow on an Air-Launched 15° Cone-Cylinder at Local Reynolds Numbers to 50×10^6 at Peak Mach Number of 6.75. NACA RM E56L03, 1957.

4. Low, George M.: Boundary-Layer Transition at Supersonic Speeds. NACA RM E56E10, 1956.

5. Moeckel, W. E.: Some Effects of Bluntness on Boundary-Layer Transition and Heat Transfer at Supersonic Speeds. NACA Rep. 1312, 1957. (Supersedes NACA TN 3653.)

6. Dunning, Robert W., and Ulmann, Edward F.: Effects of Sweep and Angle of Attack on Boundary-Layer Transition on Wings at Mach Number 4.04. NACA TN 3473, 1955.

[redacted]

LARGE AIRPLANES HAVE LESS FUSELAGE DRAG

$$C_{D,0} = C_{D,0,w} + C_{D,0,b}\left(\frac{A_b}{S_w}\right)$$

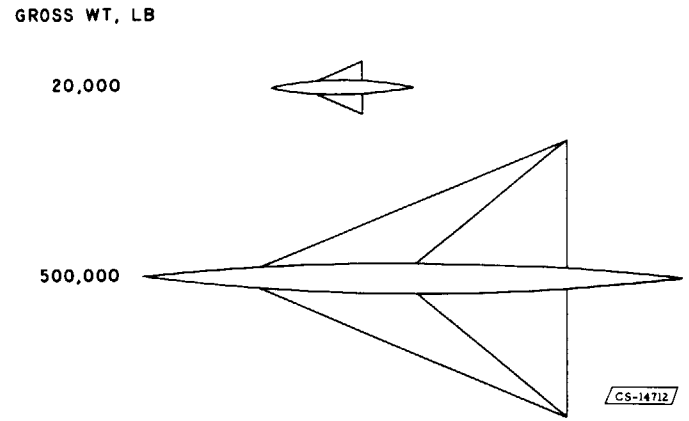

Figure 1

LARGE AIRPLANES HAVE BETTER LIFT-DRAG RATIOS

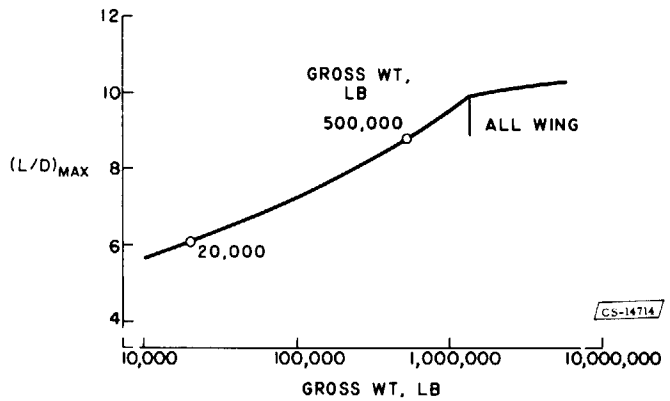

Figure 3

LARGE AIRPLANES HAVE LESS FRICTION DRAG

$M_0 = 4$, TURBULENT BOUNDARY LAYER

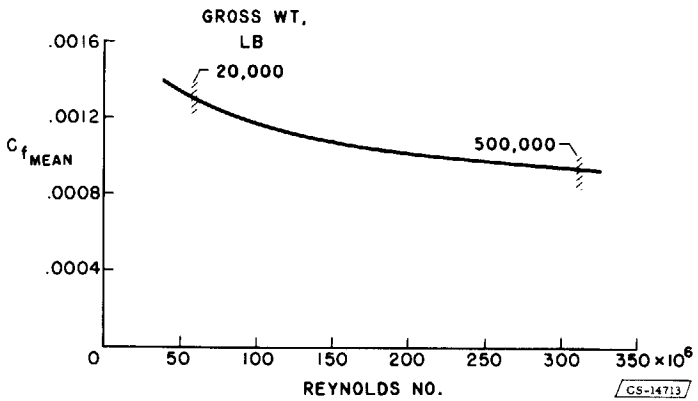

Figure 2

INCREASED MACH NUMBER LOWERS FRICTION DRAG

TURBULENT BOUNDARY LAYER INSULATED WALL

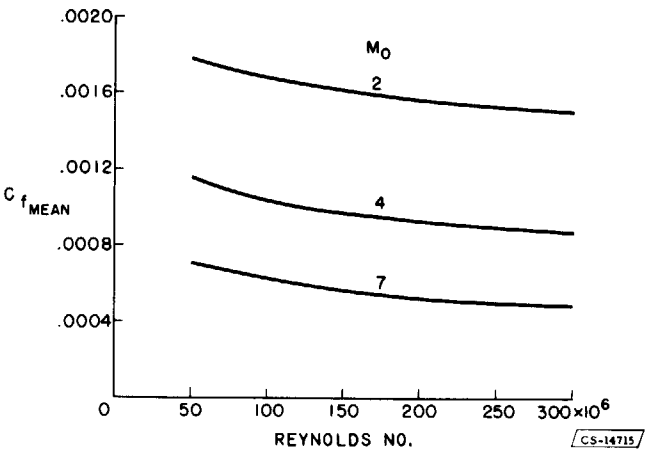

Figure 4

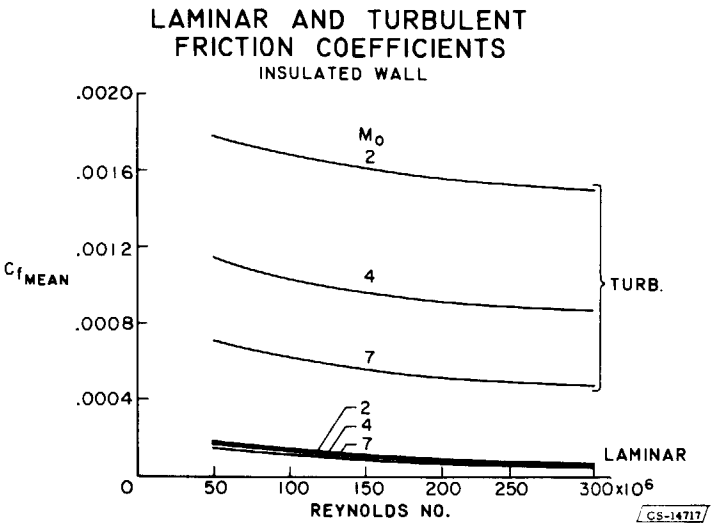

Figure 5

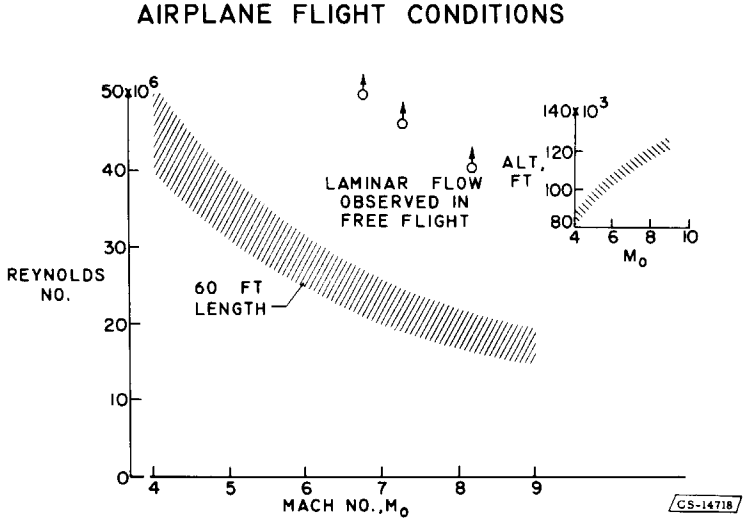

Figure 6

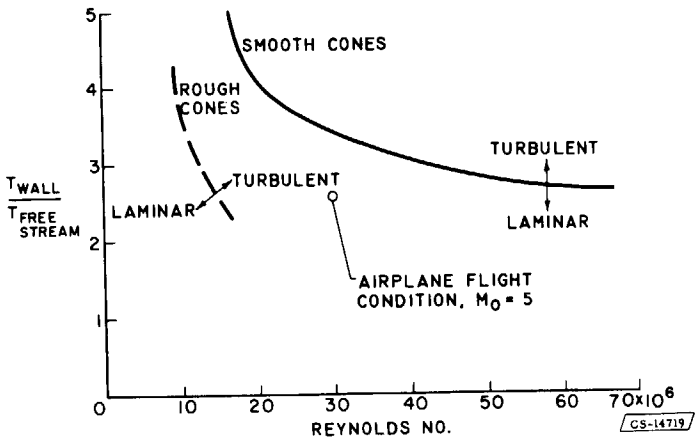

Figure 7

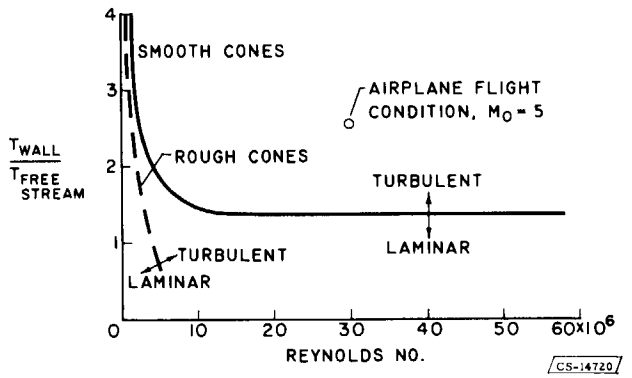

Figure 8

WING SWEEP PROMOTES TRANSITION

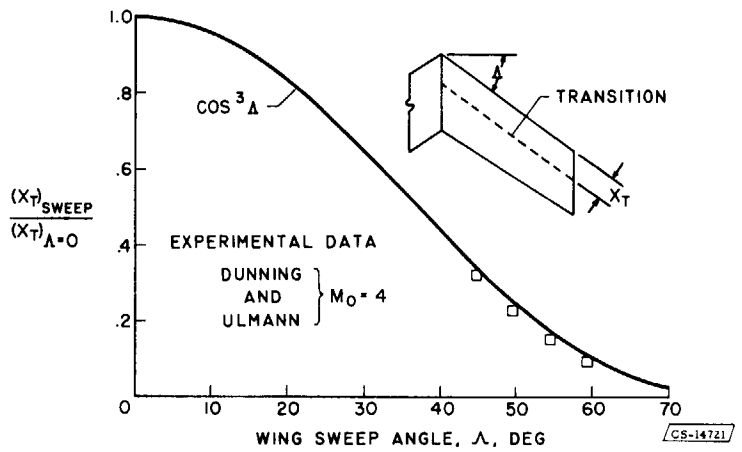

Figure 9

FUSELAGE DRAG

CIRCULAR CROSS SECTION

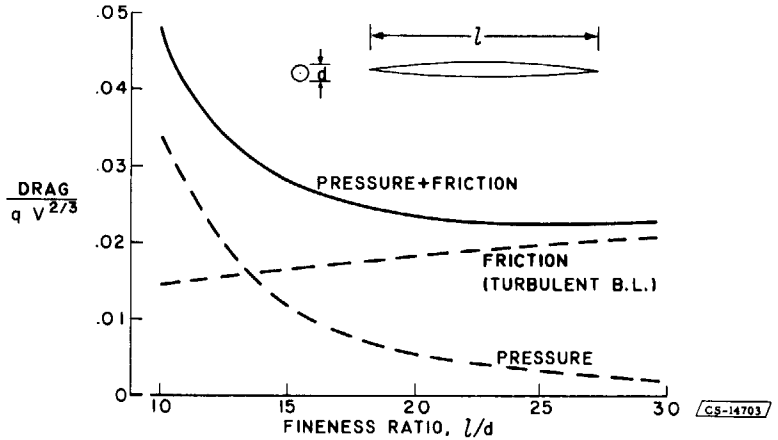

Figure 10

LIFTING FUSELAGE

CONSTANT VOLUME AND FLIGHT ALTITUDE

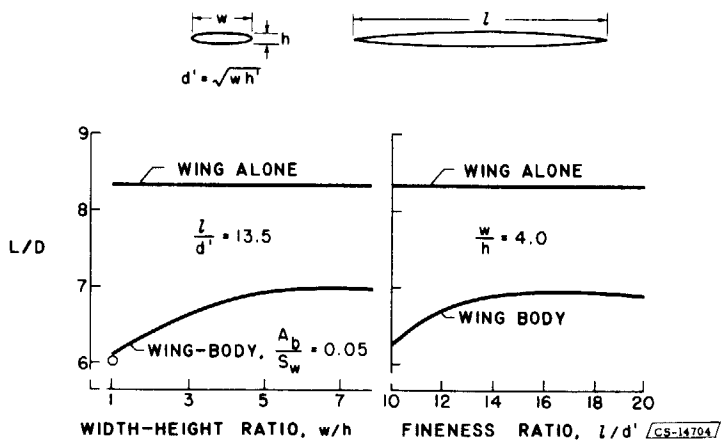

Figure 11

SOME LIFTS DON'T DRAG

2-DIMENSIONAL

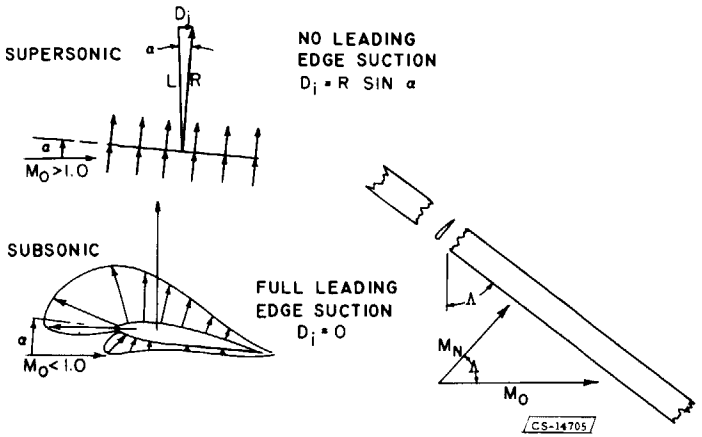

Figure 12

EFFECT OF FUEL TYPE

HYDROGEN FUEL
GROSS WEIGHT, 300,000 LB

JP FUEL
GROSS WEIGHT, 500,000 LB

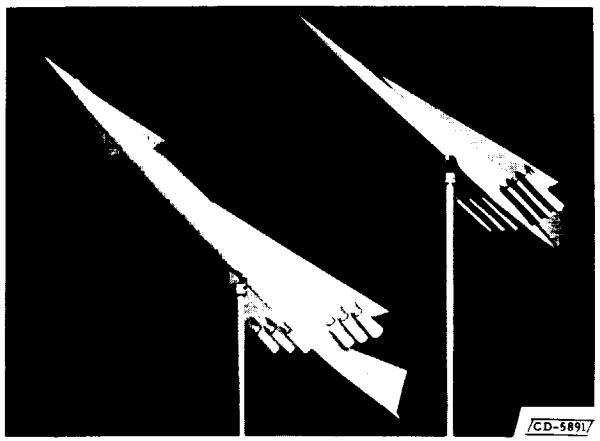

Figure 14

OBLIQUE WING LIFT-DRAG RATIO

2-DIMENSIONAL, TURBULENT BOUNDARY LAYER

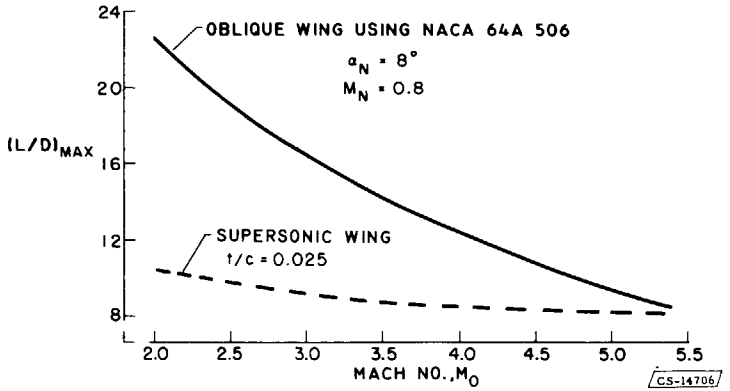

Figure 13

INLET LOCATION

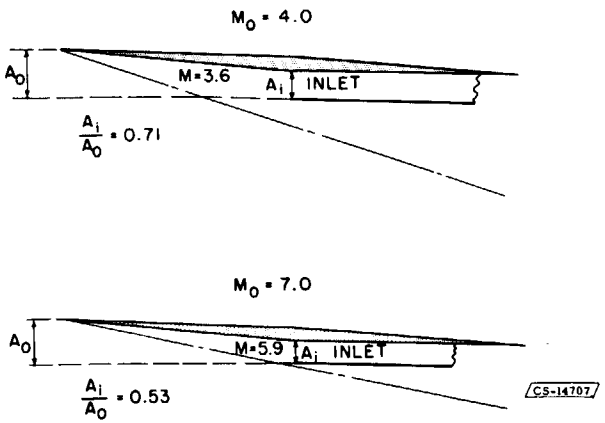

Figure 15

ENGINE FRONTAL AREA

TWO-DIMENSIONAL

ENGINE: MACH NO., 4 TURBOJET

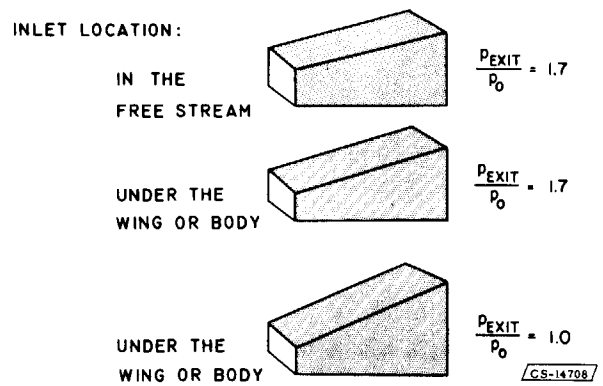

Figure 16

FUEL HYDROGEN

GROSS WT, 300,000 LB, ENGINES IN FUSELAGE

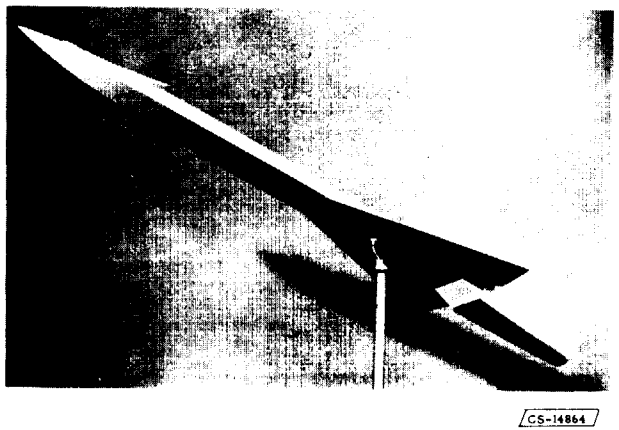

Figure 18

FUEL HYDROGEN

GROSS WT, 300,000 LB, NACELLE ENGINES

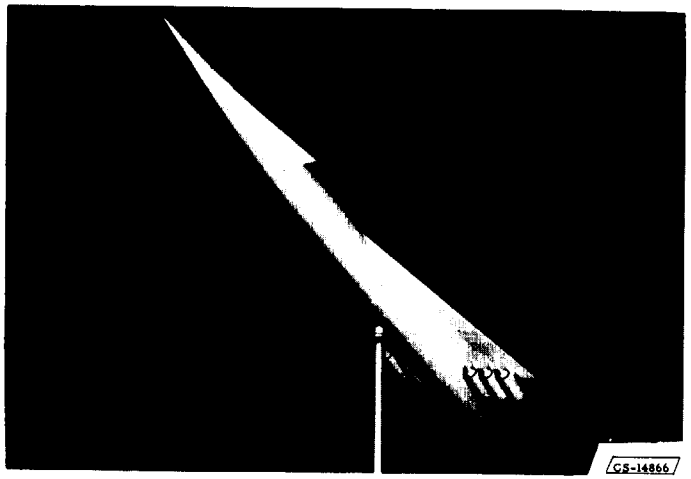

Figure 17

JET CANT FOR LIFT

TURBOJET, M=4.0 , (L/D)=7.0, T_{CYCLE} = 3000° R

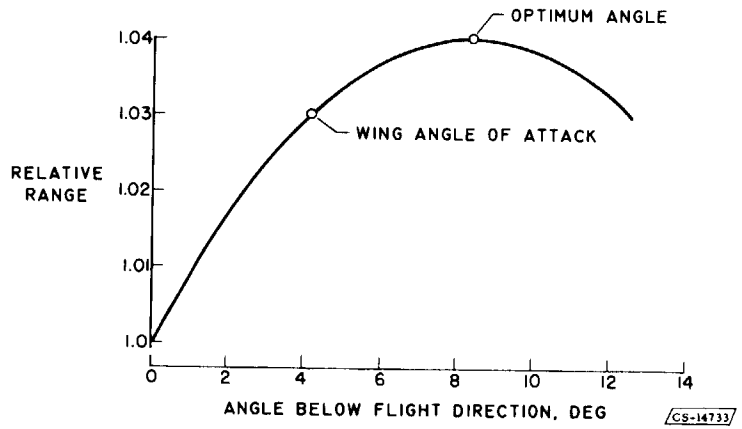

Figure 19

DIRECTIONAL STABILITY

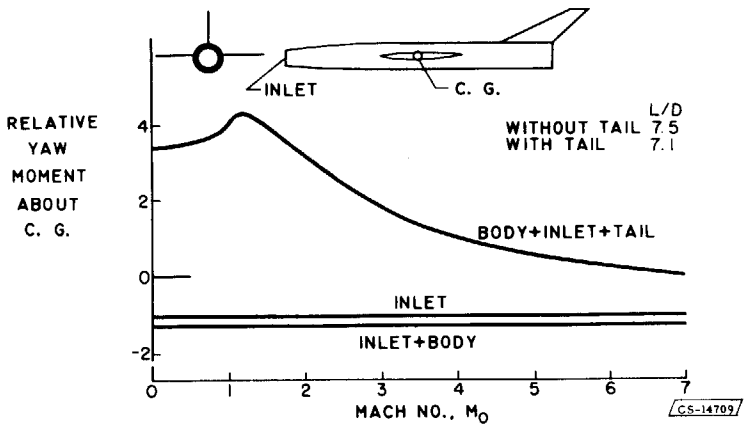

Figure 20(a)

DIRECTIONAL STABILITY

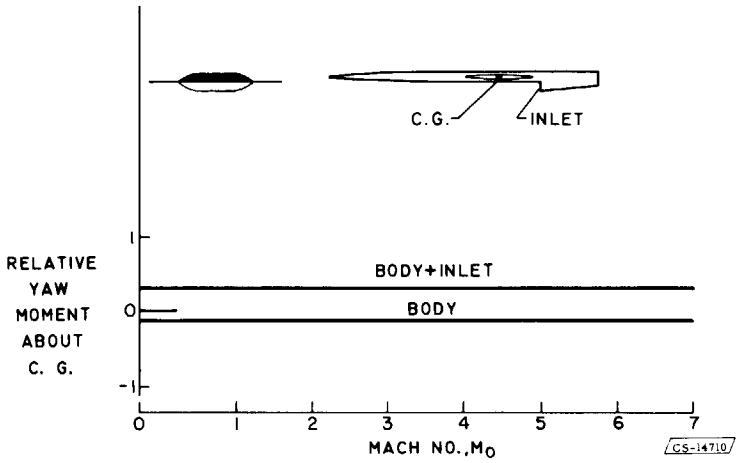

Figure 20(b)

EXPERIMENTAL MAXIMUM LIFT-DRAG RATIOS

CONFIGURATION	FACILITY	Re_l	SYMBOL
FLAT TOP	AMES (10"x14")	5.2×10^6 TO 1.0×10^6	●
FLAT BOTTOM	LEWIS (10' x 10')	29×10^6 20×10^6 6.6×10^6	○ □ ◇
CONVENTIONAL WING-BODY	LEWIS (10' x 10')	29×10^6	△

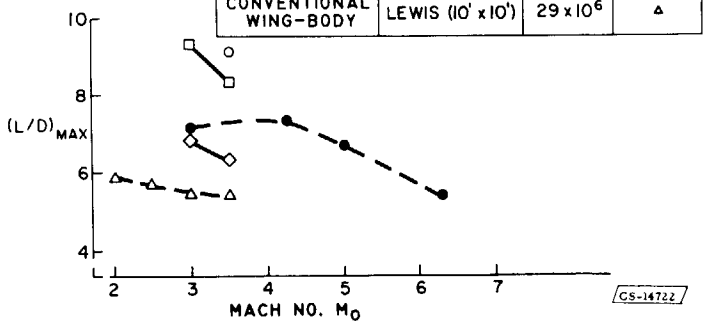

Figure 21

FLAT TOP CONFIGURATION (AMES)

10" x 14" SWT

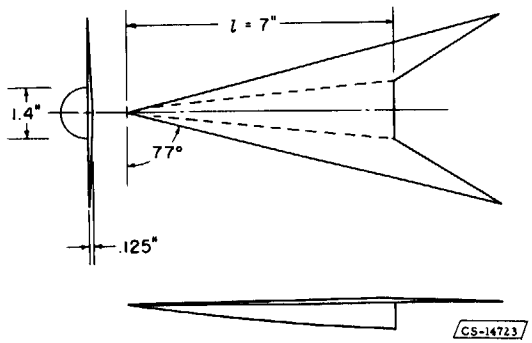

Figure 22

FLAT BOTTOM CONFIGURATION (LEWIS)

10' x 10' SWT

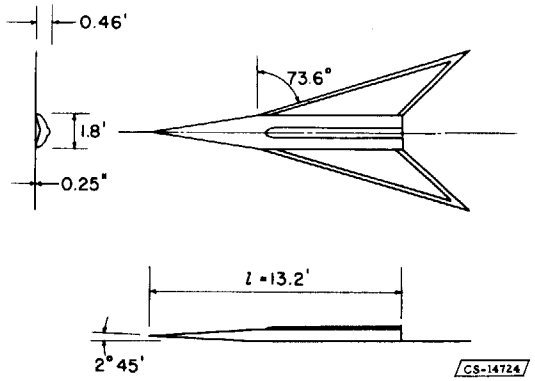

Figure 23(a)

FLAT BOTTOM CONFIGURATION

LEWIS 10 X 10 FT SWT

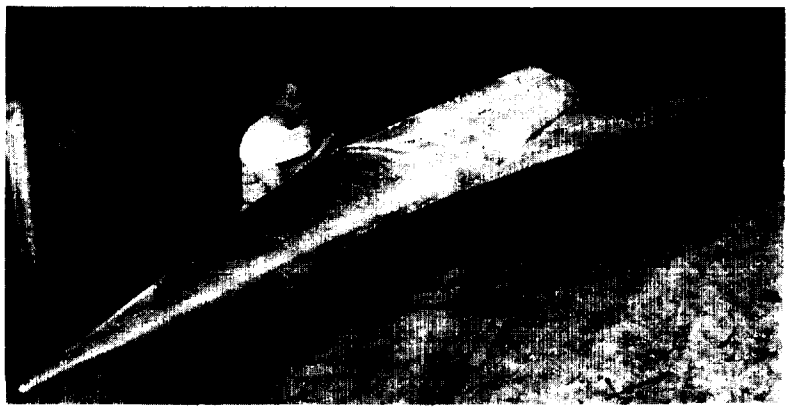

Figure 23(b)

CONVENTIONAL CONFIGURATION

LEWIS 10 X 10 FT SWT

Figure 24

RADIATION EQUILIBRIUM WALL TEMPERATURES

TURBULENT BOUNDARY LAYER 0.8 EMISSIVITY

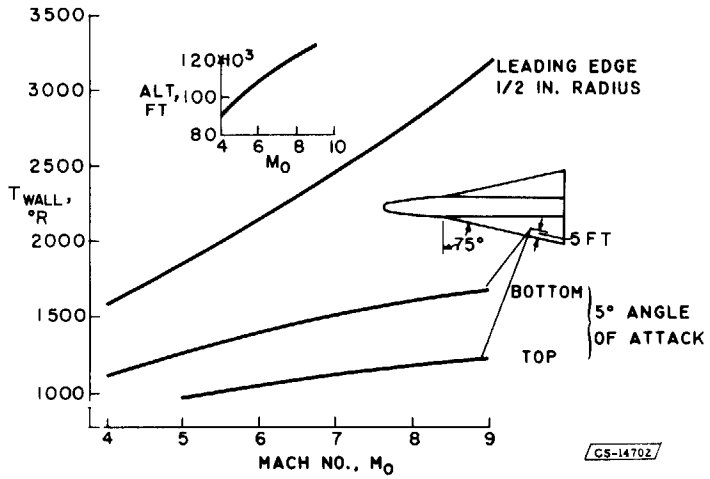

Figure 25

AIRFRAME COOLING REQUIREMENT

TURBULENT BOUNDARY LAYER

	TEMP. °F
WING LEADING EDGE	1600
WING INTERNAL STRUCTURE	600
FUSELAGE INTERIOR	170

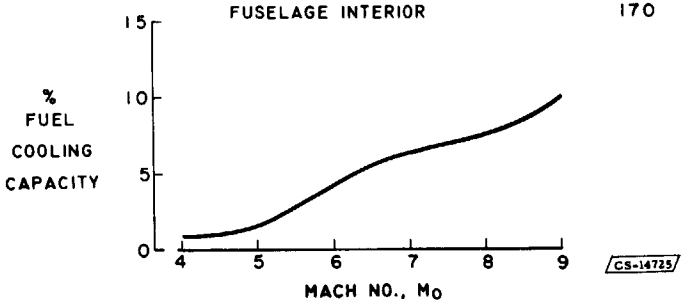

Figure 26

ESTIMATED MINIMUM HYDROGEN TANK WEIGHTS

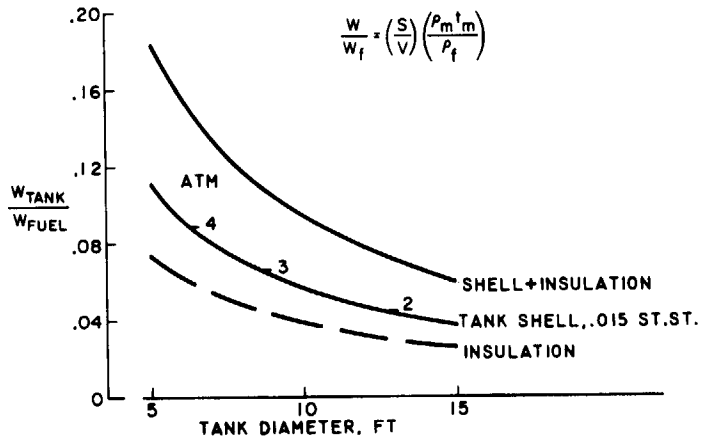

Figure 27

HYDROGEN TANK INSULATION

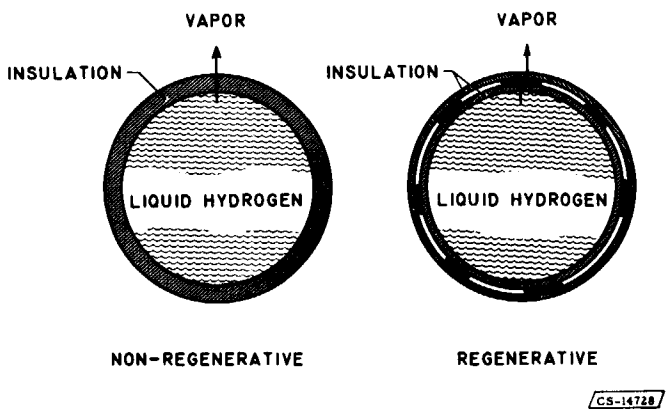

Figure 28

HYDROGEN VAPORIZATION RATES

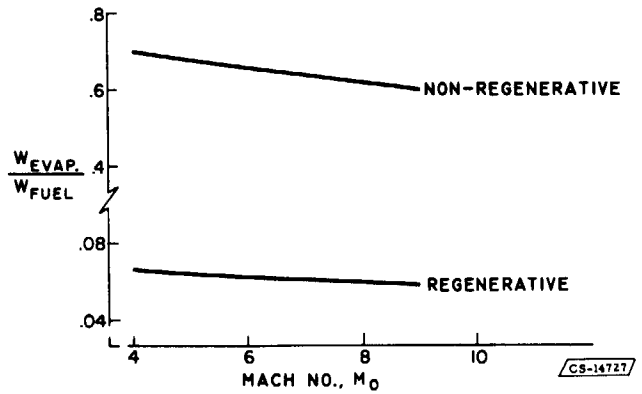

Figure 29

IDEA AIRPLANE

FUEL, JP, GROSS WT, 500,000 LB, MACH NO. 4

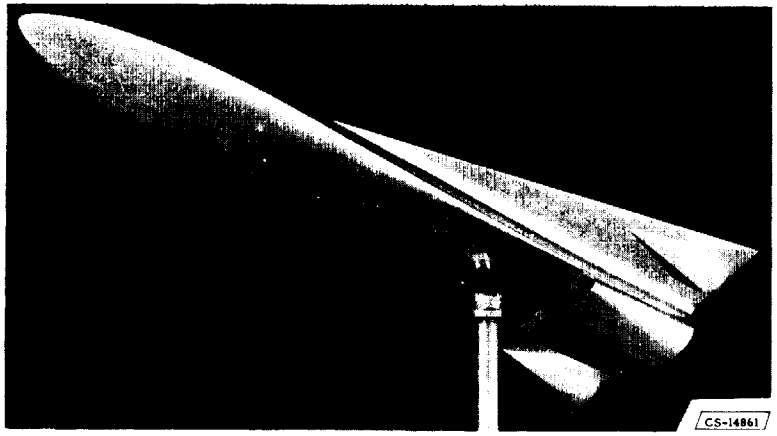

Figure 30(a)

IDEA AIRPLANE

FUEL, HYDROGEN, GROSS WT, 300,000 LB, MACH NO. 4

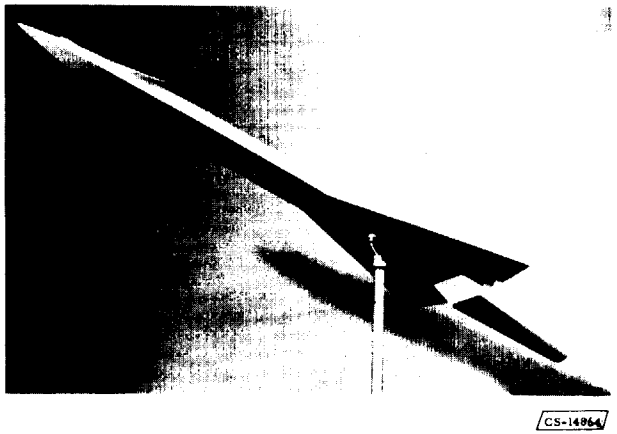

Figure 30(b)

IDEA ARROW WING AIRPLANE

FUEL, JP, GROSS WT, 500,000 LB, MACH NO. 3

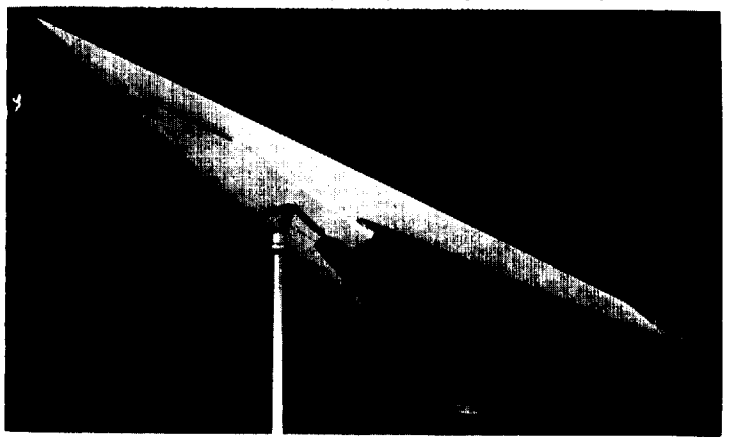

Figure 30(c)

5. MISSION STUDIES

By S. C. Himmel, E. W. Conrad, R. J. Weber,
R. R. Ziemer, and W. E. Scull

INTRODUCTION

The preceding papers have discussed in some detail the elements that go into the design of an aircraft sytem and have indicated the most promising choices for each component. It is the purpose of this paper to blend all of these elements into predictions of the performance capabilities of complete aircraft systems. The aircraft systems investigated are required to perform a particular mission - long-range supersonic bombardment. Generally speaking, there are two ways of accomplishing such a mission. The first, and most conventional, is to have a manned bomber aircraft fly out to the target, deliver its payload, and fly back to its base. The second is to send a guided missile on a one-way flight to the target. Both of these methods have been considered.

The two methods of bomb delivery required the examination of aircraft performance for the two zones indicated in figure 1, where altitude is plotted against cruise Mach number. The class of turbine engines has been considered only for the propulsion of manned aircraft. The zone of application considered for such airplanes ranges over Mach numbers from 3 to 4.5 and altitudes from 60,000 to 110,000 feet. The ramjet engine has been considered only for the propulsion of missiles. These missiles were studied over a range of Mach numbers from Mach 5 to 9 and altitudes from 80,000 and 130,000 feet.

To determine the performance potential of these bombardment systems, series of airplanes and missiles were designed for their respective zones of application and the radius or range obtainable was computed. In any such analysis the results are highly dependent on the assumptions made. Some of the major assumptions will be discussed herein. In presenting the results, the effects of such variables as flight speed, target altitude, fuel type, and system and payload weights will be examined. It is neither the purpose nor intention of this paper to argue the merits of any one system of payload delivery over another. Rather, it is desired to present, in a factual manner, the performance capabilities the analyses have indicated for the systems studied.

[redacted]

MANNED AIRPLANES

Engines

Of the gas-generator type powerplants discussed in paper 3, two of the more promising types have been chosen for discussion of flight capabilities in terms of absolute radius. These are a single-spool turbojet and an air-turborocket with air liquefaction. Although some of the more complicated engines such as the fuel-rich ducted fan and the hydrogen expansion cycle indicated radii of the same magnitude, the turbojet was chosen because, being a relatively familiar and simple engine, it would require less time to develop and also it can accommodate various types of fuels. The air-turborocket was chosen as a representative of the more complicated engines that indicated a relative range somewhat greater than the turbojet.

Some of the pertinent design parameters of representative engines that appear to hold promise of good flight capabilities at Mach numbers between 3.0 and 4.5 are listed in table I. For the Mach 3.0 engine, designed for an altitude of about 65,000 feet, a sea-level compressor pressue ratio of 5.0 was used. At the higher design flight Mach numbers and altitudes where the engines operate more like ramjets, a sea-level pressure ratio of 2.3 was selected. Turbine-inlet temperatures of 1900° and 2500° R were chosen. The 2500° R temperature assumes either turbine cooling or coated molybdenum turbine blades. This higher turbine-inlet temperature indicates improvements in aircraft radius, but the engine would be somewhat more complicated. For all engines considered, the afterburner temperature during takeoff and acceleration is 4000° R. The air-turborocket cycle with air liquefaction uses hydrogen as fuel. It has a sea-level pressure ratio of 1.71 and a turbine-inlet temperature of 2000° R.

In general, the mission capabilities to be discussed will employ engines that have inlets and outlets with some variation in geometry. A variable inlet was chosen to reduce additive drag during the transonic flight conditions below that of a fixed inlet but far from that of an ideal inlet with no additive drag. The ejector-type exhaust nozzle has a variable throat and a fixed divergent section. Penalties in nozzle efficiency were imposed at flight conditions other than design.

Airframe Considerations

Airframe configuration. - The model shown in figure 2 illustrates an airplane typical of those chosen to investigate the flight performance afforded by turbine-type engines. Since this study was limited to vehicles capable of unassisted takeoff and acceleration to their supersonic cruising speed, the design incorporates a series of compromises in order

[redacted]

to achieve not only good supersonic radius in the range of flight speeds from Mach 3 to 4.5, but also satisfactory low-speed acceleration capability.

The particular model shown in figure 2 represents a hydrogen-fueled aircraft designed to cruise at Mach 4.0 with a target altitude of 95,000 feet, while carrying a 10,000-pound payload. The actual airplane would weigh 300,000 pounds and have a fuselage length of 300 feet. Salient features are the highly swept delta wing, the canard control surface, and the six underslung engines with inlets within the pressure field of the wing.

The airframe constitutes a design considered possible by an extension of existing aerodynamic and structural practice. Alternative configurations such as those discussed in paper 4 will probably provide improved performance. However, this design will probably yield reasonable values for radius with a minimum of additional unknowns beyond those implicit in the use of hydrogen fuel.

Flight plan. - The flight plan during a typical mission is shown in figure 3, where altitude is plotted as a function of flight Mach number. The airplane takes off, accelerates, and climbs under its own power, following a path chosen to provide near-maximum radius after due regard for structural limitations on both the engine and airframe. Cruise out to the target and return are along a Breguet flight path at a constant supersonic Mach number. The airplane is required to have a 5-percent fuel reserve when landing. In the radii presented, full credit is given for distance covered during the initial climb and final descent phases of flight.

Critical regions during the flight influence the optimum combination of flight plan, engine design, and airplane design. A maximum cruise radius is sought without incurring unsatisfactory transonic acceleration or excessively long takeoff run. To achieve a good compromise among these sometimes conflicting requirements, factors such as airplane gross weight, design altitude, wing loading, and engine size have been varied. This optimization procedure was repeated, at least in part, for every engine design considered.

Airplane size and payload. - Before actual radii obtainable with such manned aircraft are discussed, there are several other factors affecting the flight analysis that should be considered. One of the more important of these is aircraft size. As a first step, calculations of airplane performance were made for several different gross weights; some of the results are shown in figure 4. Relative radius is given as a function of gross weight, where each point represents a different airplane.

[redacted]

The best airplane size is largely determined by the load it is desired to carry. The airplanes represented by the upper curve are designed to deliver a payload of 3000 pounds and to have on board 5000 pounds of other fixed equipment; the lower curve is for a payload of 10,000 pounds and a fixed load of about 30,000 pounds. (Fixed load is defined to include such items as controls and electronic and hydraulic gear, etc.)

For both curves, increasing airplane weight improves the radius, mainly because most of this additional weight can be put into fuel. Also, as was noted in paper 4, the lift-drag ratio improves as airplane size increases. The point is soon reached, however, beyond which larger airplanes show no advantage. This optimum point is obviously different for the two curves shown. Equally obvious is the fact that the lighter load permits much better radii.

Payload weight is determined by the amount of destructive power the target requires and by the accuracy with which the payload can be delivered. The fixed weight is determined largely by the ingenuity of the manufacturers of airframe and accessories as well as by tactical considerations. In order to arrive at realistic results, the examples of recent proposals for similar aircraft were accepted, and it was decided to use a payload of 10,000 pounds and a fixed weight on the order of 25,000 to 35,000 pounds. All of the following figures are based on these values.

After deciding the size payload and fixed weight that should be carried, another factor must be considered before fixing an airplane weight. This factor is the fuel used by the engine. The effects of gross weight on radius and airplane size for two fuels, hydrogen and JP, are illustrated in figure 5. For JP fuel, radius is still increasing with gross weight at an airplane weight of 500,000 pounds. For still heavier airplanes, the rate of increase rapidly diminishes. It was therefore decided to compare all the JP-fueled airplanes on the basis of the radius attainable with 500,000-pound airplanes.

For hydrogen-fueled airplanes, the radius also increases with gross weight. In this case, however, additional factors enter the picture. First, there is the problem of physical size. For the same gross weight, a hydrogen-fueled airplane is much larger than a JP airplane because of the much lower density of the hydrogen. As is shown at the top of figure 5, a 500,000-pound JP airplane is about 150 feet long, while the same weight hydrogen airplane is about 360 feet long, a ratio of more than 2 to 1. A second factor to consider is the weight of the hardware going into an airplane, which may be related to the construction cost. A JP airplane grossing 500,000 pounds has about 60 percent of its weight in fuel and thus has an empty weight of about 200,000 pounds. Because of the low fuel density, only about one-third of the weight of a hydrogen airplane is fuel, and a 200,000-pound empty weight is reached by a

[redacted]

hydrogen airplane grossing about 300,000 pounds. By striking a balance among the factors of radius, airplane size, and empty weight, a gross weight of 300,000 pounds was chosen for the hydrogen-fueled airplanes to go along with the 500,000 pounds assumed for the JP airplanes. These values are used throughout the remainder of the analysis.

Wing size. - From structural and aerodynamic considerations, a given wing type was selected for the airplanes; that is, a delta plan form of 1.5 aspect ratio, with $2\frac{1}{2}$-percent thickness ratio. The best wing size must still be determined, however. The concepts involved in sizing the wing for each application are indicated in figure 6. As a measure of wing size, wing loading is plotted along the abscissa (where low values correspond to large wings, and vice versa).

At the top of the figure, the cruise lift-drag ratio is shown for airplanes designed for various wing loadings. For the conditions considered, the maximum L/D is obtained at a wing loading of 25 pounds per square foot. Also shown are the lift-drag ratios obtained at a critical area during the climb (Mach 1.5, 36,000 ft). Highest L/D is achieved in this case at a much higher wing loading, as a result of the higher ambient dynamic pressure at this flight condition.

Wing loading also affects the weight apportionment of the airplane. Low wing loadings give large heavy wings. On the other hand, higher wing loadings increase the airplane drag, thereby affecting the required engine size. These factors in turn react on the fuel load, as shown by the middle curve. The engine is normally made larger than needed for good cruise performance in order to improve the low-speed thrust. This results in fairly low cruise afterburner temperatures.

Combining these considerations finally results in the variation of radius shown at the bottom of the figure. The optimum wing loading of 43 is materially higher than that for maximum cruising L/D. It was found necessary to repeat this optimization of both wing loading and afterburner temperature each time the design altitude or an engine parameter was changed.

Airplane Capabilities

Now that the methods used in the analysis have been described, the results for the manned airplanes are presented. The reader should be cautioned that the greater the departure from conventional configurations and the higher the flight speeds, the less precise the results become.

Target altitude. - The radius obtained by designing for various altitudes is shown in figure 7 for turbojet engines at Mach 4.0 cruise and

1900° R turbine-inlet temperature. Radius in nautical miles is plotted against altitude over the target. Airplanes fueled with JP, JP and ethyldecaborane in the afterburner, and hydrogen have maximum radii of 1650, 2270, and 2720 nautical miles, respectively. Designing for low altitudes results in small wings with poor cruise lift-drag ratios, and also in small engines which provide marginal acceleration during takeoff or transonic flight. These factors increase the fuel consumption during both climb and cruise. Designing for high altitudes where the air is less dense requires large, heavy engines and wings. These reduce the amount of fuel that can be carried. Because of these factors, an optimum altitude exists for all fuel types - about 90,000 feet for both the JP engines and the engines using EDB in the afterburner, and 95,000 feet for the hydrogen-fueled engines.

The hydrogen airplanes with their bulky fuselages require a proportionate increase in wing size to maintain a good lift-drag ratio. With a larger wing, it is necessary to operate at a higher altitude, which accounts for the higher optimum altitude for the hydrogen-fueled airplanes. It should be mentioned that the airplanes chosen have excellent takeoff performance and can leave the runway in distances of 3000 to 4000 feet.

Although EDB is used only in the afterburner, it appreciably improves the all-JP radius. This is true because, at high Mach numbers, the engine operates essentially as a ramjet. For example, at Mach 4 approximately 90 percent of the total heat addition occurs in the afterburner; thus, the higher heating value of the EDB substantially lowers the fuel-consumption rate.

High-energy fuels such as hydrogen and EDB are particularly advantageous for the self-boosting type of mission being considered here. Not only do they lower the cruising fuel-consumption rate but they also provide more fuel at the start of cruising, since less fuel is consumed during the climb.

By going from conventional JP fuel to hydrogen fuel with all its associated problems, the radius goes up from 1650 to 2720 miles, a 65-percent increase. This is certainly a large improvement, but the radius is disappointingly low in view of the 5500 miles often quoted as a desirable minimum radius for a long-range mission.

Assuming that the structural techniques for hydrogen-fueled airplanes can be developed without too many unanticipated difficulties, the design of such manned airplanes could be initiated immediately using the current background of engine and aerodynamic technology. This does not mean that there are no ways to improve this performance, however. The possibility of lighter payloads and fixed weights has already been mentioned. Another possibility more within the scope of this paper is that of modifying the engine or using a different type of engine.

Air-turborocket. - Up to this point, the discussion has concerned only the turbojet engine. Similar calculations have been made for the other engine types mentioned in earlier papers. Radius as a function of target altitude for airplanes using air-turborocket engines is shown in figure 8. Data are given for three fuel combinations, again for a cruise Mach number of 4.0. Hydrogen plus liquid oxygen extends the radius somewhat over that attained with methyl acetylene and JP. The hydrogen-air liquefier engine gives the longest radius, however, at an optimum altitude about the same as for the turbojets using hydrogen fuel. The maximum radius is about 3100 miles. This is better perhaps than the turbojet, but the improvement is not outstanding. This is also about the best that can be attained with other cycles such as the fuel-rich turbofan and the hydrogen-expansion engine.

These air-turborockets have used what are considered to be practical components - things that can probably be built without a long research effort. If a little more optimism as incorporated into the analysis and it is assumed that the inlets have no additive drag during boost and that the exhaust nozzles can be designed to avoid the penalties for under- or over-expansion, performance can be improved. The maximum air-turborocket radius then rises from 3100 to about 3500 miles, as shown by the "idealized engine" symbol, a 13-percent improvement. Similar improvements can be made for the other engine types.

Design cruise Mach number. - Thus far, all the discussion has centered about Mach 4.0. The effect of cruise Mach number on radius is shown in figure 9 for two engine types, the air-liquefier air-turborocket and the turbojet using various fuels. Again, an optimistic viewpoint has been taken, in that it is assumed that the inlets have no additive drag and the exhaust-nozzle efficiency is constant. Also, the turbine-inlet temperature for the turbojets has been raised to 2500° R.

These assumptions favor the higher Mach numbers; nevertheless, designing for Mach numbers above 3.0 is detrimental to the radius. Some of the reasons for this are: (1) The engines and airframes are required to operate over a wider range of off-design conditions; (2) more energy is needed to accelerate the airplane to the peak Mach number, leaving less fuel for cruising; and (3) aerodynamic and structural efficiency deteriorates at higher speeds.

The air-turborocket affords a rather small improvement in radius over that of the turbojet. In view of these small improvements and because of the lack of practical experience with this engine, it does not seem worthwhile to develop such engines for the application being considered.

Since the air-turborocket apparently does not offer much improvement, what can be concluded about the use of turbojets? First, hydrogen seems to provide the longest radii at all the speeds considered. This is

[redacted]

especially true at speeds above Mach 4.0, as it does not appear that either air-cooling or fuel-cooling with JP or EDB would be adequate for the engine. In going from Mach 3.0 to Mach 4.5 with hydrogen, however, the radius with idealized engines drops from 4000 to 2900 nautical miles. Four thousand miles is the best radius computed thus far, and even that is far from as much as is desired. Should 1100 miles be discarded so lightly, for the sake of higher flight speed? Cruising at Mach 4.0 or 4.5 probably reduces vulnerability to interception. On the other hand, cruising at Mach 3 gives longer radius; and such airplanes are undoubtedly easier to build. Thus, choosing the most desirable design speed is not easy.

In view of current events, the radii and speeds shown in figure 9 are not especially spectacular. It should be recalled, however, that manned airplanes are being considered. They have a human crew, carry out a round-trip mission, and takeoff and land under their own power. This performance represents a very substantial improvement over the best airplanes in existence today.

What further gains can be expected? Further engine improvements can undoubtedly be made, but there is no real reason to predict any startling breakthrough. Airframe improvements do seem possible, however, and should be examined.

Advanced airframe. - The performance of the hydrogen-fueled configurations previously discussed was based on a consideration of lift-drag ratios and aircraft design techniques thought to be moderate extensions of present aerodynamic practice. The model shown in figure 10 represents a configuration incorporating some further aerodynamic improvements that can possibly be built into an aircraft. Designed for Mach 4.0 cruise at 90,000 feet, the aircraft would be 300 feet long. Important features are the flat-bottomed fuselage and the highly swept delta wing and canard control surface. Gross weight is 300,000 pounds and payload is 10,000 pounds. Hydrogen is used in four engines mounted in the rear of the fuselage with a common exhaust through one large nozzle.

A common engine inlet is located on the bottom of the fuselage near the trailing edge of the wing. The fuselage of this aircraft is somewhat larger in volume than the previous model; not only are the engines mounted in the fuselage, but the space utilization for the flat-bottomed shape is assumed to be less efficient than with the circular shape. However, no penalties due to the larger fuselage were used in the performance estimates, it being assumed that structural techniques will advance concurrently.

A comparison of the radius obtainable with the standard and the improved configurations at Mach 4, using idealized engines, is given in figure 11. The standard configuration has a radius of 3400 nautical

[redacted]

miles, and the improved configuration has a radius of 4100 miles. The gain in radius is due in part to the reduction of both nacelle drag and fuselage boattail drag obtained by installing the engines in the fuselage and in part to the added lift of the flat-bottomed shape.

The improvement in radius of 700 miles with the advanced configuration results in a radius about the same as that attainable at Mach 3.0. However, this radius is still less than that desired. In addition, it should be remembered that the assumption of no structural penalties in the new configuration represents quite an advance in technology of aircraft structures.

Penalties of self-boosting. - From the analysis it has been determined that, using hydrogen as a fuel, it may be possible to design airplanes that can achieve radii from 2700 to 4100 miles at Mach 4. The lower figure is for a system representing but moderate improvements in engine and aerodynamic technique. The higher radius is for greater refinements in both of these areas. These results are for manned aircraft that takeoff and land under their own power. From time to time reference has been made to the compromises forced upon the airplanes by this mode of operation. It is of interest to look back now and see what has been sacrificed in this manner.

Consider the so-called practical engine and airframe with a maximum radius of 2720 miles. Figure 12 shows radius as a function of target altitude for Mach 4 airplanes of the standard configuration using hydrogen fuel. The lower curve is for the normal climb procedure and is reproduced from figure 7. The middle curve assumes that some other means, such as a rocket booster, has been employed to transport the airplanes with a full fuel load up to the initial cruise altitude and Mach number. For this case, the maximum radius is 25 percent higher than that obtainable with the self-boost procedure. This is but a part of the price that has been paid.

All the turbine engines for these airplanes have approached operating as ramjets at the cruise condition. Indeed, the gas-generator portion of the engine, which was required only for the climb and acceleration phase of the flight, was an undesirable appendage both in weight and engine pressure ratio at cruise. If ramjets are merely substituted for the turbine engines and the weight saved is employed to carry more fuel, the combination of the additional fuel and improved cycle performance yields the results shown by the top curve. The ramjet-powered airplane has a radius 15 percent greater than the fully boosted turbine airplane and 44 percent higher than the self-contained turbine airplane. This example is, of course, far removed from a practical man-carrying operational airplane and is used merely for emphasis.

[redacted]

RAMJET MISSILES

The advantages of the ramjet as a propulsion system are more spectacular in missiles than in the realm of manned flight. Since only a one-way flight is considered, target distances are immediately doubled. For such bombardment systems all the weight associated with a crew need not be carried; and, further, advantage can be taken of the higher flight speed capability of the ramjet.

For such missiles, as was the case for manned airplanes, all the factors of engine and airframe design have been merged into the analysis of a series of missiles. The performance potential of those missiles has been determined in terms of absolute range attainable. This has been done for Mach numbers from 5 to 9 for different fuels and methods of missile boost.

Airframe and Engines

Configuration. - The general aerodynamic configuration of the missiles analyzed is illustrated by the models in figures 13 and 14. This particular model represents a hydrogen-fueled Mach 7.0 missile having a gross weight of 38,400 pounds, including a 10,000-pound payload and a fixed weight of 1550 pounds. For the reasons discussed in paper 3, a single ramjet engine installed in the fuselage is used. A simple two-shock inlet is employed because of the research and development problems yet to be solved with the higher performance inlets. The exhaust nozzles have fixed areas, with a slightly conservative velocity coefficient of 0.96 assumed. The engines are of double-walled construction, and fuel was used as the coolant except when diborane was used for fuel, in which case water was supplied for cooling. The missile is a canard configuration with a fuselage fineness ratio of 20 and a wing sweep of 72.5°. The LOX-JP boosters (attached as shown in fig. 14) bring the total weight up to 150,000 pounds at ground launch.

Flight path. - The rocket booster carries the missile to the initial cruise altitude and cruise Mach number. After booster separation, the missile follows a Breguet flight path to the target, climbing perhaps 5000 feet. Near the target, using normal procedure, the engine is cut, a pull-up is executed to reduce velocity, and dive-in occurs.

Fuel type. - As the first step of the analysis, the suitability of various fuels was examined. This study gave the results shown in figure 15, where relative range is plotted as a function of missile plus booster weight for operation at Mach 5. The payload is 10,000 pounds, and chemical-equilibrium expansion in the exhaust nozzle is assumed. Data are given for three fuels: liquid methane, liquid diborane, and hydrogen. Liquid methane was selected as the most promising hydrocarbon fuel because of its high heat-sink capacity - more than twice that of JP.

[redacted]

For all fuels, the range increases with missile-plus-booster weight for the same reasons that the larger airplanes were beneficial. Comparison of the fuel types shows clearly that methane, with its low heating value, is inferior to hydrogen. Except for one fault, liquid diborane (the dashed curve) is as good as hydrogen. The difficulty is that diborane is a very poor heat sink and cannot be used to cool the engine. If enough water to cool the engine is carried, the range is cut in half, despite the assumption that the vaporized water provides some additional thrust with an impulse of 150 seconds.

This concern about liquid-cooling results from the fact that at Mach 5 the high stagnation temperature of air precludes the use of conventional cooling liners. One way the cooling problem might be alleviated would be to use insulation in the combustion chamber (e.g., foamed ceramics). Then the diborane would not be so heavily penalized for the cooling water. However, at Mach 5, hydrogen still seems clearly superior to the other fuels with respect to range. The superiority is even more pronounced at higher Mach numbers where aerodynamic heating becomes more severe.

It should be noted that at this Mach number (i.e., 5), liquid methane can yield 75 to 80 percent of the range attainable with hydrogen. As will be established in a following section, this represents an appreciable capability. If Mach 5 is considered an acceptable flight speed, liquid methane should be seriously considered as an alterante fuel, although results are presented primarily for hydrogen-fueled missiles.

Structural weight. - Before discussing actual performance numbers, one more important facet of this picture needs to be defined. This is structural weight. The extreme sensitivity of range to missile structural weight is illustrated in figure 16. Here relative range is plotted against ratio of structural to missile weight for cruise Mach numbers of 7.0 and 9.0 and a total missile weight of 30,000 pounds. For example, at Mach 7.0 a change from 0.3 to 0.4 in ratio of structural to missile weight reduces the relative range from 1 to 0.6, a 40-percent loss.

The schedule of structural weight used in the analysis is given in figure 17. Here the ratio of structural to missile gross weight is plotted against missile gross weight for cruise Mach numbers of 5, 7, 8, and 9. The payload is 10,000 pounds and the fuel is hydrogen. To keep structural weights realistic, the equations were based on weights of current design proposals in the industry, including boost-glide vehicles. At Mach 5.0 stainless-steel construction was assumed. At Mach 7.0, with its higher metal operating temperatures, the material was changed to a super alloy, which has a higher density. The increase in metal density and the higher operating temperatures account for the weight increase between Mach 5.0 and 7.0. Weight increases above Mach 7.0 were made to allow for leading-edge cooling and operation of the metal structure at still higher temperatures.

[redacted]

Missile Capabilities

Target altitude and Mach number. - Figure 18 shows range as a function of target altitude for missiles with cruise flight Mach numbers from 5.0 to 9.0. The missiles have a takeoff weight of 150,000 pounds with a payload of 10,000 pounds; LOX-JP rockets provide full boost to the initial cruise point. At each flight Mach number there is an optimum altitude, an optimum determined by the same factors discussed for the turbojet airplanes. The optimum altitude increases from 105,000 feet at Mach 5.0 to 110,000 feet at Mach 7.0. At Mach 8.0 and 9.0, however, it increases only slightly owing to the increase in structural weight. To reduce the contribution of aerodynamic heating to the total heat load, it has been elected at Mach 8 and 9 to operate at altitudes somewhat higher than that for maximum range, as shown by the tick marks. Accordingly, the portions of the curves where heating is considered excessive are shown by broken lines. Data given in succeeding figures correspond to the tick marks. Even at the higher altitude, it may well be necessary to provide internal insulation in regions of high heat flux in the engine to permit operation at Mach 9.

Despite the large 10,000-pound payload and relatively modest 150,000-pound missile-plus-booster weight, range is not a major problem. At Mach 5.0 the range is 10,500 nautical miles. At Mach 7.0 the range is 9000 miles. The ranges at Mach 8.0 and 9.0 are still respectable; however, it must be recognized that at these speeds the data are less certain because of more uncertainty in structural weight and the more serious consequences if chemical-equilibrium expansion in the nozzle is not fully achieved.

Gross weight. - The ranges at Mach 5 and 7 appear to be more than adequate. Suppose, then, that the problem is approached from a different viewpoint; that is, how little weight can be used and still deliver the specified payload for the ranges of interest. There is considerable interest at present in ranges between 6500 and 8500 nautical miles.

In figures 19 and 20, missile-plus-booster weight is shown as a function of payload for Mach numbers of 5 to 9 for these ranges. As is to be expected, an increase in payload requires a larger carrier and hence an increase in missile-plus-booster weight. Most of the discussion to this point has centered around a 10,000-pound payload. It has been suggested that an air-breathing missile may be able to use mid-course correction, say by map comparison, and thus reduce circular probable errors over the target. Suppose for this reason, or because bomb yields are improved, the payload weight can be reduced to 3000 pounds, for example. With this payload, the 6500-mile target may be hit at Mach 7 with a total takeoff weight of only 61,000 pounds. The range of 8500 miles would require a total weight of 81,000 pounds.

[redacted]

At the other extreme, suppose a bigger payload were needed. A 20,000-pound payload, perhaps a cluster of smaller bombs, could be delivered a distance of 6500 miles at Mach 7 for a weight at takeoff of 200,000 pounds. The corresponding value for an 8500-mile range is 239,000 pounds, which is about the same as current intercontinental ballistic missiles.

Comparison with ICBM. - To provide a familiar plane of reference, this weight and payload comparison with current ICBM's should be amplified. It should be emphasized that such ballisitic missiles reflect present technology, whereas the ramjet missile incorporates advanced concepts. It should also be emphasized that this is not an attempt to compare overall merit, since it is beyond the scope of this paper to assess factors such as relative cost, vulnerability, or target accuracy.

For equal takeoff weight, the Mach 7.0 ramjet missile will deliver seven times the payload of the current ICBM, and deliver it 1000 nautical miles farther. Or, looking at it another way, the same payload can be delivered 1000 miles farther for 27 percent of the current ICBM takeoff weight. This weight comparison may not be as unfair as it would appear at first glance, because the rocket booster for the Mach 7 ramjet missiles being considered is 75 percent of the total weight. These boosters employ the same technology as used in current ICBM's. High-energy rocket propellants should provide reductions in the takeoff weights for both systems.

Ramjets for boost. - Thus far the discussion has been confined to full rocket boost to the cruise Mach number. It is well known, however, that ramjet impulses are much higher than rocket impulses in the supersonic Mach number range of interest here. Accordingly, the use of a ramjet boost stage from Mach 3.0 to 7.0 was examined. A missile configuration incorporating a ramjet boost stage is shown in figure 21. The missile weighs 27,400 pounds, and the boost stage 7800 pounds. The ramjet booster contains a separate engine and hydrogen fuel tank. The design Mach number of the fixed-geometry engine is 4.5, using a simple 4° ramp inlet. For compatibility with the booster stage, the missile was altered to a high-wing design with twin inlets for the cruise engine. Double-shock inlets were used for the cruise engine, which is inoperative during boost.

The boost trajectory with this system is shown in figure 22 as a plot of altitude against Mach number. Conventional rocket boost is employed to Mach 3.0 at 47,000 feet, where separation occurs. Acceleration with the booster ramjet then occurs to Mach 7.0 at a constant dynamic pressure of 1800 pounds per square foot. This is followed by a constant Mach number climb on the booster engine to the initial cruise altitude of 100,000 feet. The ramjet boost stage then separates and cruise begins.

The effect of this ramjet boost stage on weight is illustrated in figure 23. Gross weight of the Mach 7.0 cruise missile is 35,200 pounds.

[redacted]

Range is constant at 6100 nautical miles with a 10,000-pound payload. Studies have shown that for some applications, such as boost-glide vehicles, the total takeoff weight is strongly affected by the size of the engine in the ramjet boost stage. Accordingly, total missile-plus-booster weight is shown as a function of the size of the ramjet booster engine, where the engine size is specified in terms of net thrust at Mach 3.0. At the left, for comparison, is shown a weight breakdown for full rocket boost. The total weight is subdivided into rocket fuel, total ramjet fuel, and total weight of hardware, which includes structure, tanks, engines, payload, and fixed weight.

Miminum total weight of 102,000 pounds is achieved at an engine size that corresponds to 32,000 pounds of thrust at Mach 3.0; and the weight is relatively constant in the thrust range covered for this application. This represents a one-third reduction in total weight from the 149,000 pounds for full boost on conventional rockets. From the weight breakdown it is seen that the hardware weight is virtually unaffected, and that the saving is entirely in rocket fuel. It may be concluded, then, that the use of a ramjet boost stage would reduce markedly the missile-plus-booster weights presented in figures 19 and 20. There is certainly a question, however, as to whether the saving in rocket fuel would warrant the added complexity of the ramjet booster stage.

Air-to-surface mission. - Within the scope of this discussion there lies the interesting possibility for launching a ramjet missile from a turbine-powered manned aircraft. At takeoff and up to Mach 3.0, the ramjet missile with its ramjet boost stage could ride "piggy-back" on a hydrogen-fueled turbine-powered aircraft. At Mach 3.0 and the maximum radius of the manned aircraft, the missile would leave the mother plane and accelerate to Mach 7.0. At this point it would drop its boost stage and continue to the target at Mach 7.0 cruise. The case analyzed would have a takeoff weight of 300,000 pounds, with the missile weight replacing fuel and payload of the mother airplane. In the following range calculations, it was optimistically assumed that the lift-drag ratio of the combination was the same as that of the mother airplane. This is perhaps compensated for to some extent, however, by the fact that no effort was made to reoptimize the bomber for this particular mission.

The capabilities of this combination of manned aircraft and ramjet missile are indicated in figure 24, where total range is plotted against ramjet-missile plus ramjet-booster weight for payloads of 1500 and 10,000 pounds. Hydrogen fuel was used for both aircraft and missile. Over-all missile length, including the ramjet booster, is cross-plotted. For example, a 155-foot missile weighing 35,000 pounds and carrying a 10,000-pound payload has a total range of 9300 miles. Of this range, 3025 miles are attributed to the distance traveled by the mother aircraft before launching the missile. If a range of only 8500 nautical miles is required, and lighter payloads are acceptable, then the extra range

[redacted]

capabilities of a given gross weight might be traded for higher delivery Mach numbers. Considerable flexibility is provided by this combined system, since the mother aircraft could still be used as a bomber.

One of the major problems when carrying a hydrogen-fueled missile is evaporation of the missile fuel during the flight time on the mother aircraft. If evaporation had been considered in the preceding example, it is estimated that the total target distance would have been reduced from 9300 to 8300 nautical miles, a 10-percent loss. This loss may be reduced by schemes of varying complexity and additional weight.

If delivery of the missile at Mach 5 is acceptable, the use of methane as a missile fuel appears attractive. The somewhat higher temperature of liquid methane would alleviate the fuel-evaporation problem to some extent and still give ranges approaching 7700 nautical miles for a 35,000-pound missile carrying a 10,000-pound payload.

CONCLUDING REMARKS

This paper has presented the estimated capabilities of missiles and manned aircraft designed for long-range bombardment missions and powered by chemically fueled, air-breathing engines. To help put these results in the proper perspective, figure 25 shows a plot of unrefueled radius as a function of flight Mach number for manned turbine-powered bomber airplanes. The curves on this figure indicate the broadening of the horizons for such aircraft over the last few years. The circled points indicate the unrefueled capabilities of current operational and prototype bomber aircraft. All but one of these airplanes have only subsonic capability and have radii from 2000 to 3500 miles. The one airplane with supersonic capability was designed for a split mission and for this reason as well as its small size has relatively poor supersonic radius capability.

In 1955 it was considered logical to perform mission studies for turbine-powered airplanes up to cruise Mach numbers of 3.0. With hydrocarbon fuels, radii of the order of 1200 miles at Mach 2 and 700 miles at Mach 3 were considered possible. At that time hydrogen entered the picture as a possible turbine-engine fuel and, with this fuel, the radius attainable rose to 2000 miles at Mach 2 and about 1300 at Mach 3.

In the meantime large advances in aerodynamics were achieved. Combining airplanes incorporating these advances with fairly conventional turbojet engines using hydrocarbon fuels may make possible radii of the order of 3000 miles at Mach 3. Such aircraft are typified by the WS-110 proposals indicated by the square symbol in the figure. If hydrogen fuel and turbine engines of varying degrees of improvement are used with such airplanes, radii lying within the shaded area are possible. At Mach 4, for example, a 3400-mile radius is predicted. If still more advanced

[redacted]

airplane configurations are employed, the latter figure can be increased to 4100 miles. This last value should not be construed as an ultimate limit, because other possible improvements, such as long runs of laminar boundary layer on the airplane, have not been included in the analysis. These radii are all for payloads of 10,000 pounds and fixed loads of the order of 30,000 pounds. If lighter weapons or lighter accessory weights can be considered, these radii can, of course, be increased still further.

To sum up the picture for turbine-powered manned airplanes, it is felt that, through the use of hydrogen fuel and improved engines and airplanes, it is possible to achieve unrefueled radii at Mach 4 at least equivalent to those currently attainable at subsonic speeds. This increase in flight speed is often considered as desirable from the standpoint of vulnerability; but, as noted before, the unrefueled radius falls short of the minimum for intercontinental missions.

When the hydrogen-fueled ramjet missile is included, the picture broadens to that given in figure 26, where unrefueled target distance is given as a function of cruise Mach number. The ramjet-missile curve represents fully rocket-boosted configurations as well as those employing partial ramjet boost. All these missiles are capable of delivering 10,000-pound payloads. The target distances for these missiles easily exceed the most stringent requirements, and targets can be reached at speeds up to Mach 9.

If the partial-ramjet-boost missile of Mach 7 cruise design is combined with a Mach 3 hydrogen-fueled airplane as a carrier, target distances ranging from 10,000 miles for the 10,000-pound payload to 14,000 miles for a 3000-pound payload may be attained, as shown by the shaded bar. Such a system has an inherent flexibility, as each component can be used separately for different applications.

This, then, is the picture that can be painted for missiles and manned airplanes for long-range applications powered by air-breathing, chemically fueled engines.

This discussion has not attempted to evaluate such factors as cost, development effort, development time, or vulnerability. Factors such as these must certainly be considered in deciding whether to develop a new weapons system, whether it be a manned bomber, a ramjet missile, or some other system such as an ICBM. It is hoped, however, that the information presented herein will provide a useful foundation on which such decisions can be logically based.

[redacted]

TURBINE POWERPLANTS SELECTED

ENGINE	TURBOJET	TURBOJET	TURBOJET	AIR TURBOROCKET (AIR LIQUEFACTION)
DESIGN FLIGHT, M_0	3.0	4.0	4.5	4.0
SEA LEVEL COMPRESSOR P. R.	5.0	2.3	2.3	1.71
TURBINE INLET TEMP, °R	2500	1900 2500	2500	2000
BOOST AFTERBURNER TEMP, °R	4000	4000	4000	4000

CS-14657

Table I

STANDARD HYDROGEN FUELED CONFIGURATION

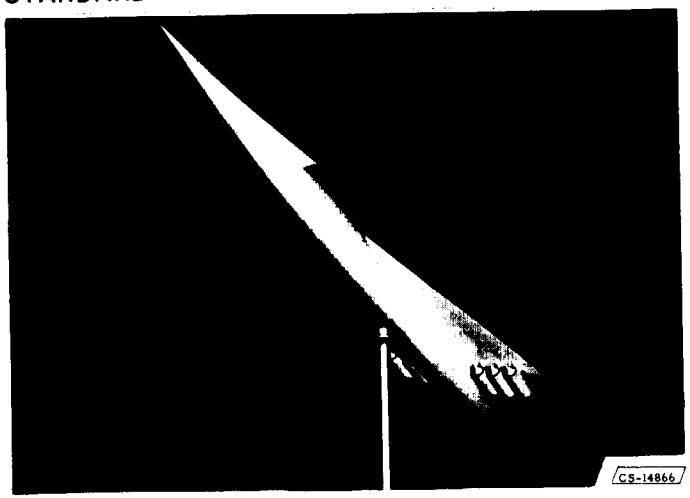

Figure 2

ZONES OF ENGINE APPLICATION CONSIDERED

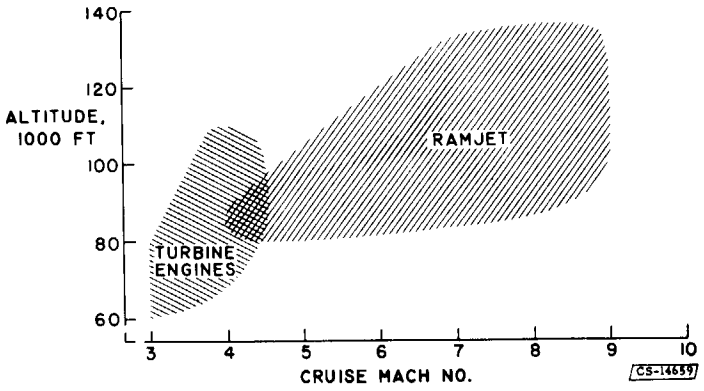

Figure 1

TYPICAL CLIMB PATH

CRUISE MACH NO., 4

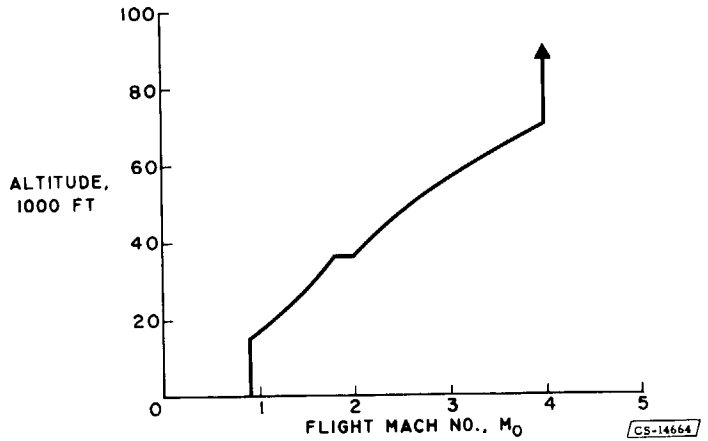

Figure 3

EFFECT OF GROSS WEIGHT ON RELATIVE RADIUS

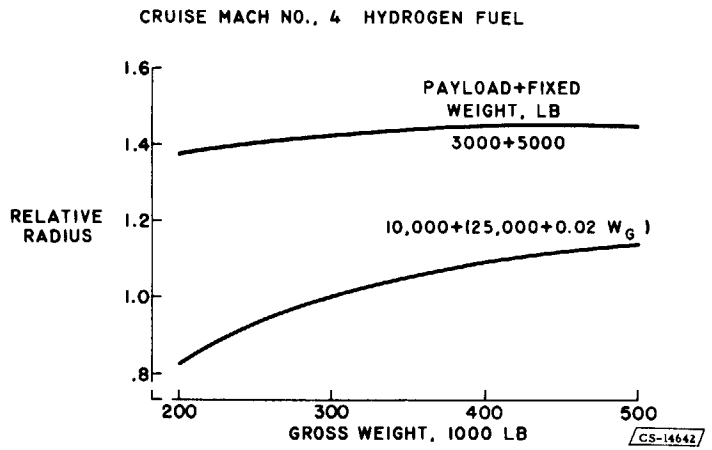

Figure 4

EFFECTS OF WING LOADING

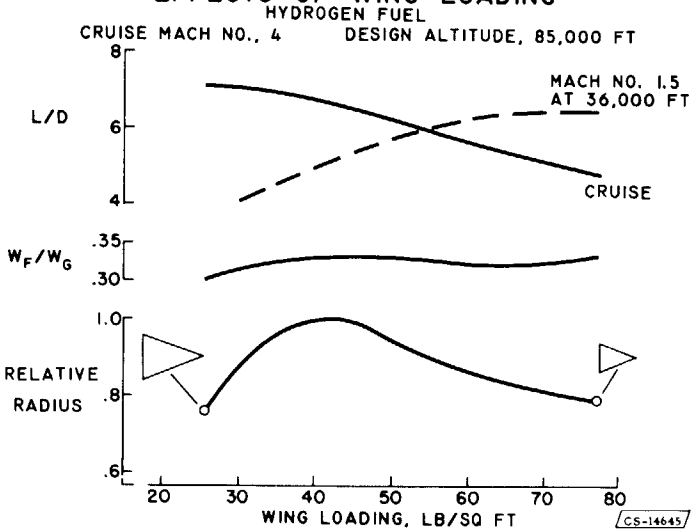

Figure 6

EFFECT OF GROSS WEIGHT FOR TWO FUELS

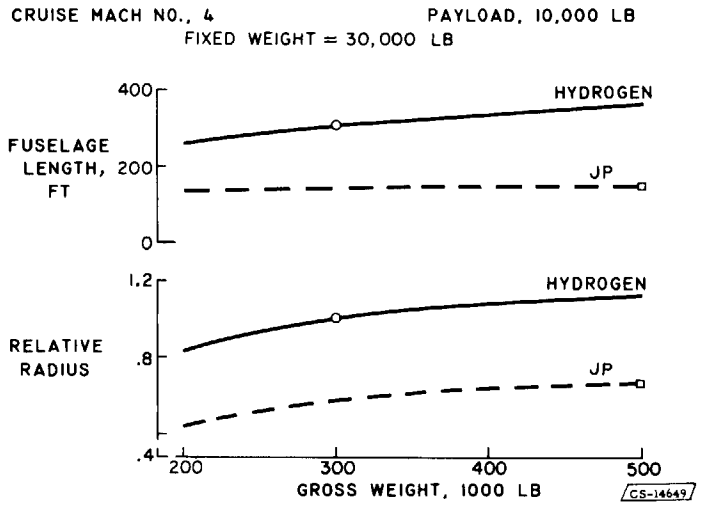

Figure 5

EFFECT OF TARGET ALTITUDE

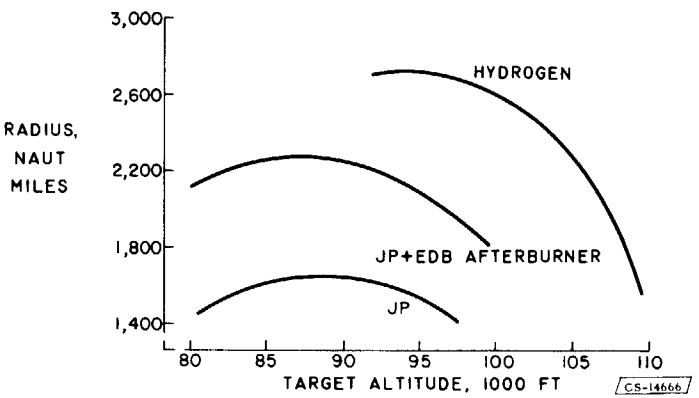

Figure 7

RADIUS WITH AIR-TURBOROCKET ENGINES

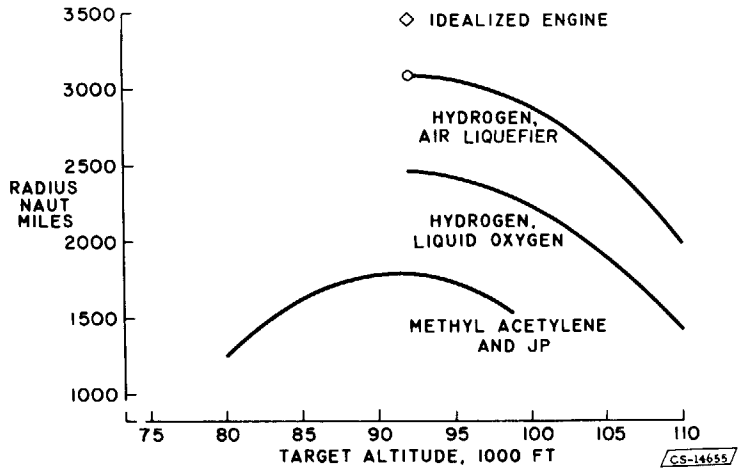

Figure 8

EFFECT OF CRUISE MACH NUMBER

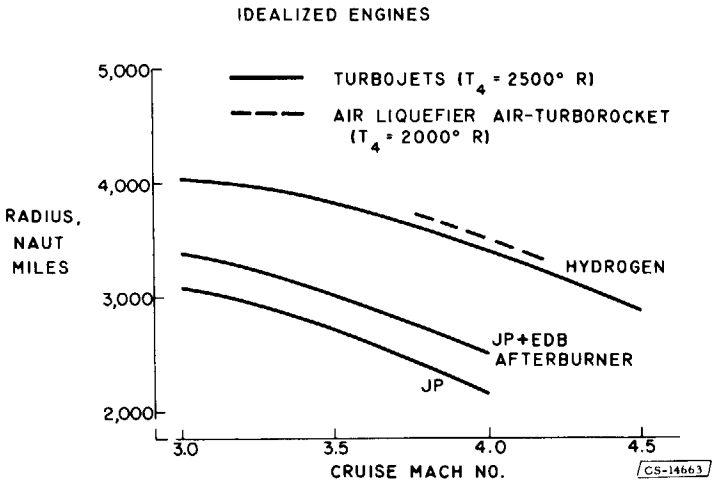

Figure 9

IMPROVED HYDROGEN FUELED CONFIGURATION

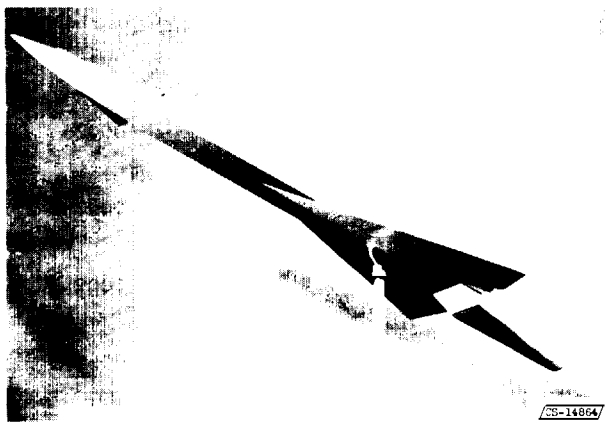

Figure 10

EFFECT OF AIRFRAME IMPROVEMENTS

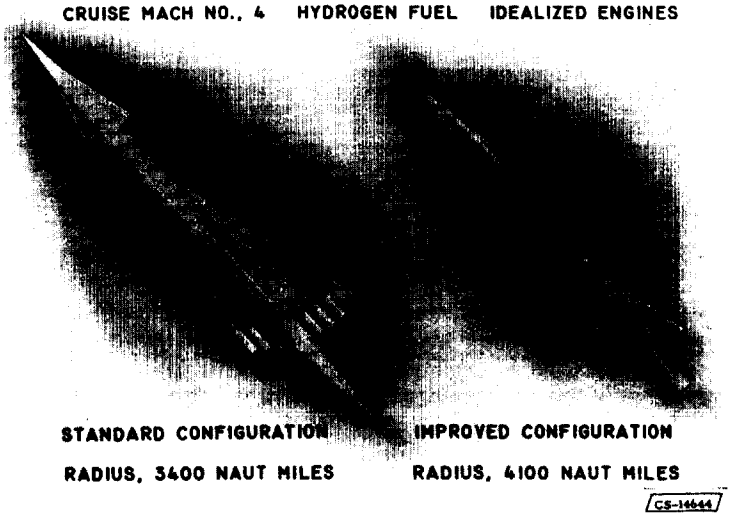

Figure 11

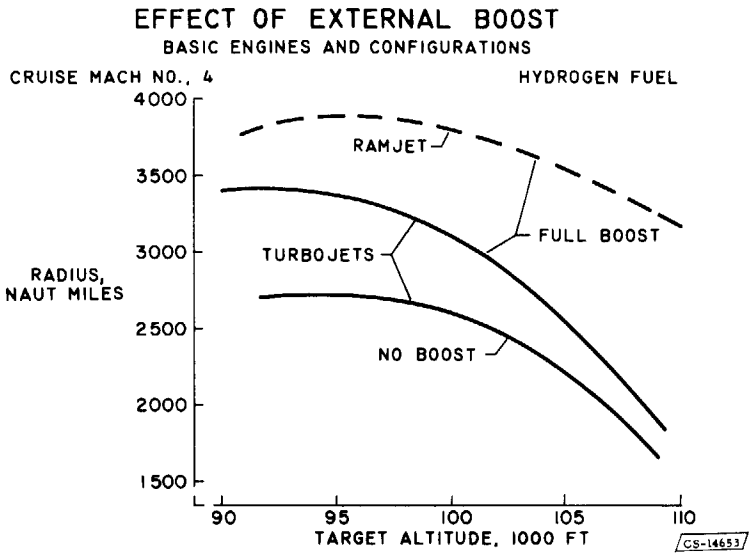

Figure 12

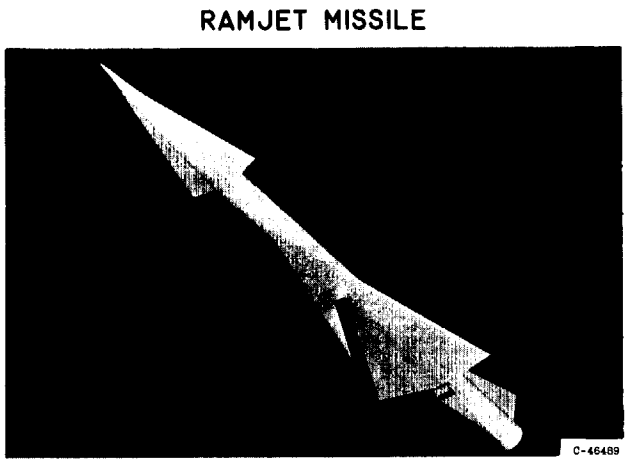

Figure 13

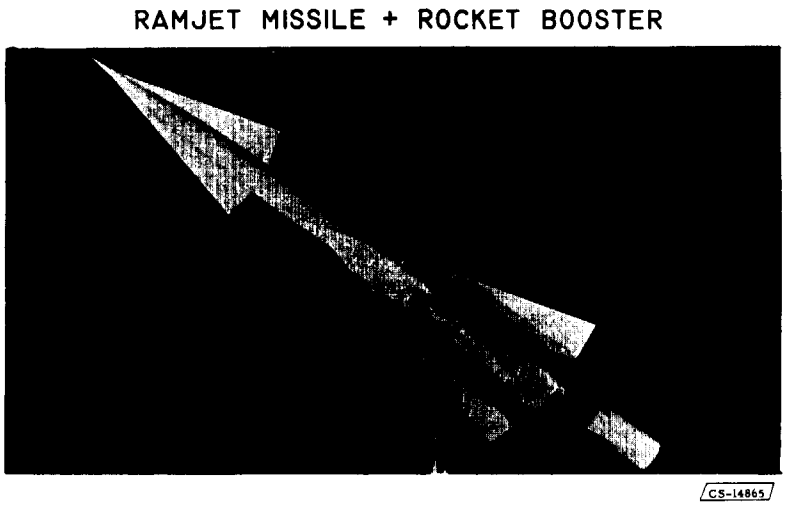

Figure 14

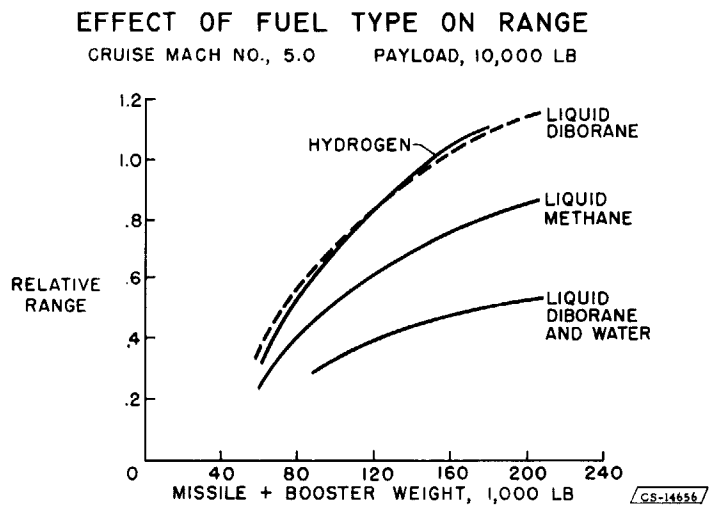

Figure 15

EFFECT OF STRUCTURAL WEIGHT ON RANGE

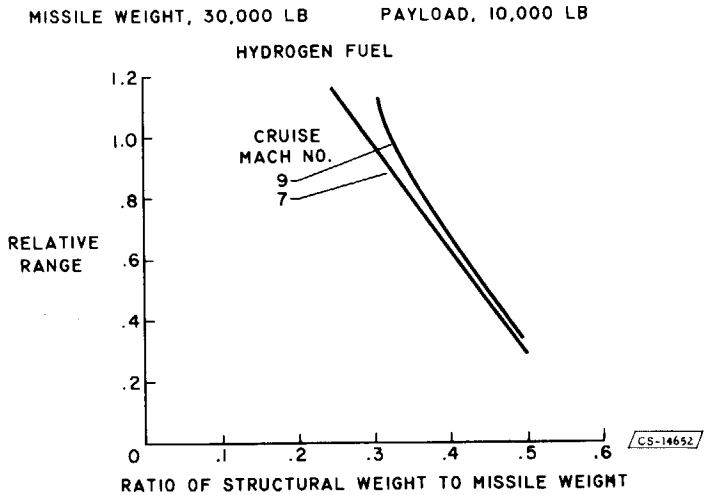

Figure 16

STRUCTURAL WEIGHT SCHEDULE

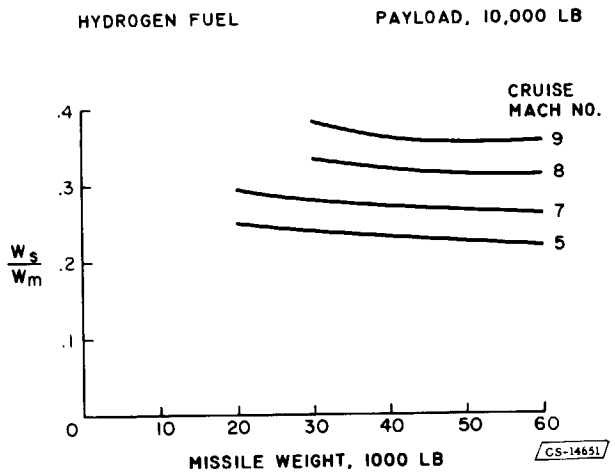

Figure 17

EFFECT OF ALTITUDE AND MACH NUMBER ON RANGE

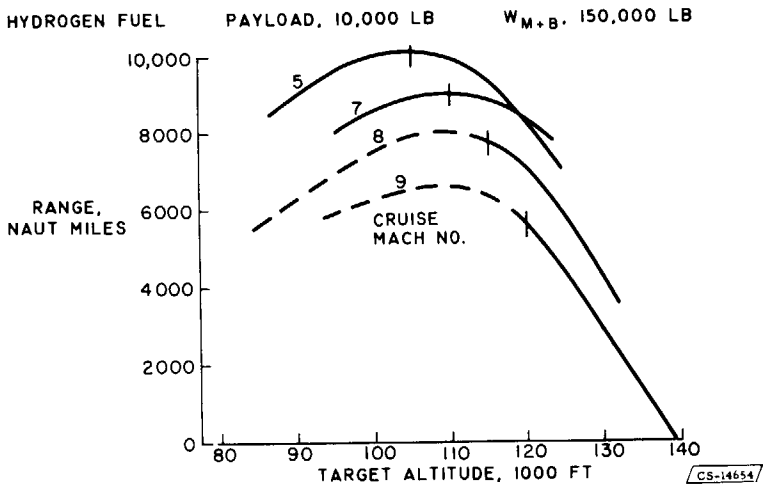

Figure 18

WEIGHT REQUIRED FOR 6500 NAUTICAL MILE RANGE

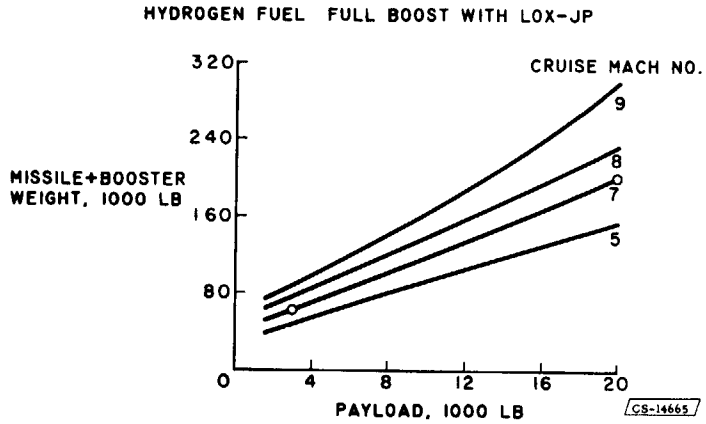

Figure 19

WEIGHT REQUIRED FOR 8500 NAUTICAL MILE RANGE

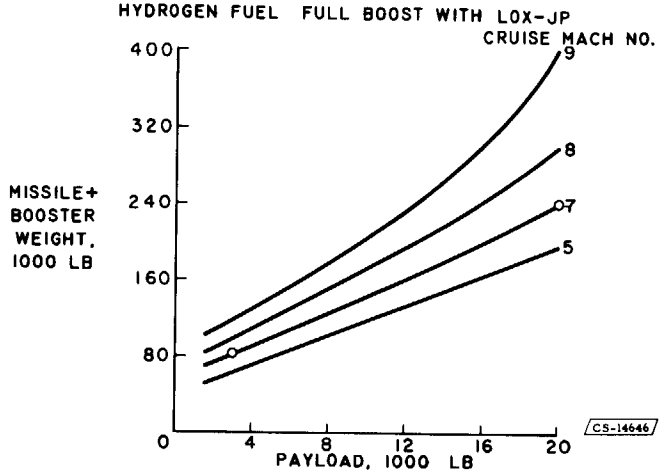

Figure 20

MISSILE WITH RAMJET BOOST STAGE

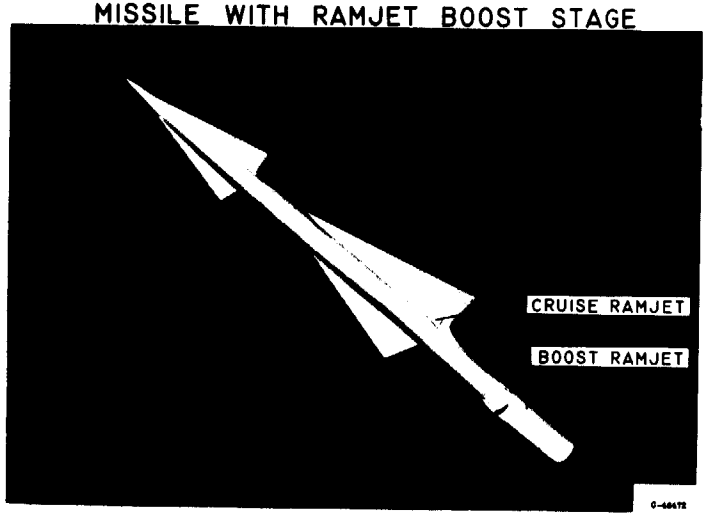

Figure 21

TYPICAL FLIGHT PATH WITH RAMJET BOOST STAGE

CRUISE MACH NO., 7

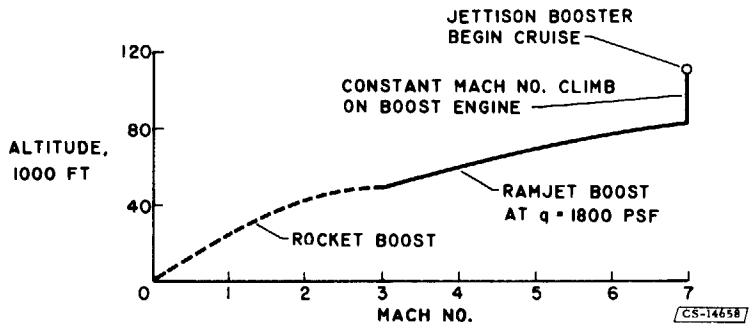

Figure 22

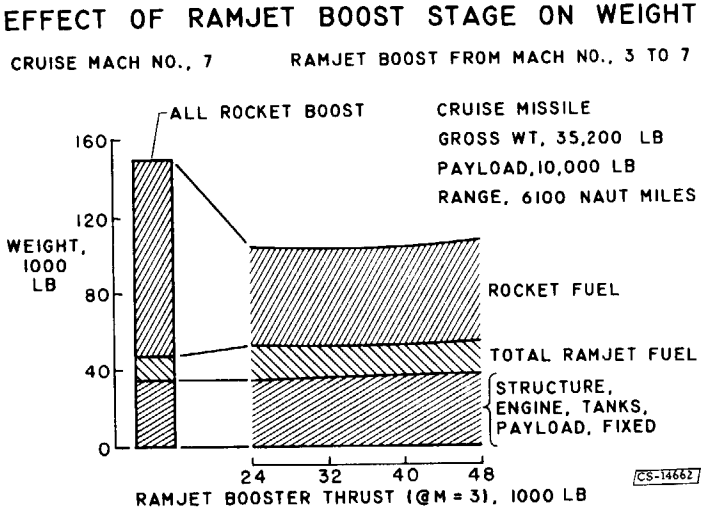

Figure 23

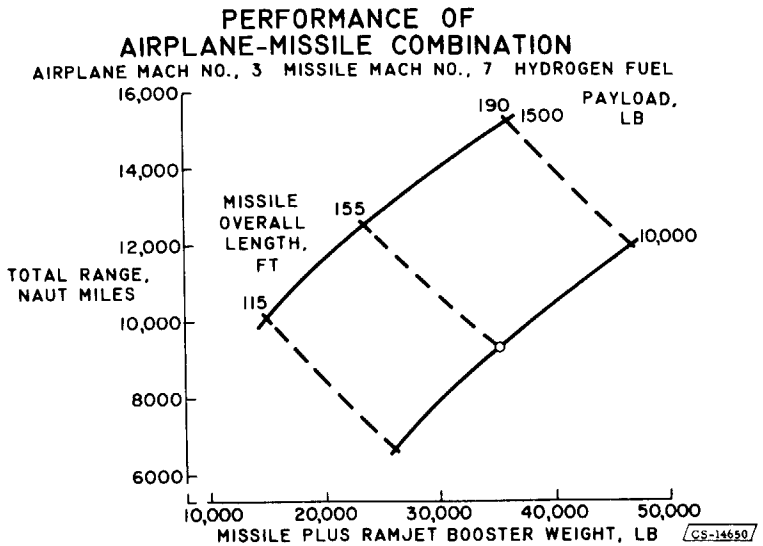

Figure 24

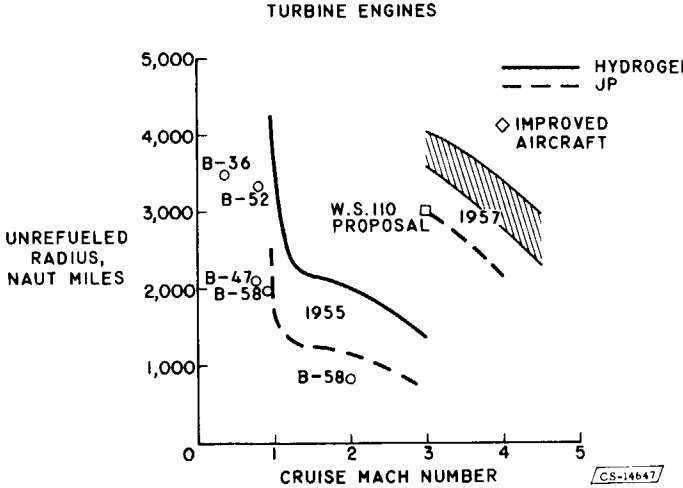

Figure 25

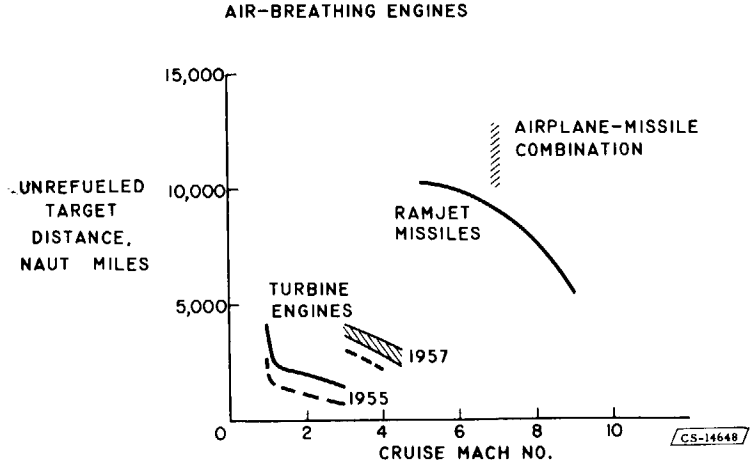

Figure 26

6. PROPELLANTS

By E. A. Fletcher, H. W. Douglass, R. J. Priem,
and G. Vasu

INTRODUCTION

The mission that a rocket can accomplish is a function of the energy supplied to it and the weight of the vehicle. The performance of a rocket is often expressed in terms of the burnout or final velocity of the vehicle. This velocity is a function of the specific impulse of the propellant and the ratio of the gross weight to the empty weight of the vehicle.

This paper discusses propellants capable of achieving high specific impulse and some of the problems associated with their use. The following topics are of primary interest in this matter:

(1) propellants available and their specific impulses

(2) combustion efficiency

(3) combustion instabilities

(4) combustor cooling

A propellant combination is of little use unless it can be burned efficiently in an engine; this presents the problem of obtaining maximum combustion efficiency in as small an engine as possible. Efficiently burning high-energy propellants are used to propel extremely complex missile systems. The various missile and engine components have oscillatory modes which can oscillate in such a way that the oscillations reinforce each other and can even oscillate badly enough to tear the missile completely apart. Thus, combustion instability is of great interest.

High-energy propellants usually produce higher temperatures; the rates of heat transfer to the walls of the thrust chambers are going to be higher. Consequently, combustor cooling achieves greater importance.

Propellants

Propellant combinations that have a reasonable chance of being used in rocket propulsion are represented by those tabulated in table I, which

122

[redacted]

gives the theoretical maximum sea-level specific impulses for a number of propellants. These propellants are divided into two groups: storable propellants, which require very little or no last minute preparation of the missile for launching, and nonstorable propellants, which require filling or topping off of the propellant tanks before the missile is launched. The propellants in the second group are nonstorable because they contain cryogenic liquids (i.e., liquefied gases).

The specific impulses are shown for combustion-chamber pressures of 300, 600, and 1000 pounds per square inch absolute. The storable liquid propellants represented by the RP-1 - red fuming nitric acid combination have higher specific impulses than the conventional solid propellants represented by the cast composite propellant.

The newer solids, represented by the polyurethane-aluminum-perchlorate and the polyvinyl chloride-diester-aluminum-perchlorate propellants, have impulses which reach into the regime between 260 and 270 and are competitive with storable liquid propellants. Solid-propellant rockets usually achieve some advantage in specific impulse by operating at higher combustion-chamber pressures than the liquid-propellant rockets. But they must pay a weight penalty for this increase in specific impulse in the form of larger, heavier thrust chambers which must be large enough to contain all the propellants and strong enough to withstand the higher pressures.

The most energetic propellant combinations are the exotic liquids, which are listed on the bottom part of table I. One combination, hydrazine with chlorine trifluoride, is storable. The remaining combinations are nonstorable because they contain the liquefied gases - fluorine, oxygen, or hydrogen. The most energetic of all these propellant combinations is the hydrogen-fluorine system which has a specific impulse of 409 at a combustion-chamber pressure of 1000 pounds per square inch absolute.

With liquid propellants, 409 is probably the highest possible specific impulse obtainable using conventional combustion reactions, unless liquid ozone is considered as a possible oxidizer. Hydrogen-ozone is expected to give a theoretical specific impulse of 386 at a combustion-chamber pressure of 300 pounds per square inch absolute. However, since this oxidizer is very difficult to handle and store, liquid ozone is not considered as a likely possibility at the present time. The cryogenic liquids now being considered give the highest specific impulses that can be reasonably expected with ordinary combustion reactions.

Solid propellants have been limited in the past by the stringent requirements of their physical properties. In addition, these propellants must be stable, unreactive, and storable. These requirements have given the solid propellants their well deserved reputation for reliability and "off the shelf" availability. Since the reactivity of the propellant

[redacted]

usually goes up as the heat of reaction increases, solid propellants having high specific impulses have been difficult to make. However, it is reasonable to expect that solid propellants having high specific impulses will be developed, and novel packaging techniques will be perfected for using these propellants.

One approach to synthesizing reliable high-energy storable packages might be to combine the advantages of fuel-oxidant separation of liquid-propellant rockets with the convenience and reliability of fuel-oxidant storage in the thrust chamber of solid-propellant rockets. Reactive propellant combinations might be stored within the thrust chamber as they are in the solid rocket, but separated from each other, as they are in the liquid rocket, by relatively unreactive but combustible plastic sheets, tubes, or capsules instead of metal tanks. One technique for doing this is illustrated in figure 1.

For obvious reasons, the resulting grain (fig. 1) is called the candle type grain. It consists of a core of lithium perchlorate oxidizer that is protected from the fuel on the outside by a polyester-styrene copolymer; this inner core, in turn, is surrounded by the fuel, in this case lithium metal. Preliminary experiments at this laboratory have shown that this kind of grain will burn smoothly and vigorously and is safe and easy to handle. If new packaging techniques are considered, there is reason to believe that specific impulses higher than those tabulated can be achieved.

The effect of the heat of reaction on propellant performance is shown in figure 2 in which the theoretical specific impulse I_s is plotted against the heat of reaction. Data are presented for conventional double-base propellants, composite propellants, and a group of N-fluoro derivatives, which were proposed by Dr. Niederhauser of Rohm and Haas at the June, 1957 meeting of the joint Army-Navy-Air Force Solid Propellants Group. There is a great deal of scatter of the points because the specific impulse does not depend on the heat of reaction alone. It is a function of the molecular weights and heat capacities of the products as well. In general, as the heat of reaction goes up, the specific impulse of the propellants increases.

In order to illustrate future trends, vertical lines (fig. 2) indicate the heats of reaction for three of many other possible propellant combinations. These are a hydrocarbon containing 10 percent lithium as fuel with nitrosyl perchlorate as the oxidizer, decaborane with lithium perchlorate, and lithium with lithium perchlorate. Although these lines have been extended to intersect the curve, the point of intersection is not significant and should not be used to estimate specific impulse. The properties of the products of these reactions will undoubtedly be different from those of more conventional propellants. The molecular weights will be higher, and the specific impulses will not be as high as might be

[redacted]

expected by extrapolating to the ordinate. However, figure 2 does indicate that there is a possibility of obtaining higher energy solid propellants.

Free radicals and the specific impulses obtainable from them are becoming of increasing interest in rocket propulsion work. Free radicals are fragments of molecules. They are obtained from ordinary molecules by breaking the chemical bonds in these molecules. In order to break the chemical bonds, energy must be supplied to the molecule, but this energy can be recovered when the fragments are either burned or allowed to recombine. For example, hydrogen molecules are composed of two hydrogen atoms that are held together by a very strong chemical bond. If enough energy is supplied, this bond can be broken and the atoms can be separated. For hydrogen, 93,000 Btu's are needed to separate 1 pound of hydrogen into its atoms. When these atoms are allowed to recombine, all this energy is liberated. In comparison, the heat of combustion of hydrogen with oxygen is only 6800 Btu's per pound.

Very high specific impulses should therefore be obtainable from free radicals. But, unfortunately, the problem is not one of allowing the free radicals to recombine but to keep them from recombining until recombination is wanted. The Bureau of Standards is currently studying the fundamental chemistry and physics of free radicals. Included in their studies are attempts to isolate, stabilize, and concentrate free radicals. However, the possibilities of their use for rocket propulsion appear dim, as the highest concentration as yet reported of the free radicals which might be useful in rocket propulsion is about 1 percent. There are theoretical reasons for believing that the highest concentration capable of being stabilized will be about 16 percent.

Still, free radicals present an intriguing if remote possibility. This is illustrated in figure 3 where the specific impulse I_s of hydrogen atoms frozen in a hydrogen matrix at 0° R is plotted against atom concentration. The reaction products are expanded from a pressure of 300 pounds per square inch absolute in the combustion chamber to atmospheric pressure. The bottom curve assumes that thermodynamic equilibrium is achieved in the combustion chamber and that the gases are expanded in the frozen state through the nozzle. The middle curve assumes the same condition in the combustion chamber but assumes that thermodynamic equilibrium is maintained in the nozzle. The top curve uses the ordinate at the right and indicates the combustion-chamber temperature associated with this reaction.

The system of hydrogen atoms in a hydrogen matrix gives the highest specific impulse. If nitrogen atoms are substituted for hydrogen atoms, a maximum specific impulse of about 500 is reached at a nitrogen atom concentration of slightly over 20 percent. If imine radicals are substituted for the hydrogen atoms, a maximum specific impulse of about 450

[redacted]

is obtained at about 45 percent. It might be expected that, as the nitrogen atom or imine radical concentration increases, the performance should increase. However, the substitution of the heavy nitrogen atom for a light hydrogen atom increases the molecular weight of the product gases so that the specific impulse actually reaches a maximum at the points shown (fig. 3) and then begins to decrease again.

Combustion Efficiency

An idealized rocket model is shown in figure 4 in order to explain the important concepts in the combustion of rocket propellants. The oxidant and fuel are injected into the combustion chamber through holes in the injector. This figure shows two propellant streams impinging upon each other, a characteristic of a like-on-like injector. After some time and distance, the propellants are atomized into oxidant and fuel drops which vaporize as they move down the combustion chamber. Since there are both large and small drops, the rate of vaporization will vary both between drops and with distance. As the propellants vaporize, they mix and then react to form the desired hot combustion gases.

Considering atomization, mixing, vaporization, and reaction and their dependence on various design and operating parameters produces a very complex problem. One might expect that this problem might be simplified by isolation of the process that requires the greatest distance.

The rocket engine can be compared with the more familiar ramjet. The three significant differences between these two propulsion systems are shown in the following table:

Operating conditions	Rocket	Ramjet
Combustion-chamber pressure, atm	40	1/2
Propellant concentration, percent		
Fuel	20	3
Oxidant	80	20
Cross-sectional area, sq in./(lb/sec)	1	1000

The rocket operates at high combustion pressures, but the ramjet functions at a very low pressure. The propellant concentration of the ramjet is considerably lower than that for the rocket. A great amount of liquid propellant must be burned in a very small cross-sectional area in the rocket because its area is so much smaller than that of the ramjet.

These operating conditions affect the time and distance required for the processes that take place in the combustion chamber. This distance is analyzed in the following table:

[redacted]

Process	Relative distances	
	Rocket	Ramjet
Atomization	1	1
Vaporization	30	5
Mixing	1	4
Chemical reaction	<1	20

Since the atomization distance is about the same in both systems, it has been assigned a relative value of 1 for both systems. The lengths for the other processes are therefore relative to the distance required for atomization.

The length necessary to vaporize the propellants in the rocket engine is about six times that of the ramjet. This increase in length is due to the larger drops produced in the rocket engine. Mean drop sizes in a rocket engine are about 200 microns, whereas in the ramjet the drop size is in the order of 50 microns.

The slightly lower mixing length in the rocket engine is due to a very low cross-sectional area in the rocket. As a result, the distance between the streams which control the mixing distance is reduced.

The chemical reaction process requires a distance of <1 in the rocket engine as compared with 20 in the ramjet. This greatly reduced length occurs because the reaction distance decreases as the temperature is increased and the concentration of the propellant or the pressure increases. The increase in pressure in the rocket decreases the reaction length by a factor of 80. In addition, the increase in concentration and temperature will also reduce the length.

The previous table indicates that in the rocket engine the greatest distance is for vaporization, while the distances for atomization, mixing, and chemical reaction are all small in comparison. Thus, the distances required for atomization, mixing, and chemical reaction can be neglected, and the combustion efficiency in a rocket engine is assumed to be proportional to the fraction of the total propellant that has been vaporized in the engine.

The way in which the various parameters affect combustion efficiency should be considered. Varying the length of the combustion chamber is the first thing to consider. By using known vaporization equations the percent of propellant vaporized can be calculated as a function of chamber length as shown in figure 5. The engine efficiency is approximately equal to the percent of propellant vaporized. The slope of the curve for the calculated results continually decreases because the drops get smaller and smaller as they vaporize. The curve asymptotically approaches 100 since the largest drop is never completely vaporized.

[redacted]

The experimental results for a hydrogen-oxygen engine using the same injector agree well with the analytical curve.

The curves for all the propellants are characterized by two properties: where the knee occurs and where high efficiency is obtained. In the following discussion the length for 90-percent efficiency will be used to represent where the knee occurs in the curve, and the length for 99-percent efficiency will be used to show where high efficiency is obtained.

Since vaporization is the important parameter in the combustion of rocket propellants because of larger drop sizes, the drop size can be reduced in order to improve the efficiency. One of various fundamental concepts that can be used to reduce drop size is orifice diameter. The results of this test are shown in figure 6. Drop diameter is plotted against orifice diameter for an injection system similar to the like-on-like injector where two streams impinge upon each other. Gas was introduced behind the liquid stream to carry the drops down the chamber. Drop size reduced as the orifice diameter was decreased. The curve ends at an orifice diameter of 0.020 inch as this is the practical minimum that can be used in a rocket engine without the injector becoming plugged by foreign particles. Increasing the velocity difference, that is, the difference between the gas and liquid stream velocities also decreases the drop size.

The two chamber lengths defining the efficiency curve (i.e., those for 99- and 90-percent efficiencies) are plotted against injector orifice diameter in figure 7. The results of the analytical study, which calculates the percentage of propellant vaporized, are shown by the solid line. The experimental results for a JP-4 - liquid-oxygen system are shown by the squares. The length required for high efficiency decreases as the injector orifice size is decreased. The slope of the experimental results is even greater than that predicted analytically, which indicates that more is gained by decreasing injector orifice size than predicted. The results for the hydrogen with liquid-oxygen system, represented by the triangles, show the same characteristics.

Another parameter that affects engine efficiency is the difference in velocity between the drops and the combustion gases. Increasing this velocity difference increases the heat-transfer rates to the drop by reducing the boundary layer around the droplet. Increasing the gas velocity is the easiest way to increase the difference between the velocities of the gases and the drops; this can be done by building engines with lower chamber-to-throat diameter ratios.

The importance of slimmer engines on the combustion-chamber length required for high efficiency is shown in figure 8. A ratio of chamber-to-throat diameter of 3, compared with a ratio of 1, has resulted

[redacted]

analytically in a reduction of one-half the chamber length required for high efficiency. Since the slope of the curve through the experimental values for a JP-4 - liquid-oxygen engine using a like-on-like injector is greater than the slope through the analytical calculations, the actual effect of diameter ratio is even greater than had been predicted.

A comparison of the experimental results obtained using the analytical model with various propellants is presented in table II. These experiments were all done in a 200-pound-thrust engine, and the numbers represented in the table are the average of 15 or more tests. The same injector, chamber diameter, and liquid-propellant orifice size were used for all the tests. The ammonia and JP-4 fuels, both with liquid oxygen as the oxidizer, required 60- and 48-inch distances, respectively, in order to achieve 99-percent efficiency. Liquid ammonia and hydrazine, using liquid fluorine as oxidizer, required lengths of 65 and 56 inches, respectively. These four propellants are characterized by having fuels with high boiling points relative to the boiling points of the oxidizers, oxygen and fluorine. When gaseous hydrogen was used as a fuel with the cryogenic oxidizers, the lengths required to achieve 99-percent efficiency were reduced to 17 and 19 inches. This indicates that cryogenic fuels with cryogenic oxidizers vaporize faster and give higher combustion efficiencies in shorter thrust chambers.

Since drop size is a function of the injection velocity difference, another way of improving combustion efficiency is to decrease the drop size by having a high gas flow behind the liquid-propellant stream. The results of this test are plotted in figure 9 in which chamber lengths for 90- and 99-percent efficiencies are plotted against the injector pressure drop. The higher the pressure drop, the higher will be the velocity of the hydrogen. The injector with a high pressure drop has a very small orifice behind the liquid stream; for a low pressure drop a large-diameter orifice is needed behind the liquid stream. Increasing the gas velocity by increasing the pressure drop resulted in a shorter length for high efficiency. This indicates that a high hydrogen pressure drop is beneficial.

A model has been described which uses vaporization as the rate-determining process in establishing combustion efficiency and which gives results that are consistent with experimental data. This suggests that engines, in order to achieve maximum efficiency, should have thin chambers and small holes in the injector. Although these conditions are important in achieving the desired efficient combustion, the complete system should maintain its mechanical stability.

Combustion Instabilities

Figure 10 illustrates the flexible, elastic nature of a missile, which is represented as four mass concentrations - the motor, the oxidant

[redacted]

tank, the fuel tank, and the nosecone. The springs represent the flexible framework between the masses; the tank bottoms, cooling passage walls, and injector faces are also shown as flexible surfaces.

There are many ways in which such a structure can oscillate or vibrate. For example, aerodynamic loading at the nosecone can introduce disturbances which oscillate the propellant tanks and lines, thereby affecting the flow of propellants to the motor. The thrust produced by the motor can similarly cause pulsations or oscillations in propellant flow. Variations in combustion-chamber pressure also affect the flow into the motor by deflecting the cooling passage walls and by directly affecting the pressure drop across the injector.

Disturbances such as those produced, for example, by drag or thrust forces do not determine whether the system is stable or unstable. These forces only shake or vibrate the system, and this is not an instability in itself.

On the other hand, several paths have been indicated through which the combustion-chamber pressure can affect the flow. Since flow in turn affects the chamber pressure, a situation is present where even a very small disturbance can be perpetuated and amplified if conditions are right. For example, consider the effect of combustion-chamber pressure on flow through the cooling passages. Chamber pressure affects propellant flow, flow affects pressure, the new pressure affects flow, and so forth. Thus, an unstable system drives itself. In general, the oscillations that are generated build up until the system oscillates violently and sometimes destroys itself.

At this point it will be helpful to examine one of these feedbacks more closely. Figure 11 shows a sketch of a motor, an injector, and a tank supplying propellant to the injector at a constant pressure. The important elements which determine whether oscillations, chugging, will occur in this system are the variation of propellant flow with pressure drop, the variation of combustion-chamber pressure with propellant flow, and the time constants associated with these processes.

The time constants are related to the motor response. If the flow to the motor is suddenly changed, as indicated in figure 11, there is no immediate change in combustion-chamber pressure p_c. After a period of time α, the combustion-chamber pressure will rise. As propellant is added to the chamber at the new flow rate, the chamber pressure will continue to rise. The time between the start of the pressure rise and the attainment of the new equilibrium value is represented by τ, the time for this portion of the response to be 63 percent completed.

Two factors are important in determining if a system will oscillate. The first is the sensitivity of the system, which is called the gain or

[redacted]

amplification factor, and the second is the response of the system, which determines the conditions under which a reinforced signal is obtained. The amplification factor is related to $\Delta p/p_c$, which is the ratio of the injector pressure drop to the combustion-chamber pressure, and the response is related to α and τ.

A stability diagram for the engine-injector loop is presented in figure 12. The curve defines the regions of stable and unstable operation in terms of $\Delta p/p_c$ and α/τ. High ratios of $\Delta p/p_c$ and low ratios of α/τ improve stability. Low values of α are associated with short atomization, vaporization, and mixing times. These were previously shown to improve efficiency; they are shown here to improve stability. The time constant τ is proportional to the ratio of the chamber area to the throat area. Since low area ratios improve efficiency, good stability, therefore, may not always be compatible with good efficiency.

As shown in figure 12, stability can always be achieved by increasing the pressure drop across the injector sufficiently. If it is undesirable from the standpoint of the engine performance to do this, the same result can be achieved by inserting a restriction in the line ahead of the injector. However, any increase in pressure drop necessitates increased weights of the feed system in order to withstand the higher pressures.

Chugging stabilizers have been proposed also. Although these devices add complexity to the system, they do offer the hope of being able to operate at low values of injector pressure drop.

As previously indicated, there are a number of feedback paths to be considered in a missile system. Figure 13 presents some of the results of a study in which only one feedback is included through the framework. The system is represented as one mass for the upper portion of the missle, a flexible framework for the motor supports, and another mass for the motor.

At low time-constant ratios the stable range is decreased because of the flexibility, but for high values of α/τ the stable range is increased. The shape of the curve and the range of stable operation available depend on the masses, spring rates, fluid inertia, and compressibility effects, among other things. With many feedback paths and under other operating conditions the stable range can be changed considerably more than indicated here.

Figure 13 indicates that a larger stable range was available with the rigid system than with the original engine-injector system alone. This increase in stable operating range is the result of including propellant line and pump dynamics.

[redacted]

Another form of oscillation that rocket engines are subject to is the oscillation of the gases in the combustion chamber or "screaming." Screaming is associated with a pressure wave that travels back and forth in the combustion chamber and leads to high local rates of chemical reaction, high rates of heat transfer, and hot spots in the engine. Such hot spots can cause an engine to burn out in less than 1 second.

Screaming usually consists of oscillations in one of two modes. The first, a longitudinal mode, travels from the nozzle to the injector, reflects, and then travels back to the nozzle. The frequency of this wave is associated with the length of the chamber. The second is a transverse mode in which the wave travels around or across the chamber. The frequencies in this wave are associated with the diameter or the circumference of the chamber. Harmonics of either of these types of waves can also occur and have been observed experimentally.

The type of wave obtained is dependent on the geometry of the chamber as illustrated in figure 14. With a longitudinal mode the energy dissipated decreases as the length-to-diameter ratio increases. For the rotary mode (a transverse mode), the energy required is independent of the length-to-diameter ratio. Since the wave requiring the lowest energy will prevail, a large length-to-diameter ratio engine should give the longitudinal wave, and the low length-to-diameter ratio engine should have the rotary wave. For engines having length-to-diameter ratios in the region of 5, either wave may be expected as the energy required is about the same for either wave.

The mechanism for sustaining a pressure wave was postulated in 1877 by Rayleigh who said: "If energy is added to the gas at the moment of greatest pressure, or absorbed at the moment of lowest pressure the vibration is encouraged". The rate of energy addition to the wave can be perturbed by at least two factors: (1) a change in chemical reaction rate,

$$r = P^m e^{-K/T}$$

where

r rate

P pressure

m constant

K constant

T temperature

and (2) a change in vaporization rate,

$$r \approx \left(\frac{V_{diff}P}{\mu T}\right)^{1/2} \frac{\Delta T}{D_{drop}^{3/2}}$$

where

V_{diff} velocity difference between drops and gas

μ viscosity of gases

ΔT temperature difference between drops and gas

D_{drop} diameter of drops

The most obvious method of adding energy to a wave is by a perturbation in the chemical reaction rate. The chemical reaction rate is dependent on the pressure at which the reaction is occurring and the temperature of the reaction. Increases in either pressure or temperature will increase the reaction rate. Thus, the perturbation in energy released is in phase with the pressure and temperature waves.

Vaporization rates should also be considered since vaporization is very important in rocket-engine combustion. The vaporization rate is proportional to the velocity difference between the gas and the drop, the pressure of the system, and the temperature difference between the drops and the surrounding gas. Increasing the velocity difference, pressure, or gas temperature will increase the reaction rate.

Increased pressure leads to increased temperature, and increased temperature gives increased reaction rates. A pressure wave should be accompanied by a velocity wave that is 90° out of phase with it; the velocity change will affect the evaporation rate. These waves have been observed experimentally in a rocket engine, and the results are shown in figure 15, which shows the pressure, temperature, and velocity histories inside the combustion chamber. The temperature is in phase with the pressure; the velocity is 90° out of phase with the pressure.

Screaming is related to the energy release under steady-state conditions as is shown in figure 16. The solid symbols represent longitudinal and rotary screaming, and the amount of shading is characteristic of the fraction of the runs that screamed. For low-energy propellants, a system having a rapid conversion rate of the propellants to hot gases and a performance curve in the shaded area was inherently unstable. A system having a lower conversion rate and producing a performance curve in the unshaded region was stable.

This same phenomenon has been observed for the high-energy propellants. An engine with a rapid conversion rate was inherently unstable; however, with a lower conversion rate the system was stable. One interesting difference between these two systems is that the high-energy propellant system with the rapid rate of conversion and high energy release reduced the region in which screaming was obtained. This can be observed by comparing the shaded areas for the high- and low-energy systems.

The screaming region can also be reduced by increasing the damping in the system. Screech in turbojet afterburners was eliminated by inserting perforated liners to introduce damping. A similar approach was used in rockets by placing baffles in the combustion chamber. The results of this investigation are shown in figure 17. Without baffles, 78 percent of the tests with the engine were screaming runs. With baffles, the percent of the screaming runs was reduced to 5 percent.

Screaming is a major problem because it is accompanied by an increased heat-transfer rate which burns out the engine. In addition, during screaming the combustion process is changed. A localized increase in combustion rate seems to produce localized hot spots next to the injector, which can also cause the engine to burn out.

Cooling

Although the higher energy propellants produce higher heat-transfer rates, these propellants can absorb greater quantities of heat when they are used for cooling. The simplest and cleanest way to cool a rocket engine is to pass one of the propellants through the cooling passages before it goes to the combustion chamber. This process is called regenerative cooling.

The cooling capacities for several rocket propellant combinations are presented in figure 18. The engines are assumed to operate at the oxidant-fuel ratio of maximum specific impulse and at a combustion pressure of 300 pounds per square inch absolute. The shaded bars represent the fuels, and the open bars represent the oxidants.

Generally, the limitations of cooling capacities are brought about by the physical properties of the fluid itself. For example, jet fuel, ammonia, and hydrazine are limited by their boiling points at the pressures in the cooling jacket. Hydrazine is limited further by the fact that it decomposes thermally at temperatures near this boiling point. Hydrogen, however, has no limitations due to physical properties because it is considered to be above its critical pressure. This means that there will be no phase transition, or no boiling. The limit for hydrogen cooling is imposed by the metal of the engine walls, which cannot be heated above the limits tolerable for structural integrity. Two values are shown for

[redacted]

hydrogen on figure 18 because it is used with both fluorine and oxygen as oxidants. When hydrogen is burned with oxygen, more fuel is needed, and thus a greater cooling capacity is available.

The use of oxidants as coolants presents some promise. However, as with hydrogen, liquefied gases are being considered. Since the critical points for oxygen and fluorine are somewhat high, a choice must be made as to whether or not the coolant is to be used above or below critical pressure. If the coolant is used below the critical pressure, it is limited by the boiling point. The solid portions of the oxidant bars (fig. 18) represent the heat capacities available within the limitations of the boiling points of the fluid at pressures normal for cooling. However, if higher pressures are used, for example 800 pounds per square inch, then the critical pressure is exceeded and there is no boiling point problem. Again, the engine wall provides the limit. The total heat capacity is represented by the total height of the bar for each oxidant.

The cooling capacities of various propellants have been discussed; next, the cooling needs of rocket engines must be considered. Figure 19 presents the results of an analysis of the cooling requirements for 10,000-, 100,000-, and 1,000,000-pound-thrust engines in terms of the ratio of the cooling required by the engine to the cooling available from the fuel.

Regenerative cooling would not be possible above a cooling ratio of 1. The engines of this investigation were assumed to operate at the oxidant-fuel ratio of maximum specific impulse at a combustion pressure of 300 pounds per square inch absolute. The fuel alone was considered as the coolant, and the cooling process was purely regenerative. In all cases, increasing the thrust level decreases the heat load on the coolant because, as the engine is increased in size, the surface area does not increase as fast as the volume.

For the propellant combinations containing hydrogen, the total cooling capacity required of the hydrogen, by analysis, does not reach the limit of that available. The adequate cooling capacity of hydrogen has been demonstrated experimentally by the NACA.

When JP-4 fuel with liquid oxygen is used, a carbon film is deposited on the gas side of the cooled wall as a self-renewing insulator. This carbon film was taken into account in these analyses. Experimental data are plotted for the JP-4 - liquid-oxygen combination for 1000- and 5000-pound-thrust NACA engines and for Rocketdyne sustainer and booster engines for ICBM use. Rocketdyne personnel have evidence which leads them to believe that the carbon layer builds up on the engine wall, flakes off, and rebuilds again. Thus, the local heat-transfer rate would be transient and possibly cyclic in nature. The net effect of the carbon film is to reduce heat transfer. The experimental data and the analysis for this case are in reasonable agreement.

[redacted]

For the hydrazine-fluorine combination, cooling of at least the larger engines appears to present no problem if thermal decomposition can be avoided. It is assumed that the stay time of the hydrazine in the coolant passages will be short and that the velocity of flow through the passages will be fast enough that the fluid will reach the combustion chamber before it decomposes. If decomposition occurs with hydrazine, it becomes a very good monopropellant. This sort of behavior is not wanted in the cooling jacket.

Cooling with ammonia appears to be quite marginal, at least with smaller engines. NACA data obtained at 1000-pound thrust with a water-cooled engine indicate, however, that purely regenerative cooling might even be possible with these small engines.

In experimental work, heat rejection rates are usually obtained which are only about 60 percent of those calculated. In any such calculations, certain assumptions must be made. For the present analysis, the assumptions were conservative. For example, combustion has been assumed to be perfect, which means that full combustion temperature was reached, less fuel was available because of higher performance, and hence less coolant was available. It was also assumed that the gases in the chamber would have homogeneous distribution and that the temperature along the walls was uniform, even back to the injector face. In addition, any effects of the injector such as hot and cool spots, which may be functions of the propellant distribution, were not considered.

The experimental data at 3000-pound thrust in figure 19 are from Rocketdyne for ammonia-fluorine. All measurements were made with engines of the same design, but the injectors were varied. The highest heat-transfer rate was obtained with a doublet-type injector, that is, each fuel jet impinged on an oxidant jet; the lowest heat-transfer rates were obtained with a like-on-like injector. The intermediate point was obtained with a hybrid of these two injector types. All the experimental data points in figure 19 were adjusted to conform to the operating conditions assumed in the analysis.

Data from Bell Aircraft show that cooling may be accomplished with ammonia in engines big enough to be used as sustainers. The heat-transfer rate, however, for these engines was about 5.6 Btu/sec-sq in. as compared with 1.1 for a corresponding sustainer engine using jet fuel and liquid oxygen.

Because of this high heat-transfer rate and the questionable capability of cooling with ammonia, the addition of a ceramic lining inside the wall has been considered for ammonia-fluorine engines. In this analysis, the ceramic reduced the heat-transfer rate appreciably. Bell Aircraft recently experimented with a ceramic liner in an ammonia-fluorine engine. The liner appeared to reduce the heat flux, but it eroded very rapidly.

[redacted]

Most refractories are oxides. The resistance of such refractories to attack by hot, turbulent fluorine gas is not known. Perhaps future research will result in fluoride-type refractories which will resist fluorine attack.

Cooling requirements are also influenced by engine parameters other than thrust level, oxidant-fuel ratio, and injection pattern. For example, at a given thrust level, decreasing the chamber diameter increases the gas velocity and slightly increases the heat load. Increasing the expansion ratio of the nozzle for high-altitude operation also increases the cooling demands because a bigger nozzle must be cooled. If the combustion pressure is increased, the heat load is also increased because of higher combustion temperatures, different transport properties, and higher mass-flow rates of combustion gases across the cooled wall.

Because the hydrogen-fluorine propellant combination offers the highest performance potential of any stable chemical system, further consideration will be given to this system and the cooling problems associated with it. The data in figure 19 were for 15 percent hydrogen, which gives the highest specific impulse. Missile designers, however, would prefer less hydrogen, since the low density of hydrogen appreciately increases the weights of the tanks and the pumps. Figure 20 shows the variation of the cooling requirements with various proportions of hydrogen and fluorine. While the change in specific impulse brought about by decreasing the percentage of hydrogen is not very significant, decreasing the fraction of hydrogen from 15 to 10 percent doubles the cooling load. Decreasing it to 5 percent, the stoichiometric ratio, almost requires the complete cooling potential of the hydrogen because the flame temperature is higher and only one-third as much fuel can be used for cooling.

Even though hydrogen has been shown generally to have ample cooling capacity, it is not known whether this can be actually realized in practice. The mechanism of heat transfer through the hydrogen coolant film remains a research problem. Not enough is known about the conditions in this film to which transport data are applied.

Figure 21 presents some heat flux rates and coolant velocities as functions of cooled length in typical engines for hydrogen-fluorine and JP-4 - oxygen propellant combinations. The coolant enters at the end of the nozzle and flows toward the injector. The heat flux rate at the nozzle throat for hydrogen (near 10 Btu/sec-sq in.) is about four times that encountered in present engines. The velocity of hydrogen in the coolant passages is an order of magnitude higher than that of JP-4 fuel, a condition never before experienced. Exploratory analysis such as this is valuable, but experimental work is needed to solve the cooling problems.

To determine experimentally whether hydrogen-fluorine engines running at high efficiency can be cooled with hydrogen, a 5000-pound-thrust

[redacted]

engine that operates at a combustion pressure of 300 pounds per square inch absolute has been designed and built at this laboratory. It was formed of nickel channels with 0.020-inch-thick walls; the channels were wrapped with wire and brazed. The wire takes the combustion-chamber pressure load.

This engine, which was run successfully, gave high performance and ample cooling. A specific impulse of 351 was obtained at 18.9 percent fuel. The chamber pressure (nominally 300) was 380 pounds per square inch; the thrust was 5980 pounds.

Figure 22 shows design temperature and pressure profiles as functions of the engine length. Experimental measurements at terminal points are represented by the circles. The actual rise in coolant temperature was somewhat lower than calculated; the actual pressure drop also was lower. The experimental heat flux rate of about 5 can be compared with the analytical value of 6.88 Btu/sec-sq in.

A small engine has been regeneratively cooled successfully; bigger engines should prove easier.

THEORETICAL MAXIMUM SPECIFIC IMPULSE
EXPANDED TO SEA LEVEL ATMOSPHERIC PRESSURE

CHAMBER PRESSURE, PSIA	300	600	1000
PROPELLANT	MAXIMUM SPECIFIC IMPULSE LB. THRUST / LB./SEC		
STORABLE			
CAST COMPOSITE	193	208	217
RP1 - RFNA	227	248	264
POLYURETHANE-ALUMINUM-PERCHLORATE	228	253	261
POLYVINYL CHLORIDE-DIESTER-ALUMINUM-PERCHLORATE	234	253	265
HYDRAZINE-CHLORINE TRIFLUORIDE	261	281	295
NON-STORABLE			
RP1 - OXYGEN	261	285	299
AMMONIA - FLUORINE	312	338	355
HYDRAZINE-FLUORINE	315	344	361
HYDROGEN-OXYGEN	348	374	390
HYDROGEN - FLUORINE	365	393	409

CS-14880

Table I

CHAMBER LENGTH FOR VARIOUS PROPELLANTS

PROPELLANT				LENGTH TO OBTAIN (IN.)			
FUEL	B P, °F	OXIDANT	B P, °F	99% EFF		90% EFF	
				EXP	THEOR	EXP	THEOR
NH_3	-28	LIQ O_2	-297	60	56	22	21
JP-4	209	LIQ O_2	-297	48	50	18	17
NH_3	-28	LIQ F_2	-305	65	56	24	21
N_2H_4	236	LIQ F_2	-305	56	71	21	26
GASEOUS H_2	-423	LIQ O_2	-297	17	21	6	8
GASEOUS H_2	-423	LIQ F_2	-305	19	20	7	8

CS-14766

Table II

CANDLE TYPE GRAIN

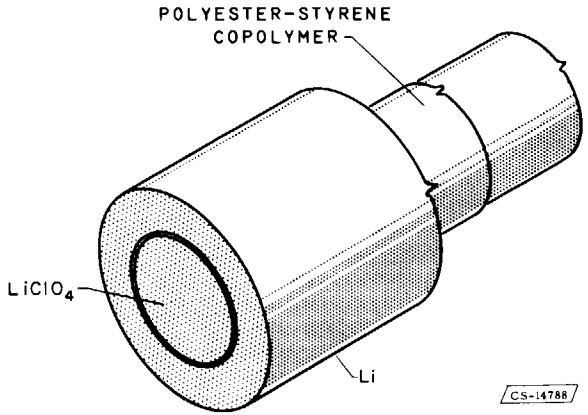

Figure 1

SPECIFIC IMPULSE OF FREE RADICALS

FROZEN AT 0° R

EXPANDED FROM 300 PSIA TO 14.7 PSIA

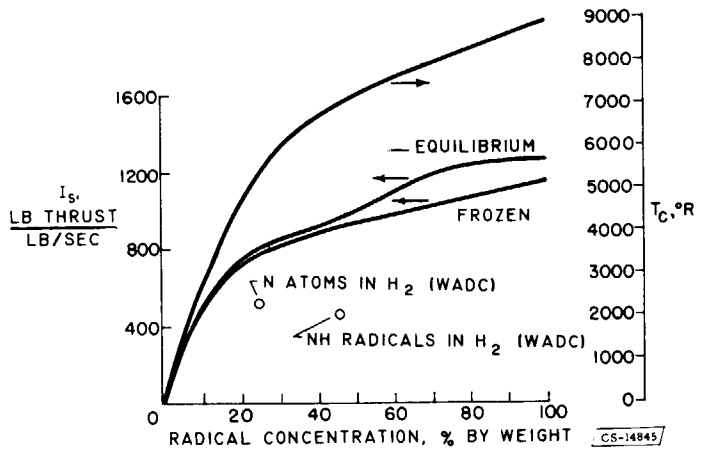

Figure 3

EFFECT OF HEAT OF REACTION ON PROPELLANT PERFORMANCE

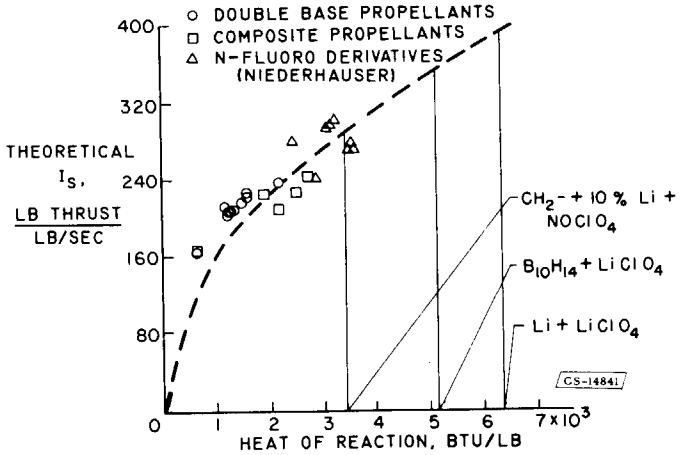

Figure 2

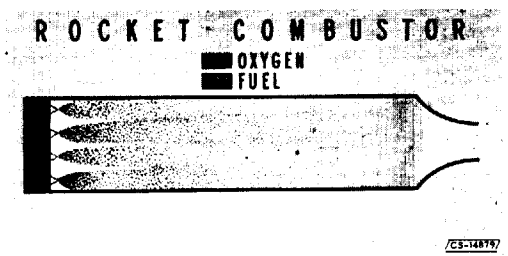

Figure 4

EFFECT OF CHAMBER LENGTH ON ENGINE PERFORMANCE

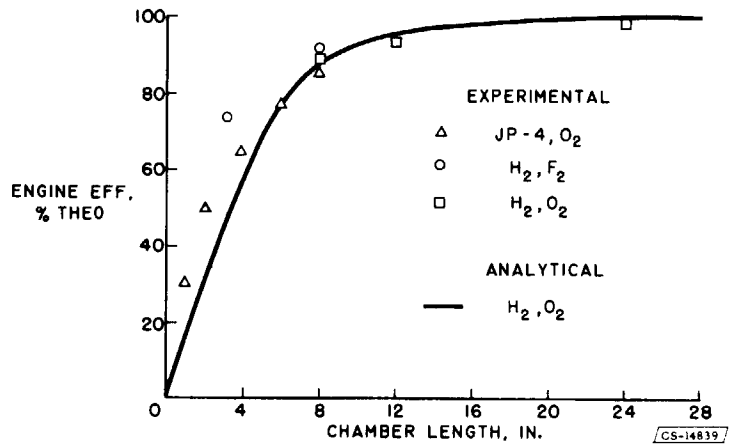

Figure 5

EFFECT OF ORIFICE DIAMETER ON DROP DIAMETER

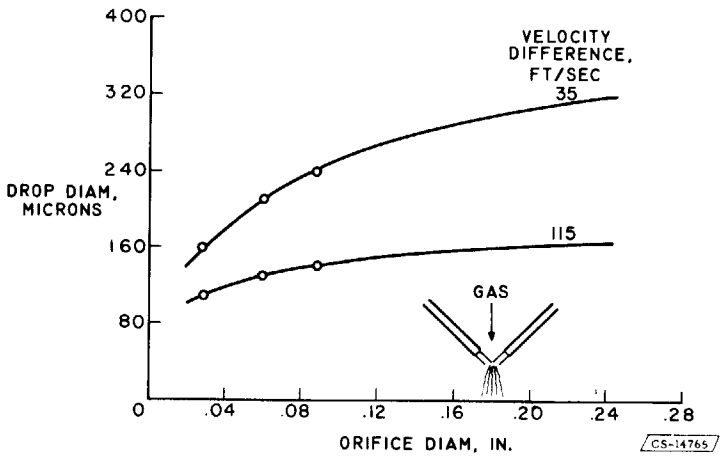

Figure 6

INJECTOR HOLE SIZE

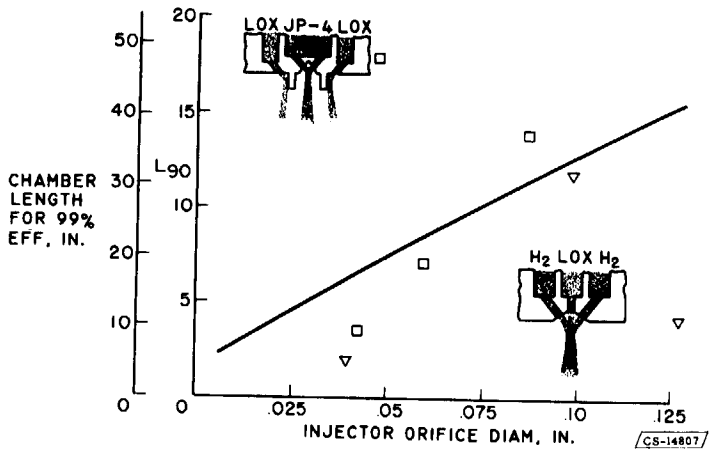

Figure 7

EFFECT OF CHAMBER-TO-THROAT DIAMETER RATIO

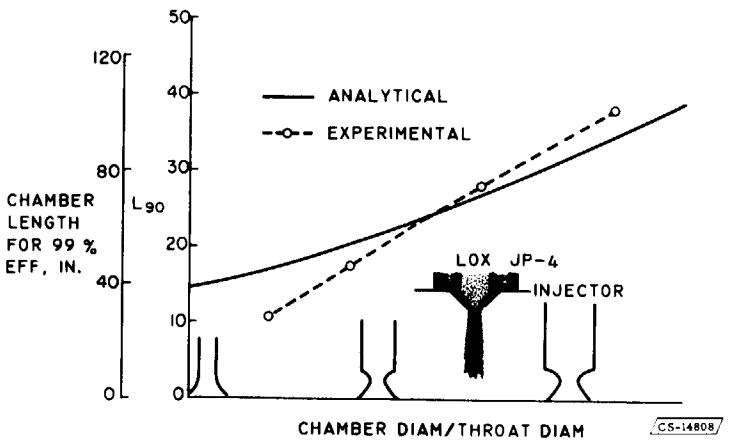

Figure 8

EFFECT OF HYDROGEN PRESSURE DROP

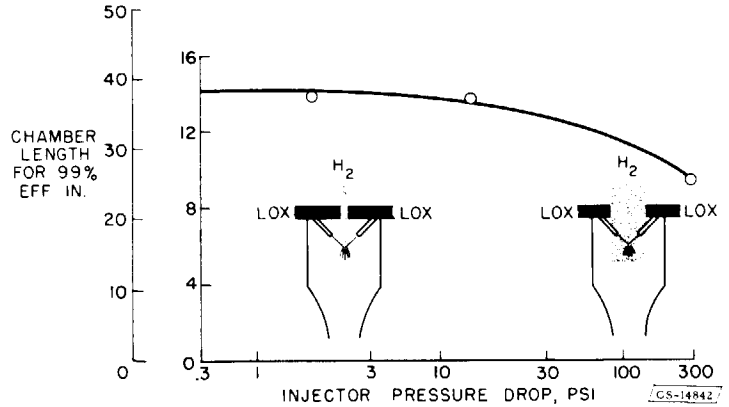

Figure 9

MODEL OF MISSILE DYNAMICS

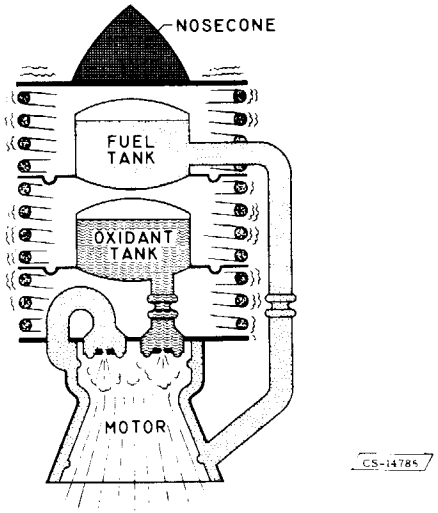

Figure 10

SCHEMATIC SHOWING INTERACTION BETWEEN MOTOR AND INJECTOR

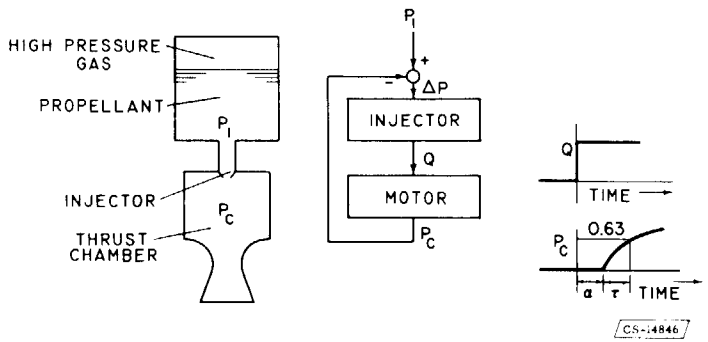

Figure 11

STABILITY DIAGRAM FOR ENGINE-INJECTOR LOOP

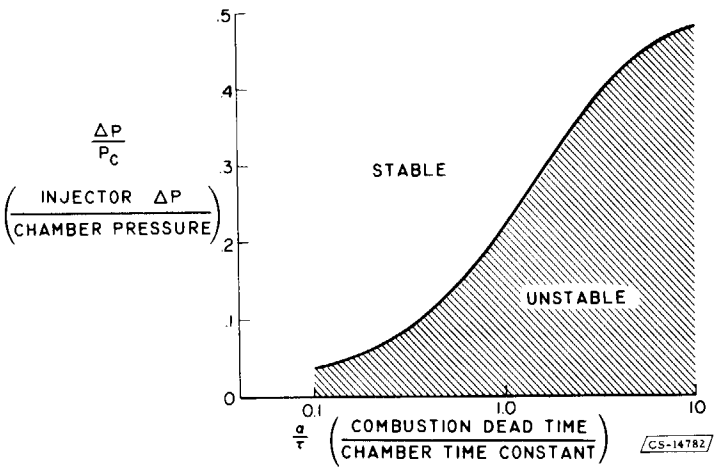

Figure 12

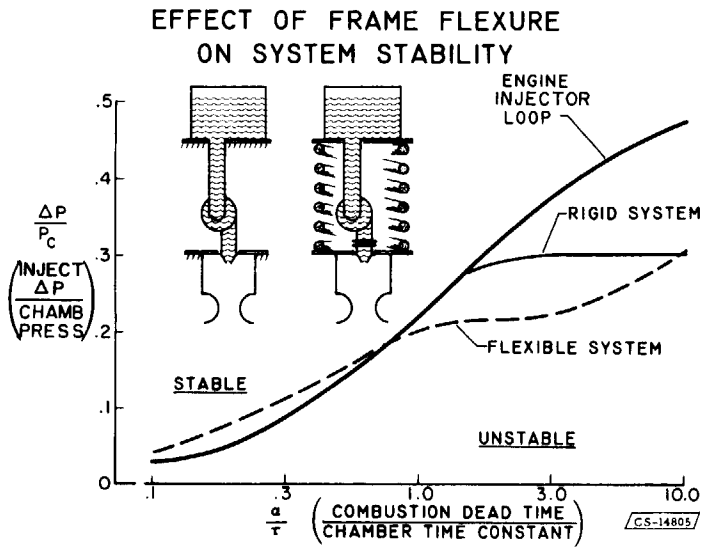

Figure 13

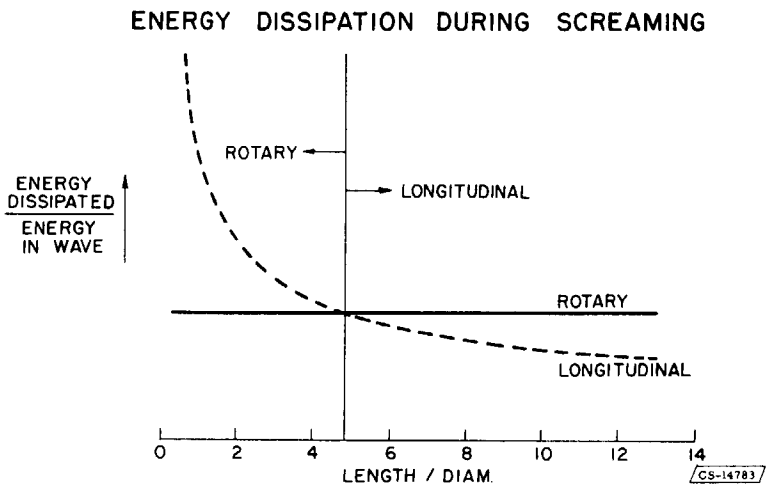

Figure 14

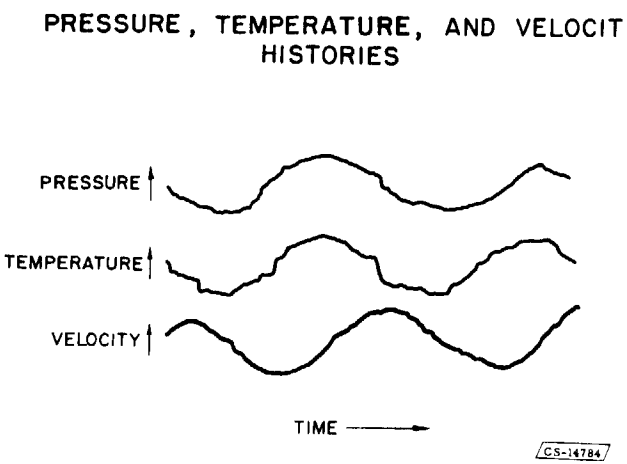

Figure 15

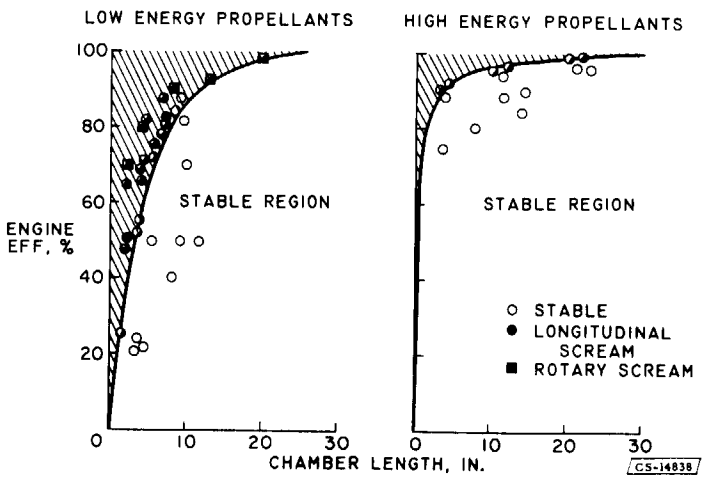

Figure 16

USE OF BAFFLES TO PREVENT ROTARY SCREAMING

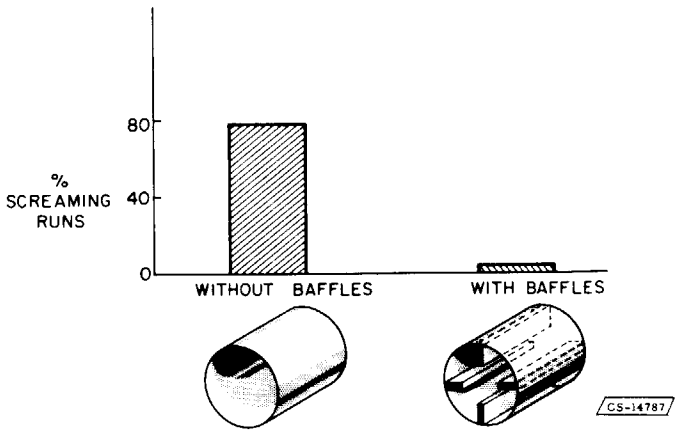

Figure 17

COOLING CAPACITIES OF PROPELLANTS

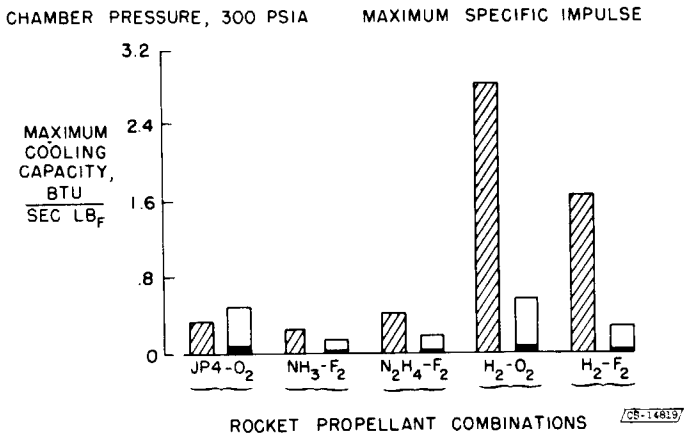

Figure 18

ENGINE COOLING POTENTIAL OF ROCKET FUELS

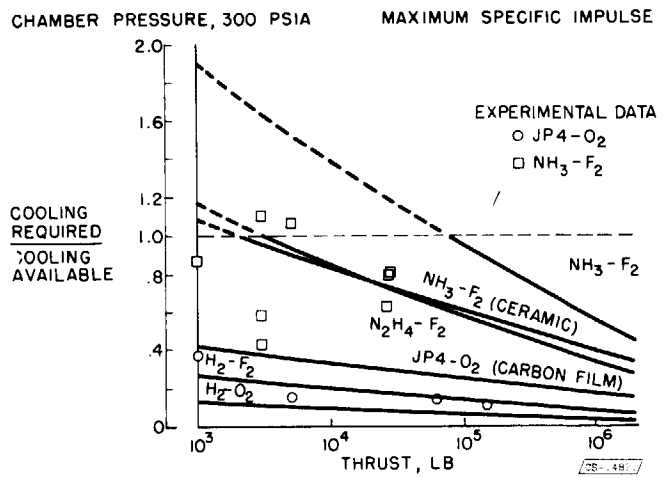

Figure 19

COOLING POTENTIAL FOR H_2-F_2 ENGINES

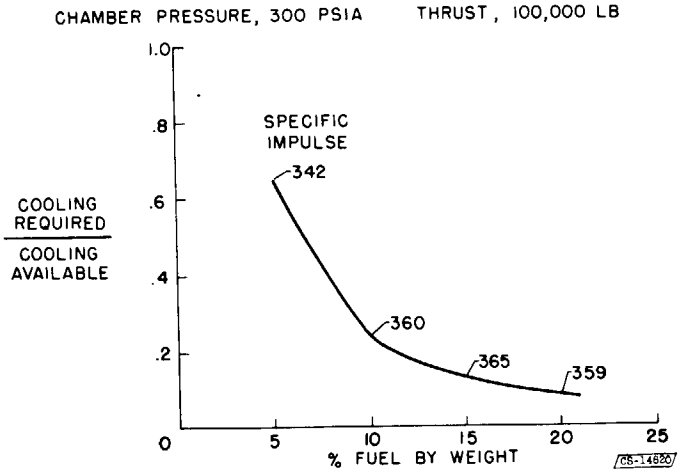

Figure 20

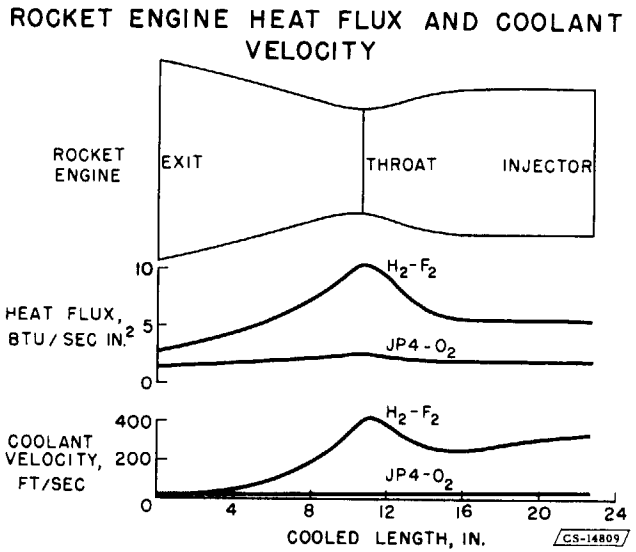

Figure 21

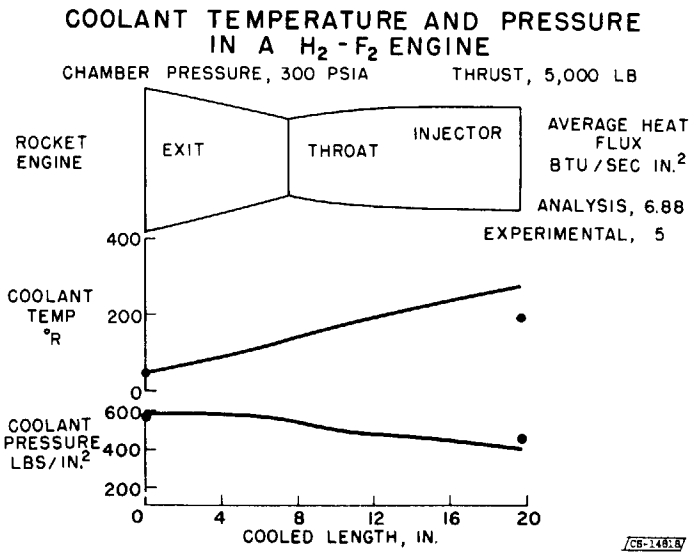

Figure 22

7. TURBOPUMPS FOR HIGH-ENERGY PROPELLANTS

By Ambrose Ginsburg, Ward W. Wilcox, and David G. Evans

INTRODUCTION

As pointed out repeatedly during the preceding papers, the fixed weight of the rocket propulsion engine must be kept to an absolute minimum. One of the components whose weight might be reduced is the turbopump. The design of pumps for liquid propellants, the turbines that drive them, and the matching of the two into a turbopump unit are considered herein.

In order to provide an illustrative example with actual weights, a mission was selected that remained the same for all propellant combinations. The mission specified a 10,000-pound payload in a satellite orbit 300 miles above the Earth. For this mission the quantity of propellants is large, but in each case a single turbopump was considered with the pump delivery pressure taken as 700 pounds per square inch at 70 percent efficiency. The liquid propellants for which component weights were determined are RP-1 - oxygen, hydrogen-oxygen, and hydrogen-fluorine. For the fixed mission, propellant combinations with a low specific impulse had correspondingly greater capacity requirements.

PUMP DESIGN CONSIDERATIONS

In this analysis only single-stage centrifugal pumps will be considered. Except for hydrogen, the pressure requirement of 1000 pounds per square inch virtual head was well within the capability of a single-stage centrifugal pump. For hydrogen this pressure requirement probably represents an upper limit beyond which multistaging would be necessary. For all the pumps shown, the conservative design practice of stationary pumps has been extended greatly into areas now representing the state of the art in the rocket-turbopump field.

The two principal hydrodynamic factors that limit pump performance are cavitation and the extent to which a pump blade may be loaded before serious flow separation occurs. The occurrence of cavitation on a hydrofoil is shown schematically in figure 1. The free-stream fluid is cavitation free. As flow accelerates over the suction surface of the blade,

[redacted]

the local pressure decreases. If the local static pressure falls below the vapor pressure of the liquid, incipient cavitation or local boiling will occur first at the point of lowest pressure. The amount of local pressure drop below the stagnation pressure that may take place before the boiling point is reached is called the suction head and is designated by the symbol H_{sv}. That is, this much pressure may be converted into velocity relative to the blade before incipient cavitation. The velocity along the blade is increased both by increasing rotational speed or by increasing the volume flow through the pump.

A semi-empirical parameter representing similar flow and cavitation conditions in geometrically similar pumps is termed the suction specific speed S and is written as

$$S = \frac{n\sqrt{Q}}{H_{sv}^{3/4}}$$

where

n rotational speed, rpm

Q flow capacity, gal/min

The higher the suction specific speed of a pump, the higher the maximum rotational speed and volume flow may be for a given suction head.

Conventional practice in pump design fixed the limit of pump operation at incipient cavitation, and the specified suction specific speed was defined for incipient cavitation. Suction specific speeds of the order of 10,000 are used in this conventional practice. Pumps designed on this basis are heavy. However, pump designs that can tolerate some cavitation without undue losses in efficiency have been developed and applied successfully to a variety of fluids including liquid oxygen. Suction specific speeds with tolerable cavitation up to 30,000 have been obtained, thus permitting lighter pump designs. However, the problem is whether hydrogen and fluorine pumps can operate satisfactorily at this level of cavitation as represented by a suction specific speed of 30,000.

When a pump is operating with fully developed cavitation, the point of incipient cavitation lies near the nose of the blade and is followed by a region of pressure which is equal to or less than vapor pressure. The cavitation bubbles grow in transit through this low-pressure region. Recent advances in missile pump design, for example, liquid-oxygen pumps, have resulted in satisfactory performance under these cavitation conditions. A comparison of the physical properties of liquid hydrogen with liquid oxygen shows this bubble growth to be less for hydrogen than for

[redacted]

oxygen. (The principal physical properties involved are the latent heat of vaporization, specific heat, absolute temperature, liquid density, and molecular weight. This matter is discussed in detail in ref. 1.) For these reasons the suction specific speed of 30,000 used successfully in oxygen pumps can be expected to be satisfactory for hydrogen pumps.

The properties of liquid fluorine are about the same as liquid oxygen. Therefore, a suction specific speed of 30,000 is used in this study for fluorine pumps. However, experience may show that the high rate of pump corrosion and erosion provided by liquid fluorine under cavitating conditions may ultimately require the use of larger and heavier noncavitating pumps.

The second hydrodynamic design limit for pumps is that of "blade loading." The term "blade loading" can best be described by considering the variation of pressure over the surfaces of an axial-flow pump blade as shown in figure 2. The pressure difference across the blade provides the force to turn and thereby to do work on the fluid. A critical condition exists on the suction, or upper, surface of the foil. If the pressure rise is too rapid, the boundary layer separates from the surface of the hydrofoil. Considerable energy is lost in the turbulent eddy motion of this separated fluid. Further losses result when the main flow and the separated boundary layer eventually mix to form a uniform flow downstream. With respect to efficient pump operation, the blade loading must be limited to prevent separation.

The use of a centrifugal pump eases the problem somewhat, since the pressure rise that results from increase in radius of rotation (that is, centrifugal force) does not contribute to separation. For a centrifugal pump, it is convenient to consider the tendency for separation on the basis of the velocity of the fluid relative to the rotating blade of the pump as shown schematically in figure 3. The flow is accelerated near the nose and then decelerates or diffuses to the trailing edge. If this deceleration is too rapid, the boundary layer will separate from the suction surface.

Simplified theoretical techniques have been developed which permit the designer to predict this velocity distribution within a given centrifugal pump. Incompleteness of boundary-layer theory and the complex three-dimensional geometry, however, prevent the designer from establishing an exact value for the limiting deceleration.

For the present pump analysis, a somewhat more empirical approach to the loading limit was taken. The approach was based primarily on past experience in the pump field. The loading was specified on the basis of two factors that influence the loading of the blades: (1) the

rotor-tip-to-inlet-diameter ratio (that is, the extent to which centrifugal force can be utilized to obtain head rise), and (2) the degree of turning done by the blade.

For pumps for heavy fluids such as fluorine, oxygen, and RP-1, a diameter ratio of 1.2 was used with the blades backward swept. The light fluids, such as hydrogen, require much greater head rise for the same pressure. In order to provide more turning, the blades are turned to the radial direction. The use of radial blades means a higher outlet- to inlet-diameter ratio must be used to avoid exceeding a loading limit. For hydrogen pumps, this diameter ratio was taken to be 2.0.

No mention has been made of the effect of fluid properties on the loading limit. However, it is felt that the fluid properties of hydrogen will be favorable to the delay of separation. This opinion, which is based on the fact that the kinematic viscosity of hydrogen is comparable to that of oxygen, and only one-fifth that of water, leads to a certain amount of confidence that the loading characteristics of hydrogen will be at least as good as those fluids that have been used in the past.

For the pumps considered herein, customary stress and rotational-speed limits have been used. These hydrodynamic limits of cavitation and loading can now be used to determine the weight of pumps.

Examination of a variety of pump designs showed that pump weight was approximately proportional to the pump diameter to the 9/4 power:

$$\text{Pump weight} \sim D^{9/4}$$

Also there was a fairly constant relation between the pump diameter and the impeller diameter. For this analysis this ratio was considered to be 1.35. The impeller-outlet diameter is fixed by the head requirement and the rotational speed as follows:

$$\Delta H = C_u \frac{U_T^2}{2g}$$

where

ΔH virtual head, ft

U_T tip speed, π (diam.)(rpm)

C_u coefficient defined by this expression and indicative of the outlet vector diagram

Substituting and rearranging, for constant C_u,

$$\text{Pump weight} \sim \frac{\Delta H^{9/8}}{n^{9/4}}$$

However, the rotational speed is limited by cavitation as represented by the suction specific speed equation given previously. For a given flow quantity and value of S,

$$n = \frac{SH_{sv}^{3/4}}{\sqrt{Q}}$$

Finally, the following equation results:

$$\text{Pump weight} \sim \frac{\Delta H^{1.125} Q^{1.125}}{S^{2.25} H_{sv}^{1.69}}$$

That is, pump weight is proportional to head and flow capacity and inversely proportional to suction specific speed and suction head.

The exponents of head and flow capacity are only slightly greater than 1; therefore, weight varies almost directly with flow and head requirements. In figure 4 the effect of the suction specific speed and the suction head on pump weight are shown for a large hydrogen pump at a constant head and flow. A very large decrease in weight accompanies a change in suction specific speed from approximately 10,000 to 30,000. This is a large gain, but that has already been obtained in oxygen pumps as pointed out earlier. Because the suction head is an exponential term, its influence becomes greater at low absolute values. From a pump standpoint, the low values of suction head should be avoided.

Thus far, the influence of cavitation limits on pump weight has been discussed but the loading limit has been ignored. The influence of loading limits may be demonstrated for a large hydrogen pump by figure 5. On a logarithmic plot of pump weight against suction head, lines of constant suction specific speed S fall on straight lines with a slope of the exponent 1.69. Such lines are shown for values of S of 10,000, 20,000, and 30,000. If a value of S of 30,000 is considered to be the cavitation limit, all the area to the left of the 30,000 line is cavitation limited. The dashed line in figure 5 represents the diameter-ratio limit of 2. Below this line the ratio of outlet to inlet diameter is less than 2 and the pump is loading limited. The intersection of these two limit lines may be shown to be dependent on the head requirement. The minimum-weight pump for a given flow and head requirement is then defined by the cavitation and loading-limit curves.

[redacted]

In a similar manner, limit lines may be established for the high-density fluid pumps where the diameter ratio was chosen as 1.2 with the backward-swept blades. For the low diameter ratio, the intersection point of the cavitation and loading-limit curves occurs at a high value of suction head. At very low values of suction head, where diameter ratio must be above 2, it is again profitable to minimize pump weight by changing to radial blades. Thus, the minimum-weight-pump curves for heavy fluids have two inflection points.

These curves can now be used to establish the effect of the properties of the various propellants on pump weight. A plot of pump weight per unit flow rate is given in figure 6 for hydrogen, RP-1, oxygen, and fluorine. Although the flow capacity of each of these pumps is different, corresponding to the original mission calculations, the effect of flow rate on these curves is secondary and does not alter the order of magnitude at any suction head. However, it is probably important to note that pump weight per unit flow rate does not generalize exactly and that the size of the pump does have some effect. From figure 6 it is evident that hydrogen pumps are much heavier for a given flow rate, primarily because of the loading limitation at higher suction heads. In fact, the weight per unit flow is arranged in the order of fluid density.

The component weight parameter that describes the effect of component weight on the rocket-vehicle gross weight is the ratio of component weight to total propellant weight. In figure 7 this ratio is shown as a function of suction head for two mixture ratios of the hydrogen-fluorine combination. For 14 percent hydrogen, the hydrogen pump is heavier than the fluorine pump at high suction heads and has equivalent weight at low suction heads. When the percent of hydrogen is reduced to 6, the hydrogen pump is the lighter pump at all values of suction head. It appears, then, that the weight increase due to use of hydrogen may be minimized at the lean mixture ratios. Also, the available suction head at the pump inlet is shown to be the most important variable affecting pump weight.

TURBINE-DESIGN CONSIDERATIONS

The turbine has a unique problem as compared with the pump: The turbine driving fluid must come from propellant aboard the missile. Thus, the turbine must be developed from two considerations, the weight of propellant it uses and the weight of the turbine itself.

The significance of turbine flow is shown in figure 8 for a theoretical mission. Hydrogen and fluorine are used as the propellants. The figure shows the percent increase in missile gross weight from a gross weight with zero turbine flow as a function of the turbine flow in percent of pump flow. .For every percent increase in turbine flow,

[redacted]

the missile gross weight increases 4 percent, thus indicating a considerable effect of turbine flow on the over-all gross weight.

Thus, keeping the turbine flow as low as possible is desirable. However, turbine weight is affected by turbine flow as illustrated in figure 9. As the turbine flow is reduced, the required work per pound of flow (specific work) increases. To achieve this increase in specific work output within given efficiency and pressure-ratio limits, additional turbine stages must be utilized, as illustrated in the figure. This increase in the number of stages increases the turbine weight and results in the observed trend.

Since turbine weight and turbine flow are interdependent, consideration of their combined effect is necessary. Figure 10 is the same plot as figure 8 with the combined turbine-flow and turbine-weight effect on the gross weight shown as a solid line. The dashed line is the same as that previously shown where only turbine flow was considered. The difference between these two curves is the effect of turbine weight. A point is reached where the increase in gross weight due to turbine weight becomes greater than the reduction due to turbine flow. The curve thus shows a minimum region. This region of minimum missile weight is termed the optimum area for the turbine.

With only turbines in this optimum range considered, turbine characteristics for different propellant combinations will be examined.

First, the turbine flow rate, which has been shown to be important, varies with propellants. Figure 11 illustrates a comparison of the required turbine flow for RP-1 - oxygen, hydrogen-oxygen, and hydrogen-fluorine propellant combinations. All the values are for the same mission. The turbine-flow comparison is made on the left of the figure. Shown in the center is the turbine horsepower per pound of pump flow, which is termed specific power. On the right is the specific heat of the turbine driving fluids, considering fuel-rich mixtures at 1400° F turbine-inlet temperatures.

RP-1 - oxygen and hydrogen-oxygen have equal turbine flows, whereas hydrogen-fluorine has less. The explanation is noted from the power requirements and the specific heats of the fluid combinations. The RP-1 - oxygen requires considerably less pump power, but it also has a low value of specific heat. The hydrogen-oxygen pump-power requirement is high, but the specific heat is also high. The net effect makes the turbine-flow requirements the same for both the RP-1 - oxygen and the hydrogen-oxygen propellants. Conversely, the hydrogen-fluorine combination, as compared with the hydrogen-oxygen, requires less turbine flow because the pumping power is reduced owing to less hydrogen being pumped, whereas the specific heat is still high. The result is that the hydrogen-fluorine propellant combination has a definite turbine-flow advantage. Although it

[redacted]

may appear that these turbine flows are a small percentage of the total (0.5 to 0.8 percent) and are not significant, it must be remembered that the turbine driving fluid is fuel rich in order to keep the temperature down, and is approximately 50 percent hydrogen. If, for example, a propellant combination of 6 percent hydrogen and 94 percent fluorine is used, the turbine is using 4 percent of the hydrogen aboard. This is a significant value in terms of tankage required to contain the turbine driving fluid.

Next to be considered is the turbine size and weight trends for the different propellant combinations. Figure 12 illustrates schematically the turbine configurations in terms of required number of stages and diameter. The RP-1 - oxygen turbine is by far the largest in diameter but with considerably fewer stages. Its large diameter is related to the large missile propellant flow rate required for this low-energy propellant in order to achieve the necessary total impulse. The multistage hydrogen-oxygen and hydrogen-fluorine turbines are necessary because of increased specific-power requirement. These multistage turbines illustrate a region for research directed toward the achievement of increased work per stage while maintaining high efficiency.

A comparison of turbine weight for four propellant combinations is shown in figure 13. Turbine weight is presented as a ratio of turbine weight to total propellant weight. The hydrogen-oxygen weight ratio is three times that of the RP-1 - oxygen. The hydrogen-fluorine combination is shown for two values of hydrogen, 14 and 6 percent of total propellant weight. This reduction in hydrogen permits a 30-percent reduction in turbine weight, assuming the total propellant weight to remain unchanged. The turbine-weight ratio of the 6 percent hydrogen-fluorine and of the RP-1 - oxygen are of the same order.

MATCHING OF PUMP AND TURBINE

Heretofore, each component of the turbopump has been considered separately. In order to make a useful device, the turbine and the two pumps must be combined in such a way that the least weight of both machinery and propellant results. Most of the difficulty in turbine and pump matching is caused by each component having its own best speed. For example, the components of a hydrogen-fluorine turbopump are shown in table I. The 116-pound fluorine pump is cavitation limited to 4100 rpm. The 214-pound hydrogen pump is loading limited at 11,000 rpm. The best turbine weighs 70 pounds and operates at 30,000 rpm.

Table II shows the results of the matching study for these pumps and turbines. Four pump and turbine arrangements were considered. If everything is run on one shaft at the fluorine speed, 4100 rpm, the fluorine pump weighs 116 pounds, the hydrogen pump, 2020 pounds, and the impossible turbine, 4000 pounds. By putting a gear with an estimated

[redacted]

weight of 294 pounds between the turbine and the two pumps, the over-all weight is reduced from 6136 to 2500 pounds.

A better way would be to run the hydrogen pump and turbine together at the hydrogen pump speed of 11,000 rpm and to gear down to the fluorine pump. In this case the gear is estimated to weigh 120 pounds and the turbine, 600 pounds. The over-all weight is now 1050 pounds, which is quite an improvement. In the final arrangement, each component could be operated at its best speed by using a gear to each pump. For this case, the total weight is 720 pounds. Mechanical considerations such as thrust-bearing requirements for the geared hydrogen pump or the turbine flow rate could govern the choice between these last two considerations.

The results of similar matching studies for four propellant combinations are shown in figure 14. The turbopump weight, consisting of complete pumps, gears, and the turbine, but without the gas generator or piping and valving, is expressed as a ratio to the total propellant weight for a range of pressures in the propellant tanks. For this example, the vapor pressures of hydrogen, oxygen, fluorine, and RP-1 were taken to be 20, 18, 18, and 0.2 pounds per square inch absolute, respectively. Mixture ratios are given by the percentage of fuel in the labels for each curve.

From figure 14 it is evident that the turbopump for RP-1 - oxygen is the lightest. The heaviest turbopump was for the hydrogen-oxygen combination, where 24 percent hydrogen was used. As the percentage of hydrogen is reduced, the turbopump weight ratio is also reduced. For the hydrogen-fluorine combination with 6 percent hydrogen, turbopump weight ratios very similar to the RP-1 - oxygen combination were obtained.

CONCLUDING REMARKS

The results of a simplified analysis of the turbopump component of a liquid-propellant rocket propulsion system indicate that:

1. Hydrogen pumps are considerably heavier per pound of propellant pumped than pumps designed for heavier liquids.

2. Although the use of hydrogen requires much higher turbine power to drive the hydrogen pump, the higher energy per pound available to the turbine allows the turbine flow (percent of pump flow) to remain the same as for more conventional propellants.

3. Turbines for use with the high-energy propellant combinations will require high specific work and multiple stages to extract the available energy.

[redacted]

4. In order to reduce turbopump weight, at least one and possibly both pumps will have to be geared to the turbine.

5. For lean mixture ratios, the over-all turbopump weight of a hydrogen-fluorine combination compares favorably with the more conventional RP-1 - oxygen combination.

6. The weight dependence of pumps at low values of suction head requires an optimization between turbopump and propellant tank weight for an optimum rocket vehicle design.

REFERENCE

1. Jacobs, Robert B., Martin, Kenneth B., Van Wylen, Gordon J., and Birmingham, Bascom W.: Pumping Cryogenic Liquids. Tech. Memo. No. 36, Rep. 3569, Cryogenic Eng. Lab., NBS, Feb. 24, 1956.

[redacted]

OPTIMUM COMPONENTS FOR HYDROGEN - FLUORINE TURBOPUMP

COMPONENT	WEIGHT	RPM
FLUORINE PUMP	116 LB	4,100
HYDROGEN PUMP	214 LB	11,000
TURBINE	70 LB	30,000

CS-14817

Table I

CAVITATION ON A HYDROFOIL

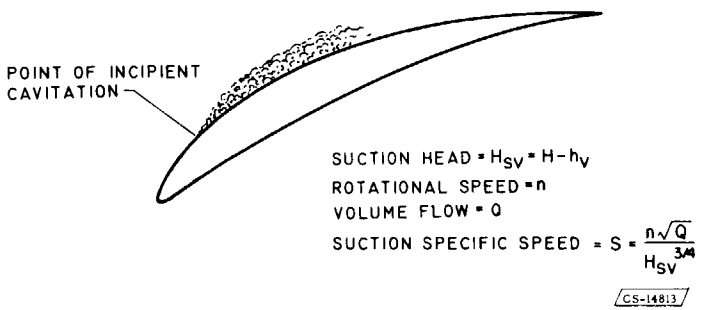

Figure 1

MATCHING OF PUMPS AND TURBINE

ARRANGEMENT	FLUORINE PUMP	HYDROGEN PUMP	TURBINE	GEARS	TOTAL
SINGLE SHAFT	116 LB 4100 RPM	2020 LB 4100 RPM	4000 LB 4100 RPM		6136 LB
GEARED TURBINE	116 LB 4100 RPM	2020 LB 4100 RPM	70 LB 30,000 RPM	294 LB	2500 LB
GEARED F_2 PUMP	116 LB 4100 RPM	214 LB 11,000 RPM	600 LB 11,000 RPM	120 LB	1050 LB
GEARED F_2 AND H_2 PUMPS	116 LB 4100 RPM	214 LB 11,000 RPM	70 LB 30,000 RPM	320 LB	720 LB

CS-14815

Table II

PRESSURE DISTRIBUTION ON A HYDROFOIL FOR AN AXIAL FLOW PUMP

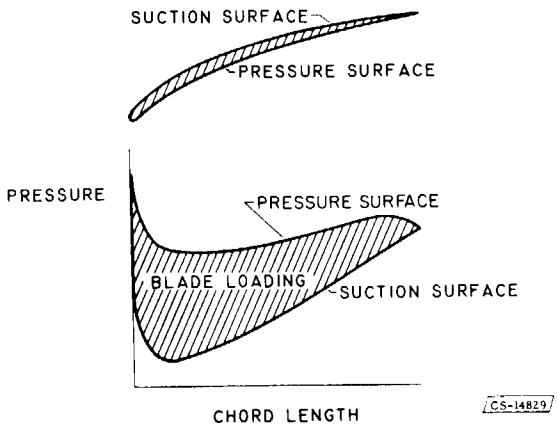

Figure 2

VELOCITY DISTRIBUTION ON A CENTRIFUGAL PUMP BLADE

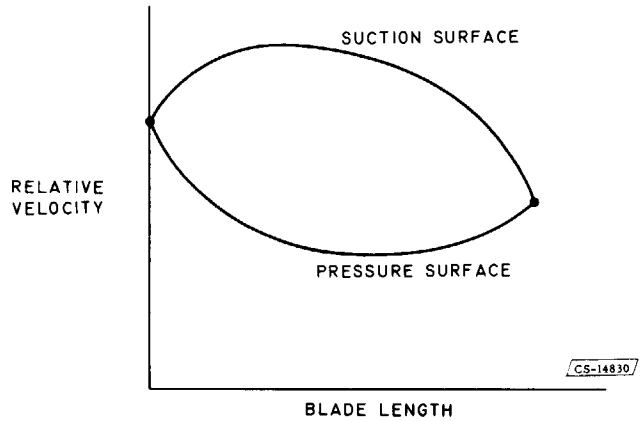

Figure 3

EFFECT OF CAVITATION LIMITS ON WEIGHT OF LARGE HYDROGEN PUMP

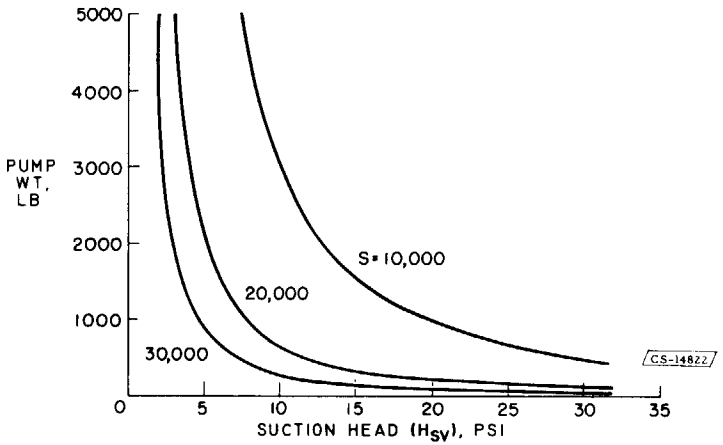

Figure 4

EFFECT OF CAVITATION AND LOADING LIMITS ON WEIGHT OF LARGE HYDROGEN PUMP

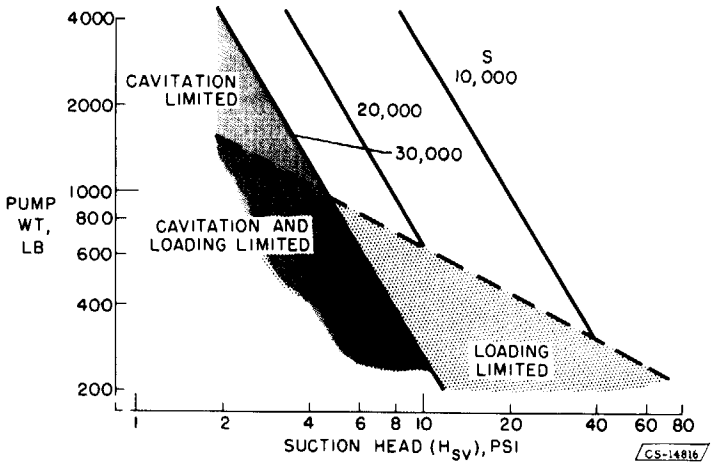

Figure 5

EFFECT OF PROPELLANT ON PUMP WEIGHT

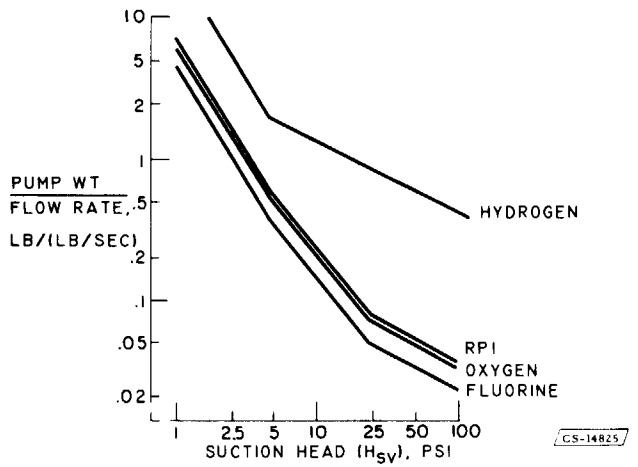

Figure 6

EFFECT OF HYDROGEN - FLUORINE MIXTURE ON PUMP WEIGHT

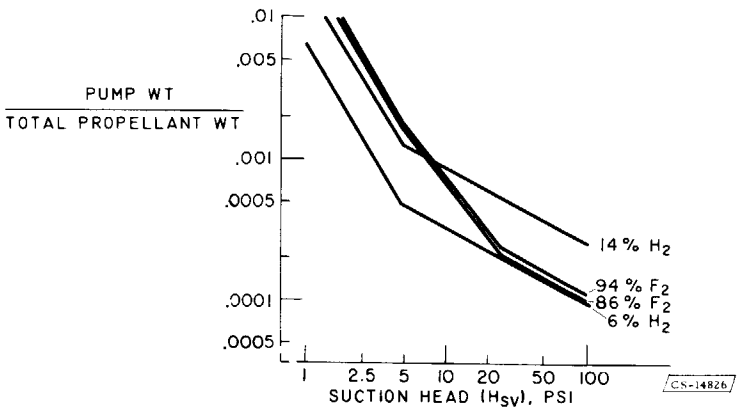

Figure 7

EFFECT OF TURBINE FLOW ON MISSILE GROSS WEIGHT

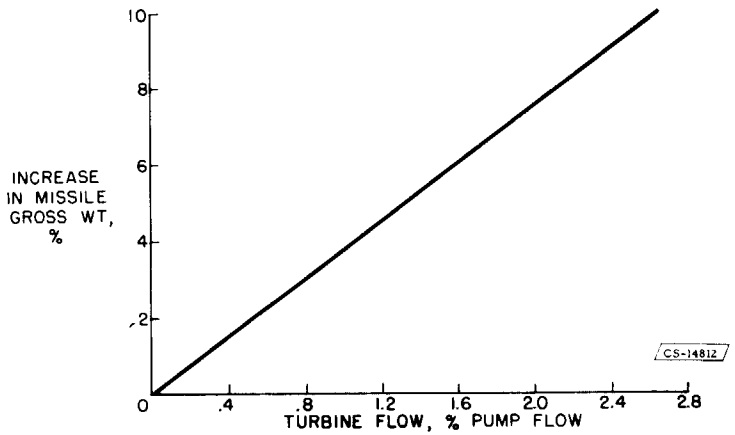

Figure 8

EFFECT OF TURBINE FLOW AND TURBINE WEIGHT ON MISSILE GROSS WEIGHT

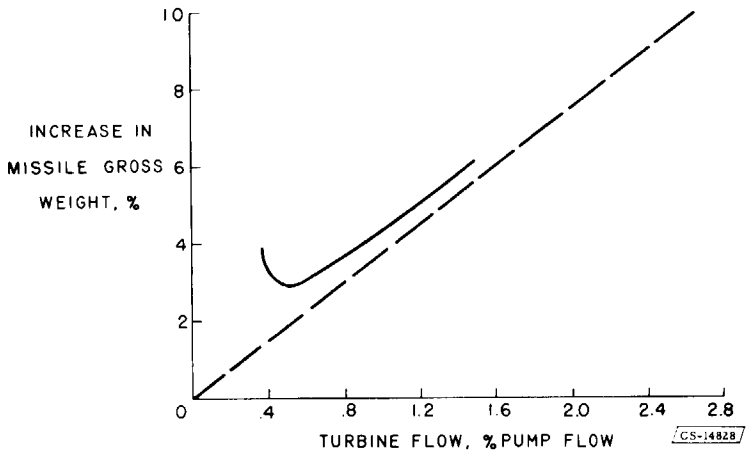

Figure 9

EFFECT OF TURBINE FLOW ON TURBINE WEIGHT

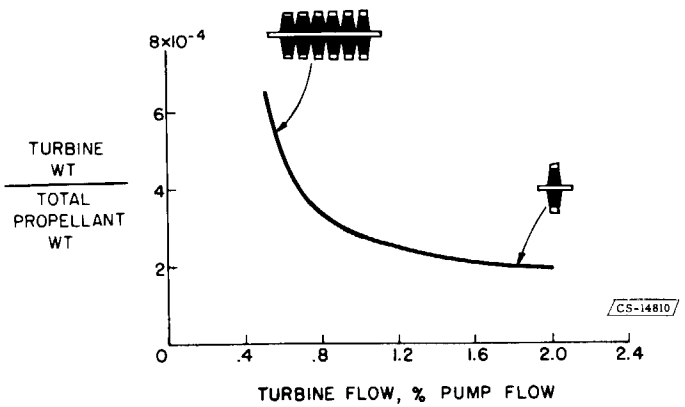

Figure 10

EFFECT OF PROPELLANT COMBINATIONS ON TURBINE FLOW

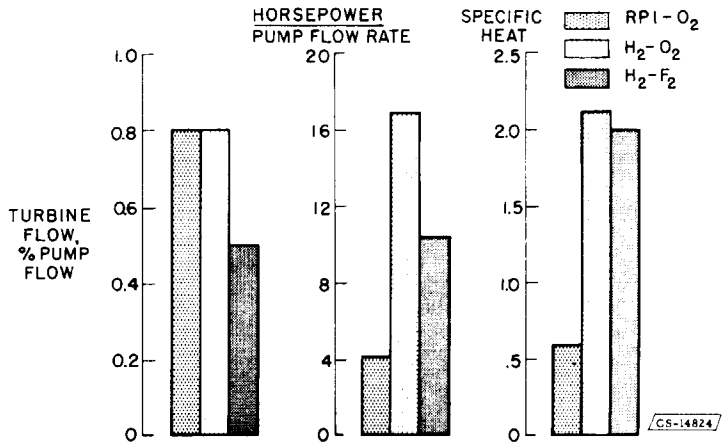

Figure 11

EFFECT OF PROPELLANT COMBINATIONS ON TURBINE DIAMETER AND STAGE NUMBER

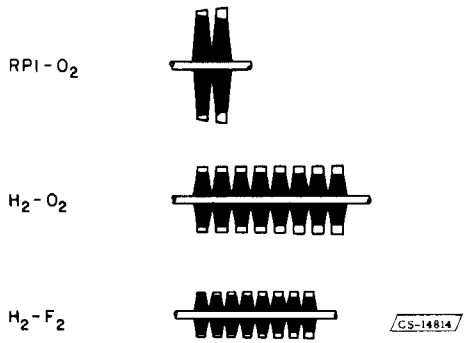

Figure 12

EFFECT OF PROPELLANT COMBINATIONS ON TURBINE WEIGHT

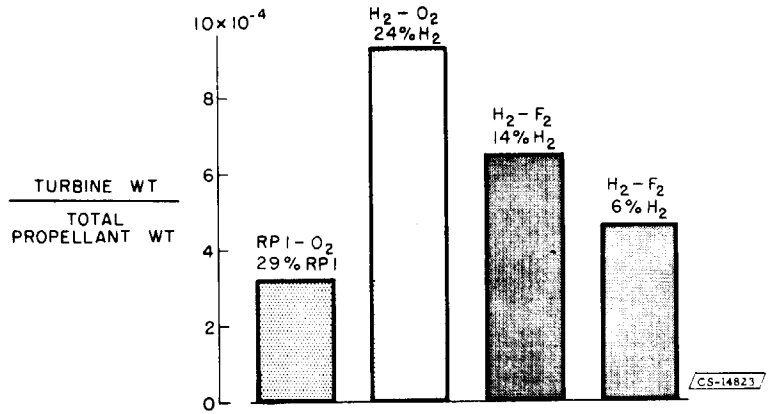

Figure 13

EFFECT OF PROPELLANT ON TURBOPUMP WEIGHT

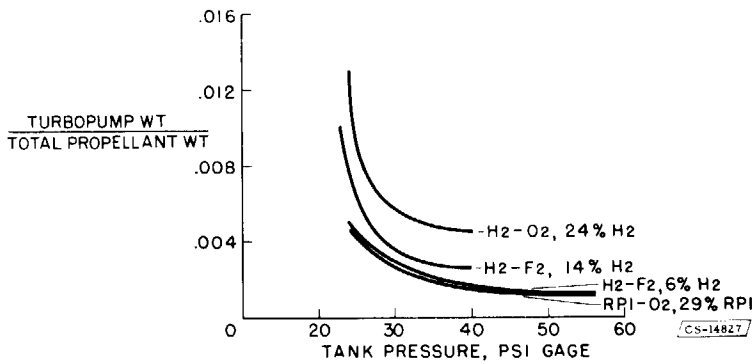

Figure 14

8. PERFORMANCE AND MISSIONS

By J. L. Sloop, A. S. Boksenbom, S. Gordon, R. W. Graham,
P. M. Ordin, and A. O. Tischler

INTRODUCTION

The purpose of this paper is to discuss propulsion requirements for accomplishing specific missions, to examine the effect of component trends on vehicle design using the information provided by the preceding papers, and to focus attention on problems where research emphasis is needed.

The missions and the propellant combinations considered in the analysis are as follows:

Missions:

Surface-to-surface
Earth satellite
Moon orbits

Propellants:

RP-1 - oxygen
Hydrazine-fluorine
Hydrogen-fluorine
Present solid
Future solid

The present and the future solid propellants were assumed to have a sea-level specific impulse of 240 and 270 pound-seconds per pound, respectively. Other propellants of current interest not considered in this analysis are ammonia-fluorine and hydrogen-oxygen. The performance of ammonia-fluorine is similar to that of hydrazine-fluorine, and the trends of hydrogen-oxygen can be deduced from those shown for hydrogen-fluorine.

[redacted]

COMPONENT WEIGHT SELECTION

Weight Designations

In order to calculate vehicle performance, it was necessary to assign specific powerplant weights and specific body weights for each propellant combination. Figure 1 is a schematic drawing of a rocket missile showing the weight designations for both liquid and solid propellants. The nose contains the load, which comprises the payload and such fixed weights as guidance mechanisms, powerpacks, and so forth. The rest of the missile is the propulsion system consisting of propellants and structure.

For liquid-propellant systems the structure is divided into the body and the powerplant. The body consists of such items as tanks, pressurization (tanks, gas, and system), lines, baffles, launching and separation gear, and residual fluids. The body weight is considered proportional to propellant weight. The powerplant consists of thrust chamber (injector, chamber, nozzle), turbopump (turbine, two pumps, gas generator, lubrication system), engine controls (gimbaling, propellant utilization, starting and shutdown systems) mounting frame, and residual fluids. The powerplant weight is considered proportional to thrust, as indicated in the figure.

The structure of the solid-propellant engine is not subdivided. It consists of such items as case, insulation, inhibitor, head closure, launching and separation gear, thrust reversal, nozzle, engine controls, mounting, and residual propellant, if any. These items are expressed as a function of propellant weight.

When the relations between thrust, propellant weight, and gross weight are known for a particular mission, the body and powerplant weights can be combined into a single structure weight and expressed as a function of propellant or gross weight. The ratio used to compare vehicle performance with different propellants and missions is the ratio of gross weight to load.

Flight Equation

The most important factors in rocket vehicle performance are related by the equation

$$\Delta V = I_S \, g \, \ln \left(\frac{1}{\frac{W_L}{W_G} + \frac{W_S}{W_G}} \right) - \Delta V_l \qquad (1)$$

[redacted]

The first term shows that velocity is a function of specific impulse and the ratios of load to gross weight and structure to gross weight. The second term accounts for velocity losses from gravitational pull (comparatively large for first-stage operation) and drag (comparatively small). These losses are considered in the analyses of this paper.

Specific Impulse

The importance of specific impulse is obvious. The specific impulse is not, however, a fixed value for a propellant combination, but depends on combustion-chamber pressure, altitude, and exhaust-nozzle design.

Altitude effect. - The theoretical specific impulse of a rocket engine with a fixed-nozzle area ratio of 13:1 (selected for the booster rockets) is shown as a function of altitude in figure 2. The remarkable change in specific impulse occurs at low altitudes. The specific impulse can be increased slightly at high altitude by increasing the area ratio of the nozzle but only at the expense of decreasing specific impulse in the low-altitude region.

Second- and third-stage engines usually fire into a nearly perfect vacuum. Consequently, the nozzles for these engines are enlarged to an area ratio of 50:1 to take advantage of the increase in specific impulse. On current ICBM missiles, these area ratios are 8:1 for the first stage and 25:1 for the second.

Efficiency. - The specific impulse also depends on the efficiency of conversion of chemical potential energy to heat. An over-all specific impulse of 90 percent of the theoretical specific impulse was assumed for these engines with a fixed-nozzle area ratio at each point along their flight path. The effective specific impulse is, of course, an integrated result.

The specific impulse values assumed in this analysis for RP-1 - O_2 in both the first- and the second-stage engines are about 15 units higher than those used in current missiles. This is partly due to the bigger nozzles, but primarily due to the higher over-all conversion efficiency of 90 percent which was assumed. NACA experiments with engines of 200 to 5000 pounds thrust indicate the 90-percent value is feasible. A 1000-pound-thrust engine with a 50:1 area-ratio nozzle was fired into a partial vacuum and gave a specific impulse of over 300 pound-seconds per pound with RP-1 - O_2.

Weight Ratios

The ratio W_L/W_G in equation (1) is directly affected by the other ratio W_S/W_G. A pound taken from the structure can be added to the

payload without affecting the flight trajectory. As previously pointed out, the structure factor includes two terms. On the basis of information given in the preceding paper and estimates of accessory weights of current vehicles, estimates were made for the powerplant weight in terms of thrust and for the body weight in terms of propellant weight.

Powerplant specific weight. - The powerplant specific weights are given in table I.

TABLE I. - POWERPLANT SPECIFIC WEIGHTS

Propellants	Propellant mixture, % fuel	W_{PP}/F	
		Stage 1	Stages 2 and 3
RP-1 - O_2	30	0.009	0.011
N_2H_4-F_2	30	.009	.011
H_2-F_2	8	.010	.012

The propellant proportions shown in percent fuel are used in the analysis; the bulk densities are 65, 82, and 36 pounds per cubic foot, respectively. The specific engine weights for first-stage engines using RP-1 - O_2 and N_2H_4-F_2 were assumed to be the same. The second- and third-stage engines were assumed to be heavier because they use more elaborate controls, such as propellant utilization devices. These weights are about one-third less than those of current engines. The hydrogen-fueled powerplant was assumed to be heavier than the others because of added turbopump weight which results from the low bulk density of the propellants. More recent estimates of the turbopump weight of a hydrogen-fluorine rocket indicate that the powerplant weights given for the hydrogen-fueled engines are conservative. (See previous paper by A. Ginsburg.)

No separate powerplant weight was considered for the solid-propellant engines.

Body specific weight. - The body specific weights, that is, the body weight per pound of propellant, are shown in table II.

TABLE II. - BODY SPECIFIC WEIGHTS

Propellants	W_B/W_P	
	Stage 1	Stages 2 and 3
RP-1 - O_2	0.04	0.06
N_2H_4-F_2	.04	.06
H_2-F_2	.06	.09
Solid (present)	.10	.10
Solid (future)	.08	.08

The body weight of solid-propellant engines is the structure weight of the vehicle or of its stage. The increased body weights for hydrogen-fueled systems are again a consequence of the low bulk density. The specific weights differ for different stages because of added support required for bending stresses in the second- and third-stage frame. The bending stresses are produced during gimbaled firing of the first-stage engine.

These assumed body weights apply only for large vehicles and are, of course, somewhat arbitrary. A body factor of only one significant figure is shown because more accurate numbers are not justified. The values for RP-1 - O_2 and present solids compare favorably with values for current advanced missiles.

A typical split of structure weight between body and powerplant is shown in figure 3. Most of the weight is in the body. Later the effects of changing the values of component weights will be considered.

SURFACE-TO-SURFACE MISSIONS

Typical trajectories for surface-to-surface missions are shown in figure 4. The IRBM, Intermediate Range Ballistic Missile, has a range of 1500 nautical miles and requires a velocity at thrust termination of about 14,000 feet per second and an angle of 35° with reference to the earth. The ICBM, Inter-Continental Ballistic Missile, has a range of about 5500 nautical miles and requires a velocity of about 23,000 feet per second and an angle of about 22° with respect to the earth. At burnout it is about 100 miles high and 300 miles distant from the launching point.

IRBM Missions

The effect of the selected propellants on the gross weight of an IRBM missile for a useful load of 5000 pounds is shown by the bar diagram

[redacted]

of figure 5. For RP-1 - O_2, a gross weight of approximately 60,000 pounds is required. This can be compared with a gross weight of 110,000 pounds for a current vehicle using RP-1 - O_2, as indicated by the dashed bar. The difference in the gross weights is due to the ratio of structure to gross weight and to the specific impulse assumed. The structure factor used for the IRBM in the design studies was somewhat lower than current practice and can be considered to be an advance in the present state of art for this mission. In addition, the specific impulse used in the design calculations was about 5 percent higher than that being developed in current engines.

With present-day solid propellants, a single-stage vehicle requires a gross weight of about 220,000 pounds; by designing for a two-stage missile, however, the gross weight is reduced to about one-half this weight. The anticipated performance of future solid propellants results in a substantial reduction in the gross weight, for both one- and two-stage missiles. The gross weight required for a storable liquid-propellant combination N_2H_4 + ClF_3 is included for comparison. The gross weight is about the same as for RP-1 - O_2 for a single-stage missile. A two-stage missile will weigh about 20 percent less.

Reducing the load results in a general reduction in the gross-weight requirements. A load of 2000 pounds would require about 40 percent of the gross weights of figure 5. For the reduced load, the RP-1 - O_2 system would weigh about 20,000 pounds, and a two-stage present-day solid-propellant system would weigh around 30,000 pounds. This last value compares well with the gross weight expected for a two-stage solid-propellant missile currently under development.

High-energy liquid propellants were not considered for this mission because they are not needed. Propellants would be selected on the basis of their performance, cost, availability, and ease of handling and storage. The safe transportation and readiness of missiles using solid propellants seem to make them well suited for this mission.

The performance and reliability of small-solid-propellant engines and their handling ease are well established; these remain to be proved for large-solid-propellant engines. At present the large-solid-propellant engines are limited to fairly narrow temperature limits and there are other problems to be solved, such as transition from normal burning to detonation, thrust termination, and thrust vector control.

ICBM Missions

Typical ICBM. - A similar comparison of gross weights of the ICBM mission for a load of 5600 pounds is shown in figure 6. The gross weight

[redacted]

for the RP-1 - O_2 two-stage vehicle is about 165,000 pounds. A current two-stage ICBM missile using RP-1 - O_2 weighs 220,000 pounds, as indicated by the dashed bar. The difference in gross weight is due primarily to the difference in specific impulse of the current engine and that assumed in the analysis.

The high performance of the N_2H_4-F_2 propellant combination results in a single-stage missile weighing about the same as the two-stage RP-1 - O_2 missile. The use of H_2-F_2 gives the minimum-gross-weight missile.

For present-day solid propellants, the gross weight of a two-stage missile is about 300,000 pounds, but decreases appreciably when three stages are used. The use of future solid propellants would result in considerable weight decrease. The gross weight of a future solid-propellant two-stage missile is about the same as the current RP-1 - O_2 missile, and a three-stage unit will reduce the weight about 30 percent further.

The gross weight can generally be reduced by adding more stages but will eventually level off or even rise as many stages are added because the structure weight of upper stages must be increased for joining and separation devices as well as for increased moments from changes in the thrust vector. The optimum number of stages depends on more detailed design considerations than are used in this analysis.

Alternate ICBM trajectories. - High-energy propellants could be used to decrease weight for ICBM missions. They could also be used to increase velocity to perform other ICBM missions. Figure 7 shows two such alternate trajectories. The missile could be lofted on a high trajectory to get a steeper angle of re-entry, for instance 47°, to improve accuracy. This requires about 3000 feet per second more velocity than the original trajectory. Or, for strategic purposes, a missile could be launched from the opposite side of the continent and go the long way to the target. Here again, the velocity requirement is greater - about 28,500 per second.

Accuracy of alternate trajectories. - There are a number of factors that will determine the accuracy and effectiveness of missiles on these trajectories: accurate measurement of the vector velocity and position at burnout, controlled fast thrust-cutoff, aerodynamic forces, and average winds on re-entry. There are also uncontrolled, indeterminate effects, such as the random winds on re-entry and mapping uncertainties. Most of these sources of error are reduced by the lofting of the trajectory.

Figure 8 shows the requirements for velocity control at burnout at an altitude of 100 miles, neglecting the effects of the earth's rotation. The effect of velocity error (ft/sec) on miss distance (miles)

is plotted against the burnout velocity for lines of constant range. The IRBM on the 1500-nautical-mile line is shown at the point of minimum burnout velocity; the miss distance due to velocity error is 0.2 mile per ft/sec. Only small improvement in accuracy would be gained for the IRBM by increasing the burnout velocity.

The ICBM for minimum burnout velocity has an error of 1.1 mile per ft/sec at a path angle of 22°. If the angle is increased, the error would decrease along the curve at the expense of increased burnout velocity. At an angle of 47°, the error can be reduced by half (to 0.5 mile per ft/sec) but at the expense of a 3000 ft/sec increase in burnout velocity.

For the backside ICBM (range of 14,400 nautical miles), the error is reduced as the velocity increases beyond satellite velocity and as the corresponding path angle increases. The point shown is for an angle of 15°; the error is 1.3 miles per ft/sec. This missile would require a burnout velocity of 28,400 ft/sec, or 5,400 ft/sec more than the conventional ICBM.

Other control factors are also improved by the lofting technique. The problems of fast thrust-cutoff time and altitude measurement are reduced in about the same manner as the velocity-measurement problem shown in figure 8. One parameter, that of path angle at burnout, is adversely affected by lofting. In figure 9 the requirements for the measurement of path angle at burnout are plotted for the four ballistic missiles. The effect of such angle error on miss distance is given in miles per minute of angle error. The missiles designed for minimum burnout velocity would be relatively insensitive to this error. If the ICBM (5500 nautical mile range) is lofted to 47°, the error would be 2 miles per minute angle. For the backside ICBM, the error is decreased for higher velocities and higher angle; at the point of burnout velocity used before, the error is 7 miles per minute angle error. These severe requirements on path-angle measurement are somewhat alleviated by the fact that the path angle is almost constant along a large part of the burning trajectory, and dynamic effects are small. The velocity, however, is continuously increasing at a high rate and must be measured instantaneously as well as very accurately.

Accuracy at re-entry. - Changing the trajectory, and therefore the path angle, affects the accuracy at re-entry. Consider the effect of winds over the target area. Because of aerodynamic heating, the nosecone may be designed to slow down appreciably on re-entering the atmosphere, which makes it subject to deviations by the winds. The average wind (if known) can be included in guidance, but the random winds cannot. Figure 10 shows the resulting possible dispersion on re-entry for the 5500-nautical-mile ICBM with estimated random winds. The standard deviation of miss distance in miles is plotted against the re-entry path angle in

degrees. For each path angle there is a coresponding re-entry velocity. These re-entry angles and velocities are almost equal to those at burnout. The lines are for constant values of weight-drag ratio (W/C_DA). Lofting can be used to decrease the dispersion due to the random winds. For example, for a weight-drag ratio of 100, which is approximately that of some present designs, the ICBM for minimum burnout velocity would have a dispersion of 1.2 mile. If the 47° loft angle is used, requiring an increase in velocity of 3000 feet per second, dispersion is reduced to 0.9 mile.

The lower drag nosecones being considered (W/C_DA of 500 or even 1000) are less affected by the winds, but they show much greater percentage improvement when lofting is used. For W/C_DA of 500, the dispersion can be reduced by a factor of 3.

All of the error factors that have been mentioned might be partially compensated by the use of terminal guidance; even so, it may be necessary to minimize the need for such compensation.

Excess velocity for ICBM missions. - The possibility of obtaining greater velocities than are now available in the ICBM by using high-energy propellants was investigated. The gross weight of the missile was assumed to be 220,000 pounds and the load 5600 pounds, as shown in figure 11. The excess velocity available from the RP-1 - O_2 propellant is about 3500 feet per second. For N_2H_4-F_2, the excess velocity is about 6400 feet per second and for the high-performance H_2-F_2 combination, about 9600 feet per second.

Excess velocity can also be obtained with the future solid propellant. A two-stage missile will provide excess velocity of about 2800 feet per second and a three-stage missile, approximately 4700 feet per second.

Excess velocities could be used for maneuvering an ICBM. After-all, a ballistic missile is really helpless after burnout. Perfection of an interceptor missile could make this weapon not nearly so effective as it is now considered. Figure 12 illustrates the requirements on excess impulse Δv for such maneuverability. A typical turn from the ballistic trajectory is shown, turning through an angle α. The Δv required to make this turn is approximately equal to the product of the angle of turn and the velocity.

Two maneuvers are shown using such a turn. For case 1, a single missile can threaten a region of target areas. By beginning the turn 1000 miles from impact, a line of 300 miles at the target can be covered if the missile is carrying fuel with a mass-ratio equivalent to a Δv of 7000 feet per second. This maneuver in three dimensions covers a

region of about 140,000 square miles, an area three times greater than the state of Ohio. For this maneuver the ratio of distances is almost independent of how fast the excess Δv is used. For the case shown, a 1-g normal acceleration is used. The dispersion would improve somewhat if higher normal accelerations were used.

The second case is a maneuver turning away from the target direction and then approaching at a different angle. For a turn angle of 6°, an excess Δv of 7000 feet per second is required. The distances required for this maneuver depend on the normal acceleration used. For example, if a 5-g normal acceleration is used, the maneuver could start 200 miles from impact, and the maximum deviation from the ballistic path would be about 5 miles.

The effectiveness of this kind of versatility built into the missile will, of course, depend on the intelligence and maneuverability of any interceptor missiles, as well as the other strategic and perhaps psychological factors involved.

Summary of Surface-to-Surface Missions

Solid propellants show promise for IRBM missions and lightly-loaded ICBM missions. High-energy liquids and solids offer weight savings for ICBM missions or, alternatively, higher velocities can be obtained and used for alternate trajectories for advantages of accuracy, surprise, or maneuverability. The choice of propellants will depend not only on the mission, but also on such other factors as readiness, mobility, size, and handling and operation problems.

EARTH SATELLITES

Guidance Requirements

Earth satellite orbits are shown in figure 13. A typical trajectory for launching a two-stage earth satellite into the orbit is shown in figure 14. The first-stage rocket boosts the vehicle to approximately 100 miles altitude and then a long coast puts the satellite into the orbital altitude of 300 miles. Then, the second stage fires and accelerates the satellite to the required orbital velocity of 25,000 feet per second.

The guidance requirements for a circular satellite orbit are shown in figure 15. In the sketch, the dotted circle is the reference desired circular orbit. If there is an error in angle and perhaps velocity at burnout, the actual orbit will be an ellipse whose height will deviate from the height at burnout, having a maximum positive deviation at apogee and a maximum negative deviation at perigee.

The plot shows the maximum velocity error that can be tolerated for each such maximum allowable deviation and angle error. For a maximum deviation of 100 miles, an expected angle error of 1° would require velocity control at burnout to within 80 feet per second. This requirement is considerably less stringent than that for the ICBM. In fact, if the satellite carried ICBM quality guidance equipment, the maximum deviation could be kept within about 1 mile.

Weight Comparisons

Figure 16 shows the gross weight - load ratio required for this mission for the propellant combinations selected. The heaviest of the two-stage vehicles is for the RP-1 - O_2 combination. It would take about 66 pounds of gross weight for every pound of load. The calculations showed that the present solid propellants would require at least three stages to put such a vehicle into its orbit. A satellite could be established with a future solid-propellant two-stage vehicle. The gross weight - load ratio for the future solid propellant appears to be as good as that of the RP-1 - oxygen vehicle. The lightest vehicle is the one with the hydrogen-fluorine propellant system. For this combination only 20 pounds of gross weight are required for every pound of load.

Also shown in figure 16 is the gross weight - load ratio for a satellite vehicle comprising an RP-1 - O_2 first stage and a H_2-F_2 second stage. Considerable weight saving over RP-1 - O_2 in both stages can be obtained by using high-energy propellants in the second stage.

Volume Comparisons

Figure 17 indicates the total propellant volume as a measure of the over-all bulk of the vehicle. Also indicated in figure 17 are the gross weights of such vehicles for a load of 20,000 pounds. The RP-1 - O_2 combination would produce the largest bulk and the hydrazine-fluorine would produce the smallest. The high density of the solid propellants offers a decided advantage in reducing the size of the vehicle. Note that the RP-1 - O_2 and the future solid-propellant vehicles weigh more than one million pounds. In contrast the high-energy propellants reduce this weight to approximately 500,000 pounds, about twice the weight of the current ICBM's. There does not appear to be a great difference in size or weight between the hydrazine and the hydrogen vehicles. In such cases the propellant would be selected on criteria other than weight and bulk.

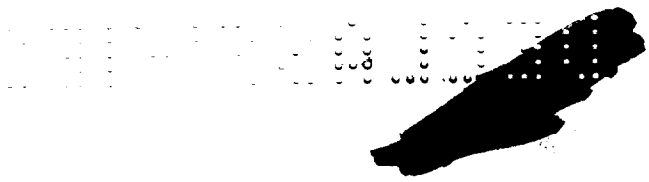

Summary of Satellite Mission

A 20,000-pound load can be placed in a satellite orbit with vehicles having gross weights from two to five times greater than those of the largest missile today, using the propellants and design values selected. For this mission more handling and operating problems can be tolerated, if necessary to gain performance advantages, than for the surface-to-surface missions.

MOON MISSIONS

Moon Circumnavigation without Load Recovery

Figure 18 is a trajectory of a moon circumnavigation. Departing from the earth requires a velocity of about 35,000 feet per second. If the guidance and timing are right, the space craft will approach the moon and be attracted by its gravitational pull. The corresponding numbers on the trajectory and moon orbit give relative positions of the space craft and moon. If correctly timed, the space craft will swing about the moon and turn back toward the earth. If the load is to be recovered, the satellite must be decelerated about 10,000 feet per second to swing into an earth satellite orbit and eventually be slowed by air braking and recovered. The moon circumnavigation with the load not recovered is first considered.

Weight comparisons. - The velocity of 35,000 feet per second required to leave the earth can be obtained with any of the five propellant combinations with the vehicle weights shown in figure 19. The gross weight needed to deliver each pount of payload is given on the ordinate. For example, a vehicle using RP-1 - O_2 has a gross weight - load ratio of 165. A 1000-pound load would require a 165,000-pound gross weight. The trend in weight ratio for the other propellants is very similar to that shown previously for the ICBM mission and the satellite mission; that is, H_2-F_2 has the lowest weight ratio and the present-day solid, the highest. For the high-energy liquids the gross weight - load ratio for H_2-F_2 is about one-third less than that for N_2H_4-F_2. The weight ratio for the present-day solid propellant can be reduced by more than half with the future solid propellant, provided the high specific impulse and lower casing weight assumed for the future solid can actually be realized.

The vehicles using solid propellants are three-stage vehicles, while those using liquid propellants are two-stage vehicles. If three stages were used with RP-1 - O_2, the gross weight - load ratio would be reduced by more than one-third, from 165 to 102.

Effect of changes in specific impulse and component weights used in analysis. - The weight ratios used in the analysis were based on the body weights, engine weights, and values of specific impulse previously given. In addition, an initial acceleration of 1.5 g's was assumed. If these parameters were to vary, the resulting weight ratios would also change.

The effect of a change in specific impulse is shown in figure 20 for H_2-F_2. A 10-percent decrease in effective specific impulse of the first-stage powerplant for the moon mission causes a 33-percent increase in gross weight - load ratio, quite a drastic change. The same trend holds for the second-stage engine and, if the specific impulse of both stages is changed, the effects are combined.

Figure 21 shows the effect of changing engine or powerplant specific weight. For the booster stage of the same mission, a 10-percent increase in powerplant weight causes only a 1.4 percent increase in the gross weight - load ratio.

Figure 22 shows the effect of changing the body specific weight for the same mission. A 10-percent increase in body weight increases the gross weight - load ratio 5.6 percent.

From the foregoing results, the factor affecting the gross weight - load ratio the most is specific impulse; changes in powerplant and body specific weights have a much lesser effect. The magnitudes of the effects depend on the severity of the mission propulsion requirements.

Moon Circumnavigation with Load Recovery

Now consider the requirements for circumnavigating the moon and returning to a satellite orbit about the earth. An initial velocity of 35,000 feet per second is required to leave the earth's surface and an additional 10,000 feet per second to decelerate for entering the earth satellite orbit. This additional velocity can be provided by adding another stage. Note that the solid-propellant vehicles now have four stages and the liquid-propellant vehicles have three stages.

Figure 23 compares the vehicle weight ratios required for this moon mission. With RP-1 - O_2, the gross weight - load ratio is 650. This is four times the weight ratio (165) that was needed to get the load around the moon. This large increase is due primarily to the fact that the additional stage (both propellant and structure) as well as the load must now be propelled around the moon.

The trend in weight ratios for the other propellants is similar to that shown for the moon mission without load recovery. H_2-F_2 again requires the smallest weight ratio and the present-day solid propellant, the highest.

[redacted]

Moon Satellites and Landing on the Moon

Assume that the problem of establishing an earth satellite platform has been mastered. The platform has been put there by perhaps several trips of vehicles with weight ratios previously described. Assume further that the space platform is orbiting about the earth at a velocity of 25,000 feet per second. Figure 24 shows a mission of a moon satellite departing from and returning to an earth satellite platform. The space craft leaves the earth satellite by increasing the velocity to 10,000 feet per second more than the platform velocity. As the craft approaches the moon, it is decelerated 2200 feet per second to swing into a moon orbit. When the space craft is ready to leave the moon's orbit, the velocity is increased by 2200 feet per second and it turns toward the earth. As it approaches the earth, the space craft must decelerate 10,000 feet per second to swing into an earth satellite orbit and contact the satellite platform. The velocity requirement for this mission is about 24,400 feet per second in addition to that needed to establish the platform.

An even more ambitious mission is a landing on the moon and return to the earth satellite platform. Figure 25 shows exactly the same steps as outlined for a moon satellite, except that for the moon landing and takeoff, landing of the moon satellite requires a deceleration of 5700 feet per second and takeoff from the moon's surface to the moon orbit, an acceleration of 5700 feet per second. These velocity requirements total 35,800 feet per second above that of the earth satellite. This is about the same velocity requirement as described for the moon circumnavigation mission.

Figure 26 shows the vehicle weight comparison for a moon landing and return. As an example, the gross weight - load ratio of the RP-1 - O_2 vehicle is only 65 as compared with 165 for the moon-circumnavigation mission requiring about the same velocity. There are several reasons for this difference. The first and most important reason is that three stages are used for this mission instead of the two stages for the moon circumnavigation. Secondly, in launching from a space platform, the specific impulse in large-area-ratio nozzles is appreciably higher than in launching from the earth's surface (see fig. 2). Finally, in launching from a space platform, there are no drag losses such as those encountered in starting from the earth.

These relatively low gross weight - load ratios can, however, be somewhat deceiving. The H_2-F_2 vehicle is chosen to illustrate this point because it has the lowest gross weight - load ratio (24). To get a 10,000-pound load off the space platform, landed on the moon, and back to the platform requires a gross weight of 240,000 pounds. This is about the weight of a present-day ICBM. However, to get these 240,000 pounds to the platform in the first place with H_2-F_2 would require a minimum initial gross weight of about 5 million pounds. If this same

[redacted]

mission were to be accomplished with RP-1 - O_2 instead of H_2-F_2, then instead of 5 million pounds, an initial minimum gross weight of over 40 million pounds is required.

SUMMARY

Propulsion requirements for the various missions have been given with selected component weights and the effect of variation in the component weights has been shown. The values given should be used more as illustrations of the trends rather than as proposed designs.

Figure 27 summarizes the propulsion requirements for the missions. Gross weight - load ratio, on a logarithmic scale, is shown as a function of velocity requirement in feet per second. The velocity represents the energy needed to accomplish the various missions. The ICBM, for example, requires a little over 23,000 feet per second; the earth satellite, about 25,000 feet per second; moon circumnavigation, 35,000 feet per second; moon circumnavigation and return, 45,000 feet per second; moon satellite, about 49,000 feet per second; and moon landing and return, about 61,000 feet per second. The upper curve is for RP-1 - O_2 or future solids and the lower curve is for H_2-F_2, representative of the high-energy liquids. The numbers on the curves refer to stages; the curves are really a minimum envelope of several curves of constant number of stages. For missions such as the ICBM or even earth satellites, the gross weight - load ratios for present propellants and high-energy liquid propellants differ by a factor of only 1.5 to 2. However, as the energy requirement becomes greater, the advantages of high-energy propellants are very significant. For the moon landing and return, the ratios differ by a factor of 8. For large payloads and extreme missions, the advantages of high-energy propellants are quite obvious.

There are many problems in the storing, handling, and operation of the various propellants, particularly the cryogenic fluids, that have barely been touched. The potentialities of chemical rockets using liquid and solid propellants have barely been tapped, and the need for intensive research and development in this area is clearly indicated.

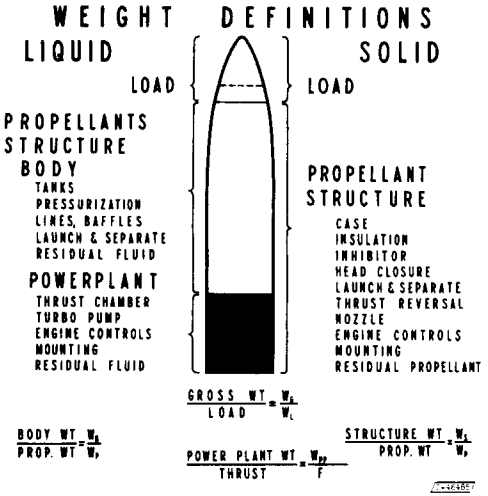

Figure 1

VARIATION OF SPECIFIC IMPULSE WITH ALTITUDE

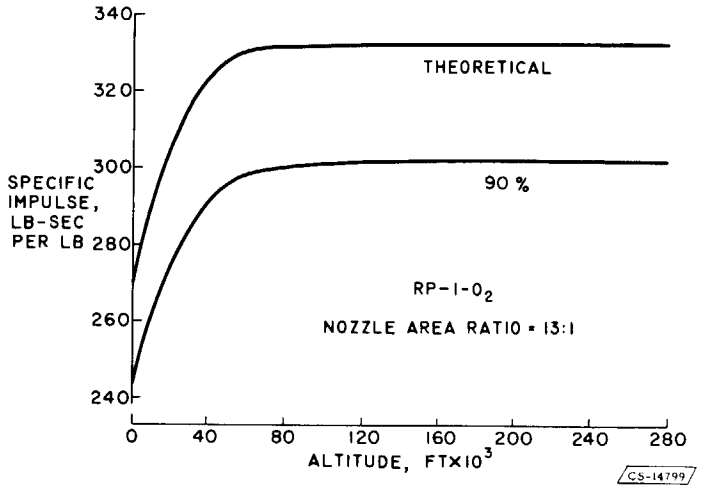

Figure 2

TYPICAL STRUCTURE WEIGHT SPLIT

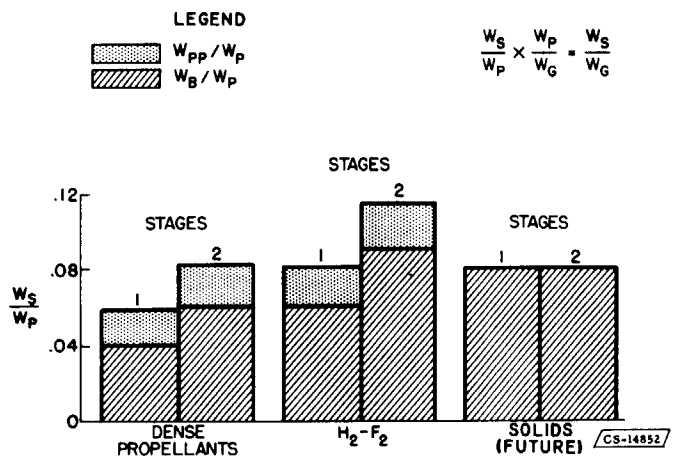

Figure 3

IRBM AND ICBM TRAJECTORIES

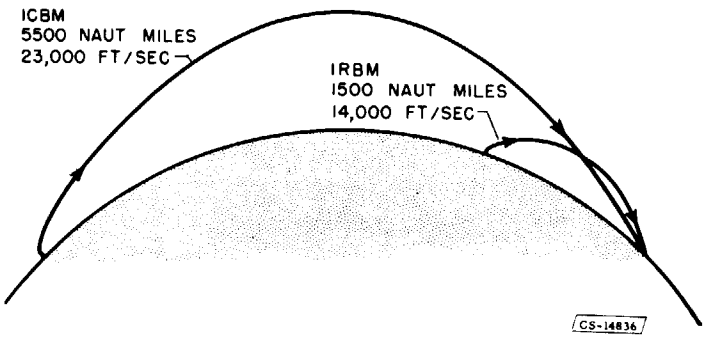

Figure 4

IRBM VEHICLE GROSS WEIGHT

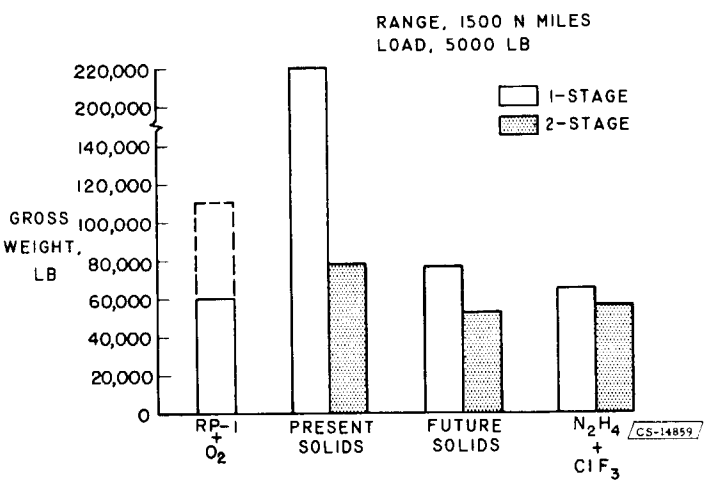

Figure 5

ICBM VEHICLE GROSS WEIGHT

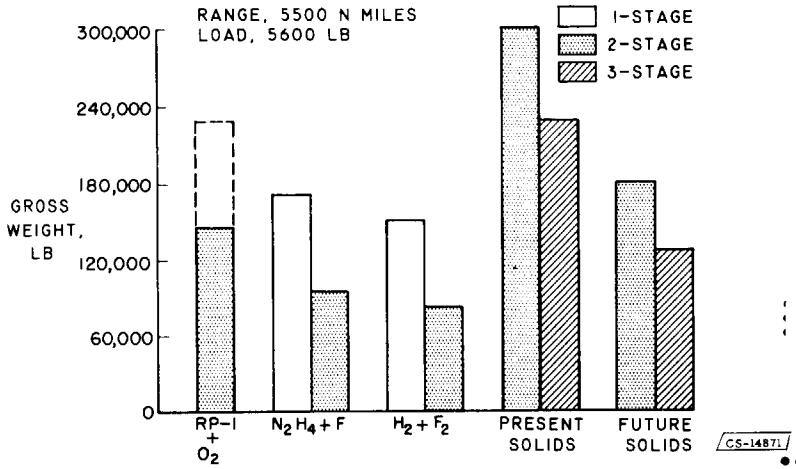

Figure 6

ALTERNATE ICBM TRAJECTORIES

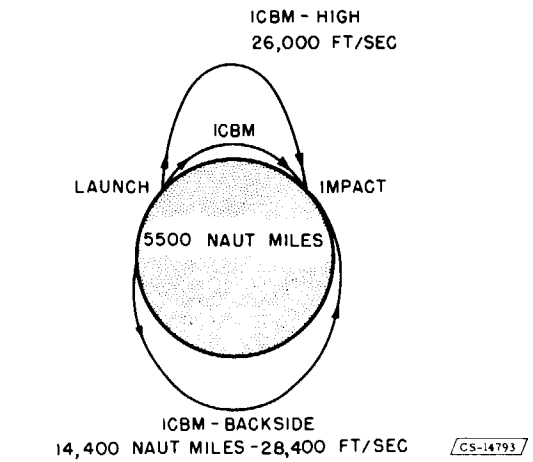

Figure 7

BALLISTIC MISSILES
REQUIREMENTS ON GUIDANCE ACCURACY

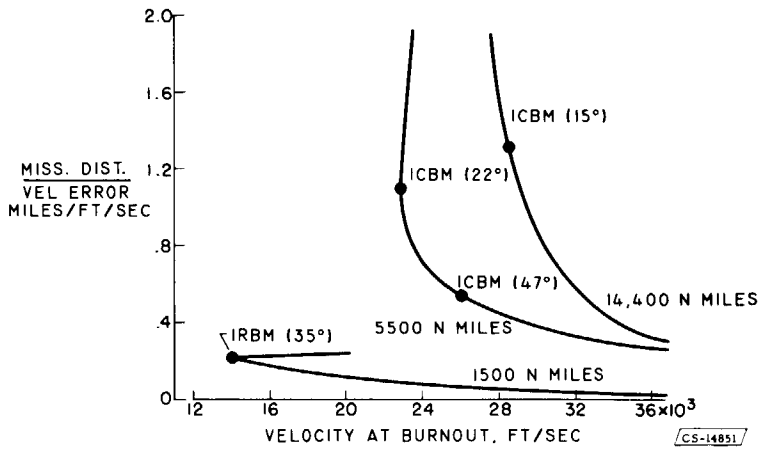

Figure 8

BALLISTIC MISSILES
REQUIREMENTS ON GUIDANCE ACCURACY

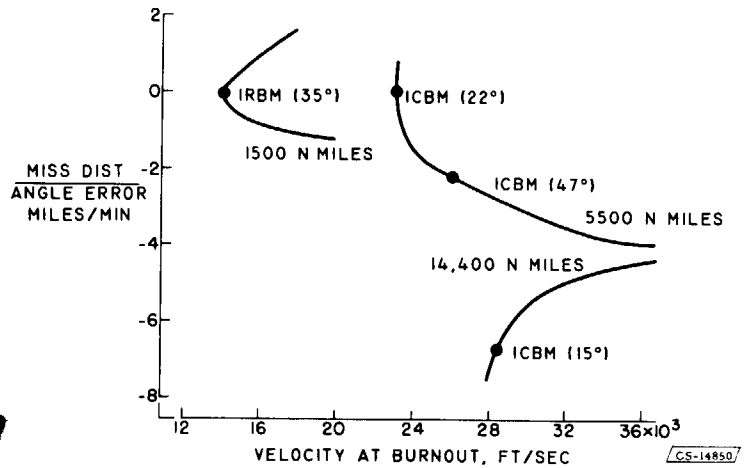

Figure 9

DISPERSION DUE TO RANDOM WINDS ON RE-ENTRY
ICBM, 5500 NAUT MILES

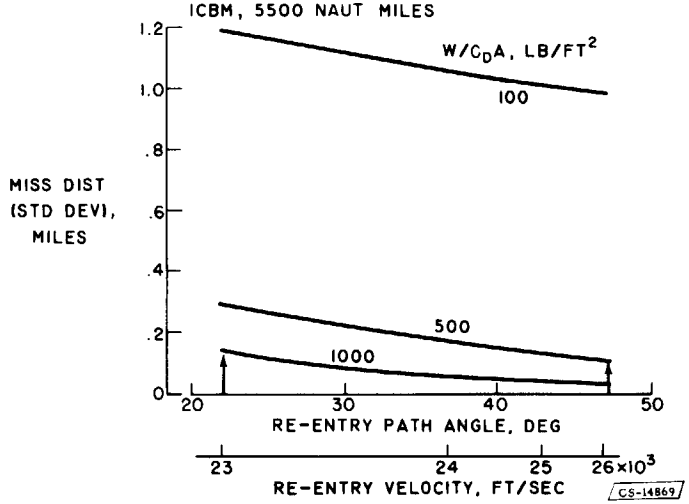

Figure 10

ICBM EXCESS VELOCITY

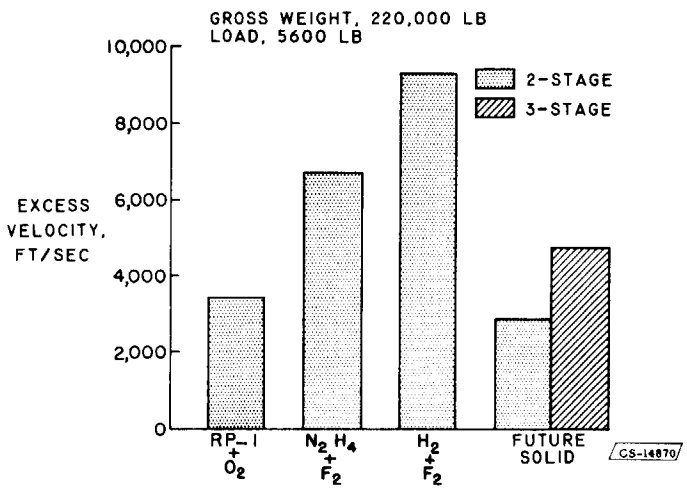

Figure 11

USE OF EXCESS IMPULSE (Δv) FOR MANEUVERS

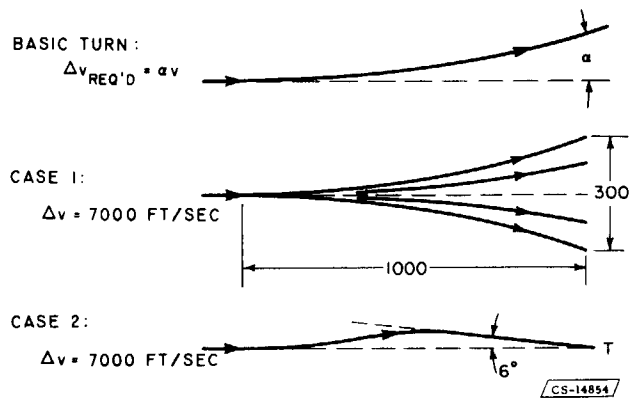

Figure 12

SATELLITE ORBITS

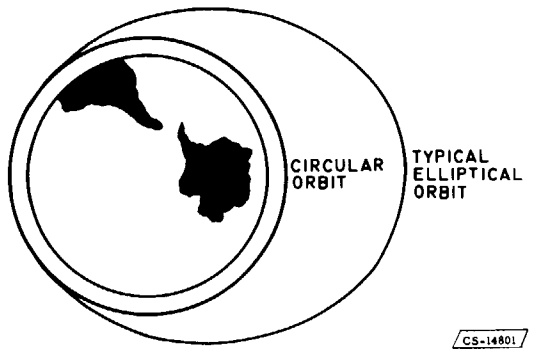

Figure 13

TYPICAL SATELLITE TRAJECTORY

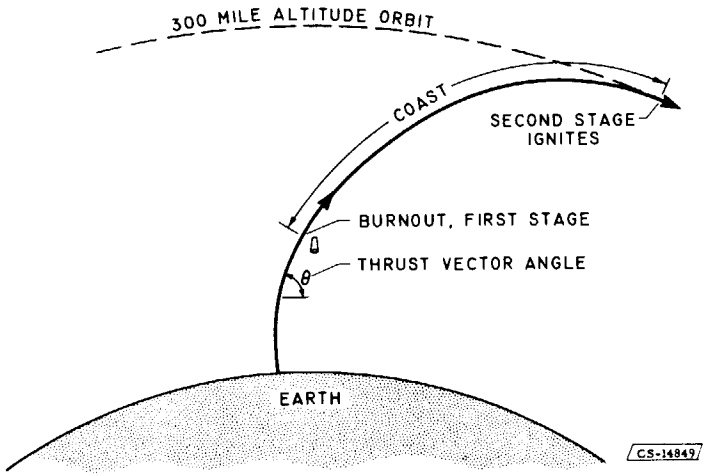

Figure 14

SATELLITE

REQUIREMENTS ON GUIDANCE ACCURACY

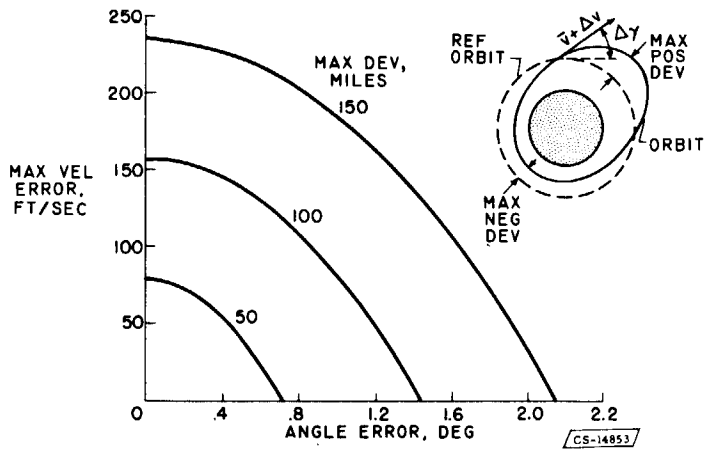

Figure 15

VEHICLE WEIGHT COMPARISON MANNED SATELLITE MISSION

2-STAGES

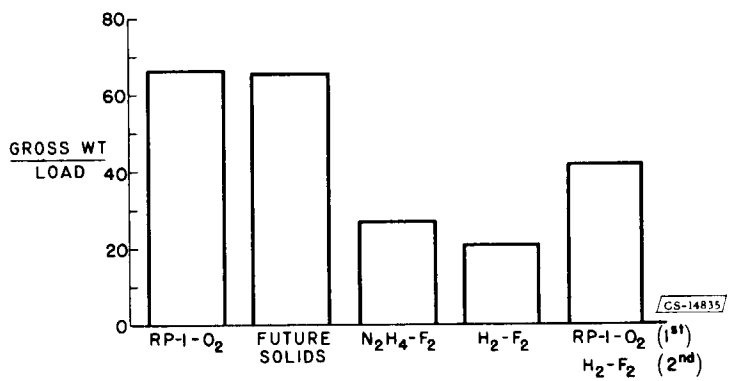

Figure 16

COMPARATIVE SIZE AND WEIGHT OF MANNED SATELLITE VEHICLES

2 - STAGE

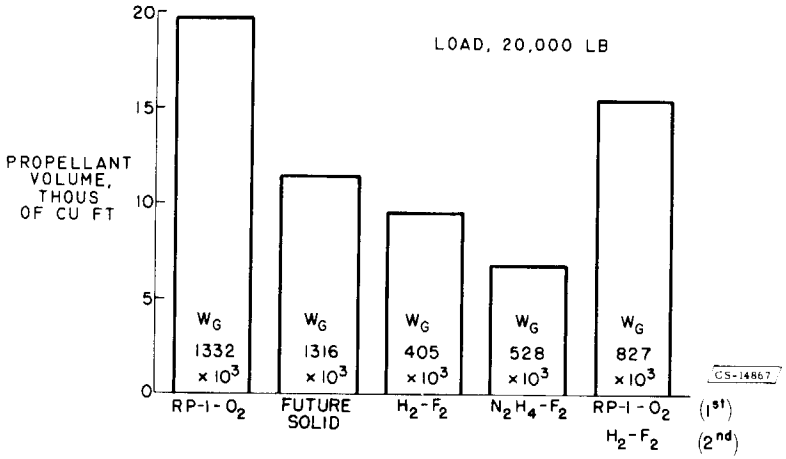

Figure 17

VEHICLE WEIGHT COMPARISON, MOON MISSION

CIRCUMNAVIGATION, LOAD NOT RECOVERED
VELOCITY REQUIREMENT: 35,000 FT/SEC

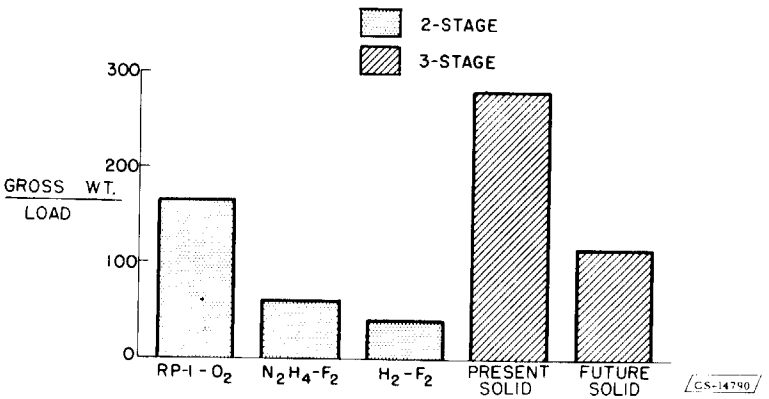

Figure 19

MOON MISSIONS

DEPARTURE FROM EARTH SURFACE

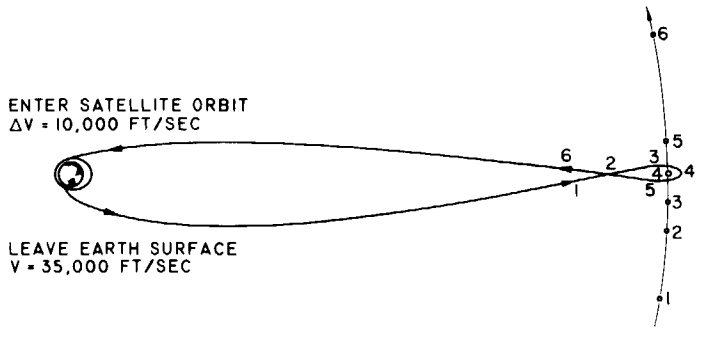

Figure 18

EFFECT OF SPECIFIC IMPULSE

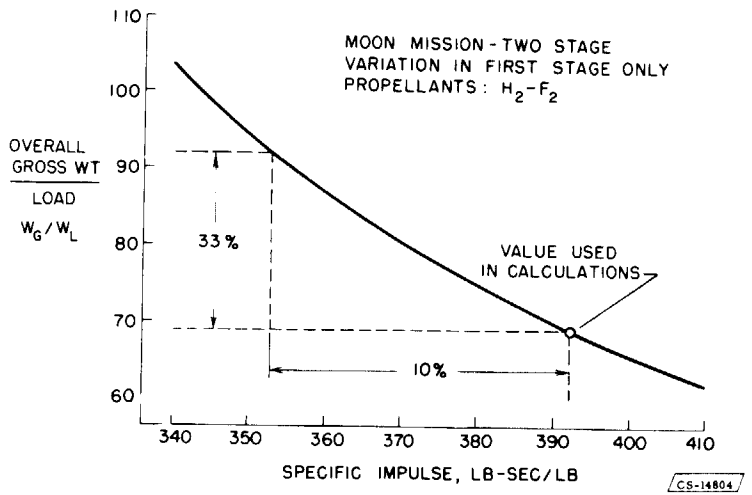

Figure 20

EFFECT OF CHANGING ENGINE SPECIFIC WEIGHT

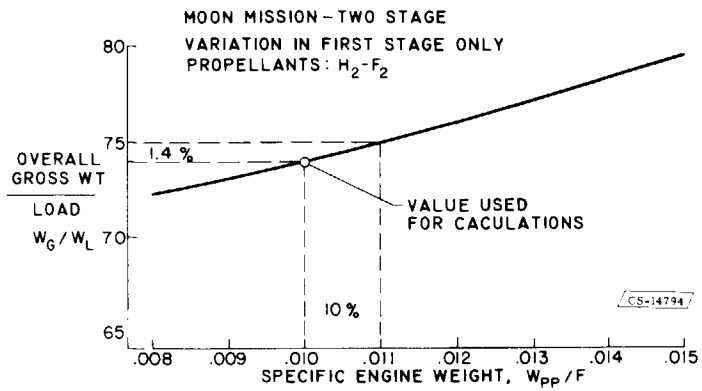

Figure 21

VEHICLE WEIGHT COMPARISON, MOON MISSION

CIRCUMNAVIGATION AND RETURN TO EARTH SATELLITE

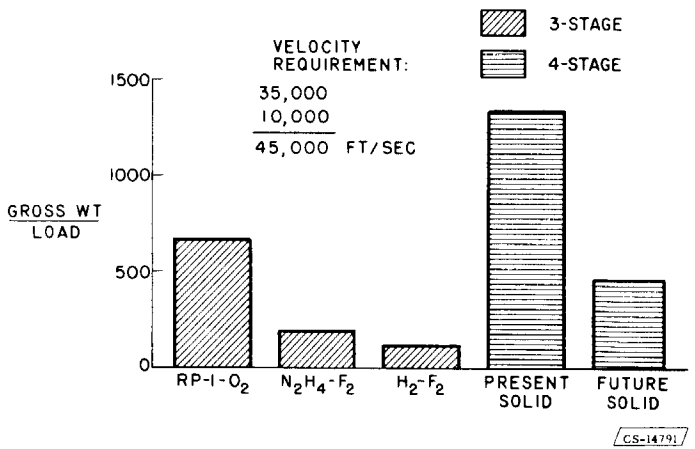

Figure 23

EFFECT OF CHANGING BODY SPECIFIC WEIGHT

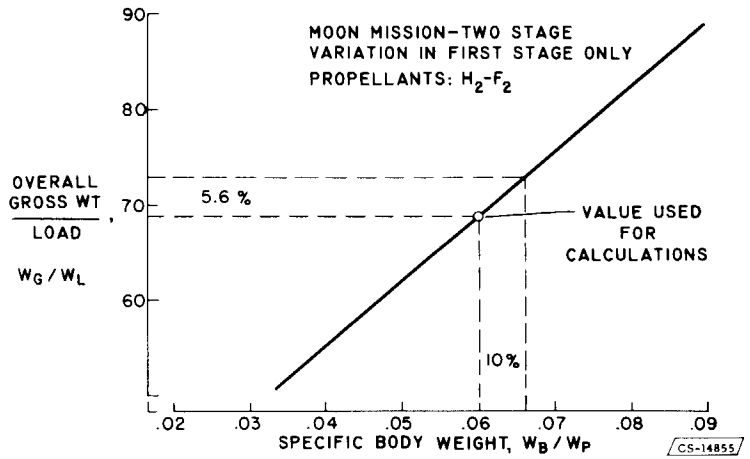

Figure 22

MOON SATELLITE

DEPARTURE FROM EARTH SATELLITE PLATFORM

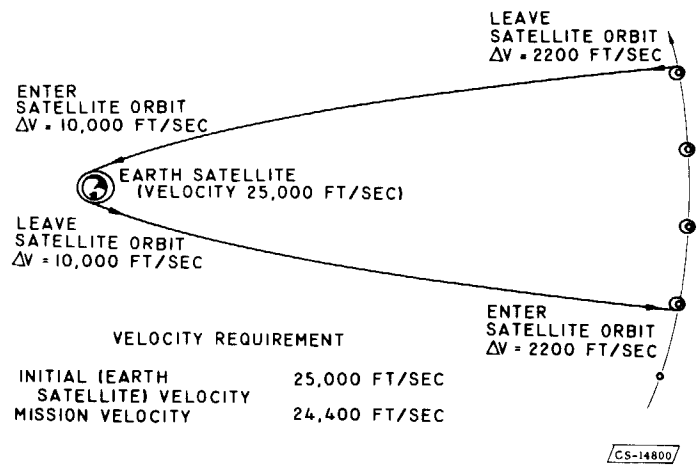

VELOCITY REQUIREMENT

INITIAL (EARTH SATELLITE) VELOCITY	25,000 FT/SEC
MISSION VELOCITY	24,400 FT/SEC

Figure 24

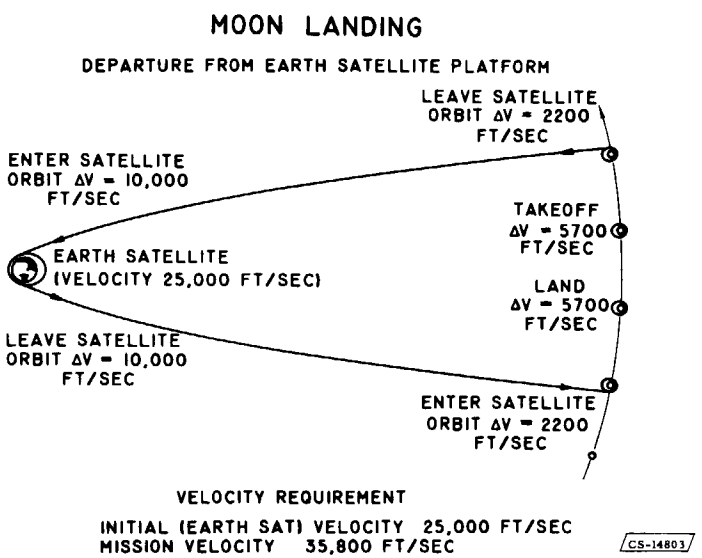

Figure 25

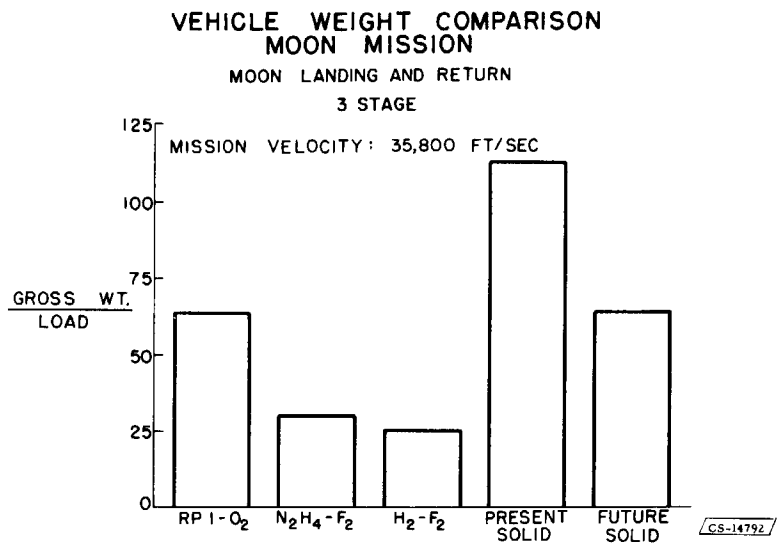

Figure 26

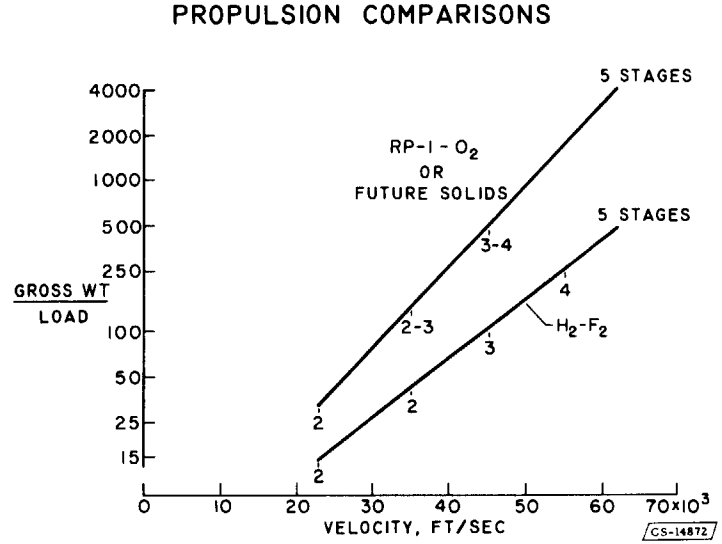

Figure 27